NASA-TM-107401 19970010710

NASA Technical Memorandum 107401

Summary Report of Mission Acceleration Measurements for STS–78

Launched June 20, 1996

Roshanak Hakimzadeh
Lewis Research Center
Cleveland, Ohio

Kenneth Hrovat
Tal-Cut Company
North Olmsted, Ohio

Kevin M. McPherson
Lewis Research Center
Cleveland, Ohio

Milton E. Moskowitz and Melissa J.B. Rogers
Tal-Cut Company
North Olmsted, Ohio

January 1997

National Aeronautics and
Space Administration

SUMMARY REPORT OF MISSION ACCELERATION MEASUREMENTS FOR STS-78

Launched June 20, 1996

Authors:

Roshanak Hakimzadeh
Lewis Research Center
Cleveland, Ohio

Kenneth Hrovat
Tal-Cut Company
North Olmsted, Ohio

Kevin M. McPherson
Lewis Research Center
Cleveland, Ohio

Milton E. Moskowitz
Tal-Cut Company
North Olmsted, Ohio

Melissa J.B. Rogers
Tal-Cut Company
North Olmsted, Ohio

Abstract

The microgravity environment of the Space Shuttle Columbia was measured during the STS-78 mission using accelerometers from three different instruments: the Orbital Acceleration Research Experiment, the Space Acceleration Measurement System and the Microgravity Measurement Assembly. The quasi-steady environment was also calculated in near real-time during the mission by the Microgravity Analysis Workstation.

The Orbital Acceleration Research Experiment provided investigators with real-time quasi-steady acceleration measurements. The Space Acceleration Measurement System recorded higher frequency data on-board for post-mission analysis. The Microgravity Measurement Assembly provided investigators with real-time quasi-steady and higher frequency acceleration measurements. The Microgravity Analysis Workstation provided calculation of the quasi-steady environment. This calculation was presented to the science teams in real-time during the mission.

The microgravity environment related to several different Orbiter, crew and experiment operations is presented and interpreted in this report. A radiator deploy, the Flight Control System checkout, and a vernier reaction control system reboost demonstration had minimal effects on the acceleration environment, with excitation of frequencies in the 0.01 to 10 Hz range. Flash Evaporator System venting had no noticeable effect on the environment while supply and waste water dumps caused excursions of $2x10^{-6}$ to $4x10^{-6}$ g in the Y_b and Z_b directions. Crew sleep and ergometer exercise periods can be clearly seen in the acceleration data, as expected. Accelerations related to the two Life Science Laboratory Equipment Refrigerator/Freezers were apparent in the data as are accelerations caused by the Johnson Space Center Projects Centrifuge. As on previous microgravity missions, several signals are present in the acceleration data for which a source has not been identified. The causes of these accelerations are under investigation.

Table of Contents

List of Tables

List of Figures

Abbreviations and Acronyms

$accel_{avg}$	root-sum-square of averaged acceleration triaxial data
$accel_{RMS}$	root-sum-square of RMS of acceleration triaxial data
AGHF	Advanced Gradient Heating Facility
APCF	Advanced Protein Crystallization Facility
APU	auxiliary power unit
ASTRE	Accelerometre Spatiale Triaxiale Electrostatique
BDPU	Bubble, Drop, and Particle Unit
EDT	Eastern Daylight Time
ESA/ESTEC	European Space Agency/European Space Research and Technology Center
FCS	Flight Control System
FES	Flash Evaporator System
g	acceleration due to gravity, 9.8 m/s^2
GMT	Greenwich Mean Time (day/hour:minute:second)
HRM	Spacelab High Rate Multiplexer
Hz	Hertz
JSC	NASA Johnson Space Center
k	number of time series intervals used in analysis
LeRC	NASA Lewis Research Center
LMS	The Life and Microgravity Spacelab
LSLE R/F	Life Sciences Laboratory Equipment Refrigerator/Freezer
LVLH	local vertical local horizontal
M	number of points in time series interval used in analysis
MAWS	Microgravity Analysis Workstation
MET	Mission Elapsed Time (day/hour:minute:second)
MEWS	Mission Evaluation Workstation System
MMA	Microgravity Measurement Assembly
MSP	Microgravity Sensor Packages
OARE	Orbital Acceleration Research Experiment
OMS	Orbital Maneuvering System
PIMS	Principal Investigator Microgravity Services
POCC	Payload Operations Control Center
PRCS	Primary Reaction Control System
PSD	Power Spectral Density
RCS	Reaction Control System
RMS	Root Mean Square
SAMS	Space Acceleration Measurement System
SIMO	simultaneous supply water and waste water
TBE	Teledyne Brown Engineering
TSH	Triaxial Sensor Head
VRCS	Vernier Reaction Control System
VV	velocity vector
X_o, Y_o, Z_o	Orbiter structural coordinate system axes
$X_{OARE}, Y_{OARE}, Z_{OARE}$	OARE coordinate system axes
X_b, Y_b, Z_b	Orbiter body coordinate system axes

Acknowledgments

Tim Reckart of Tal-Cut Company was responsible for the line drawings in and layout of this report. Nissim Lugasy, Tal-Cut Company, prepared computer software for the real-time acquisition and processing of OARE data during the STS-78 mission and for post mission processing of MMA data. The entire PIMS team provided acceleration environment interpretation during the mission. The European Space and Technology Center provided MMA data to the PIMS team.

Manny Avila of NASA Johnson Space Center provided information about the LSLE R/F. Alan Bachik of NASA Johnson Space Center provided information about the FCS Checkout. Aileen Gilbert and Beth Vann, with Teledyne Brown Engineering in Huntsville, Alabama, provided the as flown experiment timeline. Mel Buderer, Pat Kincade, Jim McAvin, and Ladonna Miller of NASA Johnson Space Center provided information about the JSC Project Centrifuge.

1. Introduction and Purpose

Microgravity science experiments are conducted on the NASA Space Shuttle Orbiters to take advantage of the reduced gravity environment resulting from the continuous free fall state of low earth orbit. Accelerometer systems are flown on the Orbiters to record the microgravity environment which is composed of quasi-steady accelerations and vibrations of the Orbiter, equipment, and local structures. The Life and Microgravity Spacelab (LMS) payload flew on the Orbiter Columbia on mission STS-78 from 20th June to 7th July 1996. The LMS payload on STS-78 was dedicated to life sciences and microgravity experiments. Two accelerometer systems managed by the NASA Lewis Research Center (LeRC) flew to support these experiments: the Orbital Acceleration Research Experiment (OARE) and the Space Acceleration Measurement System (SAMS). These accelerometers are sponsored by the NASA Microgravity Research Division. In addition, the Microgravity Measurement Assembly (MMA), designed by the European Space Research and Technology Center (ESA/ESTEC), and sponsored by NASA, collected acceleration data as part of the LMS mission. The Microgravity Analysis Workstation (MAWS), developed by Teledyne Brown Engineering (TBE) in Huntsville, Alabama, was used to calculate the quasi-steady environment of the Orbiter.

The Principal Investigator Microgravity Services (PIMS) project at the NASA Lewis Research Center supports principal investigators of microgravity experiments as they evaluate the effects of varying acceleration levels on their experiments. This report is provided by PIMS to furnish interested experiment investigators with a guide to evaluating the acceleration environment during STS-78. Section 2 of this report provides an overview of the STS-78 mission, payloads, and the experiments manifested on the payloads. Section 3 describes the coordinate systems used in this report. Section 4 describes the accelerometer systems flown on STS-78 and the means by which they recorded data and provided data to the user. Section 5 discusses specific analysis techniques applied to the accelerometer data. Section 6 discusses the microgravity environment of Columbia during STS-78 in relation to various activities which occurred during the mission. Appendix A describes how OARE, SAMS and MMA data can be accessed through the internet. Appendix B provides plots of SAMS data as an overview of the microgravity environment during the entire mission. Appendix C contains a user comment sheet. Users are encouraged to complete this form and return it to the authors.

2. Mission Overview

At 10:49:00 a.m. EDT on 20th June 1996 the Space Shuttle Columbia launched on the STS-78 mission from NASA Kennedy Space Center. Landing was at Kennedy Space Center on 7th July at 08:37:30 a.m. EDT. In terms of other time conventions used in this report, launch was at Greenwich Mean Time (GMT) 172/14:49:00 or mission elapsed time (MET) 000/00:00:00 and landing was at GMT 189/12:37:30 or MET 16/21:48:30. Both GMT and MET are recorded in day/hour:minute:second format. The primary objective of the STS-78 mission was to perform the science experiments that constituted the LMS payload. LMS experiments and facilities are listed in Table 1. As indicated, some facilities have multiple experiments and principal investigators. The payloads flown on STS-78 are listed in Table 2. The seven member crew followed a single-shift schedule, working 8 hours per day. They were both subjects for the life sciences experiments and researchers for the life and microgravity sciences experiments. The crew members are listed in Table 3.

3. Coordinate Systems

Three coordinate systems are discussed in this report: the Orbiter structural, Orbiter body, and OARE coordinate systems.

In the Orbiter structural coordinate system (X_O, Y_O, Z_O), the direction from nose to tail of the Orbiter is $+X_O$, the direction from port wing to starboard wing is $+Y_O$ and the direction from the Orbiter belly to the top of the Orbiter fuselage is $+Z_O$. This coordinate system is centered at the tip of the Orbiter external fuel tank, Figure 1. This coordinate system is usually used to specify the location of equipment within the Orbiter.

In the Orbiter body coordinate system (X_b, Y_b, Z_b), the direction from tail to nose of the Orbiter is $+X_b$, the direction from port wing to starboard wing is $+Y_b$ and the direction from the top of the fuselage to the Orbiter belly is $+Z_b$, Figure 2. This coordinate system is centered at the center of gravity of the Orbiter and is typically used as the navigational reference frame.

In the OARE coordinate system (X_{OARE}, Y_{OARE}, Z_{OARE}), the direction from tail to nose of the Orbiter is $+X_{OARE}$. The direction from the Orbiter belly to the top of the Orbiter fuselage is $+Y_{OARE}$ and the direction from port wing to starboard wing is $+Z_{OARE}$. The OARE coordinate system is centered at the OARE sensor proofmass centroid. A description of the OARE instrument is given in Section 4.

4. Accelerometer Systems and Related Studies

Three accelerometer systems measured the microgravity and vibration environment of the Orbiter Columbia during the STS-78 mission: the Orbital Acceleration Research Experiment, the Space Acceleration Measurement System and the Microgravity Measurement Assembly. One other investigation involving the Orbiter microgravity environment was performed as part of LMS, namely the real-time calculation of the quasi-steady environment of Columbia by the Microgravity Analysis Workstation.

4.1 Orbital Acceleration Research Experiment

The OARE was designed to measure quasi-steady accelerations from below $1x10^{-8}$g up to $2.5x10^{-3}$g. The OARE consists of an electrostatically suspended proof mass sensor, an in-flight calibration subsystem, and a microprocessor which is used for in-flight experiment control, processing, and storage of flight data [1-5]. The sensor output acceleration signal was filtered with a Bessel filter with a cutoff frequency of 1 Hz. The output signal was digitized at 10 samples per second and was processed and digitally filtered with an adaptive trimmean filter prior to electronic storage. Simultaneously, the unprocessed data were recorded on the Orbiter payload tape recorder and routed to the Spacelab High Rate Multiplexer (HRM). Using the HRM interface, the unprocessed OARE data were downlinked from the Orbiter to the PIMS Ground Support Equipment at the NASA Lewis Research Center Telescience Support Center. The PIMS team subsequently processed and displayed the OARE data for the LMS principal investigators on the World Wide Web.

The OARE was mounted to the floor of Columbia's cargo bay on a keel bridge, close to the Orbiter center of gravity. The location and orientation of the sensor with respect to the Orbiter structural coordinate system are given in Table 4 and Figure 3. In this report, OARE data are presented in Orbiter body coordinates. Additionally, the sign convention used is consistent with a frame of reference fixed to the Orbiter, meaning a forward thrust of the Orbiter is recorded as a negative X_b acceleration. OARE data are available from MET 000/00:10 through sensor saturation at 016/21:19. Appendix A describes how these data can be accessed through the internet.

4.2 Space Acceleration Measurement System

The SAMS was developed to measure the low-gravity environment of the Orbiters in support of microgravity science payloads. STS-78 was the fifteenth flight of a SAMS unit on an Orbiter. The SAMS unit on STS-78 was Unit D and consisted of three remote triaxial sensor heads (TSHs), connecting cables, and a controlling data acquisition unit with a digital data recording system using optical disks with 200 megabytes of storage capacity per side. This unit was located in Rack 7 of the Spacelab module. The locations of the SAMS unit and its sensor heads are shown in Figure 4. The signals from the three triaxial sensor heads were lowpass filtered with cutoff frequencies of 10 Hz (TSH A, located in Rack 8), 10 Hz (TSH B, located in Rack 3), and 25 Hz (TSH C, located in Rack 7). These signals were then sampled at 50, 50, and 125 samples per second, respectively, and the data were recorded on optical disks. In this report, the SAMS data are presented in terms of the Orbiter structural coordinate system. The SAMS data sign convention is such that when there is a forward thrust of the Orbiter it is recorded as a negative X_o acceleration. We refer to this convention as an inertial frame of reference fixed to a point in space. The locations of the SAMS heads with respect to the Orbiter structural coordinate system are given in Table 5. More detailed descriptions of the SAMS accelerometers are available in the literature [6-12].

For STS-78, 3.7 gigabytes of SAMS data are available between MET 000/06:09:27 and 015/22:11:41. Appendix A describes how these data can be accessed using the internet and how users can request that the PIMS team at LeRC make the data available to them on CD-ROM.

4.3 Microgravity Measurement Assembly

The MMA is a microgravity monitoring system capable of providing investigators and the crew with real-time display of acceleration detected by up to seven sensor heads. These sensor heads consist of up to six Microgravity Sensor Packages (MSP) and one Accelerometre Spatiale Triaxiale Electrostatique (ASTRE). Each of the MSPs are triaxial micromechanical sensors having dedicated analog-to-digital electronics. These sensors are capable of measuring disturbances in the 0.1 to 100 Hz range. The ASTRE is an electrostatically suspended proofmass sensor designed to measure quasi-steady disturbances at frequencies below 1 Hz. The ASTRE and one MSP reside within the MMA unit, and the remaining MSPs can be located remotely within the Spacelab module.

MMA without the ASTRE sensor flew on the Spacelab D-2 mission. For LMS, five of the possible seven sensor heads were used: four MSPs and one ASTRE. The ASTRE sensor and one of the MSP sensors were located within the MMA unit in Rack 3. The remaining three MSP sensor heads were located remotely at the BDPU (Rack 8), AGHF (Rack 3) and APCF (Rack 7) experiment sites within the Spacelab, Figure 4.

Following the launch of Columbia, MMA was activated at MET 000/03:45. Initially, no valid data were received from the ASTRE sensor due to saturation caused by adherence of the proofmass to its housing. The sensor was successfully knocked out of saturation by a crew member at MET 000/06:50. The ASTRE sensor data was noticed to be saturated as a result of the disturbances caused by the Torque Velocity Dynamometer at MET 000/07:35. The same recovery procedure was reapplied by a crew member at MET 000/08:04. An Operational Change Request was issued by the MMA team to apply this recovery procedure as needed throughout the mission. Other disturbances, such as intense crew activity, caused saturation of the ASTRE sensor. Post-mission analysis is being carried out by ESA/ESTEC to determine the cause of these saturations.

Throughout the LMS mission, data from the MMA sensors were continuously downlinked to ground via the HRM and the Experiment Computer Input/Output device. The HRM data were stored by the MMA Ground Station in the Marshall Space Flight Center Payload Operations Control Center and the MMA team displayed the data in both the time and frequency domains, using either real-time or playback data. Select MMA data plots were placed on the World Wide Web.

For STS-78, 30 gigabytes of MMA data are available between MET 000/03:44:57 and MET 015/22:11:05. Appendix A describes how select MMA data can be accessed using the internet.

4.4 Microgravity Analysis Workstation

The primary objectives of the MAWS were to provide real-time quasi-steady microgravity environment predictions to sensitive experiments and to provide guidance in how to optimize the quasi-steady acceleration environment. MAWS consisted of a PC-based system configured to acquire real-time Orbiter dynamics data. These data were used to calculate combined levels of aerodynamic drag, gravity gradient, and the Eulerian components of the Orbiter's quasi-steady acceleration environment. The calculation algorithms were extracted from a TBE six degree of freedom model.

MAWS successfully acquired and processed data for the entire mission. The numerical predictions from MAWS agreed well with the OARE-measured quasi-steady microgravity environment data. This was true for both local vertical/local horizontal and inertial attitudes. Notable differences between the two data sets were due to Orbiter venting operations which were not modelled by MAWS, and to OARE instrument drift. Regular OARE calibration operations consistently corrected for the drifts and returned the data sets to within a nominal $5x10^{-8}g$ difference. Some differences were also observed between the OARE data and the MAWS predictions for the Z_b-axis throughout the mission. The cause of this is still under investigation.

5. Accelerometer Data Analysis

The data recorded by SAMS on STS-78 were processed to correct for pre-mission bias calibration offsets and for temperature and gain related errors of bias, scale factor, and axis misalignment. The resulting units of acceleration are g's where 1 g = 9.8 m/s^2. The data were orthogonally transformed from the three SAMS TSH coordinate systems to the Orbiter structural coordinate system. The OARE data recorded during STS-78 and presented here have been compensated for temperature, bias, and scale factors. This processing is described in reference [5].

The MMA HRM data were recorded on CD-ROM by the Data Reduction group at MSFC. PIMS processed selected portions of the data using a conversion algorithm provided by the MMA team. The orientation of the MMA sensor axes with respect to the Spacelab axes was also provided. The calibration coefficients used to convert the MMA data into engineering values are similar to those used by the software on the MMA Ground Stations. These calibration coefficients take into account temperature change and offset detected during flight.

After this initial data correction phase, additional data analyses were applied to the SAMS, MMA, and OARE data to characterize the acceleration environment of the mission. Because of the quasi-steady nature of OARE and MMA ASTRE data versus the higher frequency character of SAMS and MMA MSP data, some data analysis techniques are more applicable to data from one system than the other. The particular processing technique used also depends on the type of information desired.

5.1 Time Domain Analysis

The time domain analysis techniques used in this report for SAMS and MMA data are acceleration versus time, interval average acceleration versus time, and interval root mean square (RMS) acceleration versus time. For OARE time domain analysis, plots of trimmean acceleration versus time and three-dimensional projections of the data are provided. The notation for all the data analysis discussed here is defined in the Abbreviations and Acronyms list.

SAMS Acceleration versus Time: These are plots of the acceleration in units of g versus time. Among the time domain plots displayed in this report, this one yields the most precise accounting of the variation of acceleration magnitude as a function of time.

SAMS Interval Average Acceleration versus Time: A plot of this quantity in units of g versus time gives an indication of net accelerations which last for a number of seconds equal to or greater than the interval parameter. The interval parameter used for STS-78 data analysis was ten seconds. Shorter duration, high amplitude accelerations can also be detected with this type of plot, however, the exact timing and magnitude of specific acceleration events cannot be extracted. The interval average acceleration for generic x-axis data is defined as

$$x_{avg_k} = \frac{1}{M}\sum_{i=1}^{M} x_{(k-1)M+i}$$

Corresponding expressions for y- and z-axis data can be combined with that for the x-axis to form the interval average acceleration vector magnitude as follows:

$$\text{accel}_{avg_k} = \sqrt{x^2_{avg_k} + y^2_{avg_k} + z^2_{avg_k}}.$$

SAMS Interval Root Mean Square Acceleration versus Time: A plot of this quantity in units of g_{RMS} versus time gives a measure of the energy in the acceleration signal due to purely oscillatory acceleration sources. Again, the interval parameter used for STS-78 data analysis was ten seconds. The interval RMS acceleration for generic x-axis data is defined as

$$x_{RMS_k} = \sqrt{\frac{1}{M}\sum_{i=1}^{M} \left(x_{(k-1)M+i}\right)^2}.$$

Corresponding expressions for y- and z-axis data can be combined with that from the x-axis to form the interval RMS acceleration vector magnitude as follows:

$$\text{accel}_{RMS_k} = \sqrt{x^2_{RMS_k} + y^2_{RMS_k} + z^2_{RMS_k}}.$$

OARE Trimmean Acceleration versus Time: A trimmean filter is applied to OARE data to reject transient, higher magnitude accelerations from analysis that is concerned with the quasi-steady environment. This filtering procedure ranks the collected data in order of increasing magnitude, measures the deviation of the distribution from a normal distribution, and deletes (trims) an adaptively determined amount of the data. The mean of the remaining data is calculated and this value is assigned to the initial time of the interval analyzed [5]. For this report the trimmean filter was applied to fifty seconds of OARE data every twenty-five seconds.

Three-dimensional Projection: This type of analysis results in a visualization of the acceleration vector alignment, projected onto three orthogonal planes, for example the top, front, and side view of the Orbiter. The time series is analyzed using a two-dimensional histogram method where the percentage of time the acceleration vector magnitude falls within a two-dimensional bin is plotted as a color. Areas showing colors toward the red end of the colorbar indicate a higher number of occurrences of the acceleration vector magnitude falling within that area. Conversely, areas showing colors toward the blue end are indicative of a lower number of occurrences. This type of plot provides overview information about the total time period analyzed. Exact timing of acceleration events cannot be extracted from this type of plot.

5.2 Frequency Domain Analysis

Transformation of data to the frequency domain is performed to gain more insight about the environment and to identify potential acceleration sources. The frequency domain analysis and displays used in this report are acceleration power spectral density (PSD) versus frequency and acceleration power spectral density versus frequency versus time (spectrogram). Frequency domain analysis of quasi-steady acceleration data is not often performed because of the relative lack of pertinent frequency information in the range of interest.

SAMS Power Spectral Density versus Frequency: Spectral analysis is performed on time series data to identify the relative magnitudes of sinusoidal signals that compose the series. The basis of this computation is the Fourier transform which indicates the magnitude of each frequency (sinusoid) present in the time history signal. The PSD is computed directly from the Fourier transform of a time series so that Parseval's Theorem is satisfied: the RMS of a time signal is equal to the square root of the integral of the PSD across the frequency band represented by the original signal. The PSD is reported in units of g^2/Hz.

Welch's Averaged Periodogram Method, or spectral averaging, is often used to produce PSDs that represent the average spectral content of a time period of interest. The PSD of k successive intervals is calculated and the k resulting spectral series are averaged together on a point by point basis.

SAMS Power Spectral Density versus Frequency versus Time (Spectrogram): Spectrograms provide a roadmap of how acceleration signals vary with respect to both time and frequency. As such, they are particularly useful in identifying when certain activities begin and end and to get a general feel for changes in the microgravity environment with time. To produce a spectrogram, PSDs are computed for successive intervals of time. The PSDs are oriented vertically on a page such that frequency increases from bottom to top. PSDs from successive time slices are aligned horizontally across the page such that time increases from left to right. Each time-frequency bin is imaged as a color corresponding to the logarithm of the PSD magnitude at that time and frequency. A color bar is included with each plot as a key to the color to $\log_{10}$(PSD) correspondence. To maximize the value of individual PIMS analyses, spectrogram color bars may vary among analyses and among mission reports. For ease of interpretation, however, within an appendix the color maps are kept constant unless otherwise noted.

6. Columbia Microgravity Environment – STS-78

The microgravity environment of the Space Shuttle Orbiters during missions, or parts of missions, dedicated to microgravity science is typically consistent. Different quasi-steady environment characteristics on different missions are related to Orbiter altitude, Orbiter attitude, and the time of the mission. The variation in atmospheric density with both altitude and date and the dimensions of the leading face of the Orbiter combine to create differences in the aerodynamic drag component of the quasi-steady acceleration environment. Different attitudes will also lead to different contributions to the Eulerian accelerations experienced on the Orbiters. For the typical altitude range of 140 to 160 nautical miles, the quasi-steady microgravity environment experienced within the Orbiters varies by about $2x10^{-6}g$ [13].

In the frequency range 0.01 Hz to 100 Hz, several microgravity disturbances are commonly seen in acceleration data collected on the Orbiters. Orbiter structural modes, while slightly different among the vehicles, are typically present at 0.43, 2.4, 3.5, 3.6, 4.7, 5.2, and 7.4 Hz [13-15]. In addition, the 17 Hz dither frequency of the Ku-band communications antenna is seen in acceleration data collected on all Orbiters. In the remainder of this section, we discuss the microgravity environment of Columbia as recorded by OARE, SAMS, and MMA during a variety of activities. The first five topics of discussion are Orbiter systems operations: a radiator deploy, a vernier reaction control system (VRCS) reboost demonstration, the flight control system (FCS) checkout procedure which occurs late in all missions, water venting operations, and effects of Orbiter attitudes.

The remaining topics are related to crew and experiment activities, some of which are common to numerous missions. The effects of having a single shift crew and having crew members exercise are discussed as is the effect of having a crew member working at an experiment rack. The disturbances caused by two experiment facilities, the Life Sciences Laboratory Equipment Refrigerator/Freezer and the JSC Projects Centrifuge, are presented. Finally, several characteristics of the acceleration data from as-yet-to-be-determined causes are discussed.

6.1 Radiator Deploy

The Orbiter has radiator panels attached to the underside (as seen when the doors are closed) of each payload bay door. The radiators are part of the Orbiter's Active Thermal Control System, used to reject heat generated on-board. While on orbit, these panels may remain next to the door or may be deployed away from the door at a nominal 33.5° angle in order to increase the amount of heat rejected from the cooling loops. Deployment of the radiators allows heat to be rejected on both sides thus increasing the total amount of rejected heat. In order to deploy each radiator, six motor driven latches must first be unlocked, and then the radiators are moved by a motor with a torque-tube-lever arrangement [16].

The STS-78 Space Shuttle Mission Report [17] lists the time of the port radiator deploy as MET 002/03:23:53. After examining the SAMS data around this time frame, it was concluded that the time listed in the book corresponds to the end of the radiator deploy operation. Three 25-second periods were chosen to correspond to times before, during, and after the deploy operations. PSDs were computed (using a boxcar window) from the SAMS TSH A data acquired, and the Root-Sum-of-Squares (RSS) of the three axes were plotted for these three periods in an overlapping fashion in Figure 5.

There are three primary differences among the PSDs for these three periods. The PSD for the during-deploy period shows the addition of a 6.30 Hz and a 9.47 Hz peak which do not appear in either the before deploy or after deploy periods. These two peaks may be related to the motor which drives the radiators away from the payload bay doors. The after deploy period shows the addition of a 3.37 Hz peak which does not appear in the before deploy spectrum.

6.2 VRCS Reboost Demonstration

During LMS, a detailed test objective called the Vernier Reaction Control System Reboost Demonstration was performed to demonstrate reboost capability for the Hubble Space Telescope on the upcoming STS-82 mission. The effects of plume impingement on the elevons were investigated and reboost capabilities were demonstrated by pitching the Orbiter back and forth using the VRCS jets F5L, F5R, L5D, and R5D [13].

During this test, the Orbiter was in a -XLV/-ZVV attitude while two pairs of VRCS jets (F5L/F5R and L5D/R5D) were alternately fired in a precise pattern to slightly raise the Orbiter's altitude. This pattern can be seen in Figure 6 where the forward (FWD) and AFT vernier jet firings are indicated by the top and bottom rows of "+" markers, respectively. As a result, the Orbiter was ratcheted to a higher altitude as is suggested by the pitch angle data plotted at the top of Figure 6. The acceleration vector magnitude during this test did not exceed 2.5×10^{-3}g, and was nominally below about 1×10^{-3}g, not much above the background acceleration environment. The power spectral density plots of Figure 7 add some insight into the impact of this activity on the acceleration environment. Figure 7 shows the acceleration spectra below 0.2 Hz from three different time frames for all three Orbiter structural axes, X_O, Y_O, and Z_O, from top to bottom. The left-most column of plots corresponds to a time frame (MET 015/19:12:00 to 015/19:17:28) which is just before the VRCS reboost. Plots in the center column were computed from accelerations measured during the test (MET 015/19:22:00 to 015/19:27:28) and the right-most column of plots corresponds to a time frame (MET 015/19:35:00 to 015/19:40:28) which occurred not long after completion of the test. Comparison of the "during" spectrum to both the "before" and "after" spectra reveals that the VRCS reboost excited the low frequency acceleration environment (below about 0.1 - 0.2 Hz) primarily on the X_O and Z_O axes. Most notably, a payload bay door natural frequency at 0.04 Hz was excited by this activity.

The plots shown in Figures 6 and 7 are from the SAMS TSH A measurements taken in Rack 8 of the Spacelab near the BDPU experiment. By comparison, Figure 8 shows measurements taken by the MSP BDPU sensor head of MMA (also mounted in Rack 8). As expected, SAMS and MMA data are corroborative for this event.

6.3 Flight Control System Checkout

Approximately one day before the scheduled re-entry, a two-part checkout procedure is performed to verify operations of the Flight Control System (FCS). The first part of this check-out is to use one of the three Auxiliary Power Units (APUs) to circulate hydraulic fluid in order to move the rudder, elevons, and ailerons of the Orbiter. For this mission, APU number 2 was used for this checkout procedure. As the APU is activated, it vents an exhaust gas in the $-Z_b$ direction. The result of this exhaust is similar in nature to a VRCS jet firing. The exhaust gas can range from nearly 0 to 30 pounds of force. The exhaust does not vent as a steady stream, but cycles at approximately 1 to 1.5 Hz.

Typically, Phase 1 of the FCS checkout lasts for 5-9 minutes. The SAMS data from STS-78 suggest that this FCS Phase 1 checkout lasted for approximately 5 minutes (MET 015/18:01 - MET 015/18:06). The effect of the FCS checkout on the microgravity environment was to cause impulse accelerations of roughly $5x10^{-3}g$ on the X_O-axis, with the Y_O- and Z_O- axes acceleration spikes reaching above the $1x10^{-2}g$ level, Figure 9. After a spike, the accelerometer data showed a damping behavior. Impulse relaxation time appears to be roughly 4 seconds. The SAMS data do not show an excitation in the 1 to 1.5 Hz region, but this could be due to an increase in broad-band noise having masked this region of the spectrum. The impulsive transients which occur roughly every 20 seconds during the checkout procedure are the cause of the increased PSD noise floor. Phase 2 of the FCS checkout procedure tests the electronics and command channels and should not cause measurable disturbances to the microgravity environment. No disturbances to the microgravity environment were attributed to the FCS Phase 2 operations.

6.4 Venting Operations

The Orbiter Food, Water, and Waste Management Subsystem provides storage and dumping capabilities for potable and waste water [16]. Supply and waste water dumps are performed using nozzles on the port side of the Orbiter. Water dumps from these nozzles are expected to cause a steady acceleration of about $4.0x10^{-7}g$ in the Y_b-axis [18]. Figures 10 and 11 show a simultaneous supply water/waste water

dump and a supply water dump. These water dump plots show contributions to the Y_b-axis and, unexpectedly, to the Z_b-axis. The explanation for these Z_b-axis contributions is unknown at this time.

Another venting system, the Flash Evaporator System (FES), is a component of the Orbiter Active Thermal Control System. The flash evaporators are located in the aft fuselage of the Orbiter. There are two evaporators in the FES: the high-load evaporator and the topping evaporator. The topping evaporator vents steam equally to the left and right sides of the Orbiter, and is non-propulsive. The topping evaporator is used on orbit because of this feature. In addition to serving its normal Active Thermal Control System functions, the FES topping evaporator can be used to dump excess potable water from the potable water storage tanks. Examination of the OARE data during known FES operations for both thermal control and water dump periods confirms the non-propulsive nature of the FES. That is, no discernible effects of FES operations were seen in the OARE data for this mission.

6.5 Orbiter Attitude

A summary plot of the OARE data for the entire LMS mission is provided in Figure 12. Two facts regarding the LMS mission offer assistance in explaining the summary plot. The first fact is that the LMS mission was operated in a single shift environment. This manifests itself in Figure 12 as the quiet periods which occur on a daily basis. The excursions in the data in the non-quiet periods are the result of crew and Orbiter activity. The second fact is that the LMS mission was flown predominantly in two attitudes: -XLV/+ZVV and -ZLV/-XVV. This is most apparent in the X_b-axis data during the sleep periods (see Figure 12). The nominal microaccelerations observed for the X_b-axis during these quiet periods consist of two levels. The two levels observed result from the different rotational and gravity gradient effects imparted on the X_b-axis data for the two attitudes flown. Similar, less obvious level changes are observable in the Z_b-axis data as well.

Figure 13 is a 3-dimensional projection plot of the trimmean filtered OARE data recorded throughout the entire mission. The two concentrations of data in the X_b- vs. Z_b-axis and X_b- vs. Y_b-axis plots clearly illustrate the different quasi-steady acceleration vectors during the two primary LMS attitudes. Figure 14 shows eight hours of TMF OARE data from the -ZLV/-XVV attitude, and Figure 15 shows eight hours of TMF OARE data from the -XLV/+ZVV attitude. Both of these eight hour periods include a crew sleep cycle which clearly illustrates the atmospheric drag contributions (see the X_b-axis data for the -ZLV/-XVV attitude, and the Z_b-axis data for the -XLV/+ZVV attitude) to the quasi-steady acceleration environment.

6.6 Crew Sleep

Various characteristics of the microgravity environment can be discerned by using SAMS or MMA MSP data. Figure 16 shows a color spectrogram of a 24-hour period of SAMS TSH C data. Figure 17 is a color spectrogram of MMA MSP APCF data collected in Spacelab Rack 7. These plots show significant quieting of the microgravity environment between MET 003/12 and 003/18, due to a crew sleep period. Although the crew sleep time is more than six hours in duration, we assume that the entire crew does not fall asleep simultaneously.

Notice that the primary quieting is in the lower frequency (under 5 Hz) regime. In fact, due to the diminished crew and equipment activity, the structural modes quiet as well. Table 6 shows an analysis of the structural modes during a crew wake period (MET 003/03 - 003/04) and a crew sleep period (MET 003/14 - 003/15). This analysis was performed using SAMS TSH C data.

In addition to the quieting behavior noticed at each of the structural modes, it is possible (due to the overall quieting) that certain modes will be evident in the data collected during the sleep period that were not evident in the data during the awake period. This is true of the 8.35 Hz peak shown in Table 6.

Another signal that becomes more evident during the crew sleep period is the unidentified sinusoidal signal around 12.3 Hz. Some disturbances are not affected by crew sleep, such as the 17 Hz Ku-band communications antenna dither, and the activity in the 21 - 23.5 Hz region which is related to the Life Sciences Laboratory Equipment Refrigerator/Freezer.

6.7 Ergometer Exercise

During this mission, ergometer exercise was performed in both the Spacelab module and on the flight deck. The Ergometer III is a next-generation cycle ergometer, first flown on Shuttle-Mir mission STS-71 in June 1995. This ergometer was also used for JSC Projects experiments. It provided investigators with quantitative measurements of the stress induced by exercise. The Ergometer III is a horizontal cycle. Wearing a lap belt, the subject sits in a recumbent position, with legs pedaling roughly parallel to the floor. To create and maintain a constant workload, the ergometer has a large, weighted flywheel surrounded by a braking band to resist the subject's pedaling.

The frequency domain signature of ergometer exercise is typically easy to identify in the acceleration data. Energy from this type of exercise is concentrated primarily in two spectral peaks at about 2.5 Hz and 1.25 Hz. For the Spacelab-mounted ergometers on past missions the wheel was aligned with the Orbiter structural XZ-plane, thus leading us to expect the pedaling motion to induce a prominent (and fairly constant) 2 to 3 Hz disturbance, principally in the X_O- and Z_O-axes. Figure 18 suggests that this disturbance was felt on all three axes on LMS, most notably the Y_O- and Z_O-axes. While pedaling on the ergometer, crew members tend to rock their shoulders back and forth perpendicular to the pedaling plane at half the pedaling frequency. For the Spacelab-mounted ergometer, this shows up as a disturbance primarily in the Y_O-axis as is evidenced by the middle plot of Figure 18. Later in the mission, this signature changes somewhat as seen in Figure 19. In particular, the rocking frequency seen earlier on the Y_O-axis is missing. This leads us to speculate that this exercise was being performed in a different location, probably the flight deck, and possibly with the ergometer in a different orientation.

6.8 Rack Excitation

During BDPU experiment operations, it became necessary for payload specialist Jean-Jacques Favier to close the front-panel of the BDPU experiment module in Rack 8 of the Spacelab. Downlink video from the Spacelab showed that it took considerable force by Favier to move this front-panel in the $+Z_O$ direction. Acceleration data from SAMS TSH A, which was mounted in the BDPU Rack, is shown in Figure 20 for the time frame of interest. As seen, the transitory disturbance induced by this action is prevalent on the Y_O- and Z_O-axes. Figure 21 shows that the acceleration vector magnitude during this closure operation peaked at about $3x10^{-3}g$.

6.9 Life Sciences Laboratory Equipment Refrigerator/Freezer

Flown in Rack 9 of the Spacelab module, the JSC Life Sciences Laboratory Equipment Refrigerator/Freezer (LSLE R/F) was used to protect perishable biological specimens, such as blood samples. Two LSLE R/F units were flown side-by-side in Rack 9 and each could be independently controlled to hold a temperature in the -22°C to +10°C range. The LSLE R/F operates using a vapor compression freon engine.

PIMS believes the two acceleration signals around 22.00 and 23.07 Hz to be primary frequencies of the two LSLE R/F units. The cause for the difference in appearance between the two signals in Figure 22 is currently unknown. However, at MET 012/15:00 (see Figure 100 in Appendix B), the more chaotic of the two signals enters a 2.5 hour period of constant-on, and by MET 012/20:00 the two signals appear more similar in the spectrogram plots. Preliminary information indicates that one of the units was switched from refrigerate to freeze mode around the MET 012/15:00 time frame. Harmonics of the fundamental frequencies of 22.00 and 23.07 Hz are seen at approximately 44 and 46 Hz.

In addition to these harmonics, signal aliasing is believed to be present. This conclusion is supported by the presence of the non-harmonic signals at 47.01 and 48.09 Hz, as well as the inverse (or mirrored) signals at 1.84, 2.82, 51.99, and 52.86 Hz. Signal aliasing is a phenomenon caused during the analog-to-digital signal conversion process, and occurs when signals above the Nyquist frequency are present. The Nyquist frequency is equal to half the sampling rate. For the SAMS TSH C data, the Nyquist frequency is 62.5 Hz. Normally, the SAMS lowpass filter (-140 $^{dB}/_{decade}$) is sufficient to suppress signals above the Nyquist frequency, however the accelerations caused by the LSLE R/F units may appear particularly loud due to the close proximity of the LSLE R/F units (Rack 9) and the SAMS TSH C (Rack 7).

In addition to the signals, harmonics, and aliases discussed above, there is another signal which is also believed to be related to LSLE R/F activity. This third signal appears at 23.61 Hz, with a harmonic at 47.00 Hz, and aliases at 48.64 and 51.34 Hz.

6.10 JSC Projects Centrifuge

As an integral part of life science studies on this mission, blood samples were periodically collected from crewmembers. A centrifuge mounted in Rack 12 of the Spacelab module was then used to process these samples before they were frozen for postflight analysis. The centrifuge had a rotational rate of 2387 rpm (39.8 Hz) and was operated for 15 minutes at a time throughout the mission. As shown in Figure 23, centrifuge startup was marked by an exponential rise and slight overshoot in frequency, while shutdown shows an exponential decay from the steady state. Furthermore, there are at least two other lower frequency disturbances at 15.7 and 24.1 Hz which exhibit similar startup and shutdown characteristics and are concurrent with centrifuge operation. Data from SAMS TSH C were used to generate Figure 23. This sensor had a cutoff frequency of 25 Hz which accounts for the quieting at higher frequencies. By comparison, Figures 24 and 25 were generated from data recorded by MMA sensors MSP APCF and MSP BDPU which were located in Racks 7 and 8, respectively. Both of these

measurements were made with a cutoff frequency of 100 Hz. As expected from sensor proximity, the spectrogram magnitudes shown in Figures 23 and 24 match quite closely up through 25 Hz, but diverge at higher frequencies because of the different filter cutoffs. The only notable exception to this similarity is the signal seen at around 2.5 Hz near the beginning and end of the time frame covered in the SAMS data. This is an alias of the LSLE R/F 22 Hz disturbance.

6.11 Unidentified Disturbances

During the mission, the BDPU team noted unexpected oscillations in their downlink video images at MET 008/11:38. In an attempt to identify the source of these oscillations post-mission, the time history plot shown in Figure 26 was generated from SAMS TSH A data. The acceleration data leading up to this time and shortly thereafter (from about MET 008/11:12 to about MET 008/11:40) is of particular interest. During this period, there were a considerable number of impulsive disturbances primarily aligned with the Y_o-axis. These disturbances were not localized to Rack 8 of the Spacelab, because they appear in the acceleration data on the other two SAMS sensor heads, as well as in MMA MSP BDPU data as shown in Figure 27. Furthermore, these disturbances were observed intermittently throughout the mission during crew sleep periods. The source of these disturbances remains unknown.

While analyzing the SAMS data, a number of recurrent unidentified peaks have been identified by an analysis of the spectrogram plots shown in Appendix B. The peaks are at 15.79 Hz, 19.86 Hz, and 29.96 Hz. The first and last of these signals (15.79 Hz, 29.96 Hz) turn-on early in the SAMS data and remain on throughout the duration of recorded SAMS data. The middle signal (19.86 Hz) is on throughout the entire period of recorded SAMS data. The sources of these signals is under investigation.

7. Summary

The microgravity environment of the Space Shuttle Columbia was measured during the STS-78 mission using accelerometers from three different instruments: the Orbital Acceleration Research Experiment, the Space Acceleration Measurement System and the Microgravity Measurement Assembly. The quasi-steady environment was also calculated in near real-time during the mission by the Microgravity Analysis Workstation.

The OARE provided investigators with real-time quasi-steady acceleration measurements. The SAMS recorded higher frequency data on-board for post-mission analysis. The MMA provided investigators with real-time quasi-steady and higher frequency acceleration measurements. The MAWS provided calculation of the quasi-steady environment. This calculation was presented to the science teams in real-time during the mission. The SAMS data and the MMA MSP sensor data compare well for the times studied. The MAWS predictions of the quasi-steady environment compared well with the recorded OARE data. No detailed comparisons have yet been made for the OARE and MMA quasi-steady, ASTRE sensor data.

The microgravity environment related to several different Orbiter, crew and experiment operations is presented and interpreted in this report. A radiator deploy, the Flight Control System checkout, and the vernier reaction control system reboost demonstration had minimal effects on the acceleration environment. Frequency components at 6.3 and 9.47 Hz were present in the SAMS data during the port radiator deploy. These frequencies may be related to the motor which drives the radiators away from the payload bay doors. During the FCS checkout period, regular impulse accelerations of about $5x10^{-3}$ to $10x10^{-3}$g were evident in the SAMS data. This activity occurred late in the mission, so it should not have disturbed any sensitive experiments. Flash Evaporator System venting had no noticeable effect on the environment while supply and waste water dumps caused excursions of $2x10^{-6}$ to $4x10^{-6}$g in the Y_b and Z_b directions. Crew sleep and ergometer exercise periods can be clearly seen in the acceleration data, as expected. Accelerations related to the two Life Science Laboratory Equipment Refrigerator/Freezers were apparent in the data with fundamental frequencies of 22 and 23 Hz. These signals showed different characteristics than on previous missions. The cause for the differences is being investigated. Accelerations caused by the Johnson Space Center Projects Centrifuge were evident at about 40 Hz. Disturbances at 15.7 and 24 Hz appear to be temporally related. As on previous microgravity missions, several signals are present in the acceleration data for which a source has not been identified (15.79, 19.86, 29.96 Hz). The causes of these accelerations are under investigation.

8. References

[1] R.C. Blanchard, M.K. Hendrix, J.C. Fox, D.J. Thomas and Y.J. Nicholson, Orbital Research Experiment. J. Spacecraft and Rockets, Vol. 24, No. 6, (1987) 504-511.

[2] R.C. Blanchard, J.Y. Nicholson and J.R. Ritter, STS-40 Orbital AccelerationResearch Experiment Flight Results During a Typical Sleep Period. NASA Technical Memorandum 104209, January 1992.

[3] R.C. Blanchard, J.Y. Nicholson, J.R. Ritter, Preliminary OARE Absolute Acceleration Measure ments on STS-50. NASA Technical Memorandum 107724, February 1993.

[4] R.C. Blanchard, J.Y. Nicholson, J.R. Ritter and K.T. Larman, OARE Flight Maneuvers and Calibration Measurements on STS-58. NASA Technical Memorandum 109093, April 1994.

[5] Canopus Systems, Inc.,OARE Technical Report #149, STS-78 (LMS-1) Final Report. CSI-9604, September 1996.

[6] R. DeLombard, B.D. Finley, Space Acceleration Measurement System, Description and Opera tions on the First Spacelab Life Sciences Mission. NASA Technical Memorandum 105301, November 1991.

[7] R. DeLombard, B.D. Finley and C.R. Baugher, Development of and Flight Results from the Space Acceleration Measurement System (SAMS). NASA Technical Memorandum 105652, January 1992.

[8] C.R. Baugher, G.L. Martin and R. DeLombard, Low-Frequency Vibration Environment for Five Shuttle Missions, NASA Technical Memorandum 106059, March 1993.

[9] M.J.B. Rogers, C.R. Baugher, R.C. Blanchard, R. DeLombard, W.W. Durgin, D.H. Matthiesen, W. Neupert and P. Roussel, A Comparison of Low-Gravity Measurements Onboard Columbia During STS-40. Microgravity Science and Technology VI/3 (1993), 207-216.

[10] B.D. Finley, C. Grodsinsky and R. DeLombard, Summary Report of Mission Acceleration Measurements for SPACEHAB-01, STS-57. NASA Technical Memorandum 106514, March 1994.

[11] M.J.B. Rogers and R. Delombard, Summary Report of Mission Acceleration Measurements for STS-62. NASA Technical Memorandum 106773, November 1994.

[12] M.J.B. Rogers and R. DeLombard, Summary Report of Mission Acceleration Measurements for STS-65. NASA Technical Memorandum 106871, March 1995.

[13] R. DeLombard, Compendium of information for interpreting the microgravity environment of the orbiter spacecraft, NASA Technical Memorandum 107032, August 1996.

[14] C. Cooke, M. Koenig, J. Lepanto, G. Levine, J. Miller, D. Sargent, and R. Schlundt, SDI Space Shuttle Based Experiments for Acquisition, Tracking, and Pointing - Definition of Space Shuttle Operational Environment, The Charles Stark Draper Laboratory, Cambridge, Massachusetts, R-1868, 1986.

[15] M. J. B. Rogers, and J. I. D. Alexander, Data Analysis for Spacelab Missions. Microgravity Science and Technology V/1 (1992).

[16] Shuttle Operational Data Book, Volume 1, JSC-08934, Rev. E, Johnson Space Center, Houston, TX, January 1988.

[17] STS-78 Space Shuttle Mission Report, NSTS-37409, August 1996.

[18] M. J. B. Rogers, B. P. Matisak, and J. I. D. Alexander, Venting Force Contributions-Quasi-steady accelerations on STS-50. Microgravity Science and Technology VII/4 (1995) 293-295

Table 1. LMS Experiments and Facilities

Experiments and Facilities	*Location*	*Contact*	*Affiliation*
J. S. C. Project, 13 experiments	Spacelab	Ladonna Miller	NASA Johnson Space Center, Houston, TX
Space Tissue Loss Configuration B	Middeck	Alex Pranger	NASA Ames Research Center, Moffet Field, CA
Animal Enclosure Module	Middeck	Randall Berthold	NASA Ames Research Center, Moffet Field, CA
Plant Growth Facility	Middeck	Debbie Vordermark	NASA Kennedy Space Center, Cape Canaveral, FL
Bubble, Drop, and Particle Unit (BDPU), 6 experiments	Spacelab	Pasquale DiPalermo	European Space Agency Noordwijk, The Netherlands
Space Acceleration Measurement System	Spacelab	Ronald Sicker	NASA Lewis Research Center Cleveland, Ohio
Microgravity Measurement Assembly	Spacelab	Maurizio Nati	European Space Agency Noordwijk, The Netherlands
Advanced Gradient Heating Facility (AGHF), 6 experiments	Spacelab	Claus Alfermann	European Space Agency Noordwijk, The Netherlands
Advanced Protein Crystallization Facility (APCF), 12 experiments	Spacelab	Klaus Fuhrmann	European Space Agency Noordwijk, The Netherlands

Table 2. STS-78 Payloads

Payloads	*Location*	*Contact*	*Affiliation*
LMS	Cargo Bay	J. Patton Downey	NASA Marshall Space Flight Center, Huntsville, AL
Orbital Acceleration Research Experiment	Keel Bridge	William Wagar	NASA Lewis Research Center, Cleveland, OH

Table 3. STS-78 Crew

Crewmember	*Position*
Terence T. "Tom" Henricks	Commander
Kevin R. Kregel	Pilot
Susan J. Helms	LMS Payload Commander, Mission Specialist 2
Richard M. Linnehan, D.V.M.	Mission Specialist 1
Charles E. Brady, Jr., M.D.	Mission Specialist 3
Robert B. Thirsk, M.D.	Payload Specilalist 2
Jean-Jaques Favier, Ph.D.	Payload Specialist 1
Pedro Duque	Alternate Payload Specialist
Luca Urbani, M.D.	Alternate Payload Specialist

Table 4. STS-78 OARE Head Location and Orientation

Sensor Head	*Serial Number, Frequency*	*Sample Rate (samples/sec)*	*Location*	*Location of CG of Sensor Head*
OARE Sensor	0 to 1 Hz	10	Orbiter Cargo Bay Keel Bridge	X_O= 1153.3 in Y_O= -1.3 in Z_O= 317.8 in

Table 5. STS-78 SAMS Head Location and Orientation

Sensor Head	*Serial Number, Frequency*	*Sample Rate (samples/sec)*	*Location*	*Location of CG of Sensor Head*
TSH A	821-36 10 Hz	50	Rack 8 (behind front panel)	X_0= 1041.12 in. Y_0= 32.41 in. Z_0= 442.68 in.
TSH B	821-39 10 Hz	50	Rack 3 (behind front panel)	X_0= 984.03 in. Y_0= -40.27 in. Z_0= 432.15 in.
TSH C	821-40 25 Hz	125	Rack 7 (behind SAMS)	X_0= 1049.85 in. Y_0= -69.59 in. Z_0= 390.01 in.

Table 6. Comparison of structural modes during crew wake and crew sleep

Peak Frequency (Hz)	μg_{RMS} *during awake period*	μg_{RMS} *during sleep period*
3.69	18.67	5.27
4.66	66.58	18.35
5.65	51.99	7.32
6.20	25.37	4.37
7.15	41.76	6.98
7.63	38.00	4.74
8.35	not observed	3.70
8.99	37.65	5.23

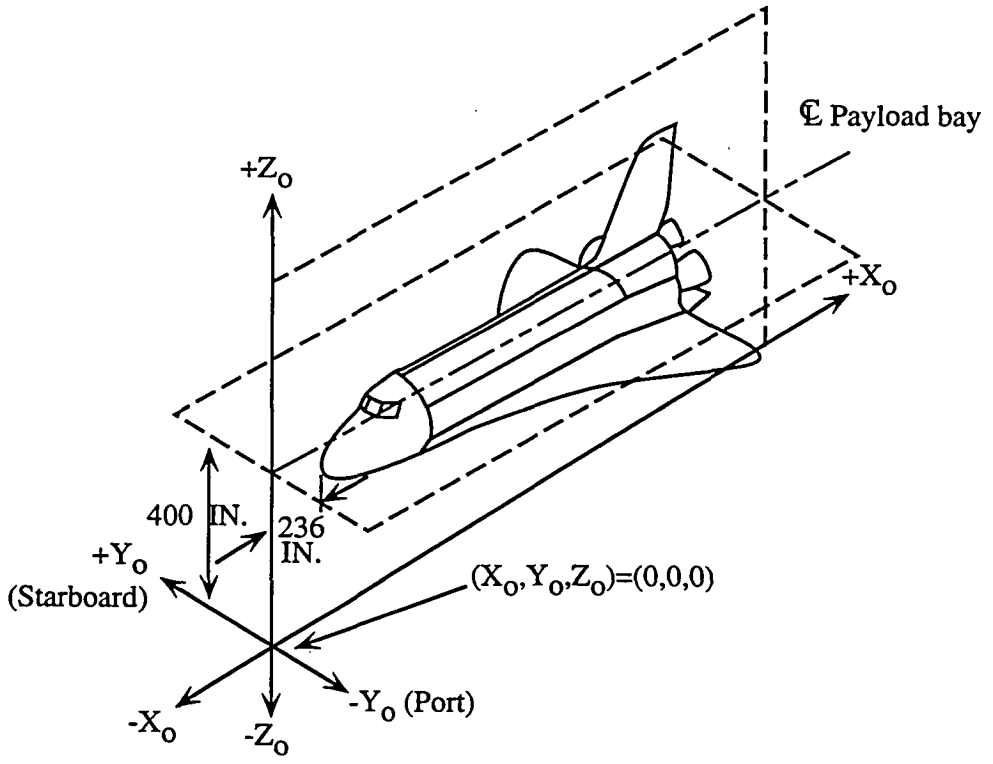

Figure 1. Orbiter structural coordinate system.

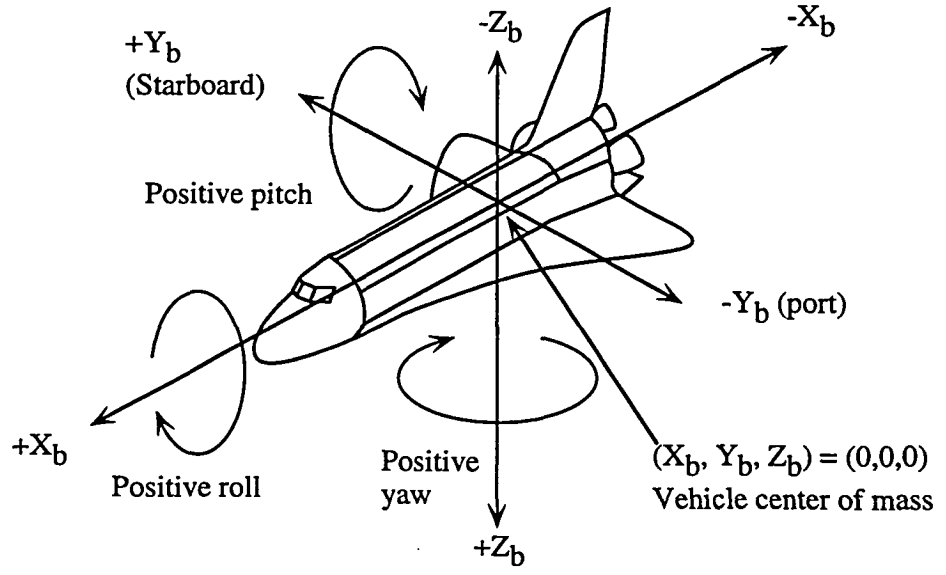

Figure 2. Orbiter body coordinate system.

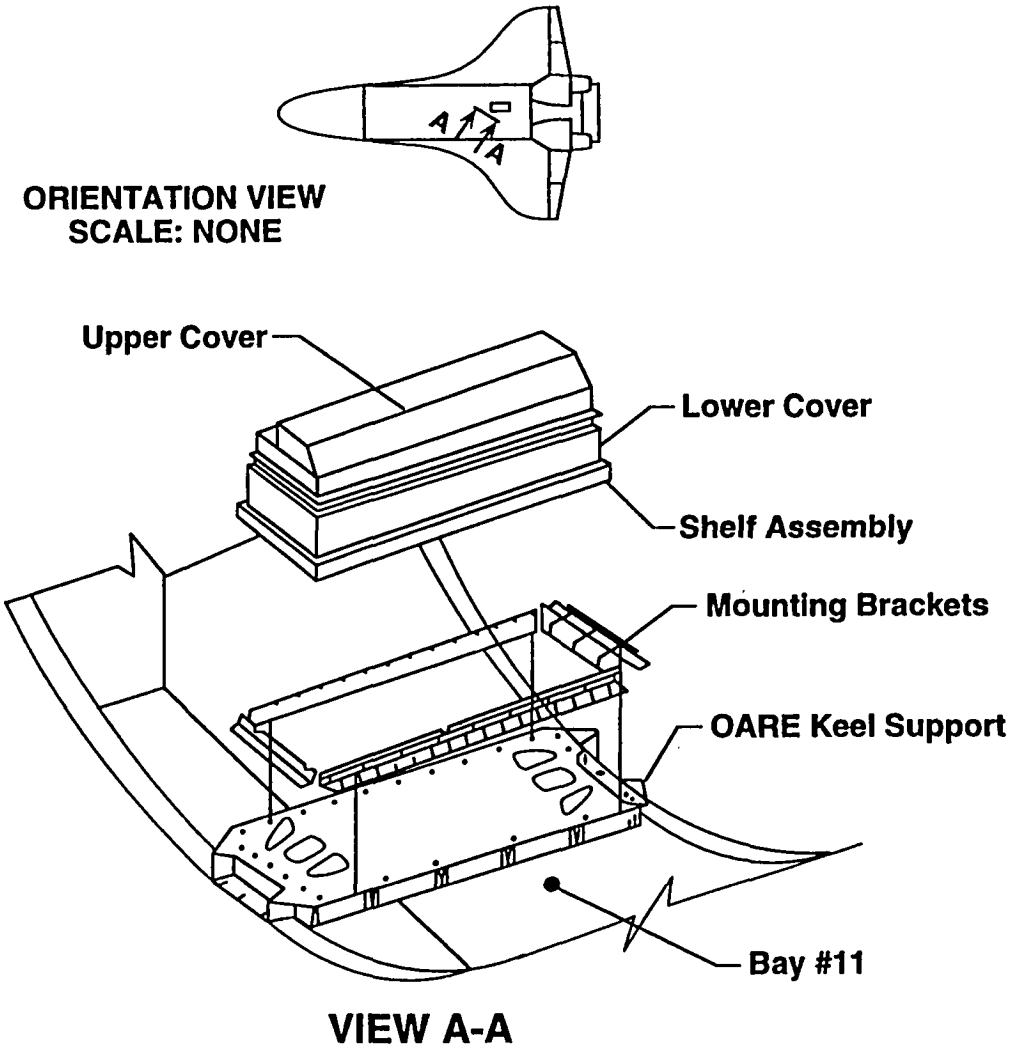

Figure 3. OARE instrument location on STS-78.

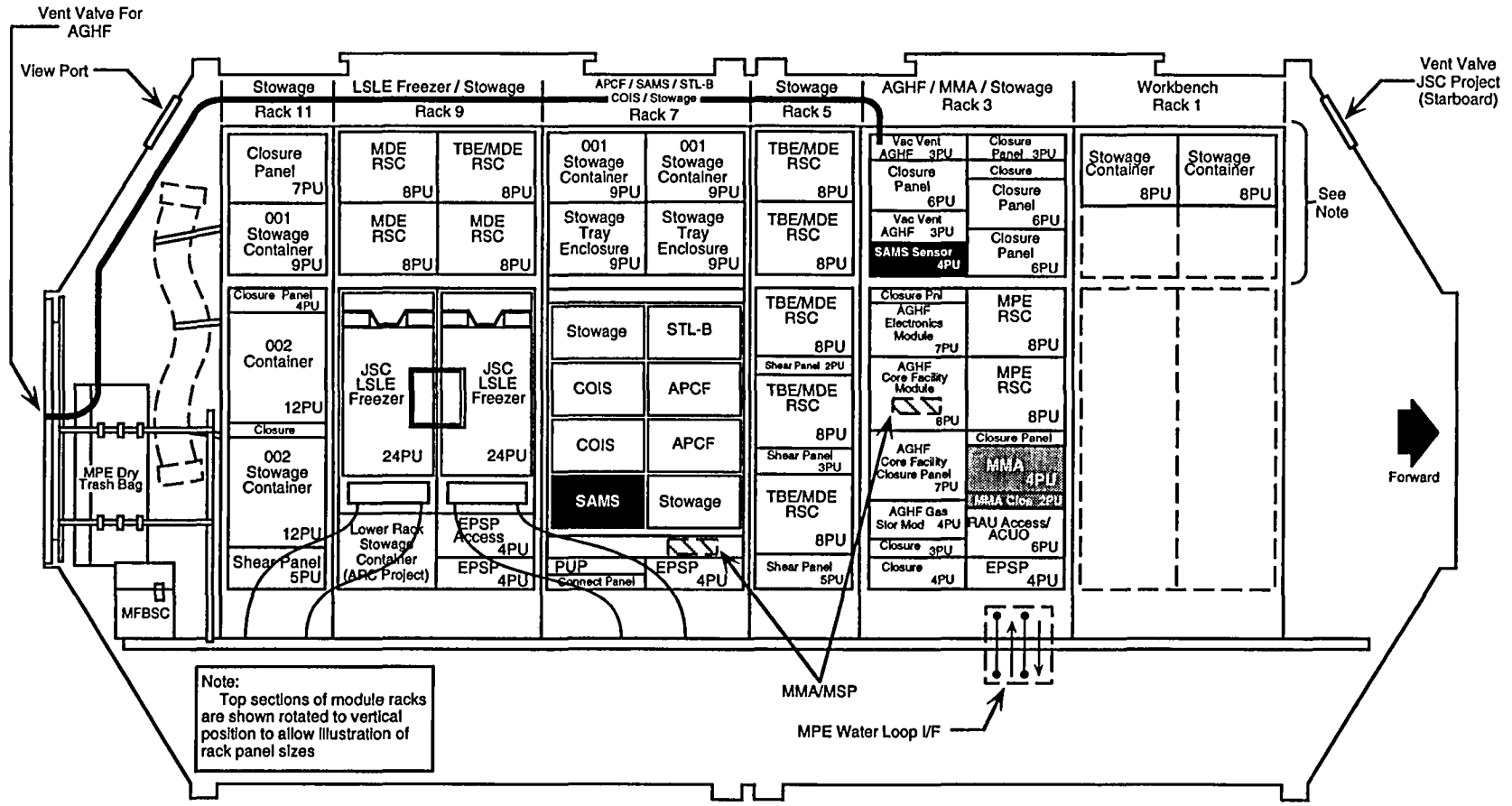

Figure 4a. Approximate location of SAMS and MMA sensors on STS-78, Spacelab port side.

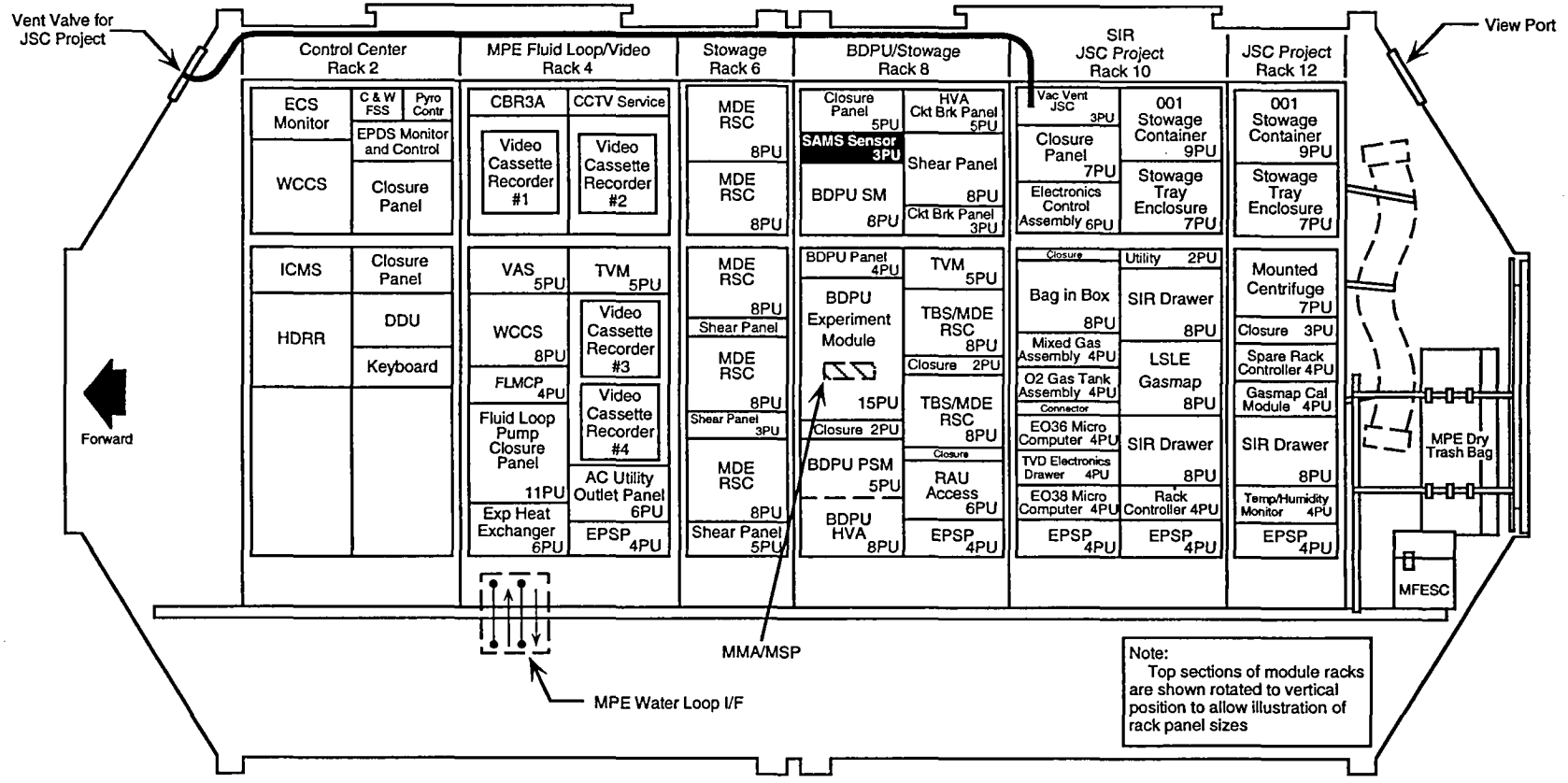

Figure 4b. Approximate location of SAMS and MMA sensors on STS-78, Spacelab starboard side.

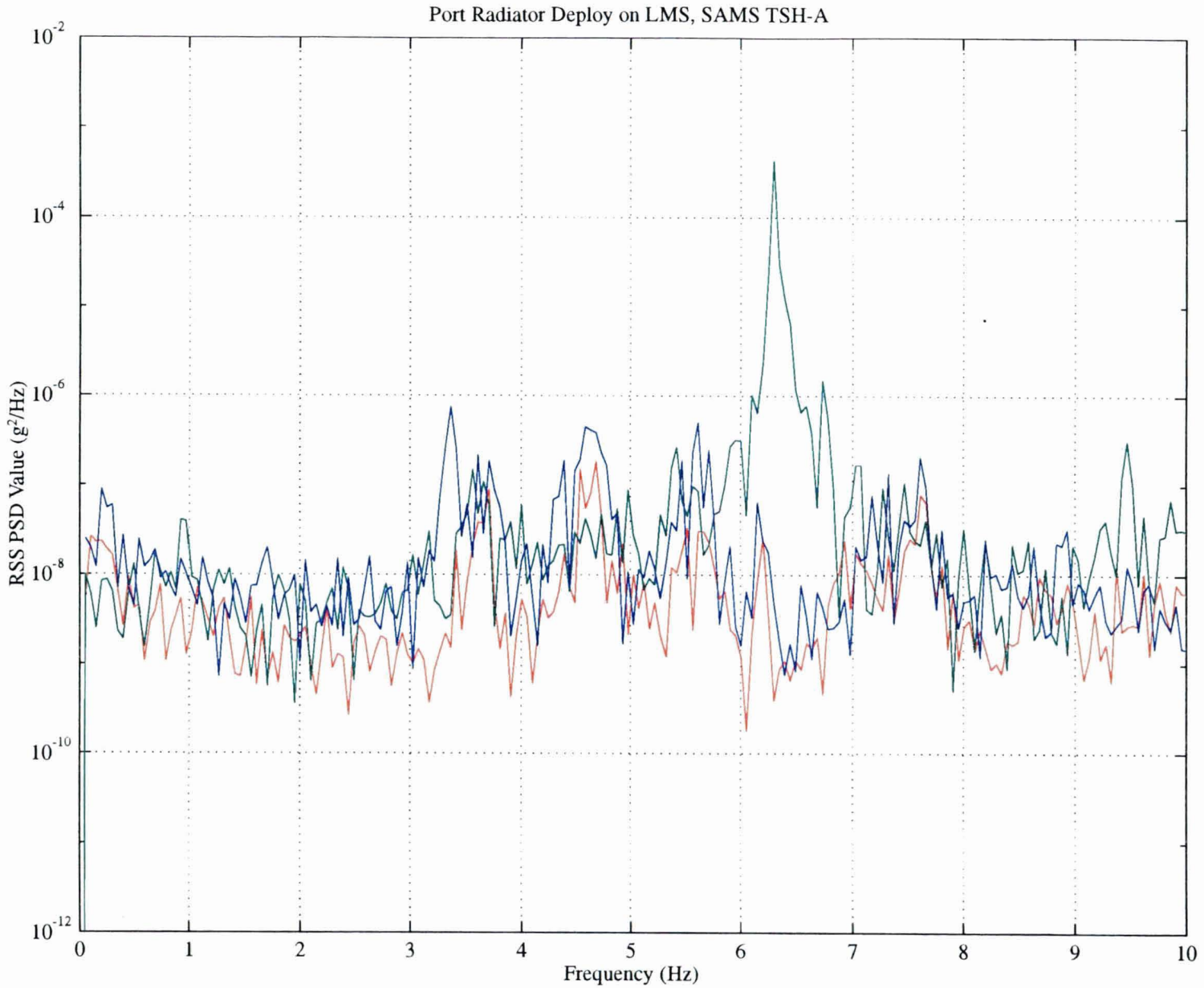

Figure 5. SAMS TSH A data PSDs for periods before, during, and after port radiator deploy. Note differences at 3.37, 6.30, and 9.47 Hz. Red: Radiator next to door, Green: during Deploy Operation, Blue: Radiator deployed away from door.

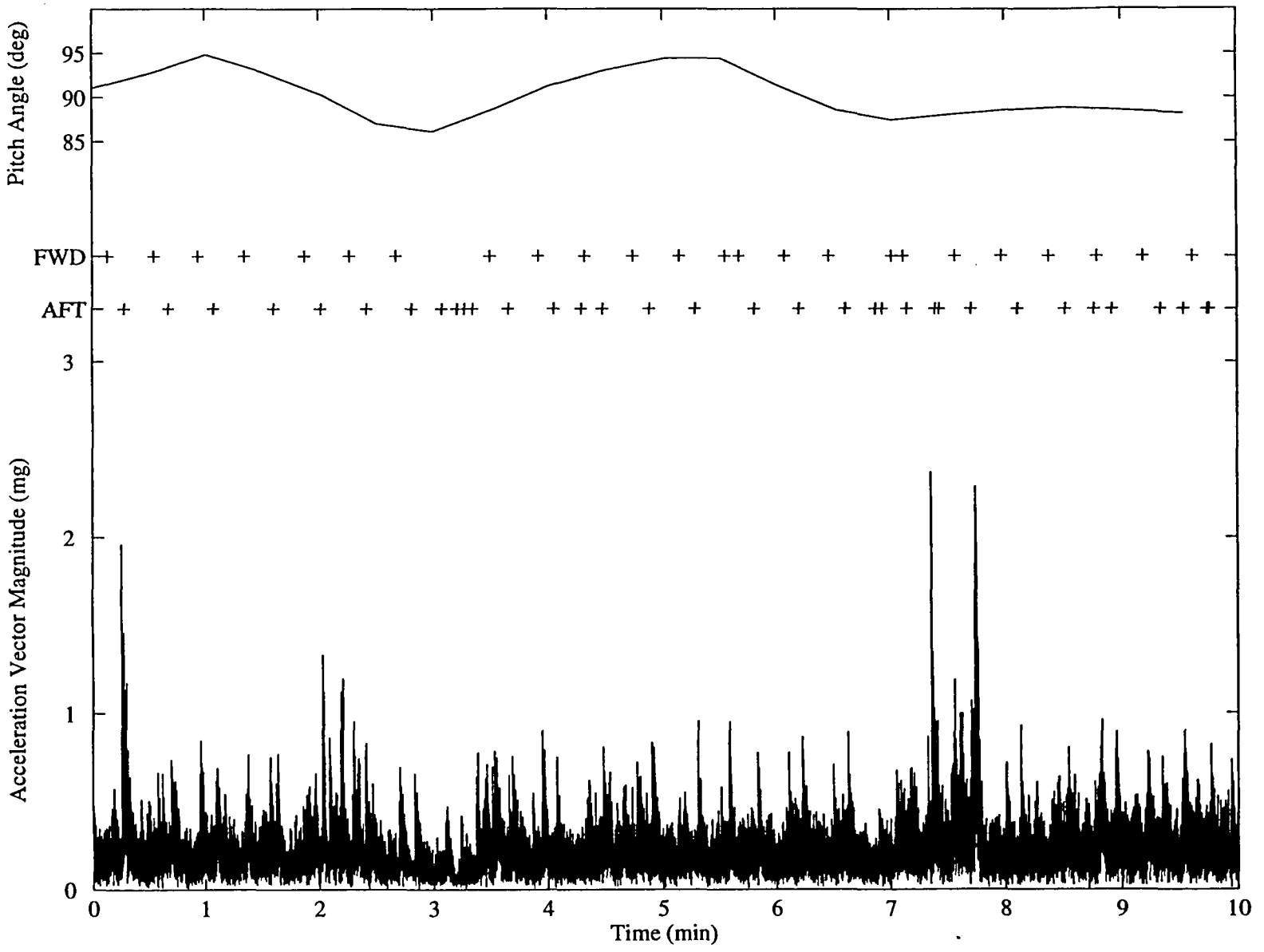

Figure 6. SAMS TSH A data for VRCS Reboost Demonstration. Also indicated are the firing events for two pairs of VRCS jets (FWD and AFT) and the Orbiter pitch angle for this period.

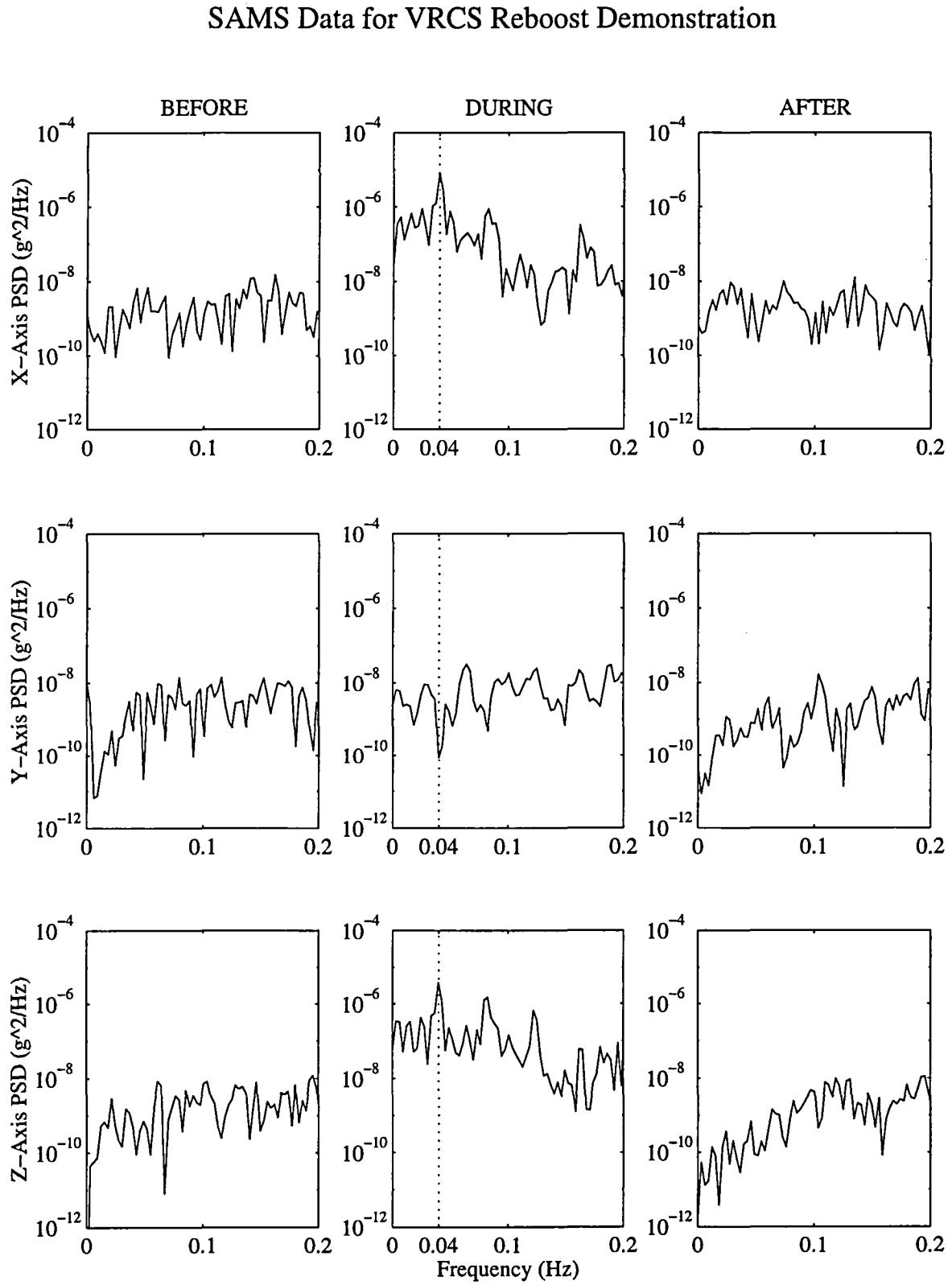

Figure 7. SAMS TSH A data PSDs before, during, and after the VRCS Reboost Demonstration. Note excitation at 0.04 Hz (dotted line) during the test

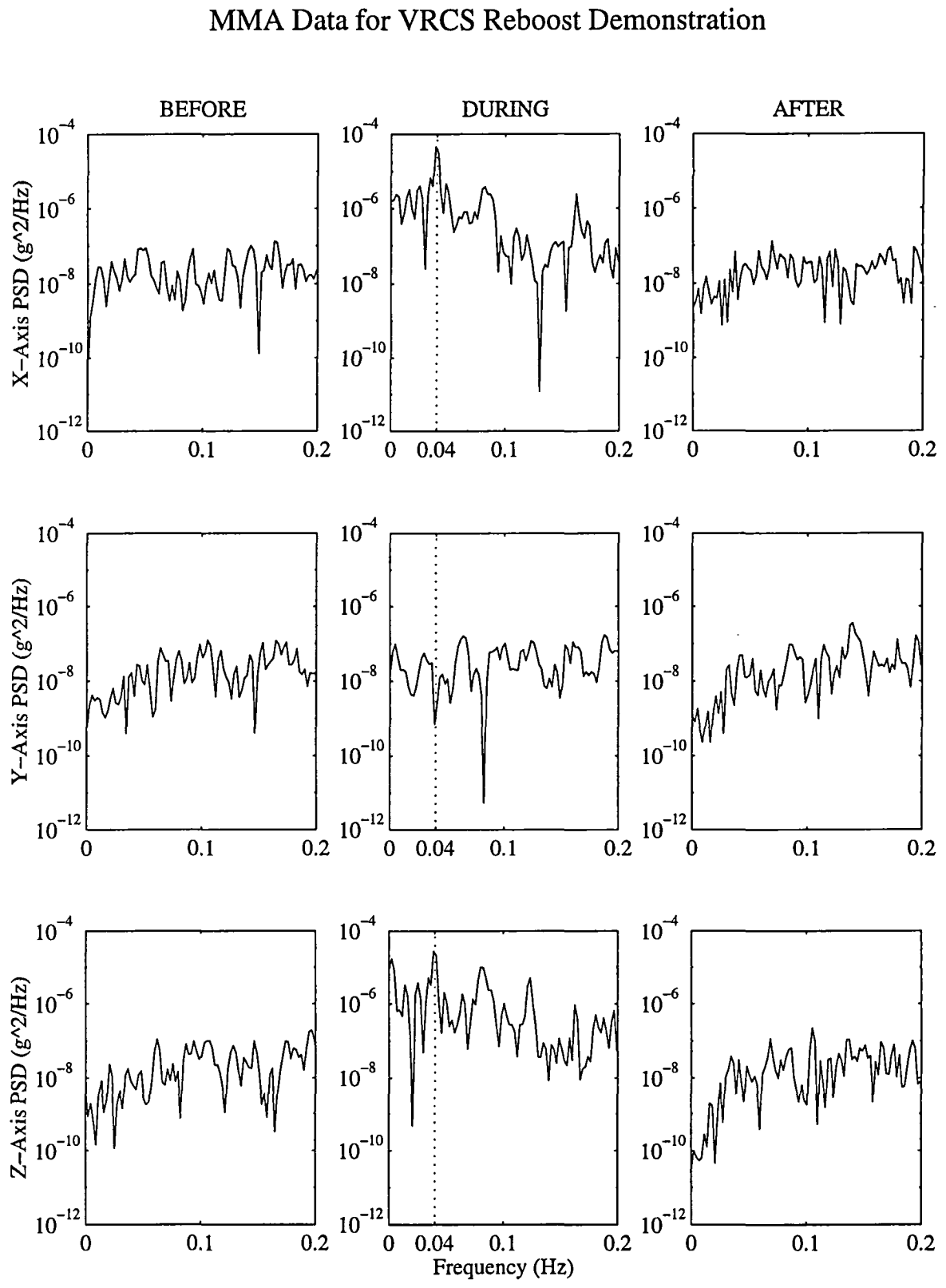

Figure 8. MMA MSP BDPU data PSDs before, during, and after the VRCS Reboost Demonstration. Note excitation at 0.04 Hz (dotted line) during the test

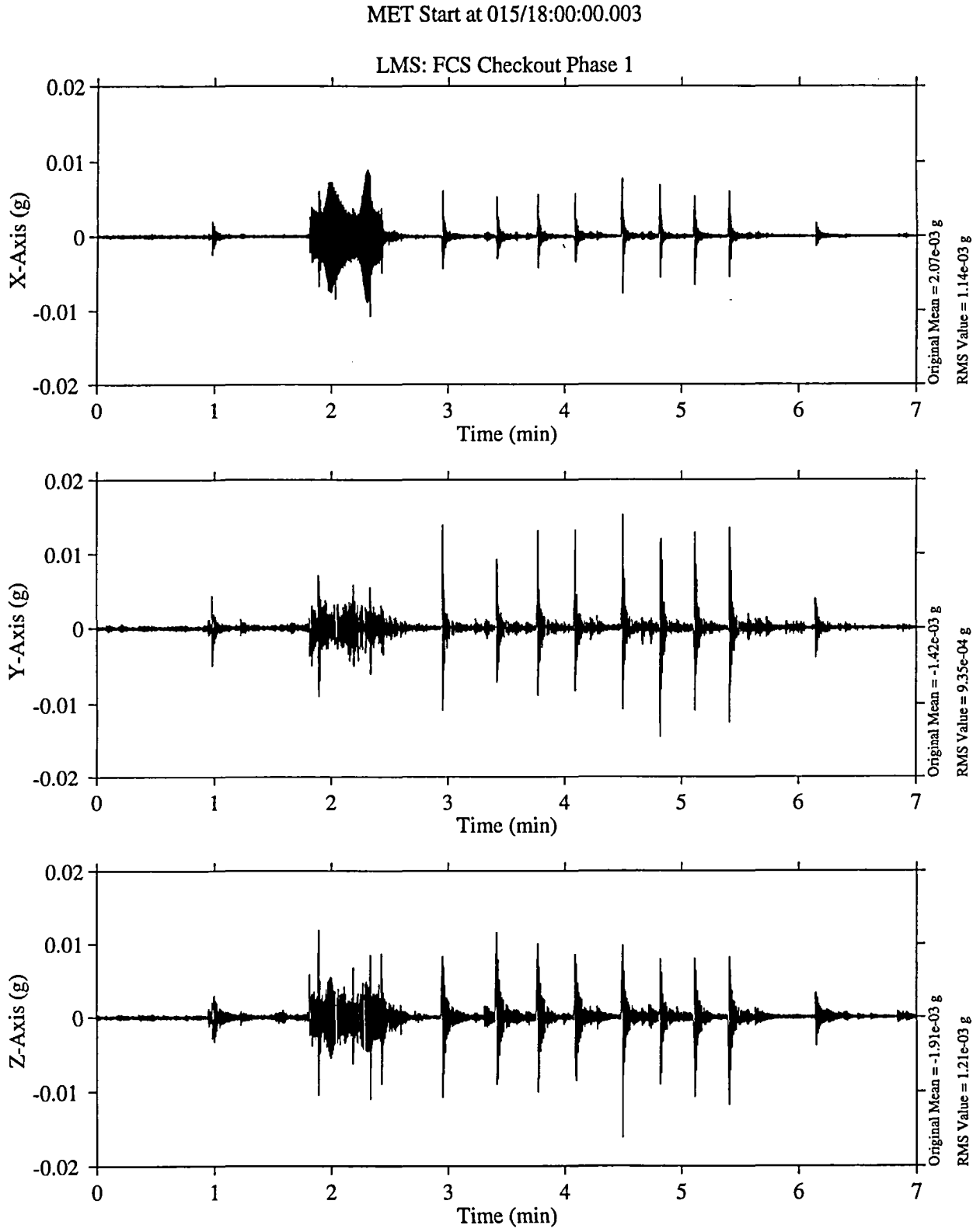

Figure 9. SAMS TSH A data for Flight Control System checkout phase 1

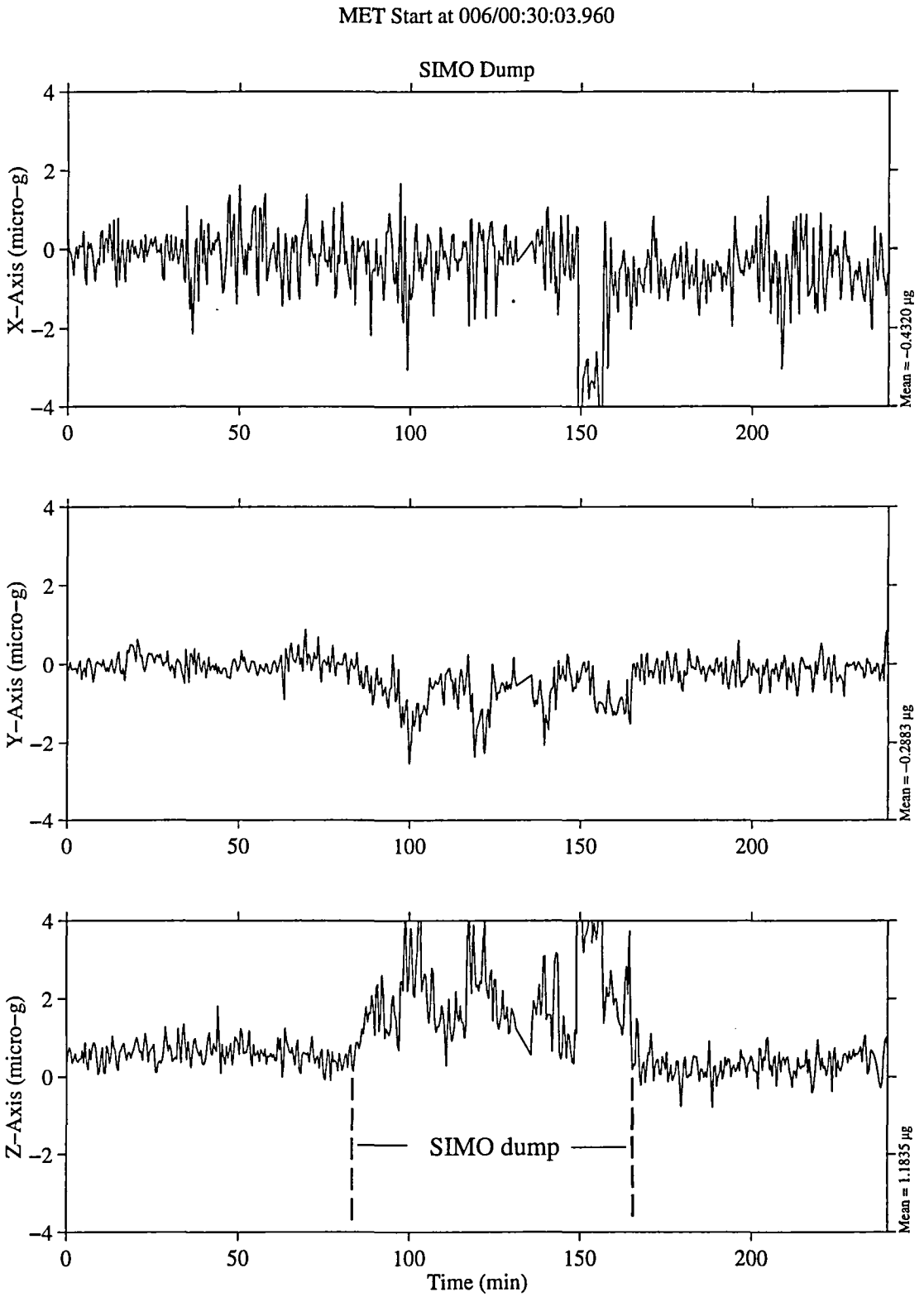

Figure 10. OARE data collected during a simultaneous supply and waste water dump at MET 006/00:30

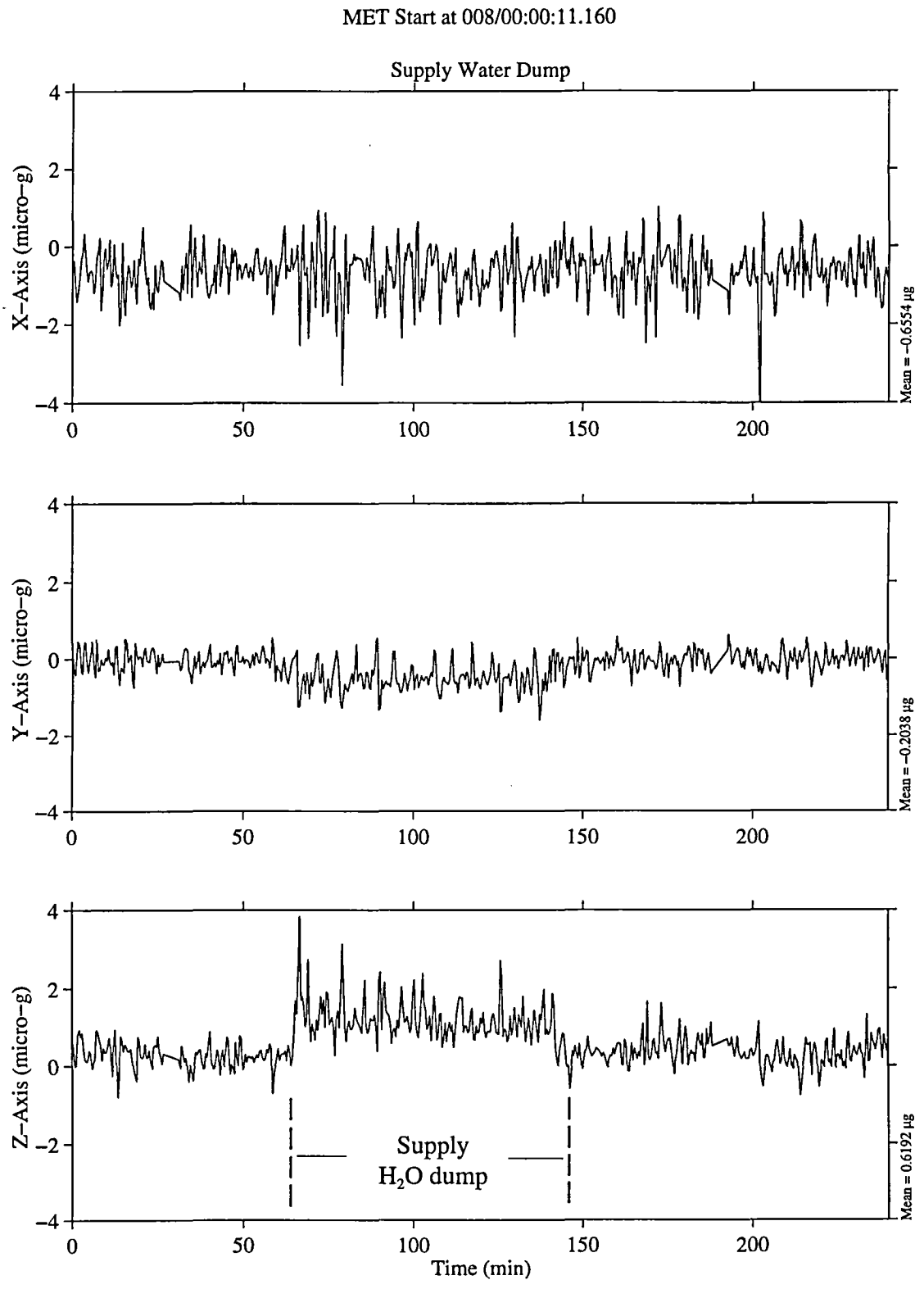

Figure 11. OARE data collected during a supply water dump at MET 008/00:00.

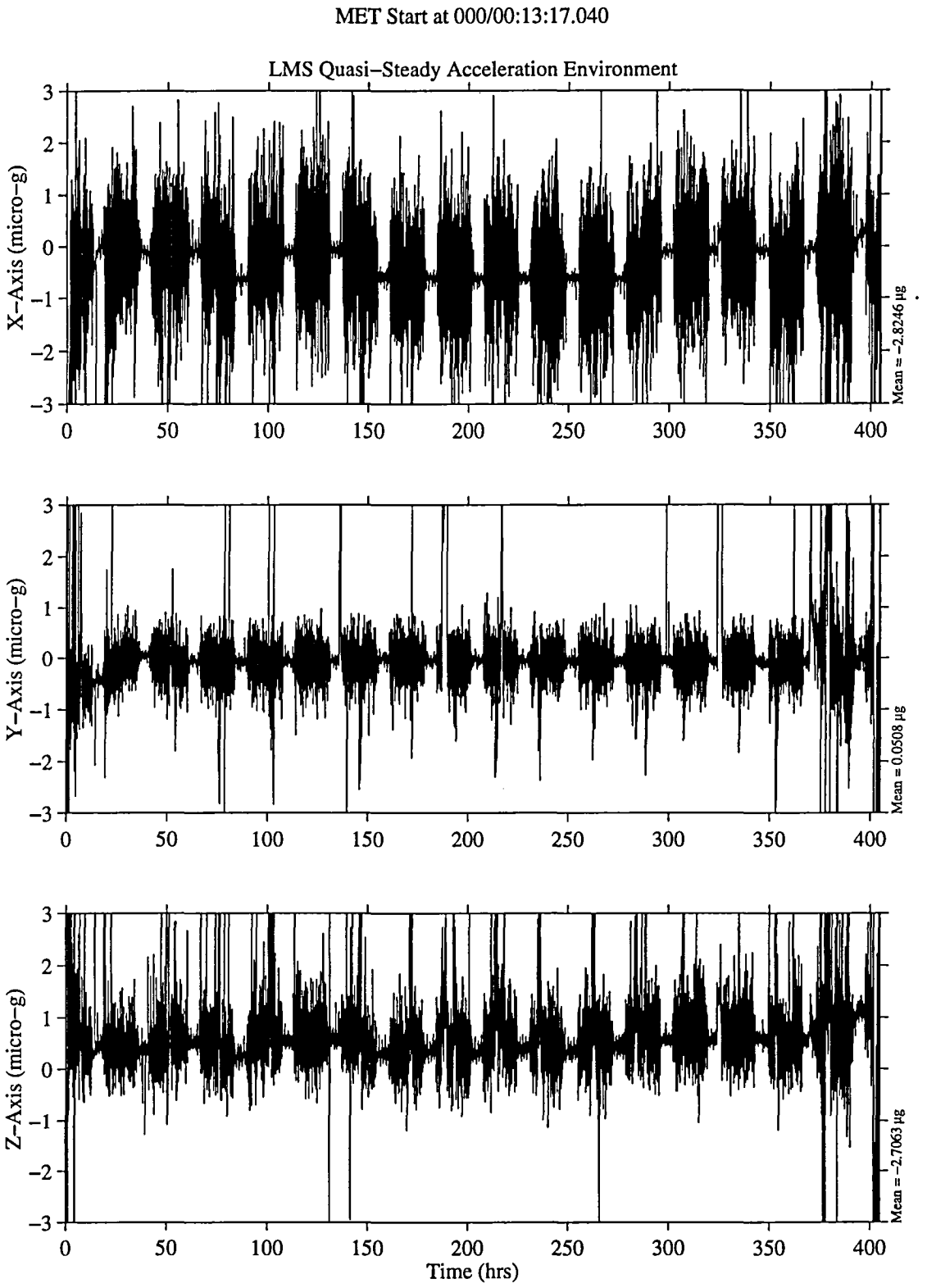

Figure 12. Trimmean filtered OARE data for the STS-78 mission.

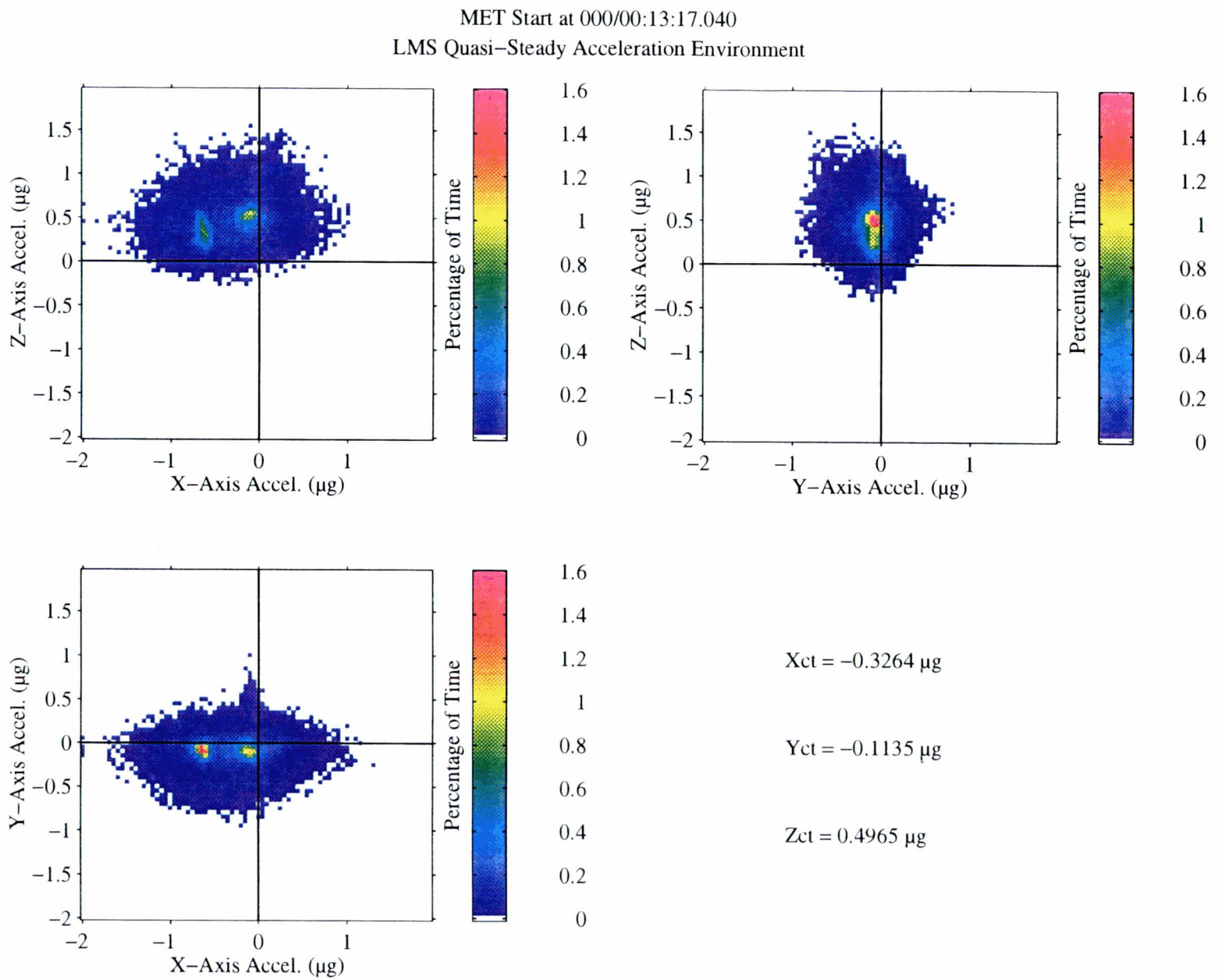

Figure 13. Three-dimensional projection of trimmean filtered OARE data for the STS-78 mission.

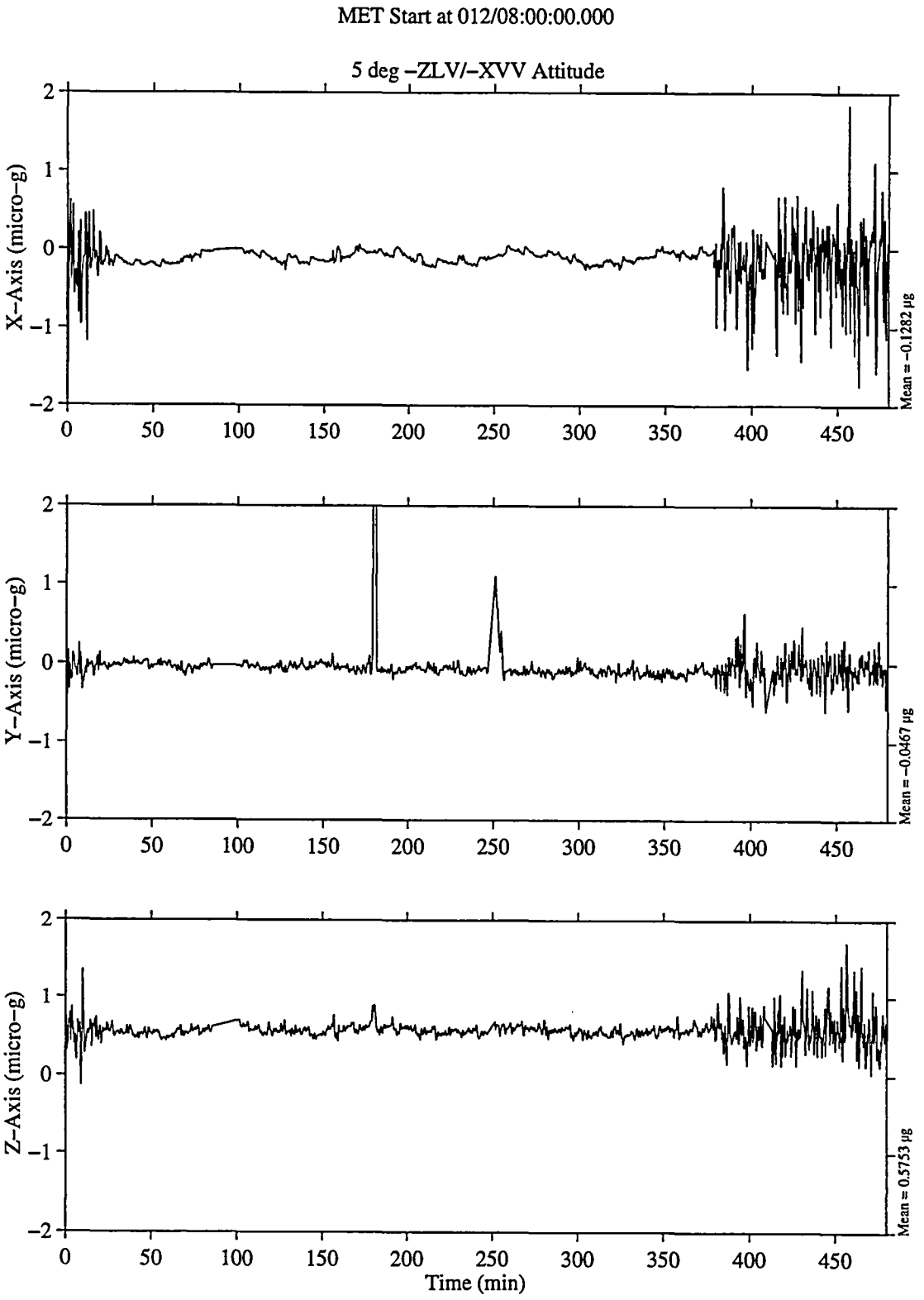

Figure 14. Trimmean filtered OARE data for STS-78 with Columbia in -ZLV/-XVV attitude, MET start 012/08:00.

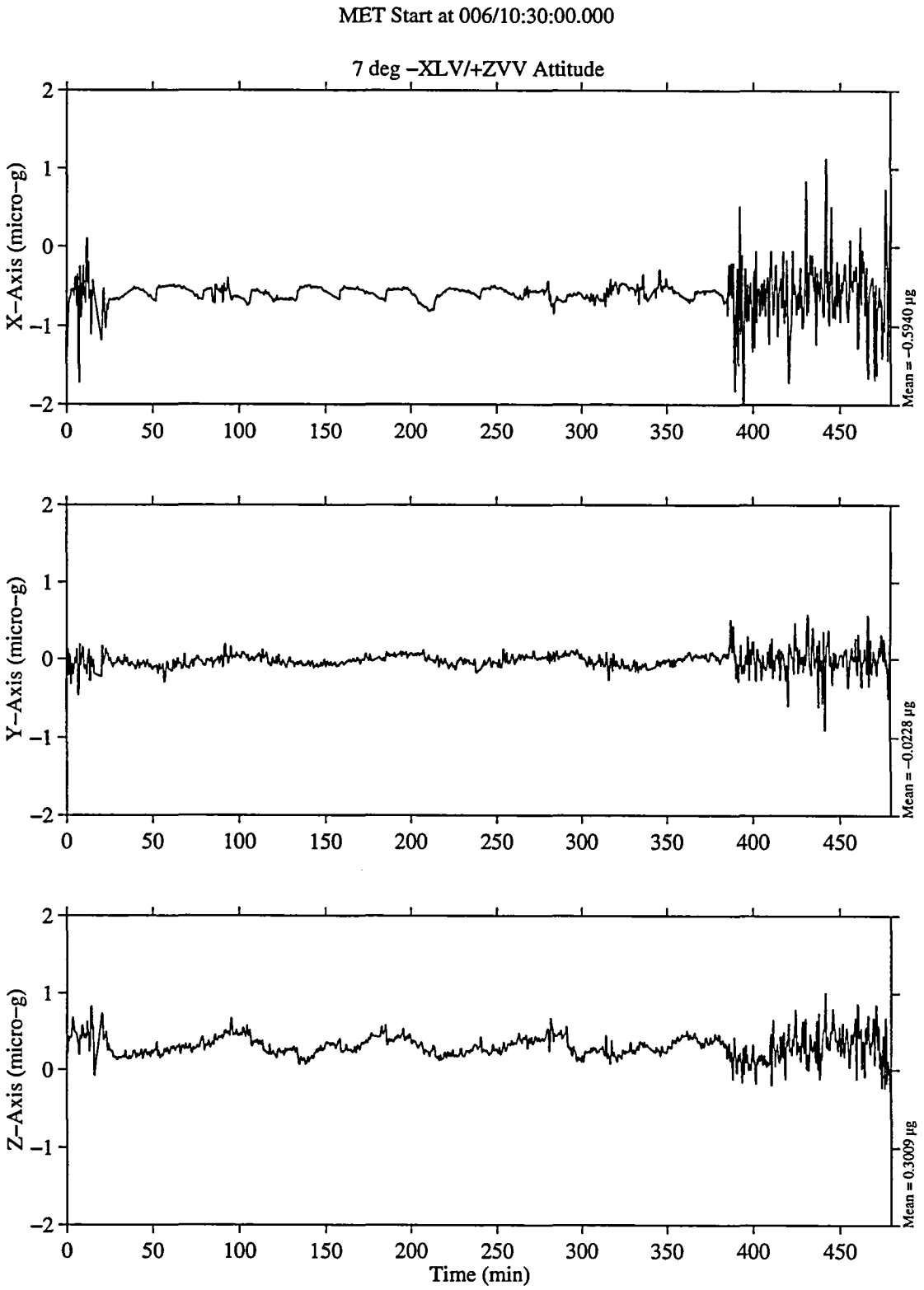

Figure 15. Trimmean filered OARE data for STS-78 with Columbia in -XLV/+ZVV attitude, MET start 006/10:30.

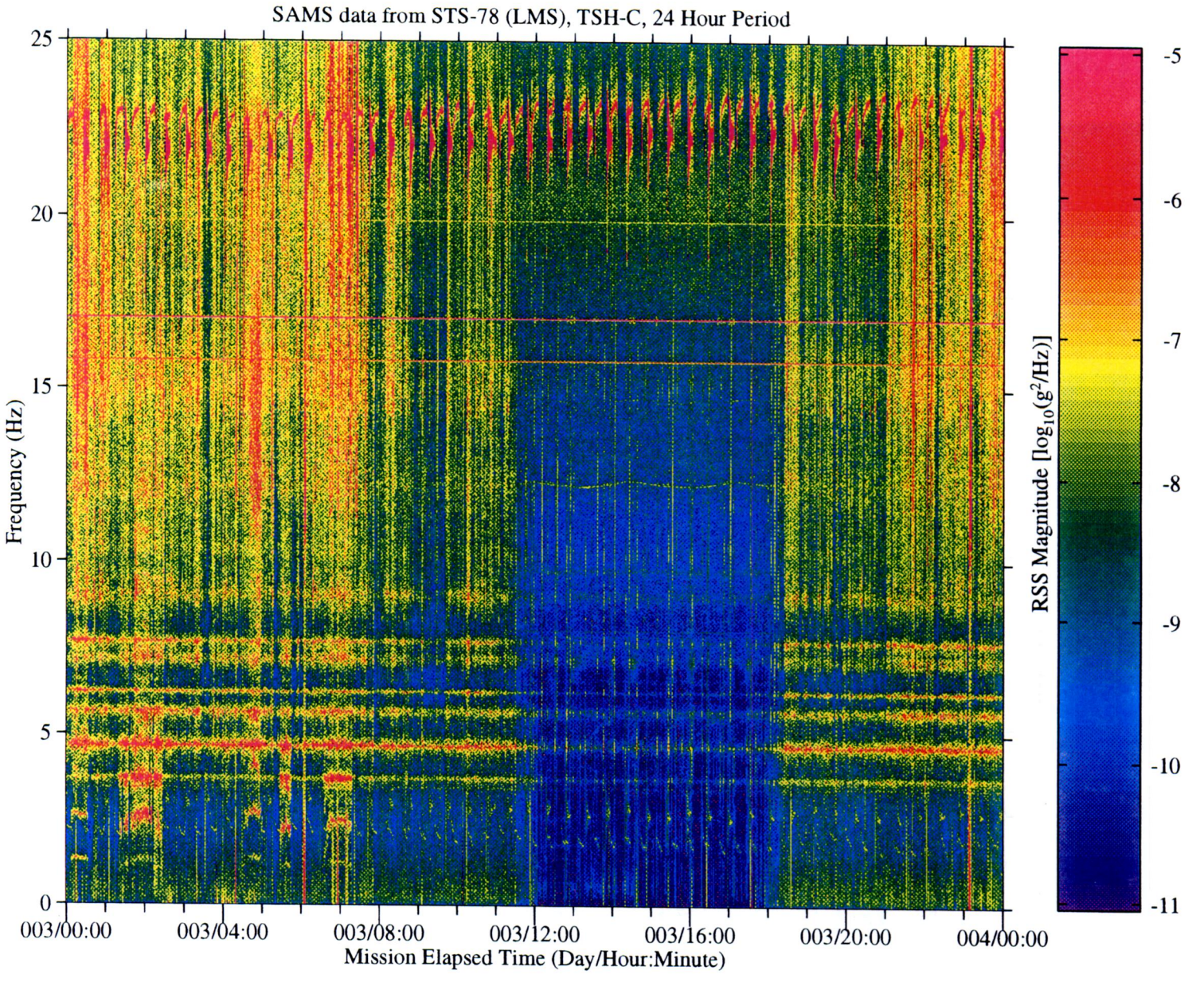

Figure 16. SAMS TSH C spectrogram for 24 hour period starting at MET 003/00:00.

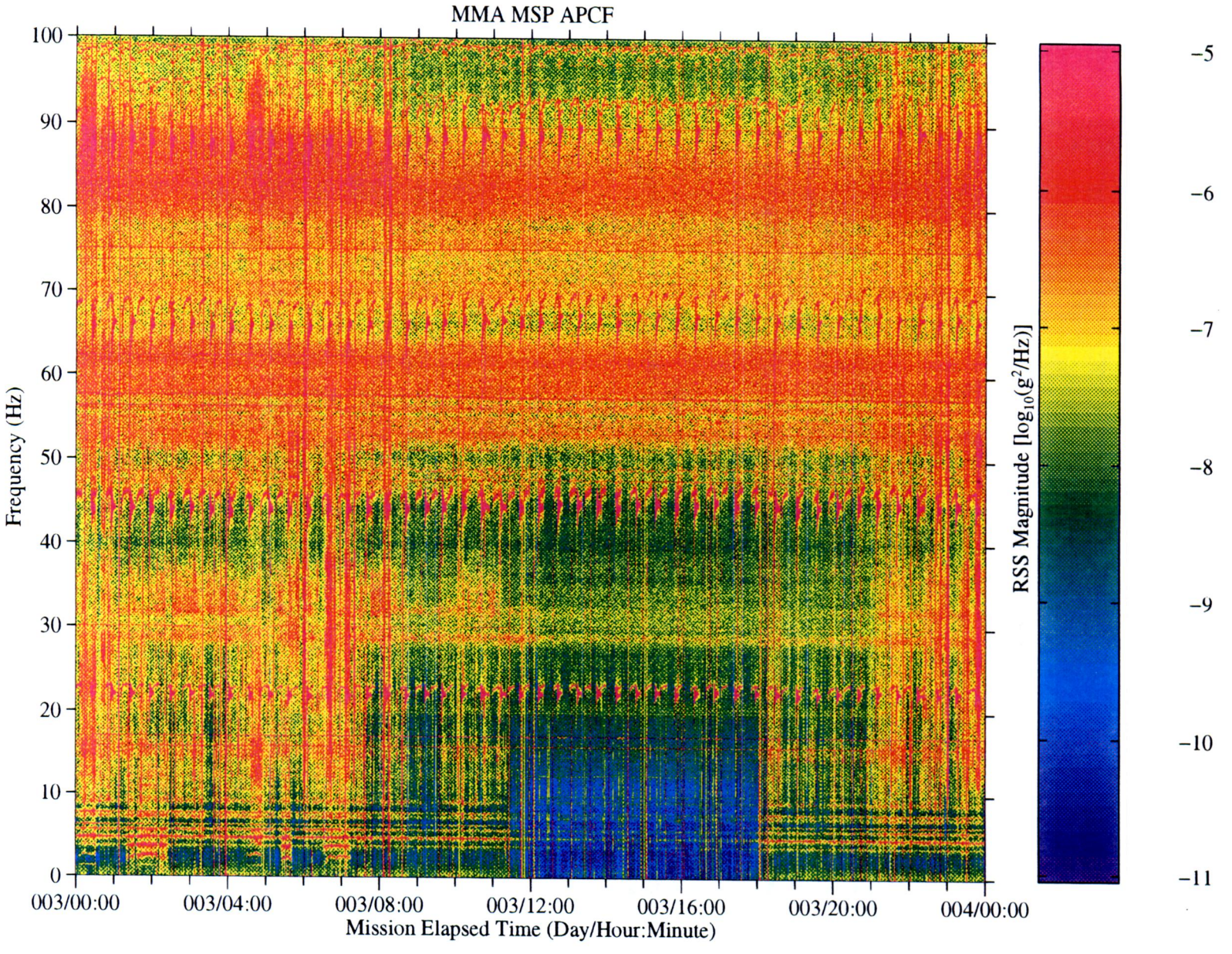

Figure 17. MMA MSP APCF spectrogram for 24 hour period starting at MET 003/00:00.

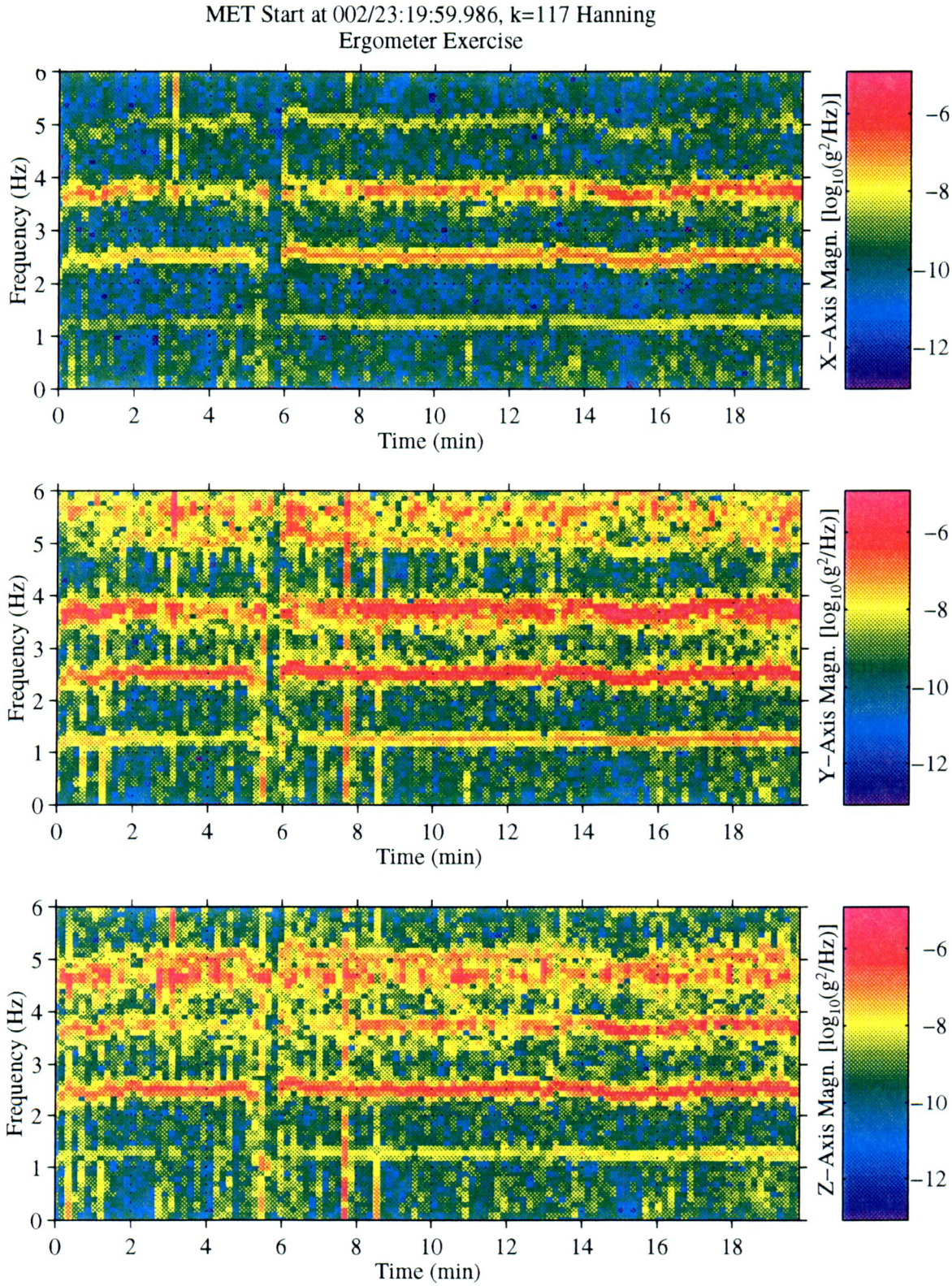

Figure 18. SAMS TSH A data for ergometer exercise in Spacelab module, MET 002/23:20.

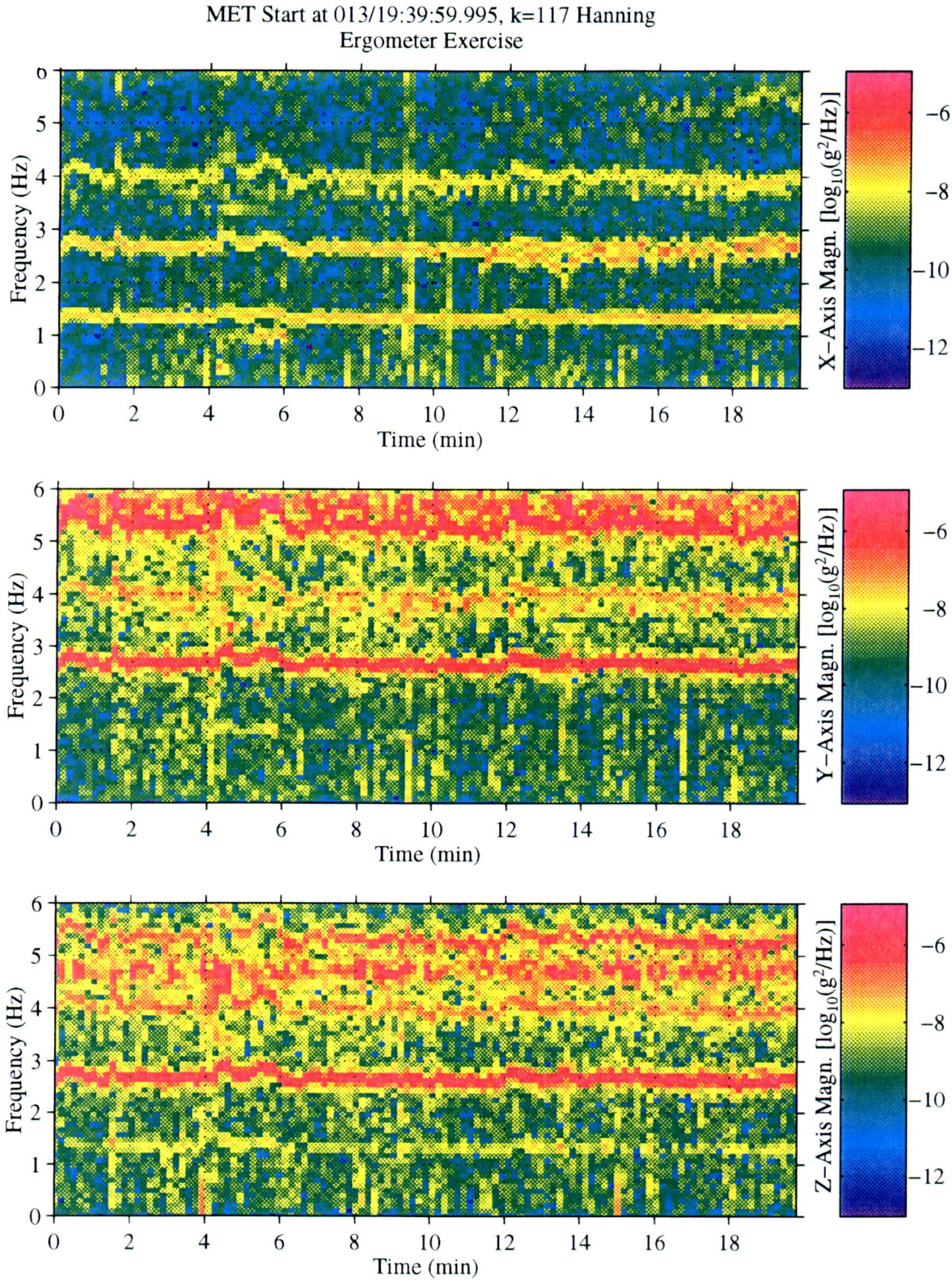

Figure 19. SAMS TSH A data for ergometer exercise assumed to be in flight deck, MET 013/19:40.

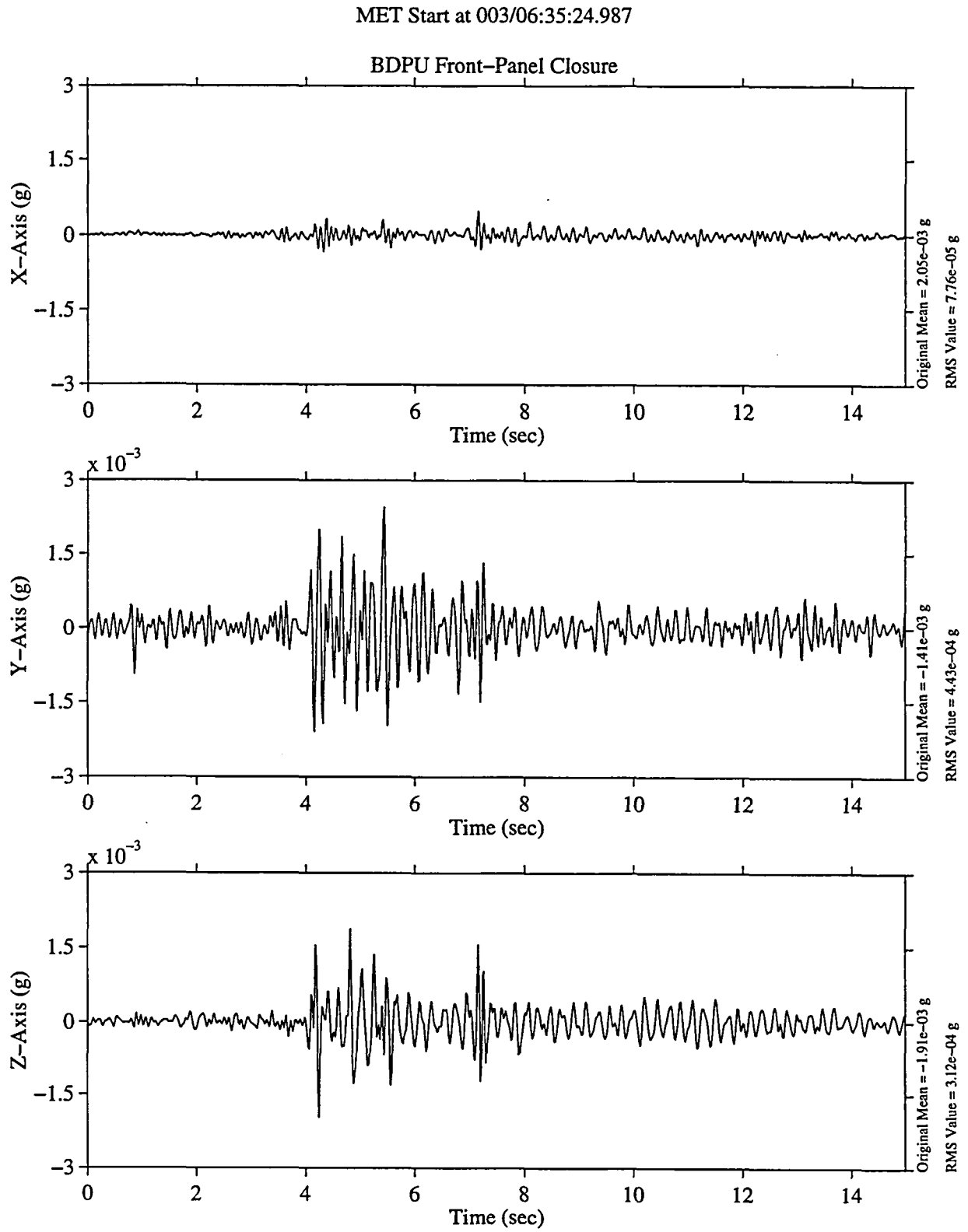

Figure 20. SAMS TSH A data for BDPU panel closing, MET 003/06:35:24.987.

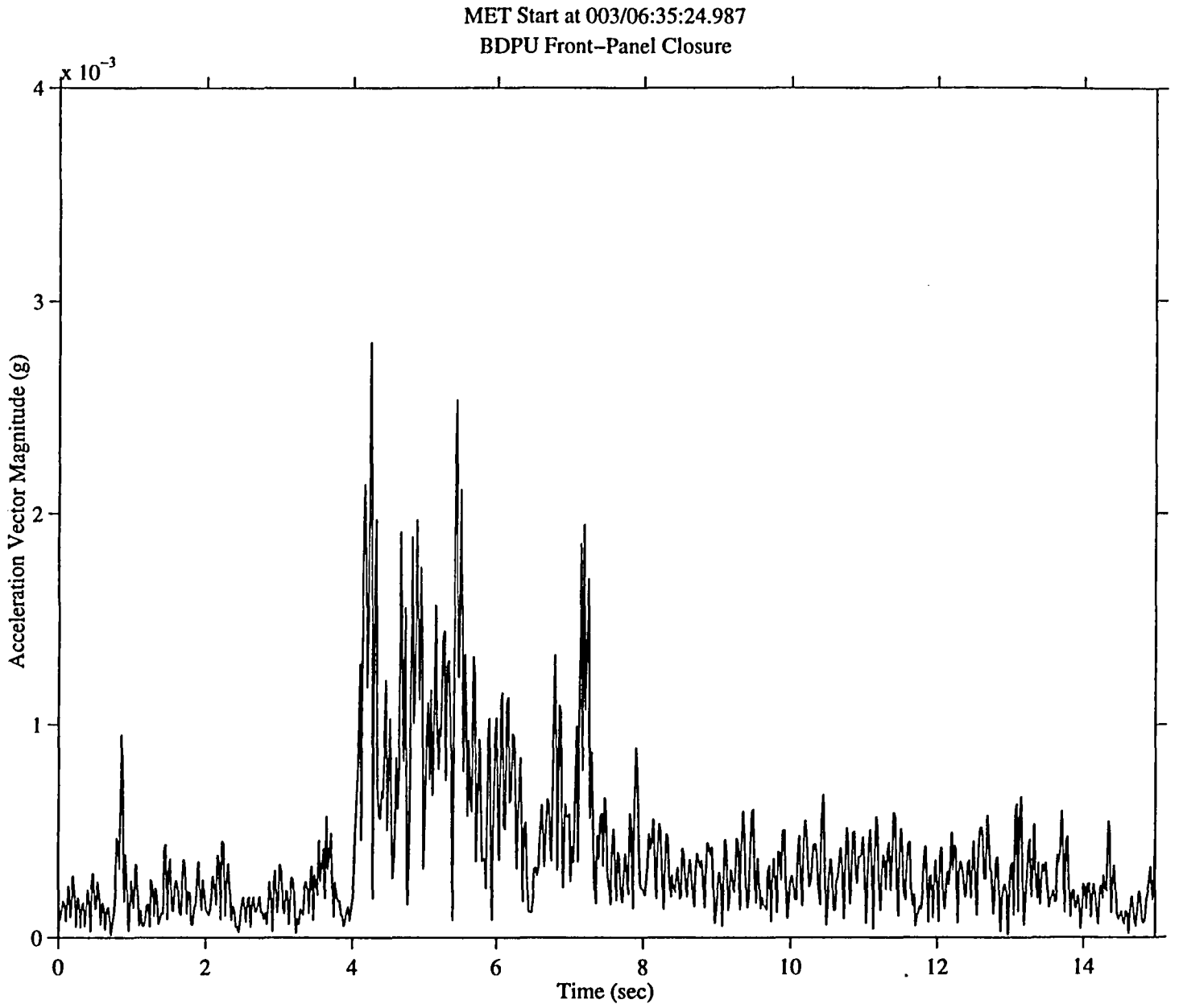

Figure 21. SAMS TSH A data for BDPU panel closing, acceleration vector magnitude.

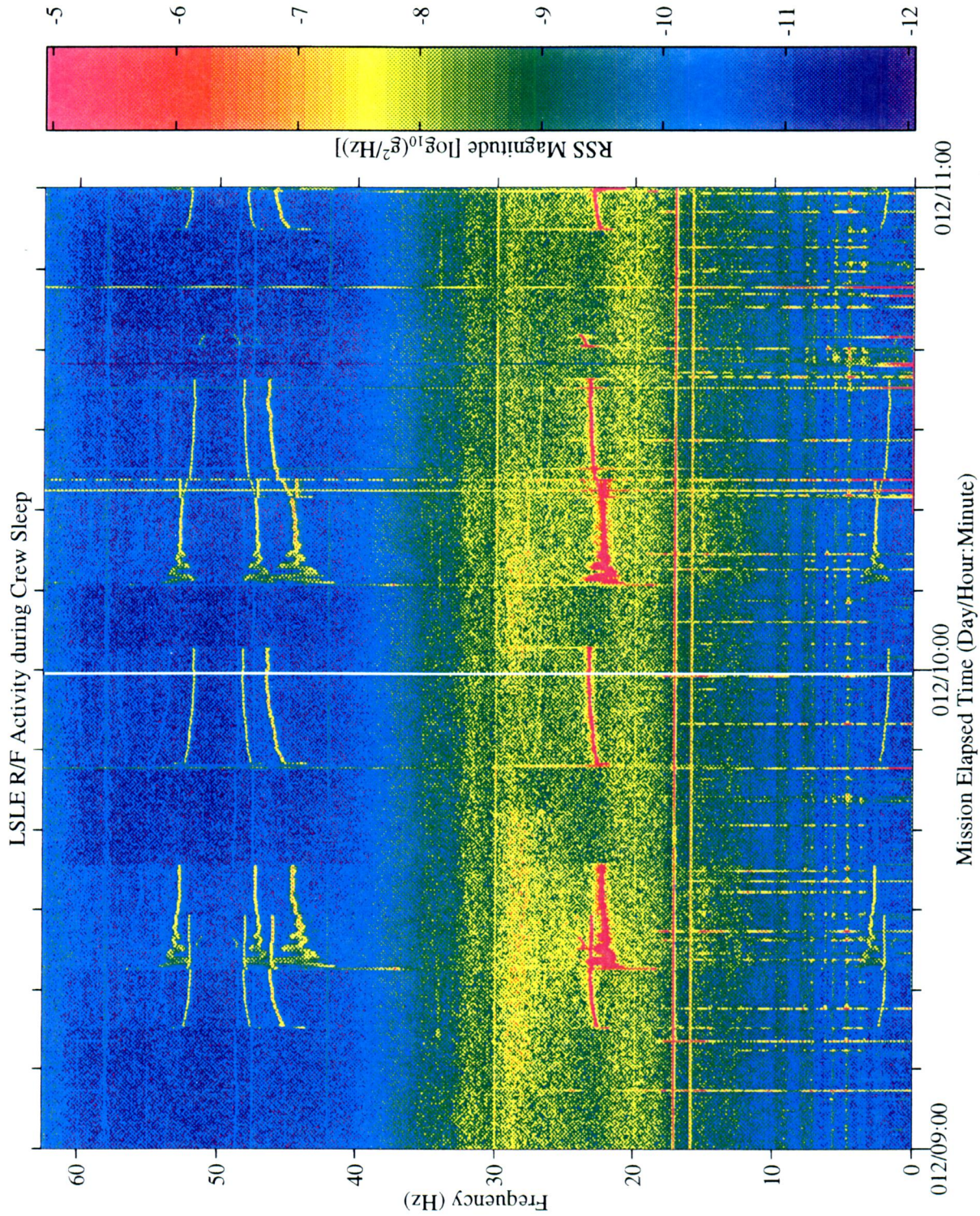

Figure 22. SAMS TSH C spectrogram showing LSLE R/F frequencies. MET start at 012/09:00

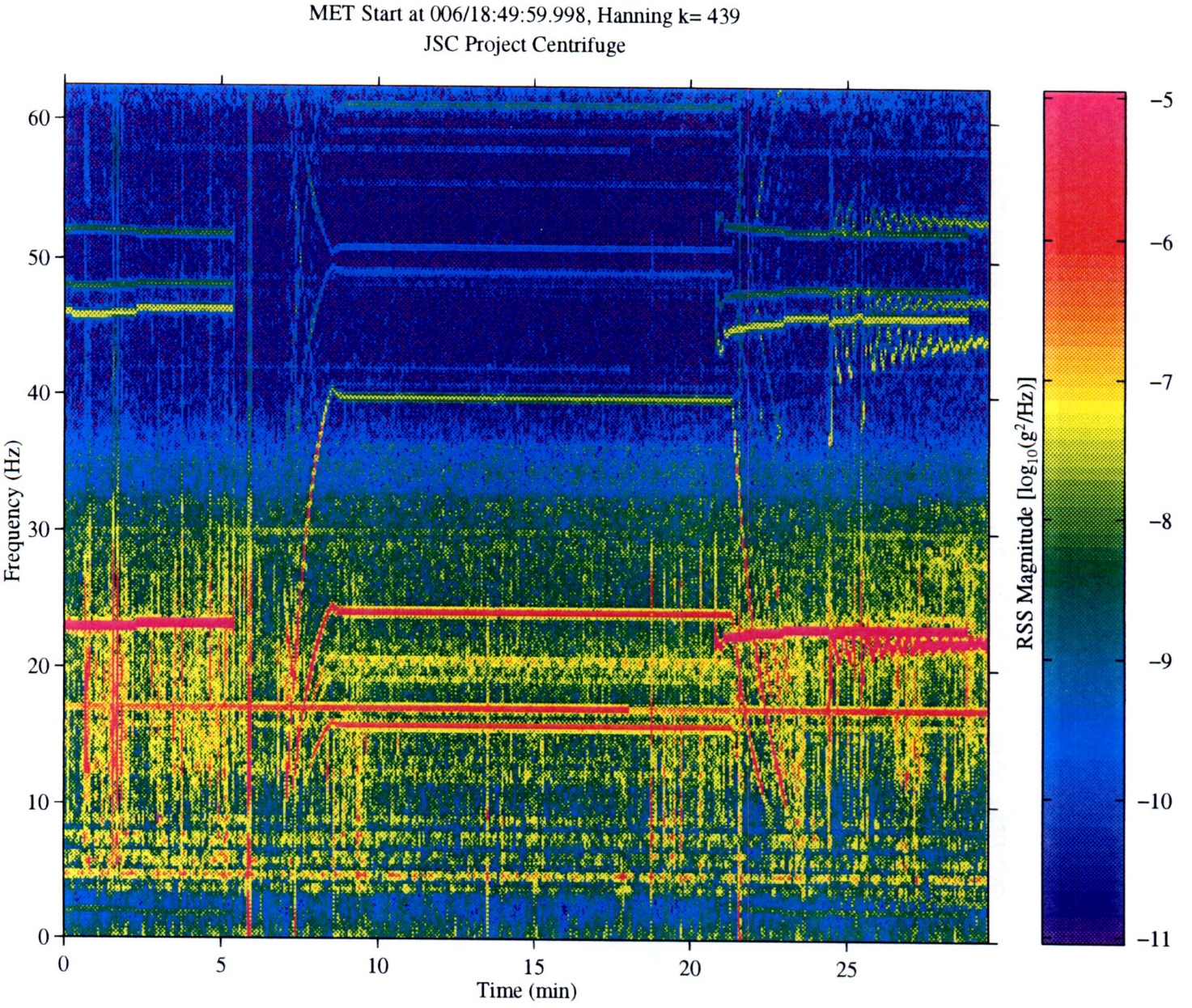

Figure 23. SAMS TSH C spectrogram showing JSC Projects Centrifuge accelerations. MET start at 006/18:49:59.998.

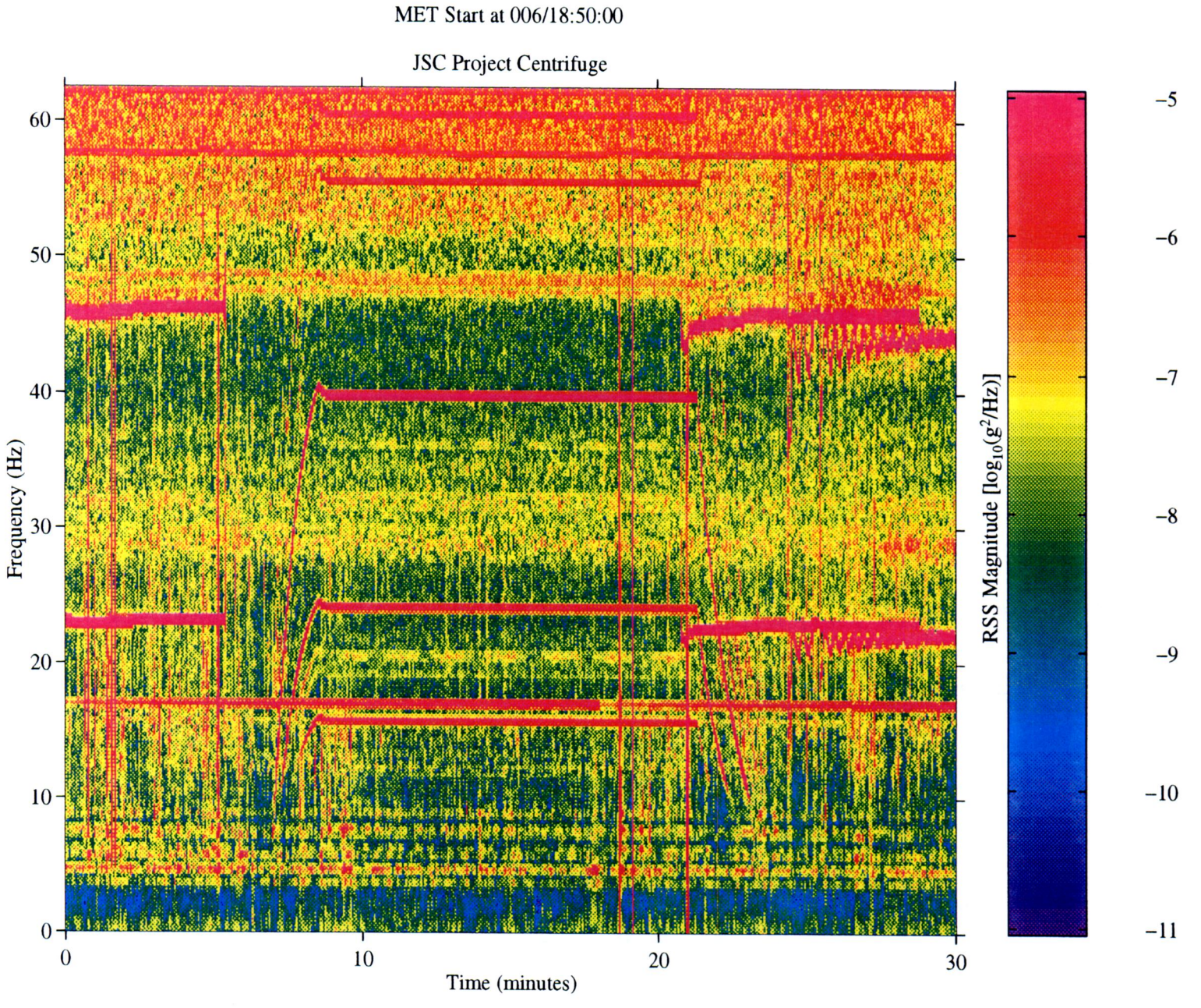

Figure 24. MMA MSP APCF spectrogram showing JSC Projects Centrifuge accelerations. MET start at 006/18:50:00.

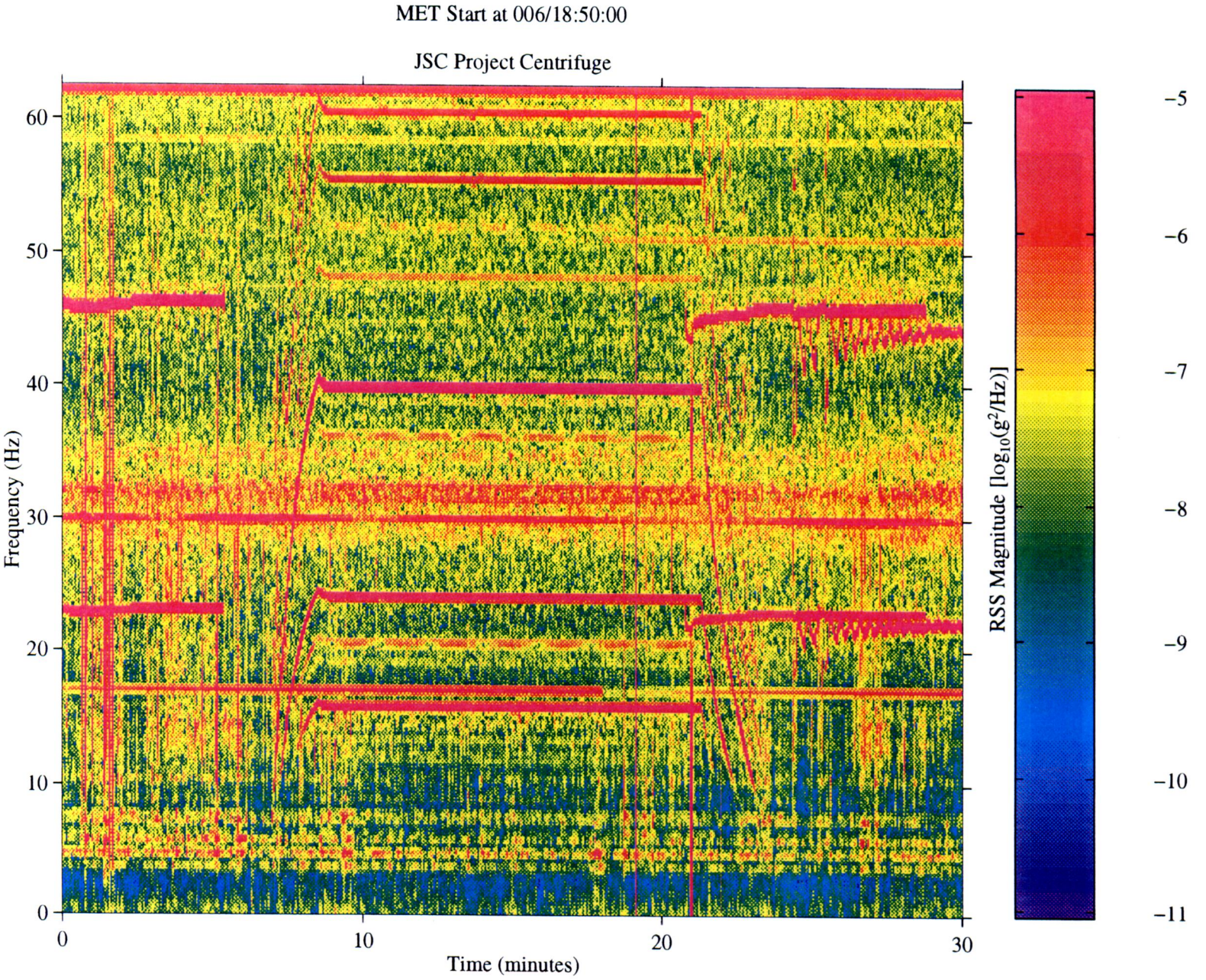

Figure 25. MMA MSP BDPU spectrogram showing JSC Projects Centrifuge accelerations. MET start 006/18:50:00

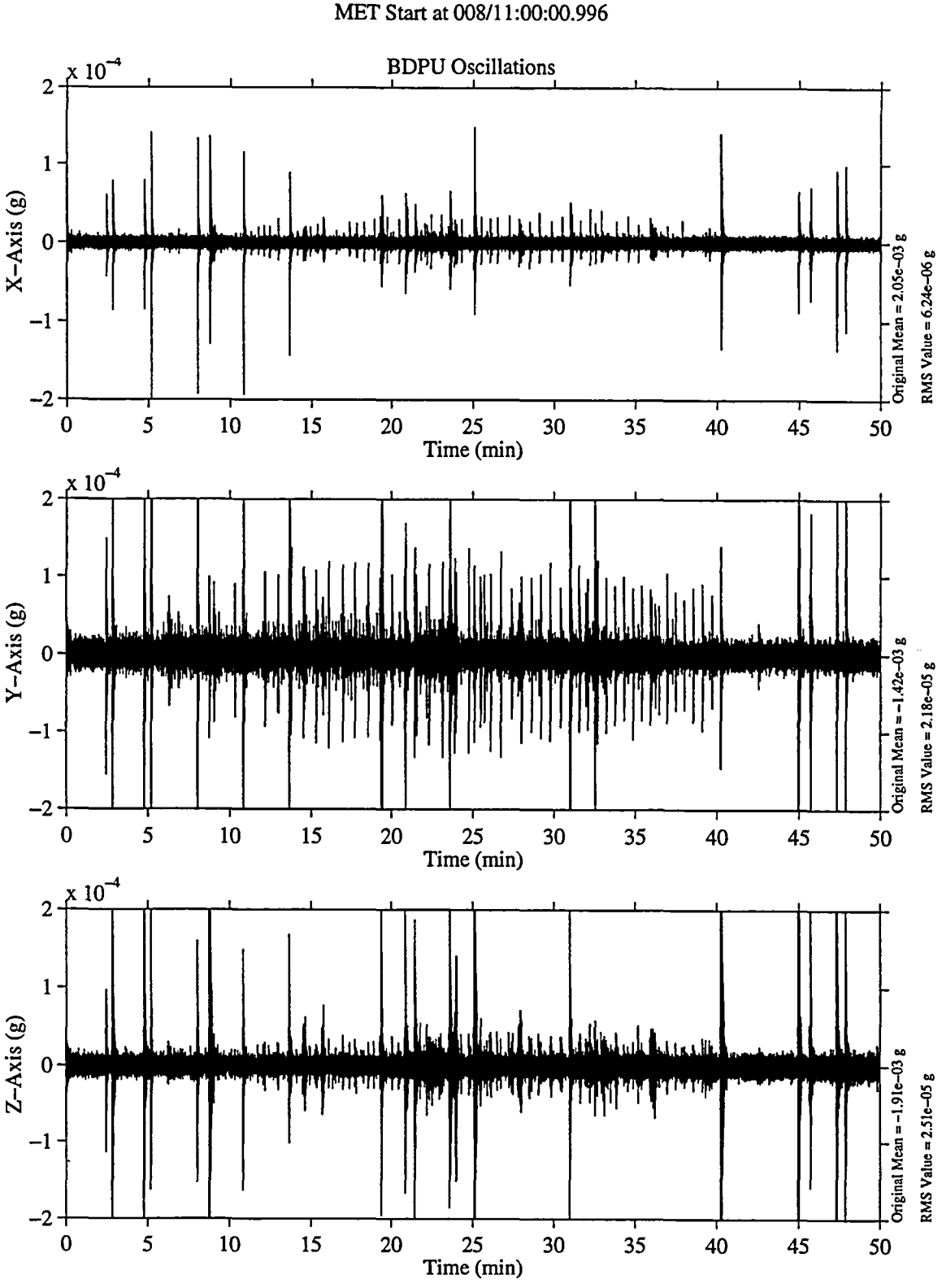

Figure 26. SAMS TSH A data for unidentified disturbances, MET start 008/11:00:01.

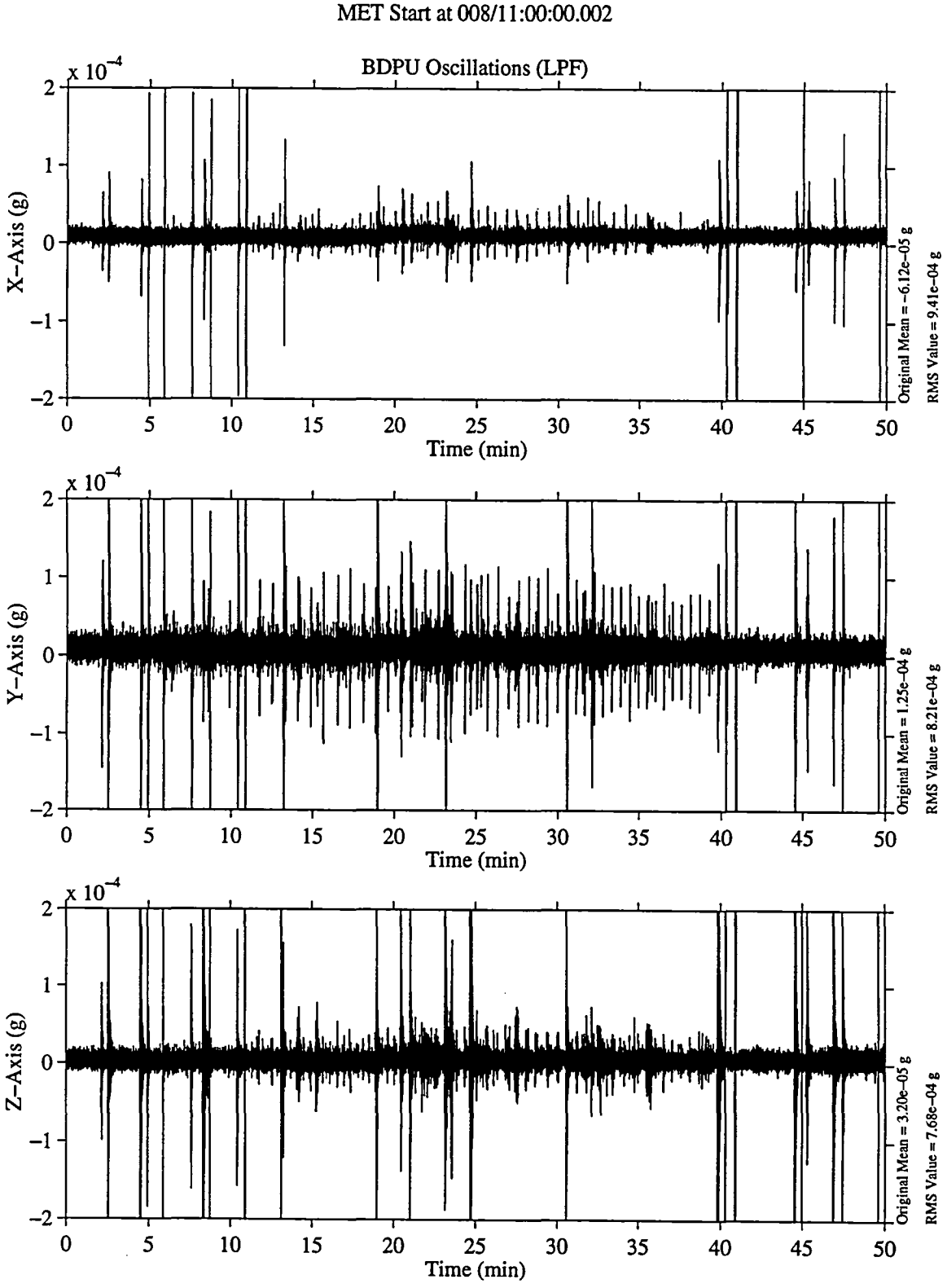

Figure 27. MMA MSP BDPU data for unidentified disturbances, MET start 008/11:00:00.

Appendix A: Accessing Acceleration Data via the Internet

SAMS and OARE data are available over the internet from the NASA LeRC file server "beech.lerc.nasa.gov". Previously, SAMS data were made available on CD-ROM, but distribution of data from current (and future) missions will be primarily through this internet file server.

SAMS data files are arranged in a standard tree-like structure. Data are first separated based upon mission. Then, data are further subdivided based upon some portion of the mission, head, year (if applicable), day, and finally type of data file (acceleration, temperature, or gain). Effective November 1, 1996, there has been a minor reorganization of the beech.lerc.nasa.gov file server. There are now two locations for SAMS data: a directory called SAMS-SHUTTLE and a directory called SAMS-MIR. Under the SAMS-SHUTTLE directory, the data are segregated by mission. Under the SAMS-MIR directory, the data are segregated by year. The following figure illustrates this structure.

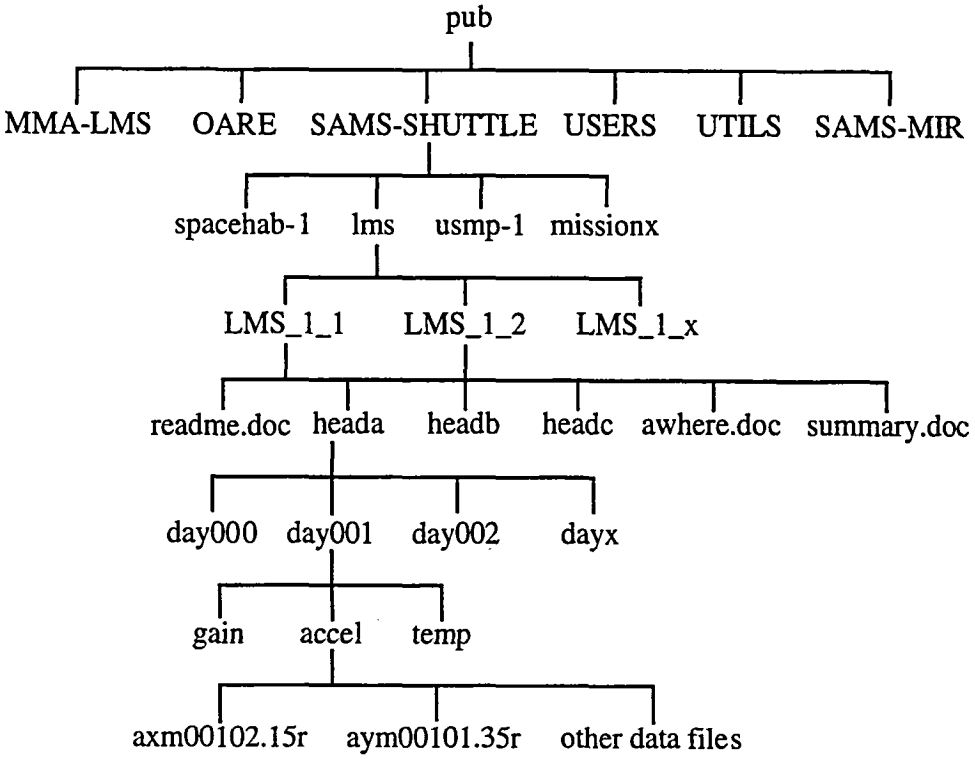

The SAMS data files (located at the bottom of the tree structure) are named based upon the contents of the file. For example, a file named "axm00102.15r" would contain head A data for the x-axis for day 001, hour 02, file 1 of 5. The readme.doc files give a complete explanation of the file naming convention.

OARE data files are also arranged in a tree-like structure, but with different branches. The data are first divided based upon mission, and then are divided based upon type of data. The OARE tree structure looks like this:

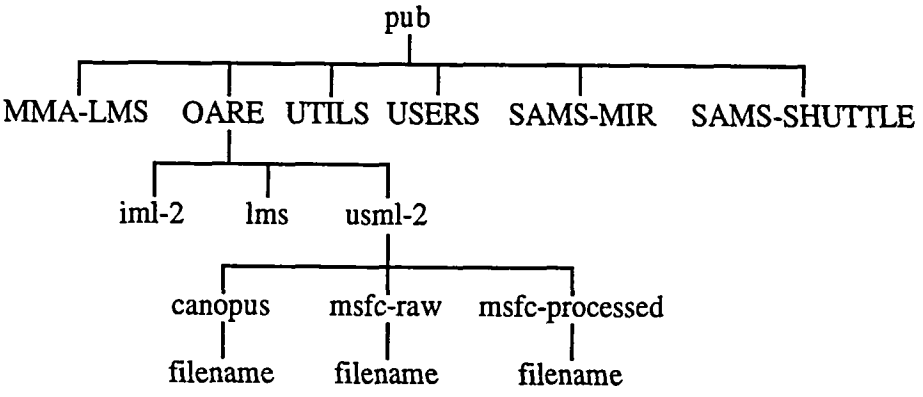

Files under the canopus directory are trimmean filter data, computed by Canopus Systems, Inc. Files under the msfc-raw directory contain the telemetry data files provided to PIMS by the Marshall Space Flight Center Payload Operations Control Center data reduction group. Files under the msfc-processed directory are raw files containing binary floating point values, listing the MET (in hours), and the x, y, and z axis acceleration in micro-g's. Selected MMA data files are located in the MMA-LMS subdirectory. See the readme files for complete data descriptions.

Data access tools for different computer platforms (MS-DOS, Macintosh, SunOS, and MS-Windows) are available in the /pub/UTILS directory.

The NASA LeRC beech file server can be accessed via anonymous File Transfer Protocol (ftp), as follows:

1) Open an ftp connection to "beech.lerc.nasa.gov"
2) Login as userid "anonymous"
3) Enter your e-mail address as the password
4) Change directory to pub
5) List the files and directories in the pub directory
6) Change directories to the area of interest
7) Change directories to the mission of interest

8) Enable binary file transfers
9) Use the data file structures (described above) to locate the desired files
10) Transfer the desired files

If you encounter difficulty in accessing the data using the file server, please send an electronic mail message to "pims@lerc.nasa.gov". Please describe the nature of the difficulty and also give a description of the hardware and software you are using to access the file server.

Appendix B SAMS Time Histories and Color Spectrograms

The Principal Investigator Microgravity Services (PIMS) group has further processed SAMS data from LMS (STS-78), Head C to produce the plots shown here. Three representations of the data are presented here: ten second interval average, ten second interval RMS, and PSD magnitude versus frequency versus time (spectrogram) plots. These calculations are presented in 6 hour plots, with the corresponding average and RMS plots on one page, and the spectrogram on the facing page.

The ten-second interval average plots give an indication of net accelerations which last for a period of 10 seconds or more. Shorter duration, high amplitude accelerations may be seen with this type of plot, however their exact timing and magnitude cannot be extracted. The ten-second interval RMS plots give a measure of the oscillatory content in the acceleration data. Plots of this type may be used to identify times when oscillatory and/or transient deviations from the background acceleration levels occurred.

Color spectrograms are used to show how the microgravity environment varies in intensity with respect to both the time and frequency domains. These spectrograms are provided as an overview of the frequency characteristics of the SAMS data during the mission. Each spectrogram is a composite of 6 hour's worth of data. The time resolution used to compute the spectrograms seen here is 65.536 seconds. This corresponds to a frequency resolution of 0.0153 Hz.

These data were collected at 125 samples per second, and a 25 Hz low pass filter was applied to the data by the SAMS unit prior to digitization. Prior to plot production, the raw SAMS data were compensated for gain changes, and then demeaned. Demeaning was accomplished by analyzing individual sections with a nominal length of 30 minutes. Users who are interested in further details for either of these operations are encouraged to contact the PIMS group.

Interval Average and Root Mean Square Calculations

The interval average plots were produced by calculating the average of ten second intervals of data for each axis

This operation is described as: $x_{avg_k} = \frac{1}{M}\sum_{i=1}^{M} x_{(k-1)M+i}$,

where x represents the x, y, or z axis data, M is the number of points analyzed in an interval, and k refers to the kth interval analyzed.

The resulting data streams (x_{avg}, y_{avg}, z_{avg}) are then combined by a vector-magnitude operation.

This computation is expressed mathematically as: $\text{accel}_{\text{avg}_k} = \sqrt{x^2_{\text{avg}_k} + y^2_{\text{avg}_k} + z^2_{\text{avg}_k}}$.

The interval RMS plots were produced by taking the root-mean-square of ten second intervals of data for each axis and forming a vector magnitude of the resulting data stream.

The interval RMS operation is expressed mathematically as: $x_{\text{RMS}_k} = \sqrt{\frac{1}{M}\sum_{i=1}^{M}\left(x_{(k-1)M+i}\right)^2}$.

The same definitions apply for x, M, and k as in the interval average computation. The resulting data streams are combined by a vector-magnitude operation.

Power Spectral Density versus Frequency versus Time Calculations

In order to produce the spectrogram image, Power Spectral Densities were computed for successive time intervals (the length of the interval is equal to the time resolution). For the PSD computation, a Hanning window was applied. In order to combine all three axes into a single plot to show an overall level, a Vector-Magnitude (VM) operation was performed. Stated mathematically:

$$\text{VM}_k = \sqrt{\text{PSD}^2_{x_k} + \text{PSD}^2_{y_k} + \text{PSD}^2_{z_k}}.$$

By imaging the base 10 logarithm ($\log_{10}$) magnitude as a color and stacking successive PSDs from left to right, variations of acceleration magnitude and frequency are shown as a function of time. Colors are assigned to discrete magnitude ranges, so that there are 64 colors assigned to the entire range of magnitudes shown.

The colorbar limits are chosen in order to maximize the data value and visibility in a given set of spectrogram plots. Data which fall outside of these limits will be imaged as either the highest or lowest magnitude, depending on which side they have saturated. For this report, less than 1% of the total points lie below the lower limit, and less than 1% of the total points lie above the upper limit. If an area of interest seems to be saturated, care should be taken in that the actual values may lie above or below the color mapping shown on the plot.

Due to the nature of spectrograms, care should be taken to not merely read a color's numeric value as being the "amount" of acceleration that is present at a given frequency. In order to get this type of information, the PSDs must be integrated between two frequencies. These frequencies (lower and upper) form the "band" of interest. The result of this integration is the g_{RMS} acceleration level in the $\left[f_{\text{lower}}, f_{\text{upper}}\right]$ band. The PIMS group is able to provide this type of analysis on a per-request basis.

Plot gaps (if any exist) are shown by either white or dark blue areas on the page. Care should be taken to not mistake a plot gap (represented by a black vertical band) with a quiet period. If a plot gap exists for an entire plot (or series of successive plots), a comment is placed on the page to let the user know there is a gap in the data. These "no data available" comments will not show exact times for which the data are not available, but will only indicate missing plots.

Contacting PIMS

To request additional analysis or information, users are encouraged to send an e-mail to pims@lerc.nasa.gov, or FAX a request to (216) 433-8545.

Figure 1a: LMS, Head C (fc=25 Hz), Ten Second Interval Average

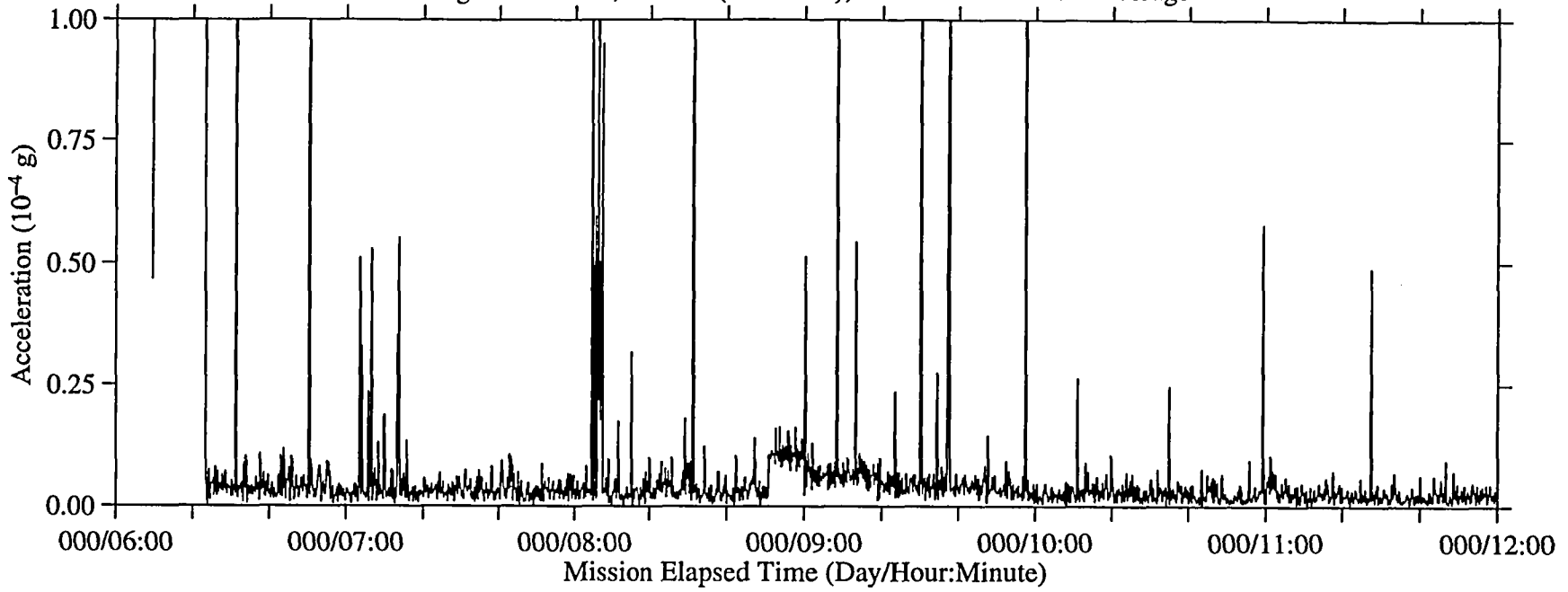

Figure 1b: LMS, Head C (fc=25 Hz), Ten Second Interval RMS

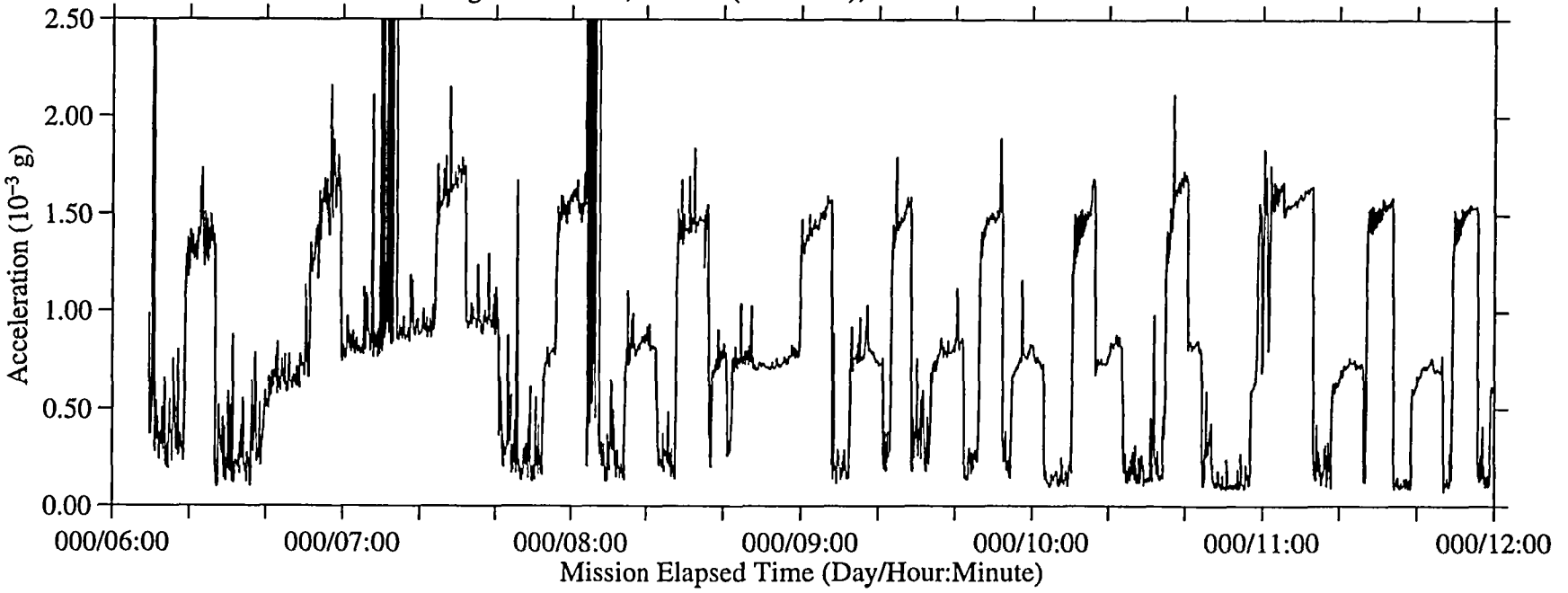

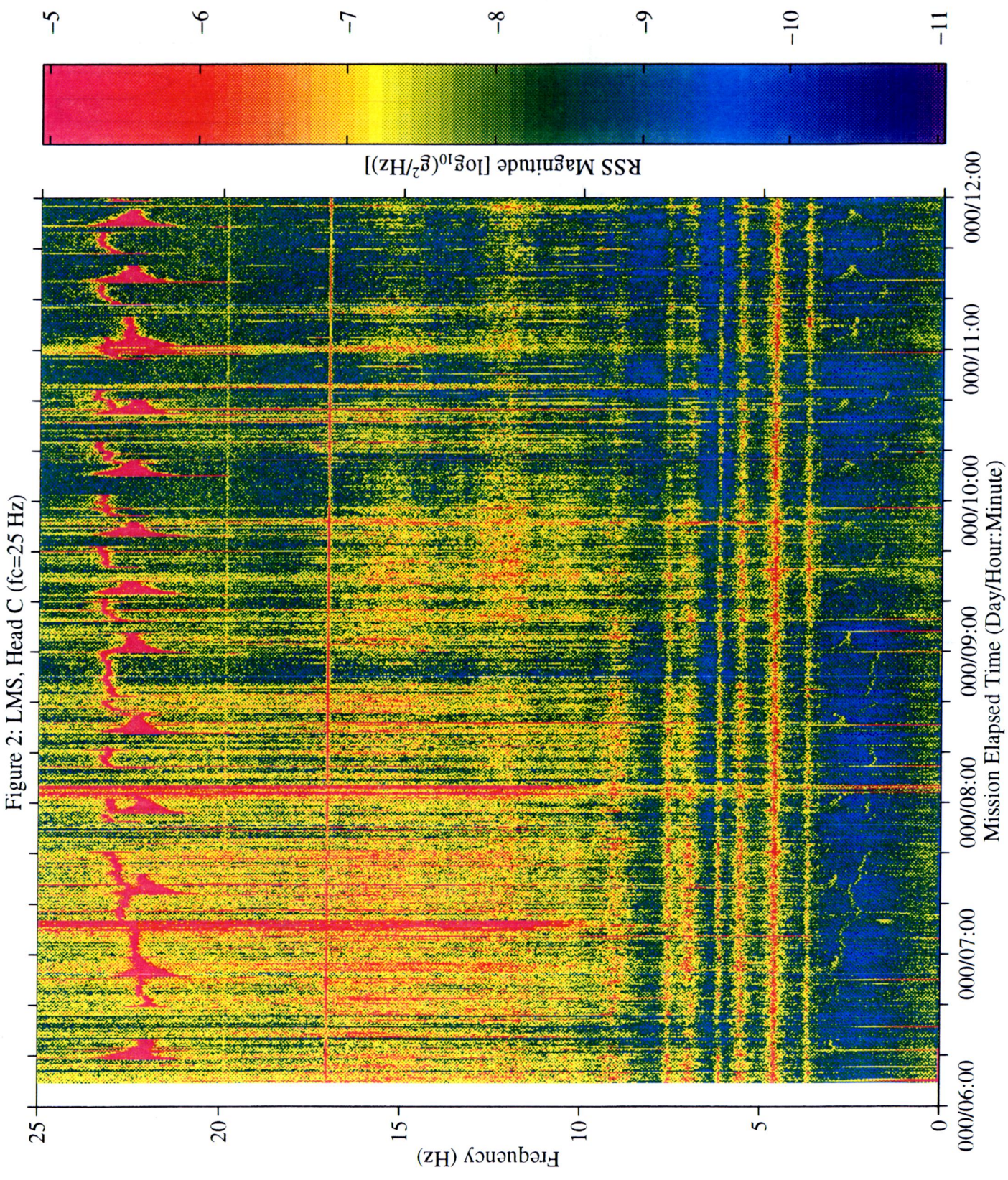

Figure 2: LMS, Head C (fc=25 Hz)

Figure 3a: LMS, Head C (fc=25 Hz), Ten Second Interval Average

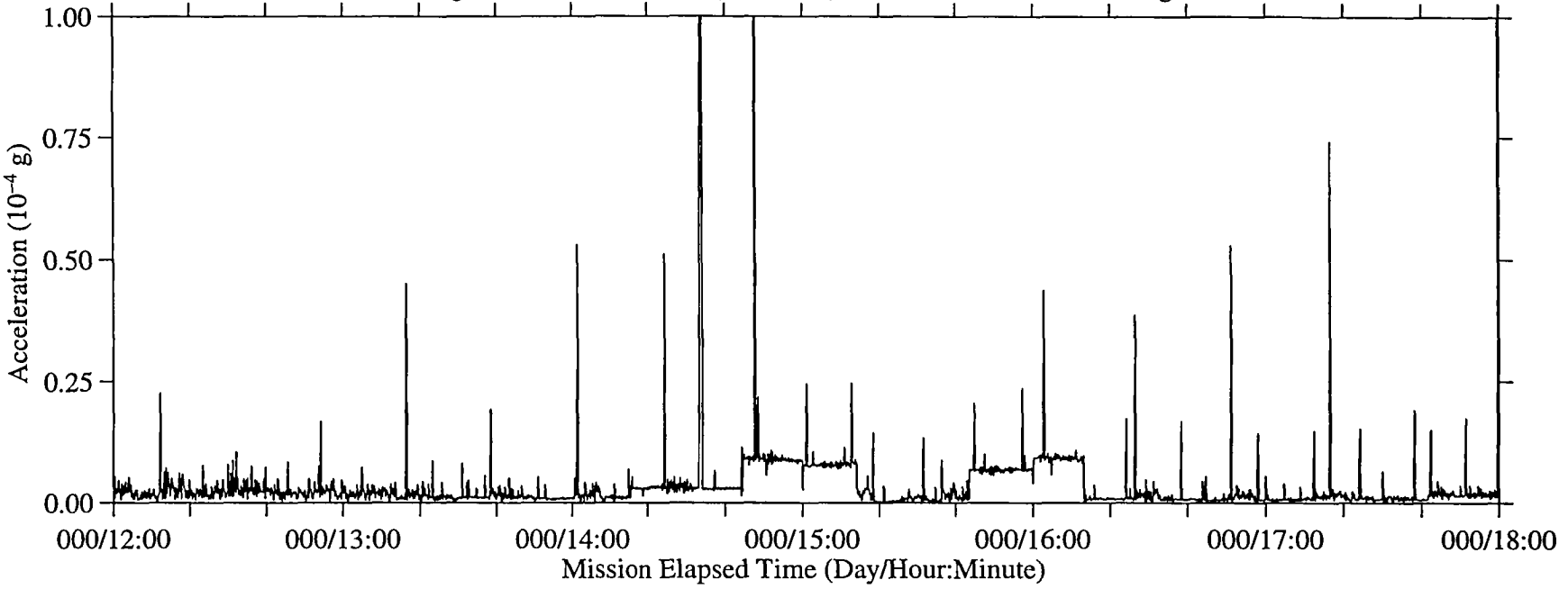

Figure 3b: LMS, Head C (fc=25 Hz), Ten Second Interval RMS

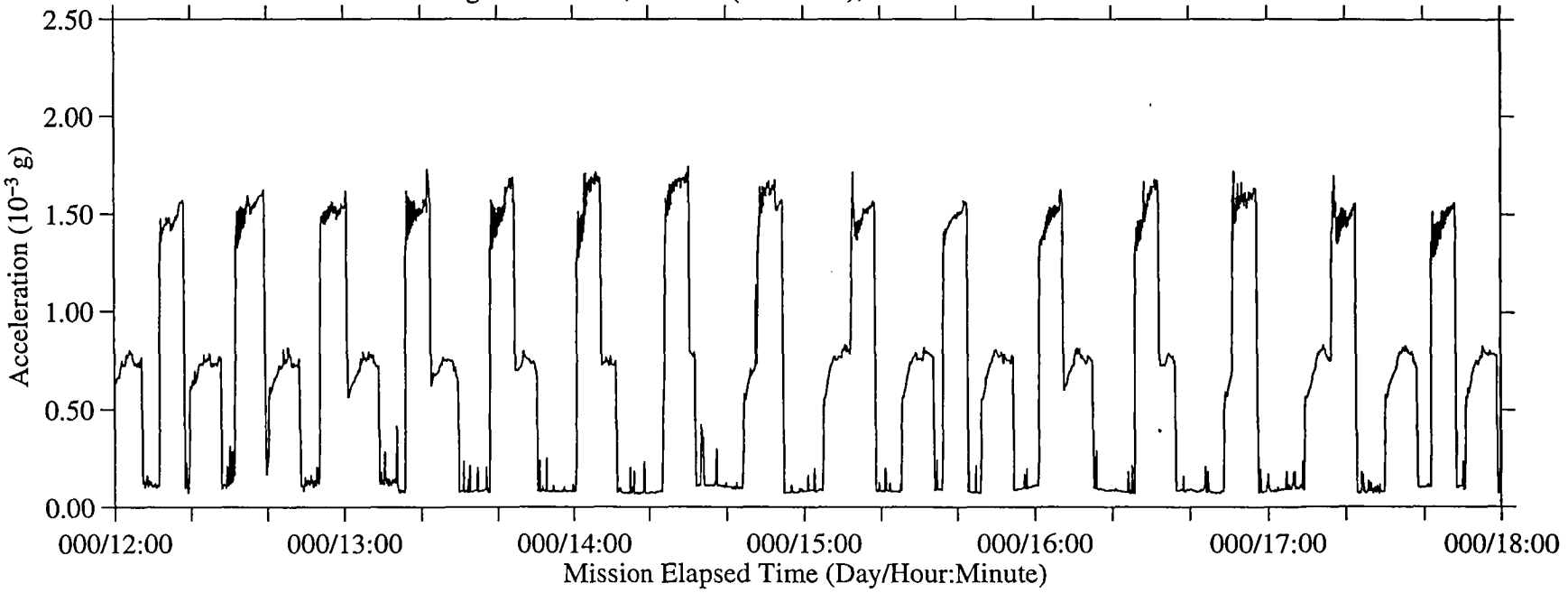

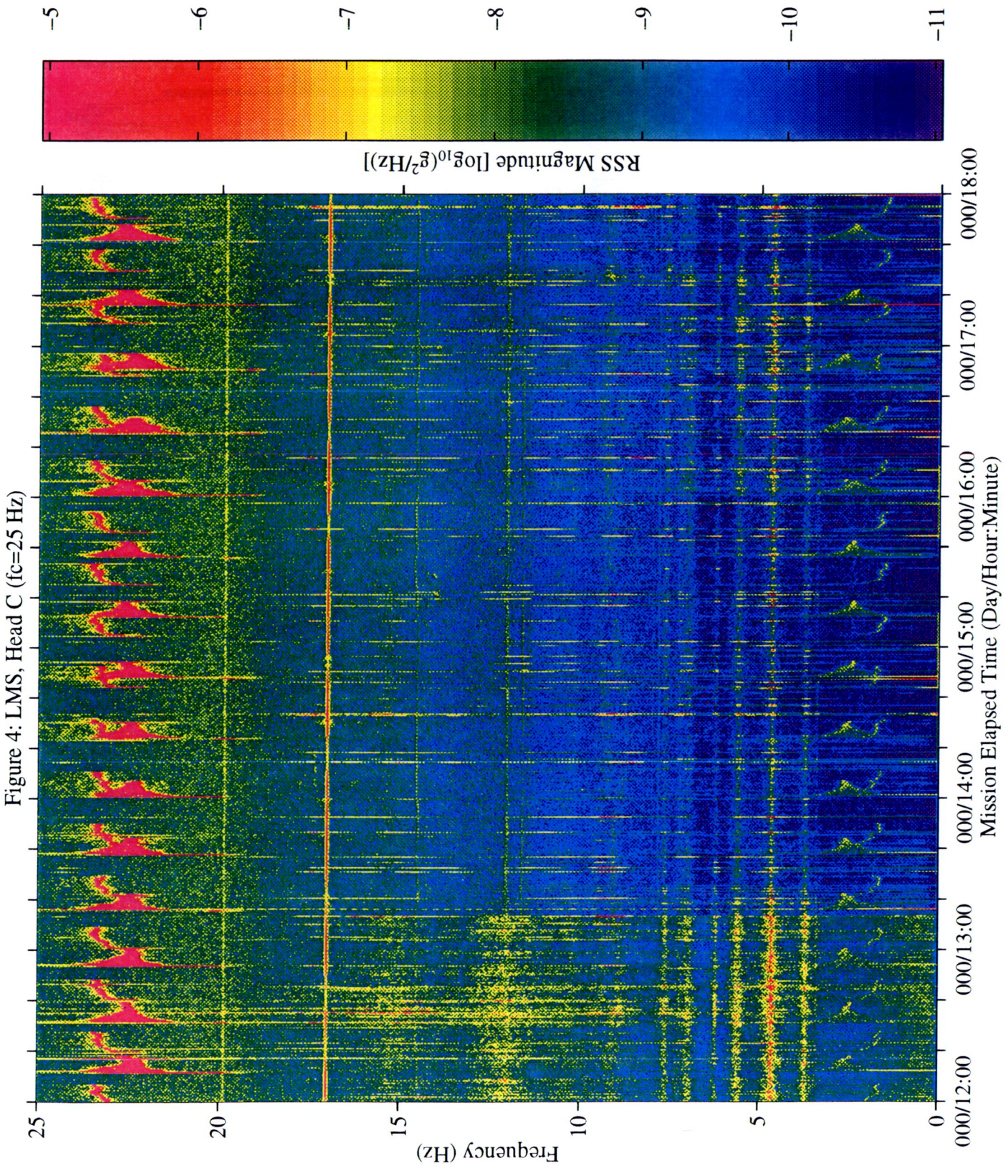

Figure 4: LMS, Head C (fc=25 Hz)

Figure 5a: LMS, Head C (fc=25 Hz), Ten Second Interval Average

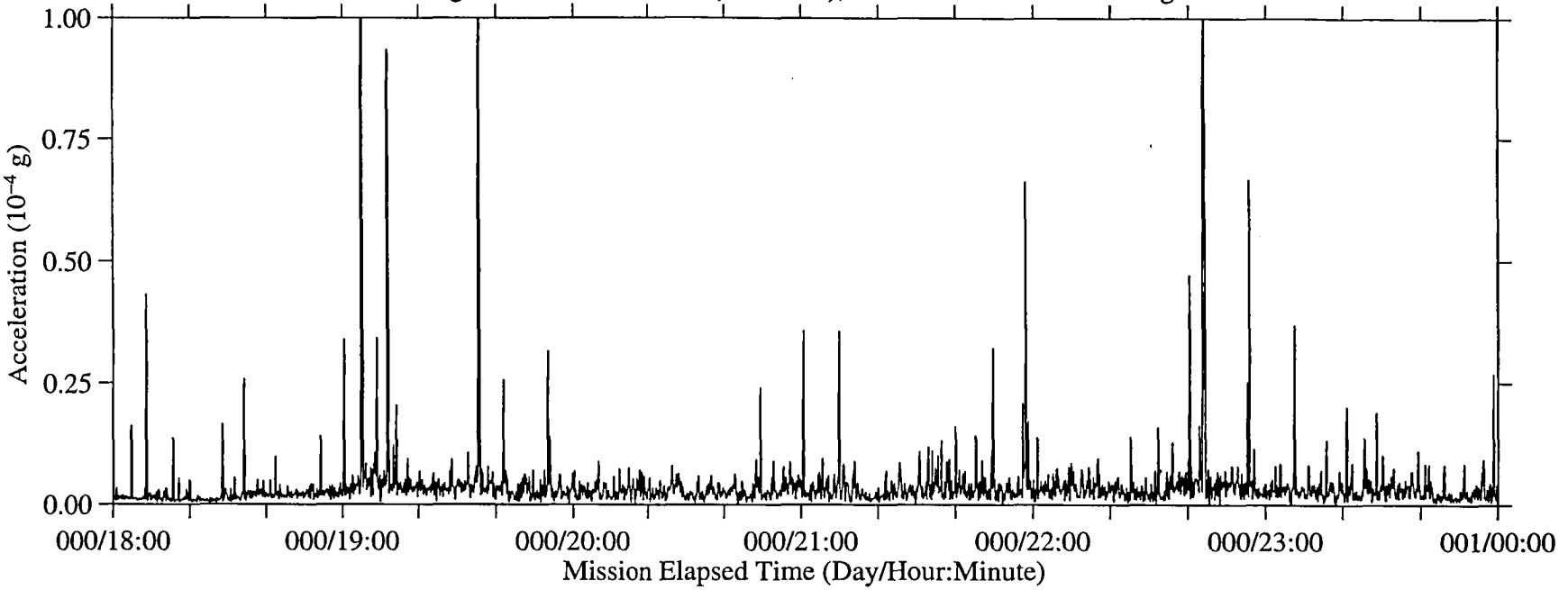

Figure 5b: LMS, Head C (fc=25 Hz), Ten Second Interval RMS

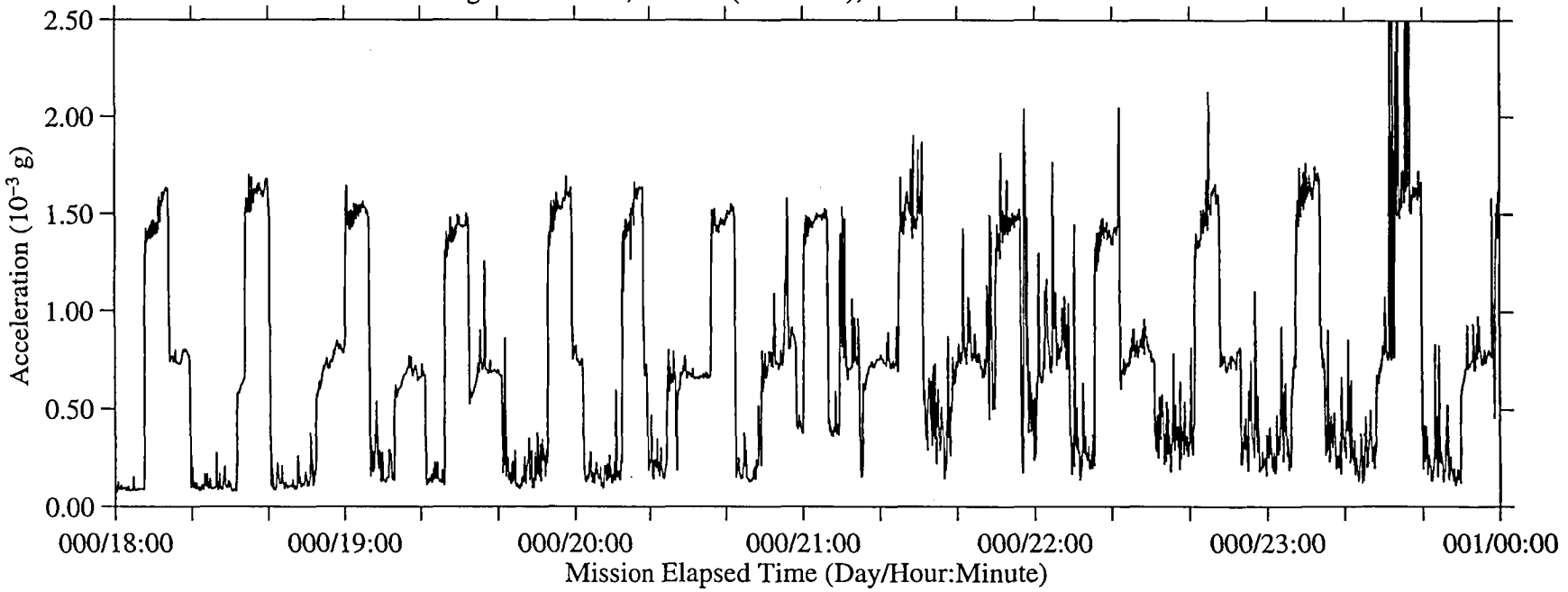

Figure 6: LMS, Head C (fc=25 Hz)

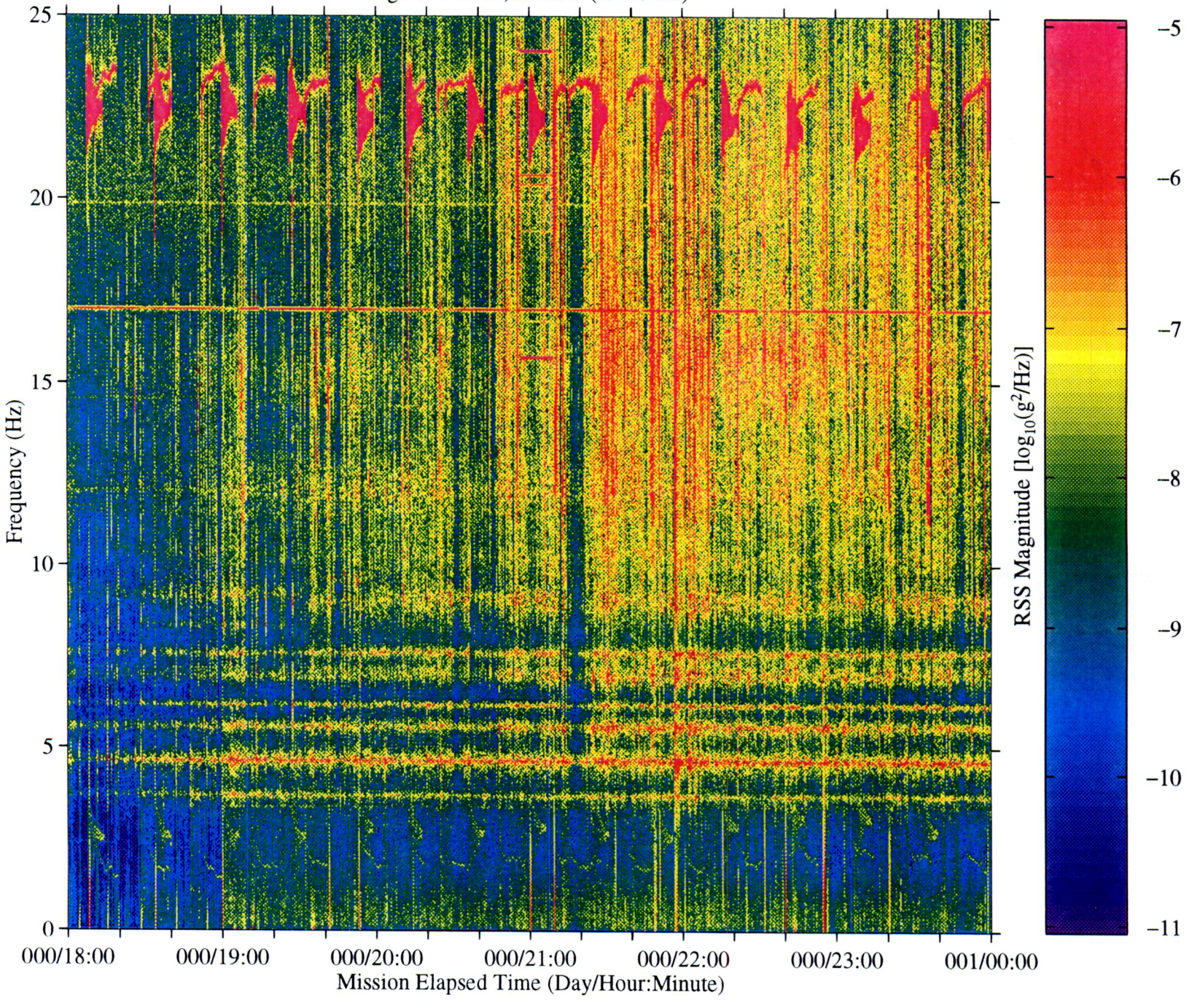

Figure 7a: LMS, Head C (fc=25 Hz), Ten Second Interval Average

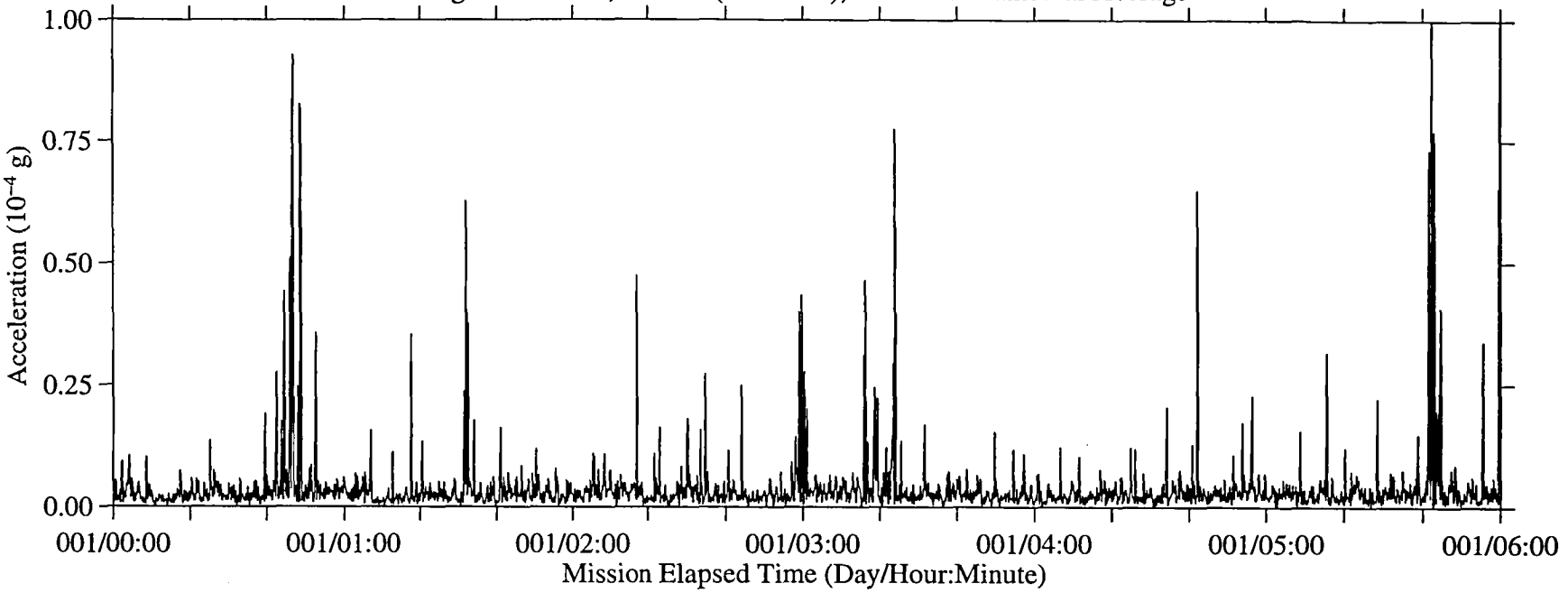

Figure 7b: LMS, Head C (fc=25 Hz), Ten Second Interval RMS

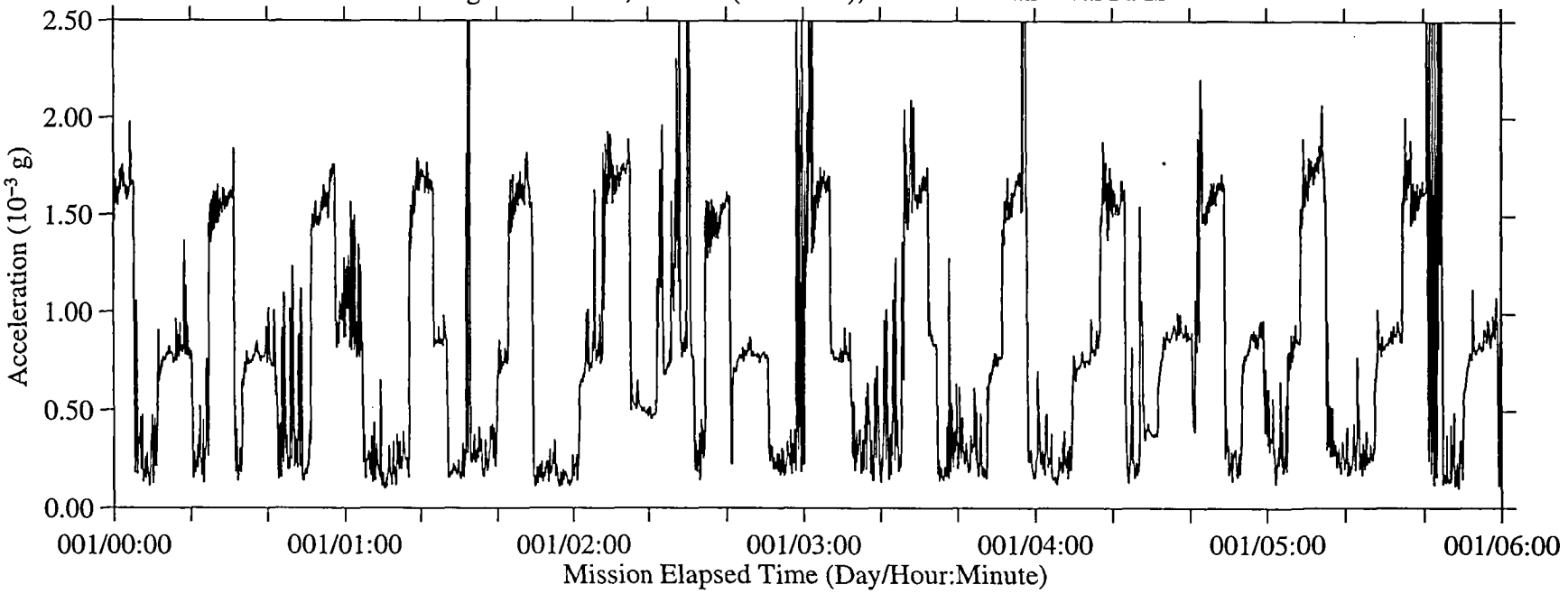

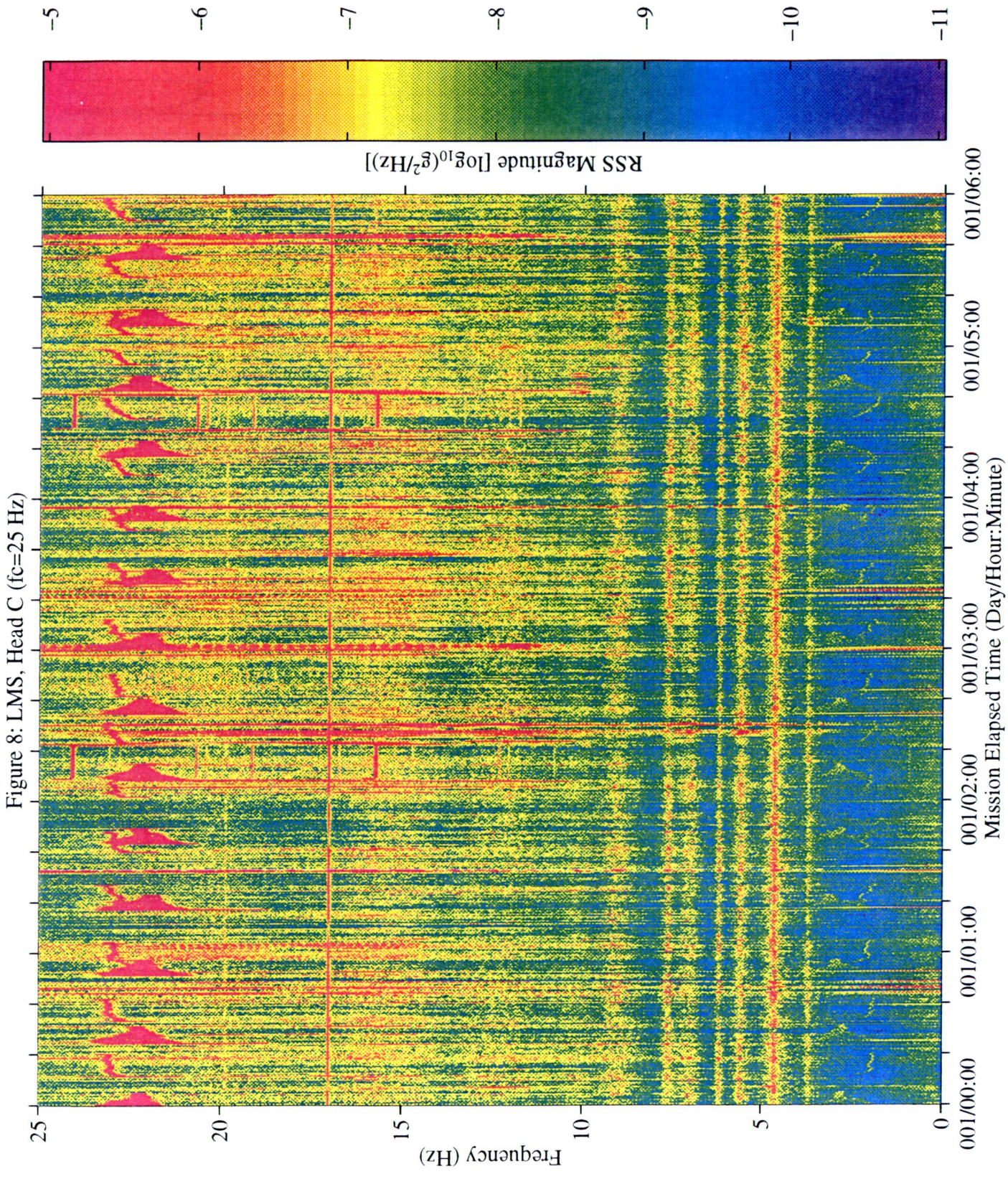

Figure 8: LMS, Head C (fc=25 Hz)

Figure 9a: LMS, Head C (fc=25 Hz), Ten Second Interval Average

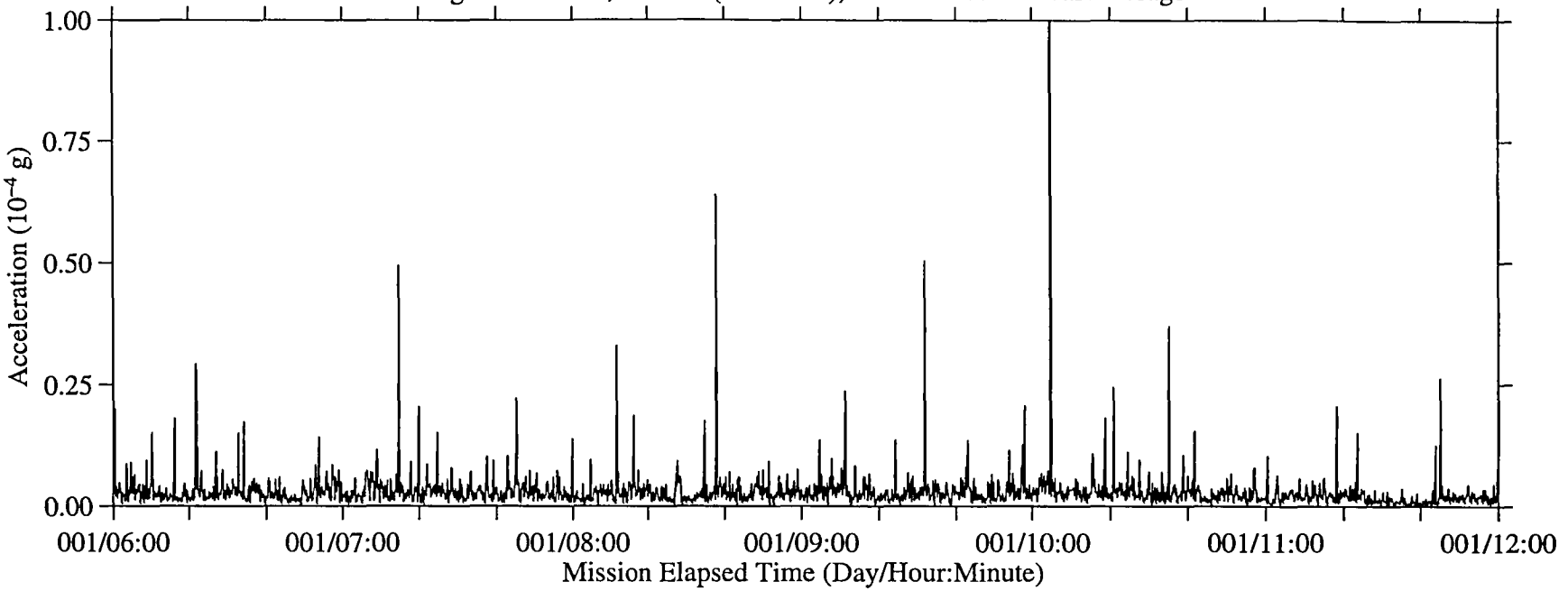

Figure 9b: LMS, Head C (fc=25 Hz), Ten Second Interval RMS

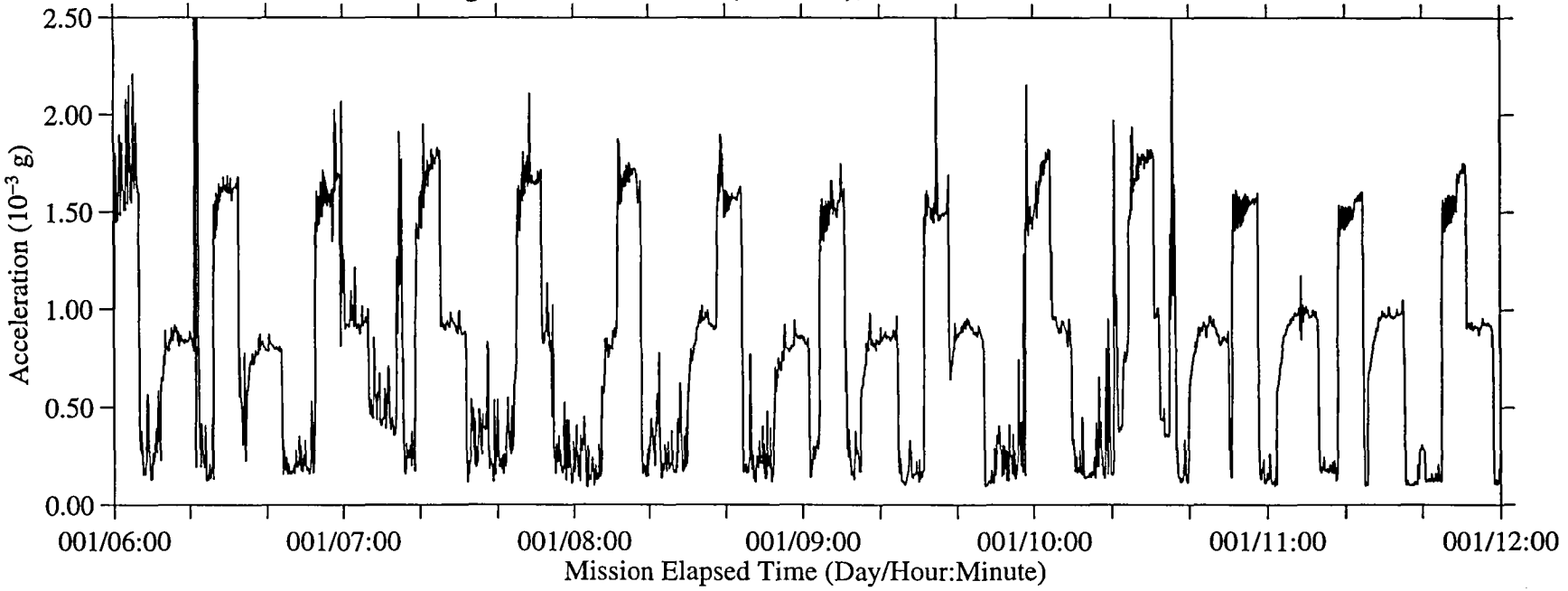

Figure 10: LMS, Head C (fc=25 Hz)

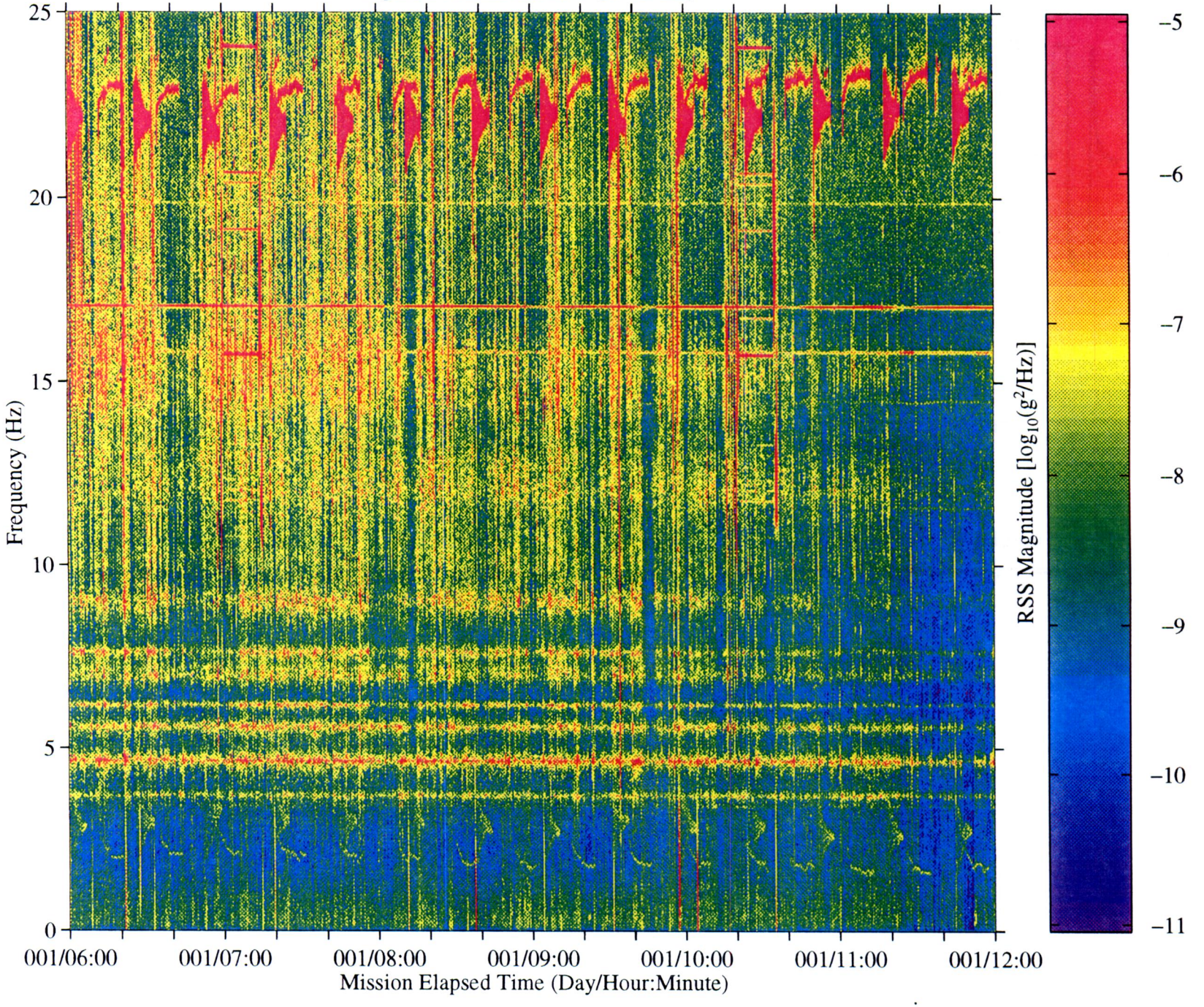

Figure 11a: LMS, Head C (fc=25 Hz), Ten Second Interval Average

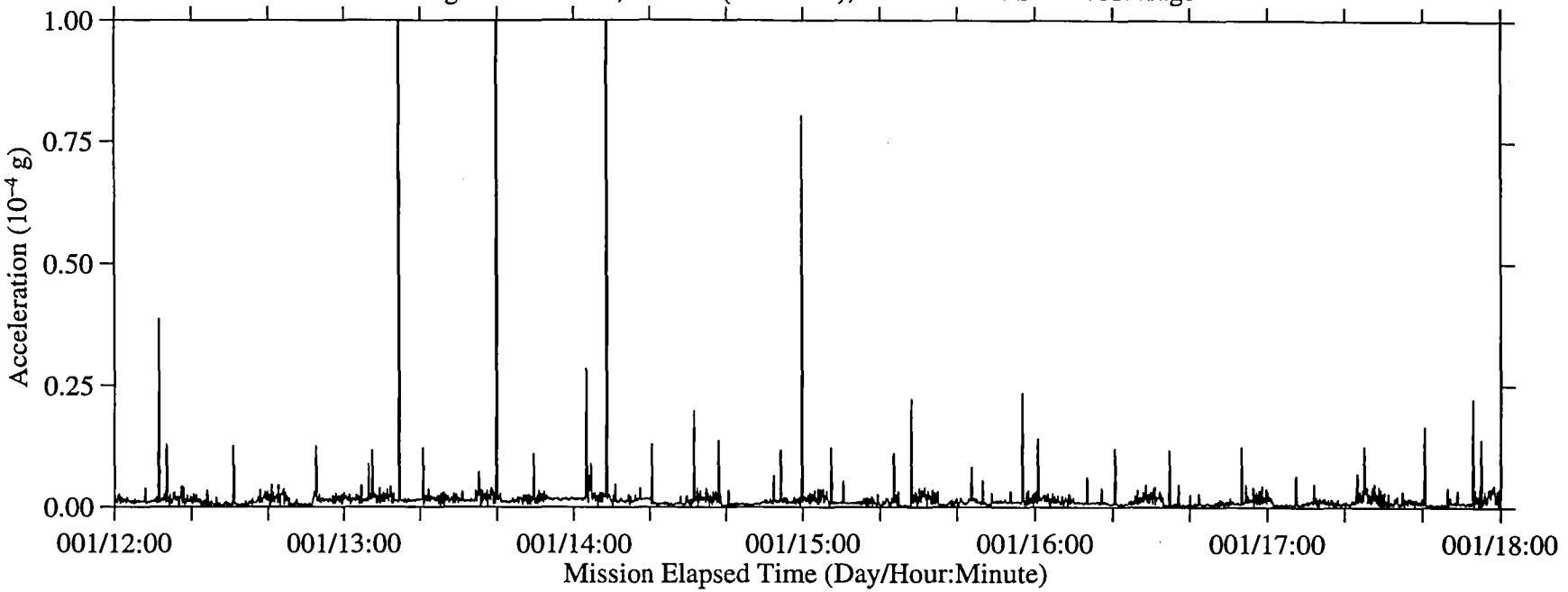

Figure 11b: LMS, Head C (fc=25 Hz), Ten Second Interval RMS

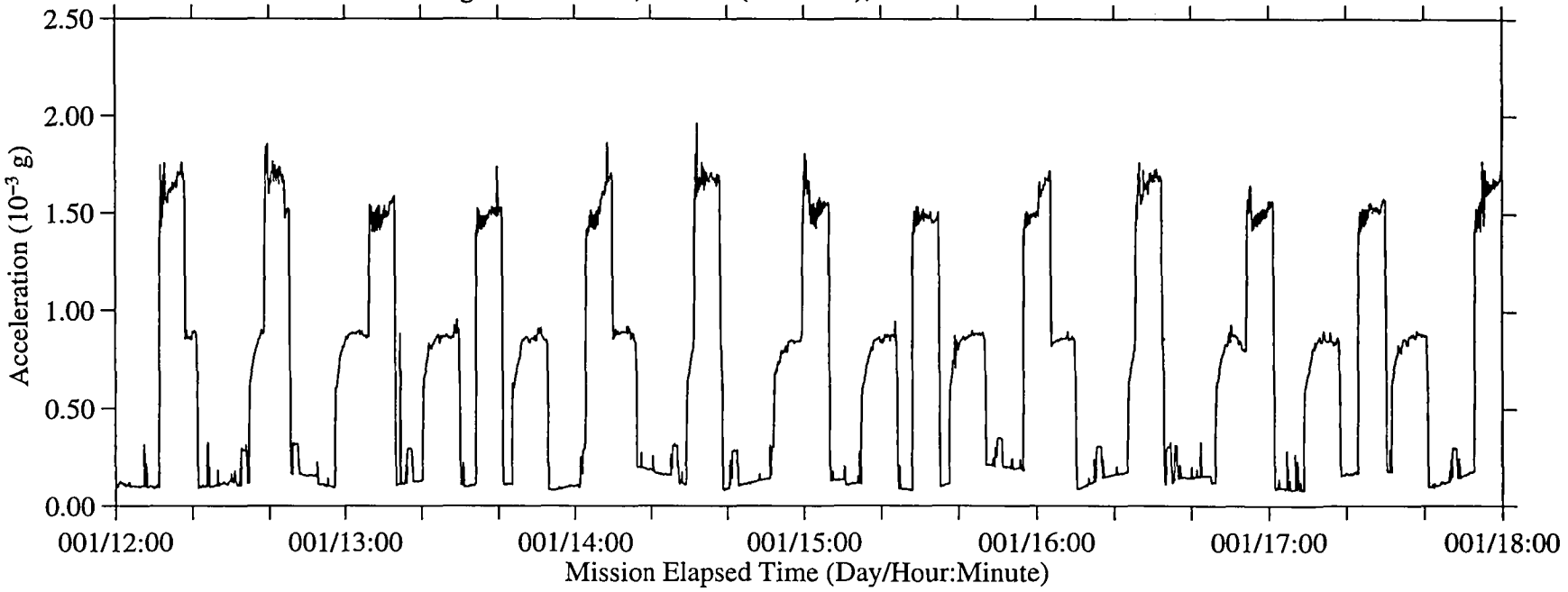

Figure 12: LMS, Head C (fc=25 Hz)

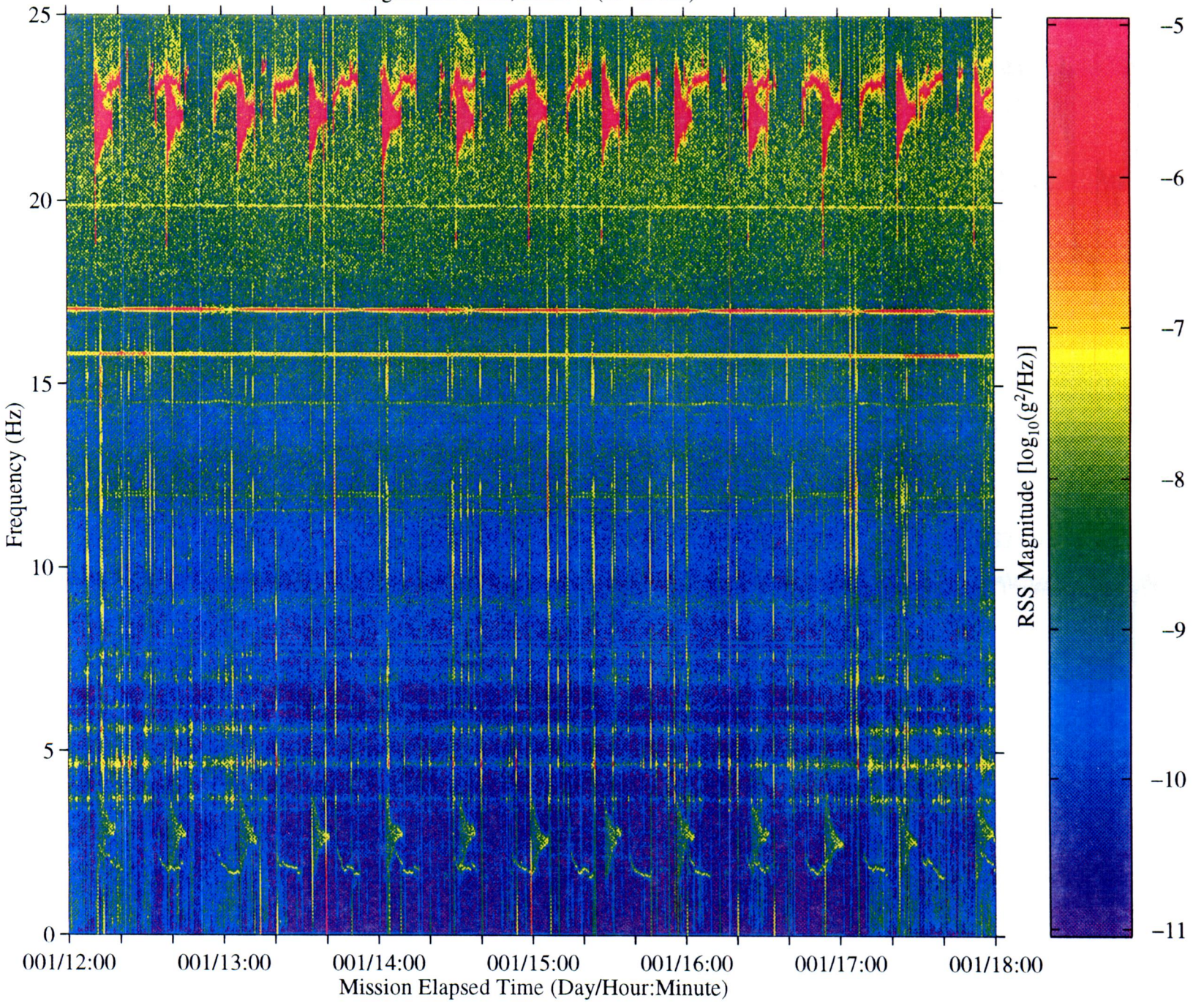

Figure 13a: LMS, Head C (fc=25 Hz), Ten Second Interval Average

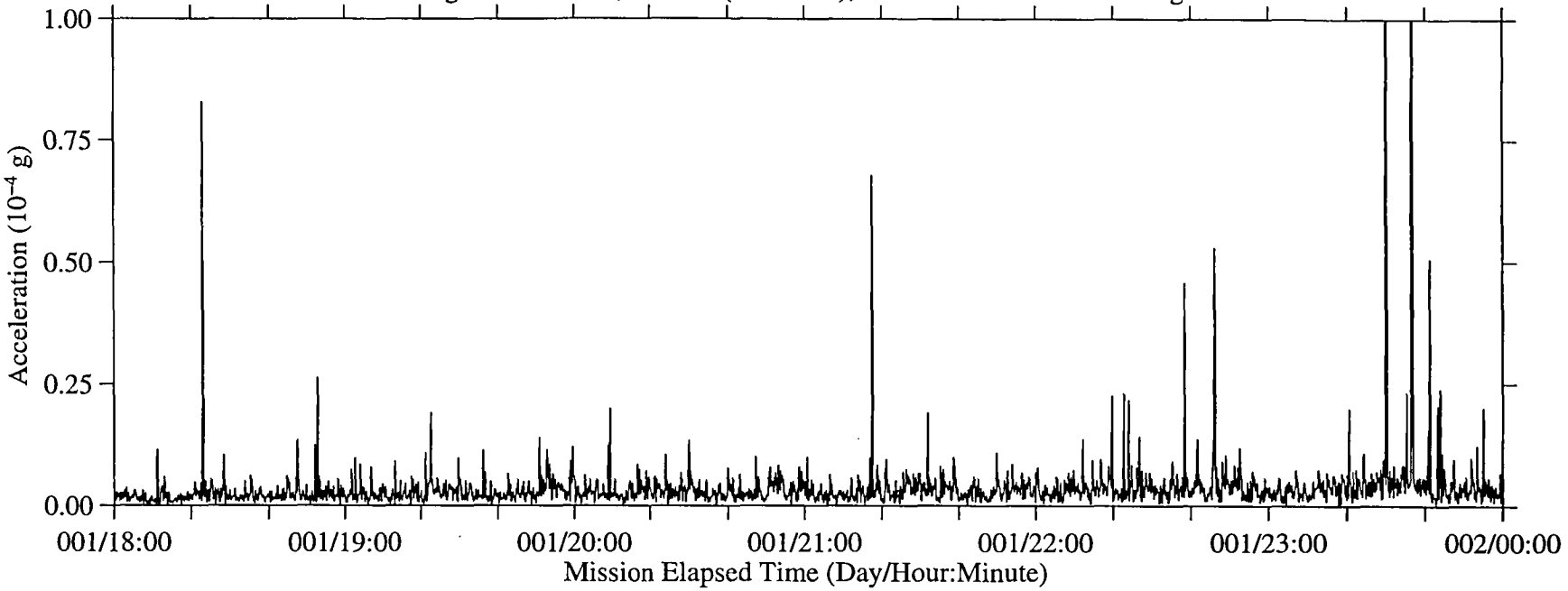

Figure 13b: LMS, Head C (fc=25 Hz), Ten Second Interval RMS

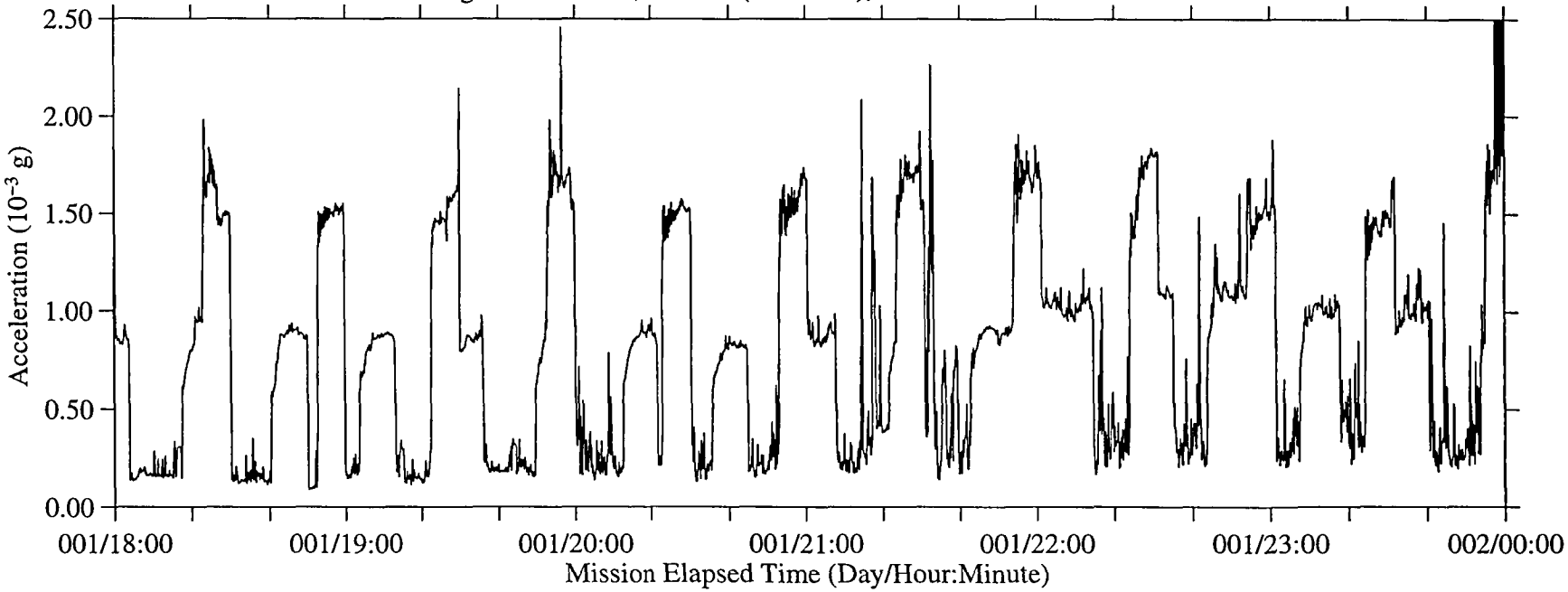

Figure 14: LMS, Head C (fc=25 Hz)

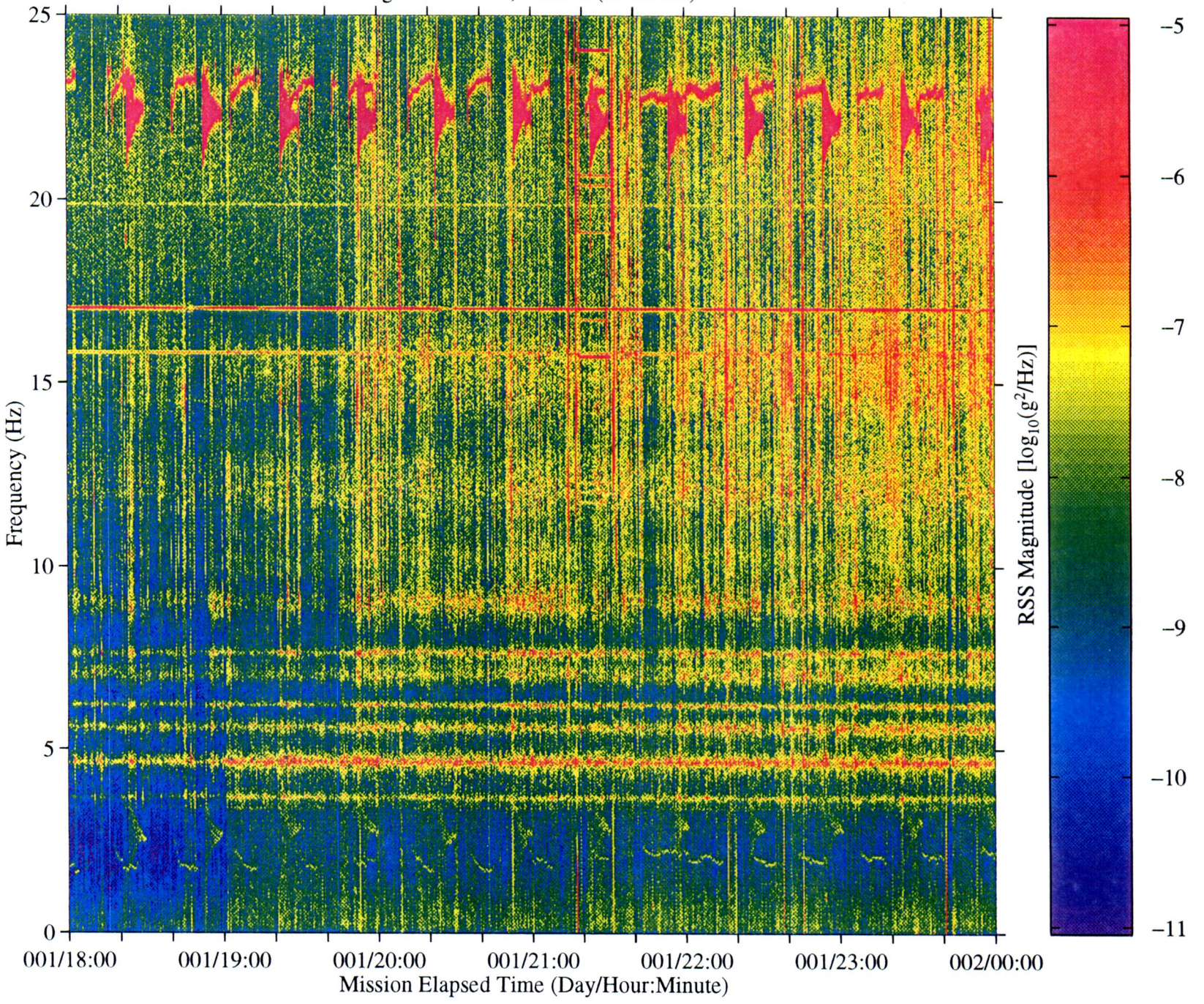

Figure 15a: LMS, Head C (fc=25 Hz), Ten Second Interval Average

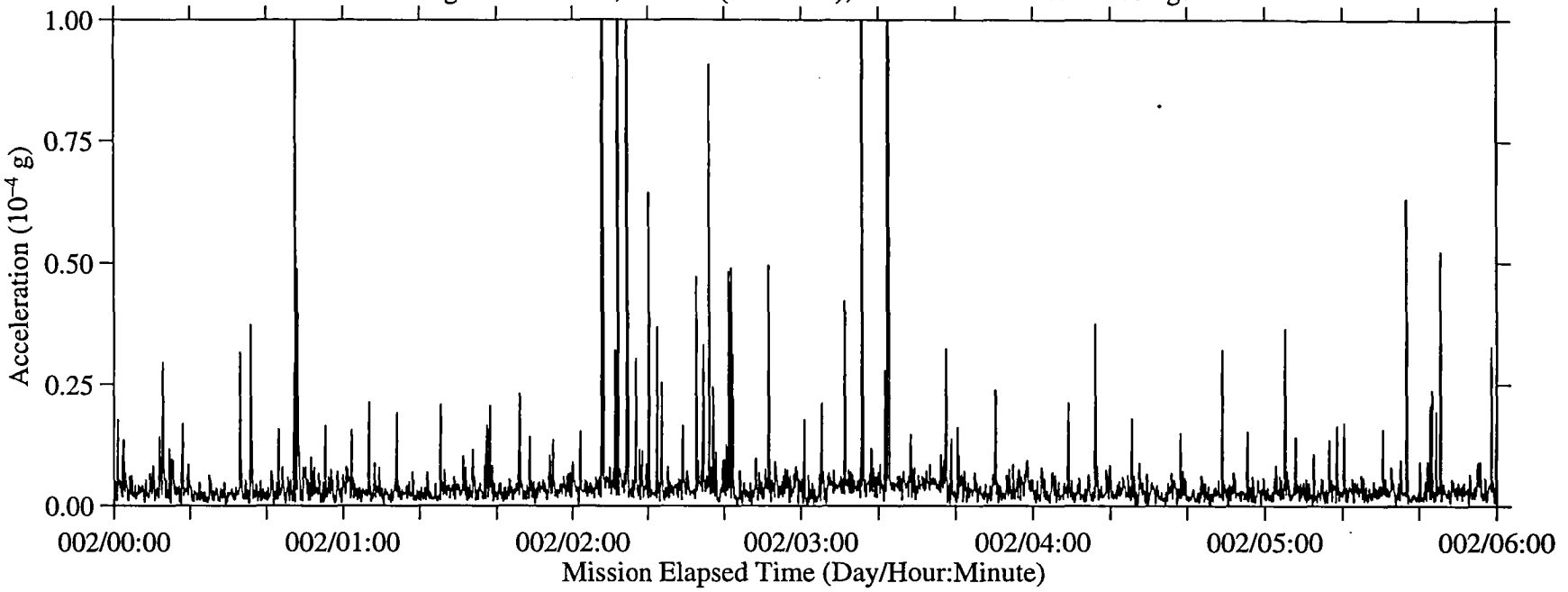

Figure 15b: LMS, Head C (fc=25 Hz), Ten Second Interval RMS

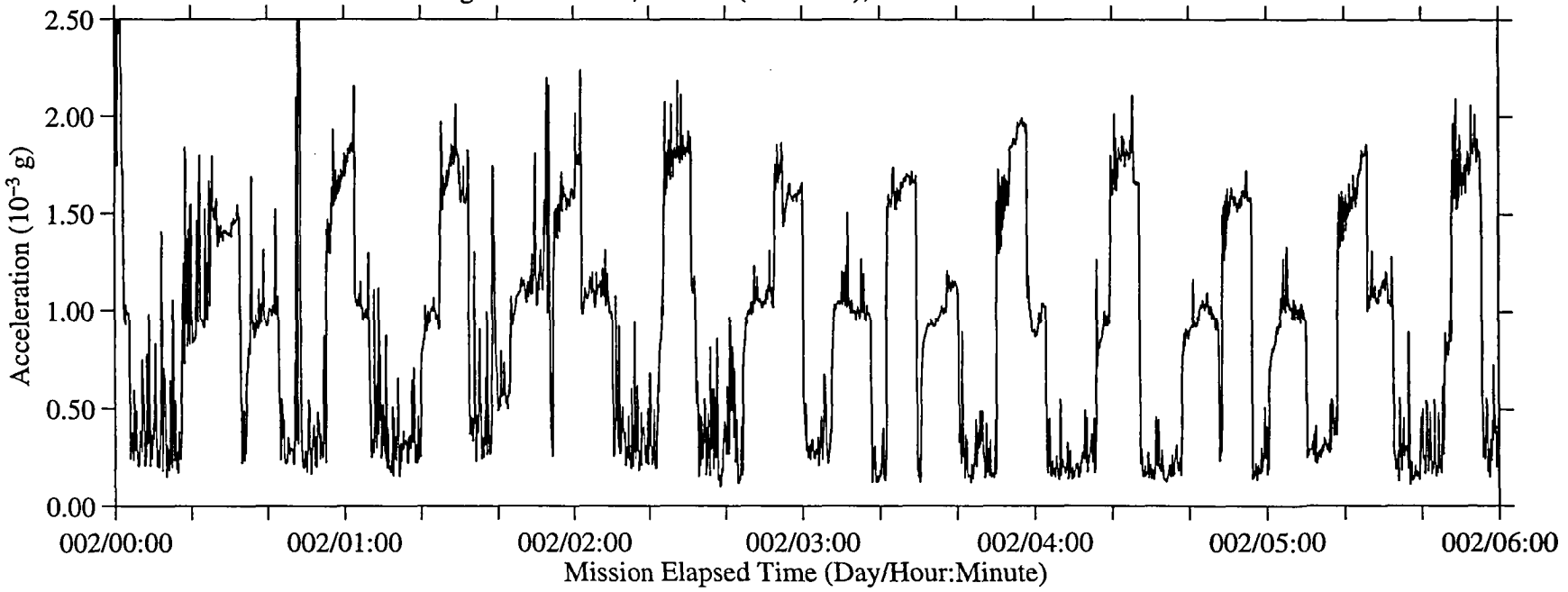

Figure 16: LMS, Head C (fc=25 Hz)

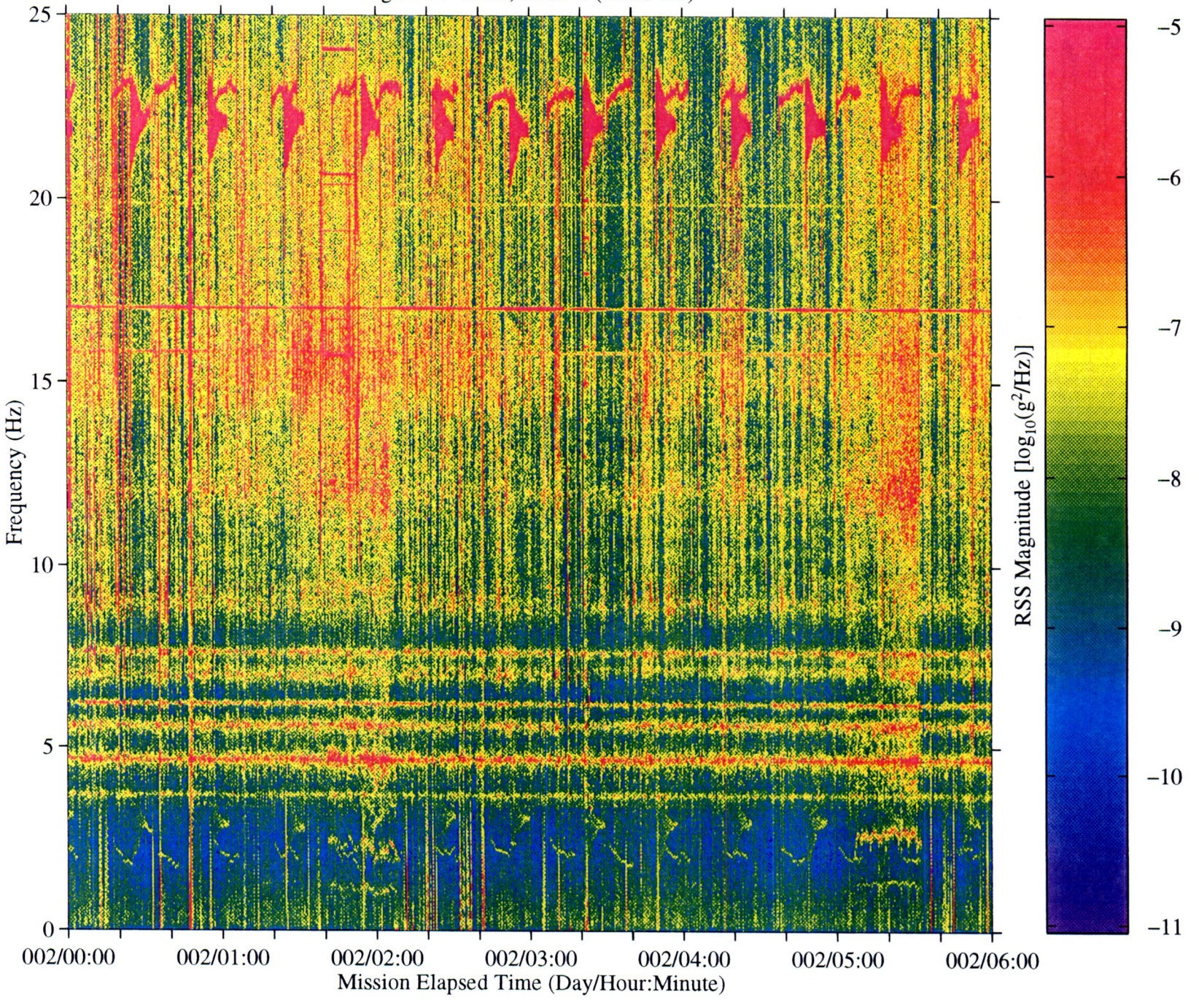

Figure 17a: LMS, Head C (fc=25 Hz), Ten Second Interval Average

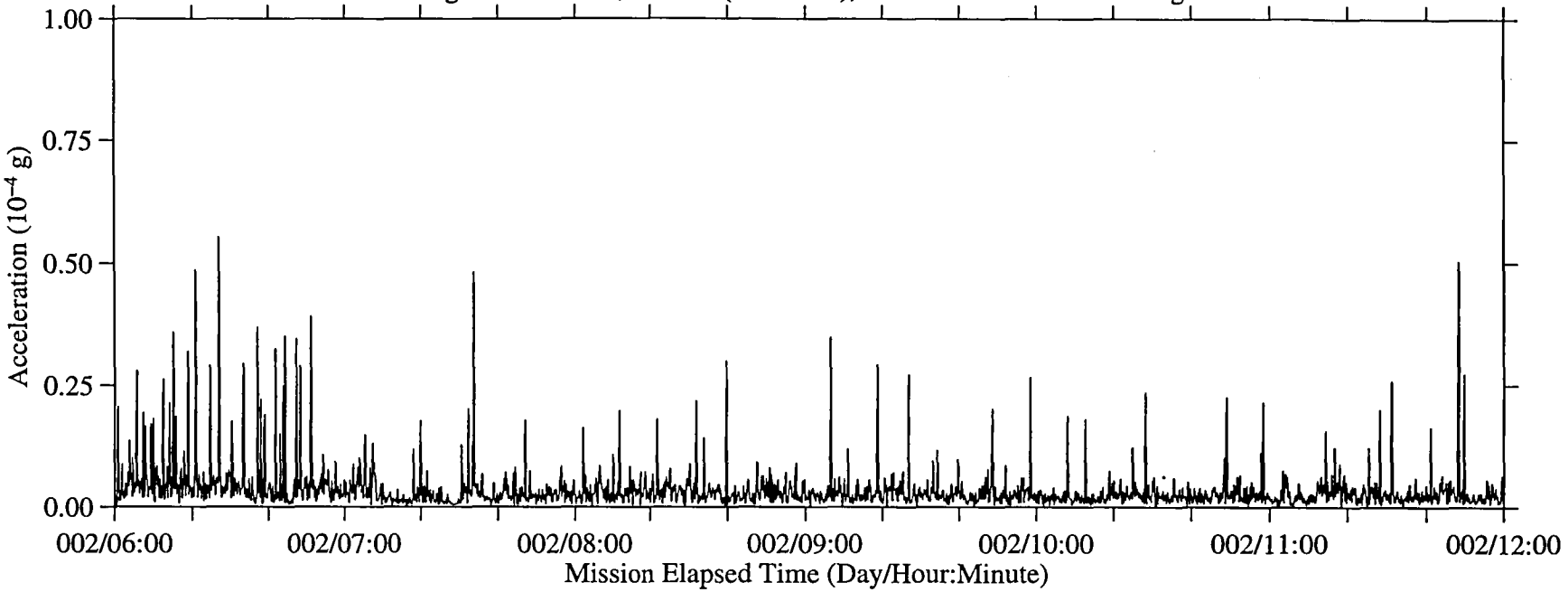

Figure 17b: LMS, Head C (fc=25 Hz), Ten Second Interval RMS

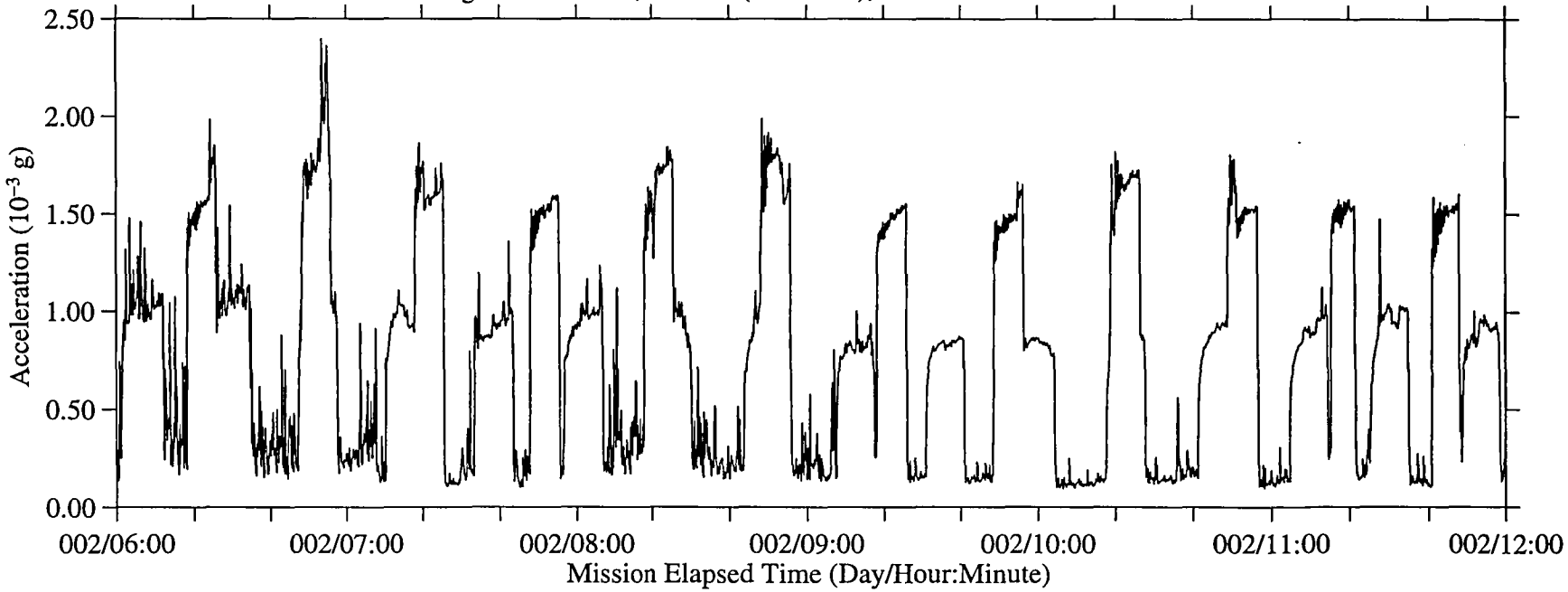

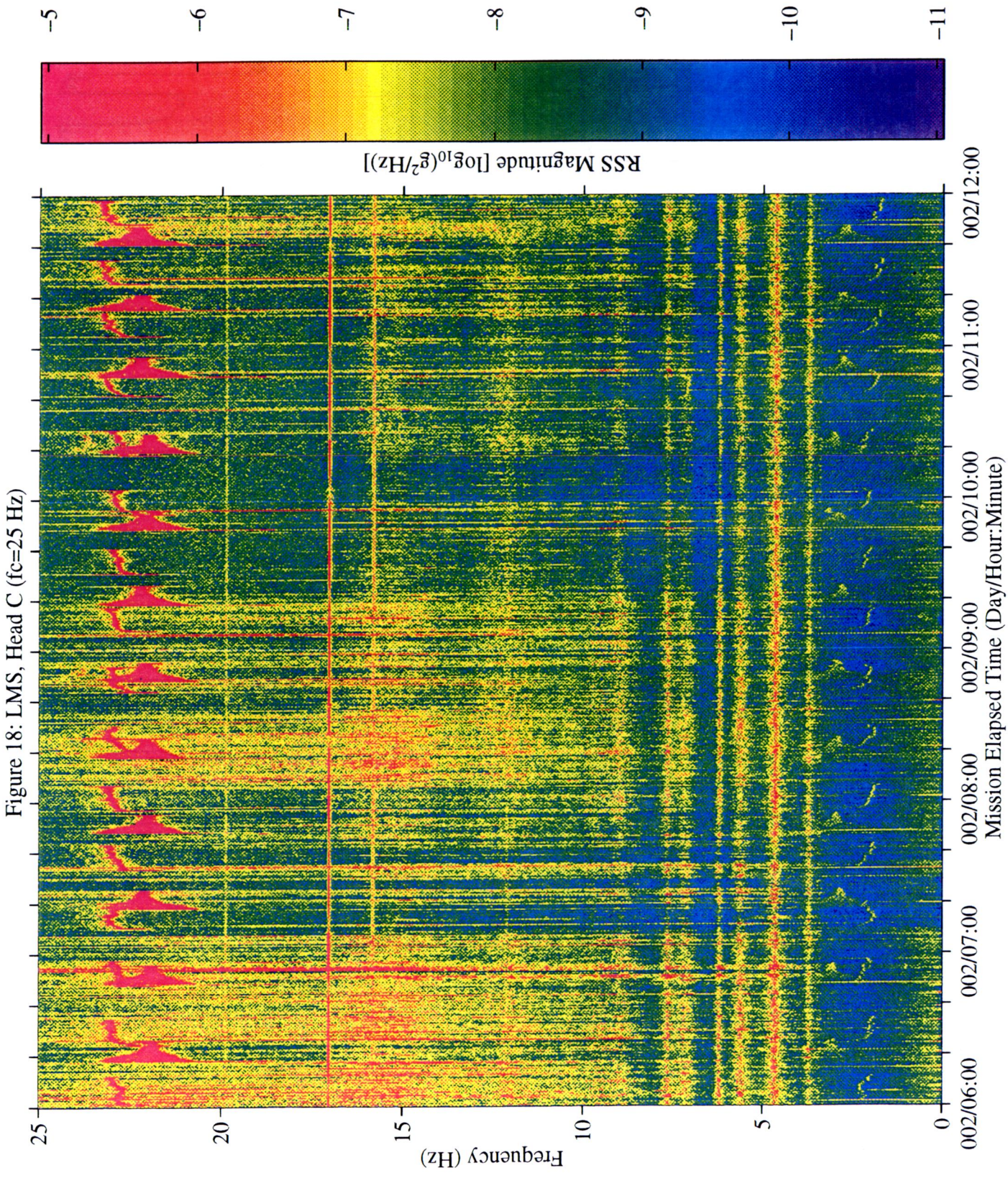

Figure 18: LMS, Head C (fc=25 Hz)

Figure 19a: LMS, Head C (fc=25 Hz), Ten Second Interval Average

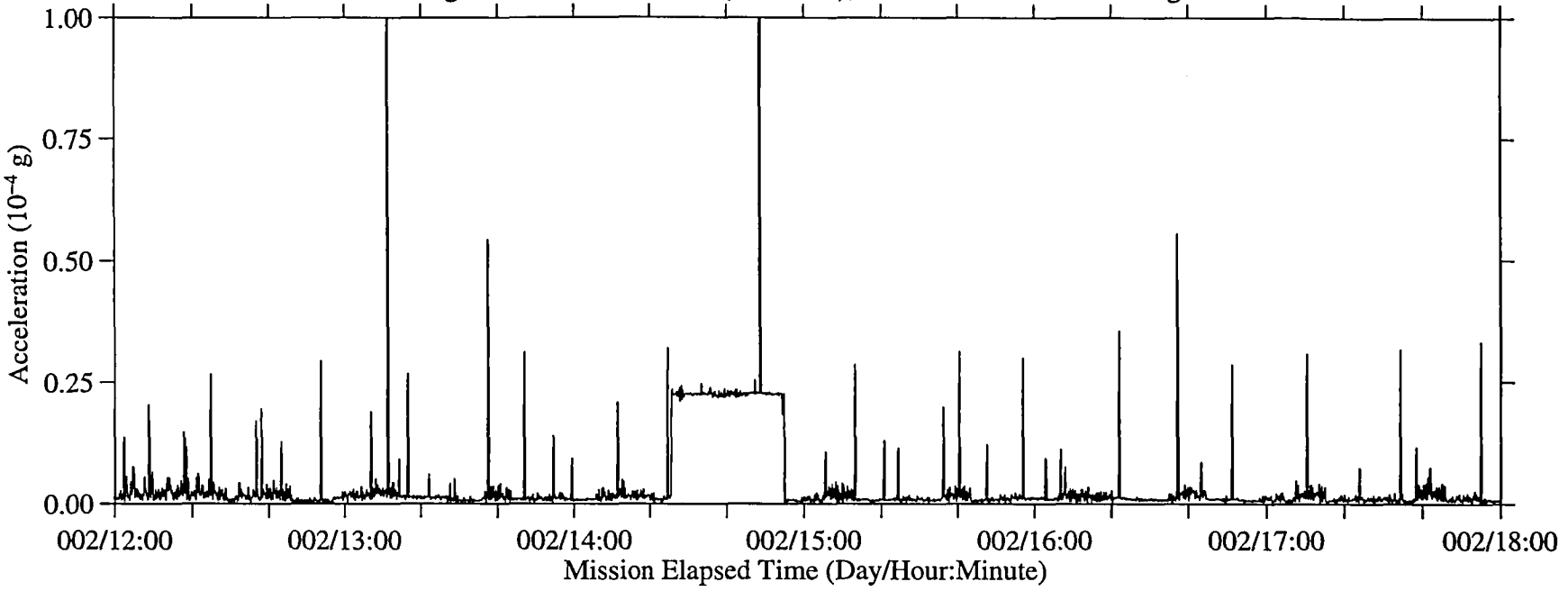

Figure 19b: LMS, Head C (fc=25 Hz), Ten Second Interval RMS

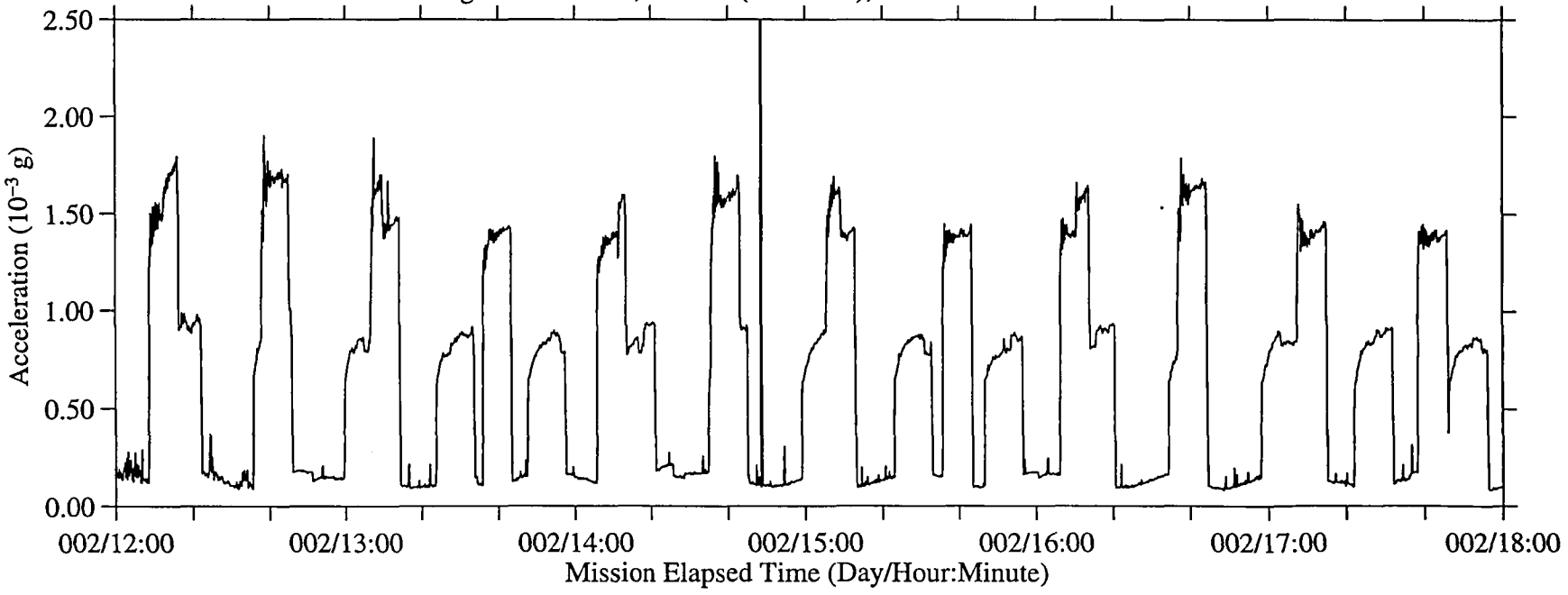

Figure 20: LMS, Head C (fc=25 Hz)

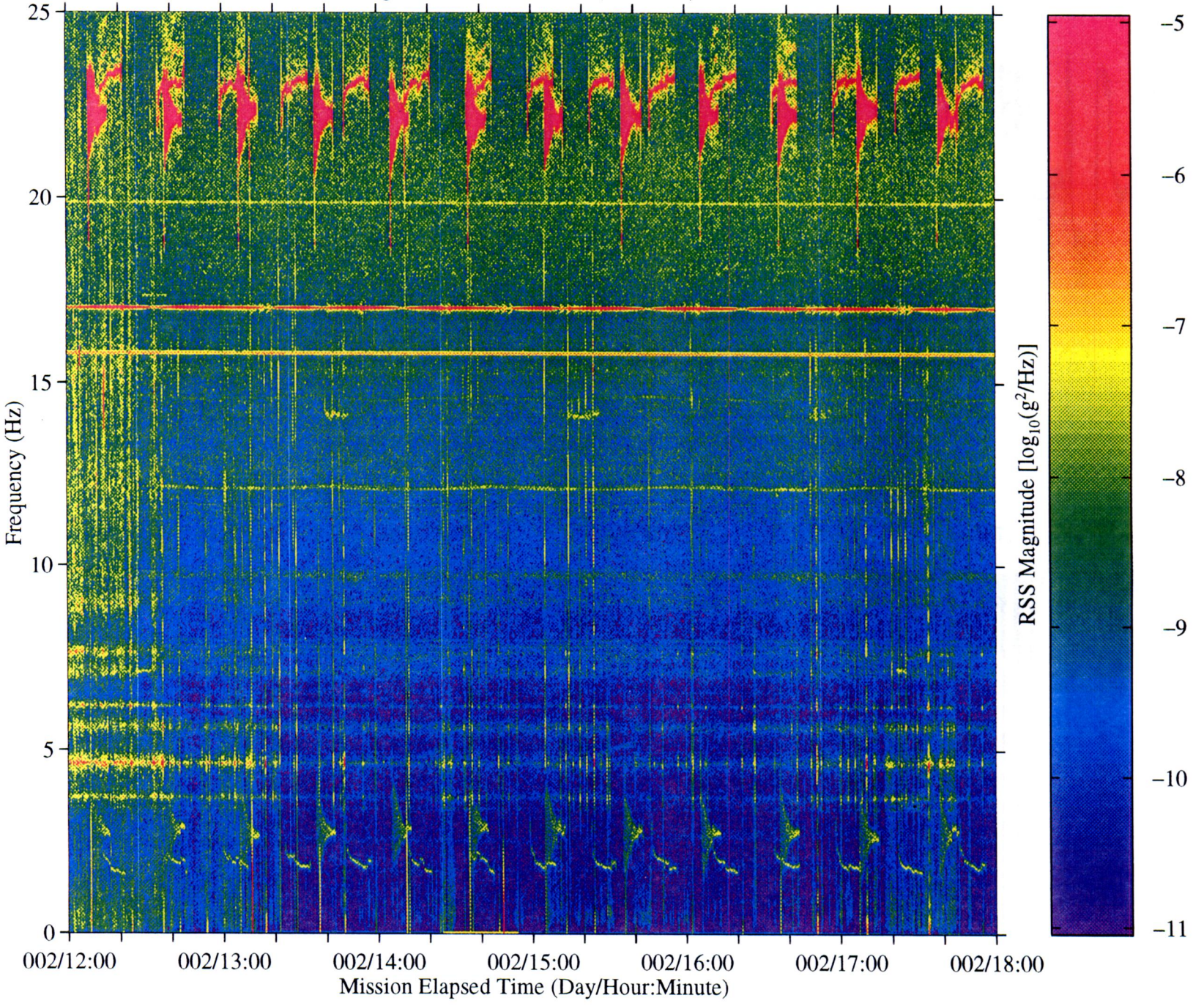

Figure 21a: LMS, Head C (fc=25 Hz), Ten Second Interval Average

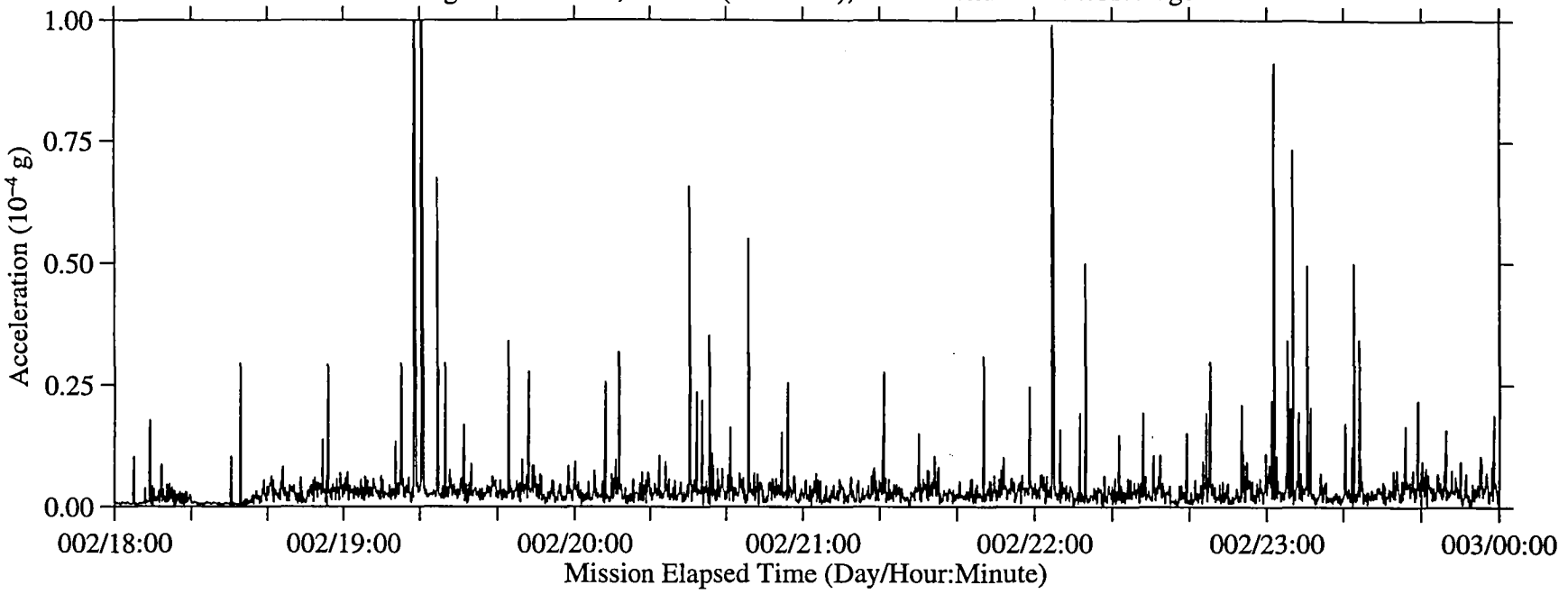

Figure 21b: LMS, Head C (fc=25 Hz), Ten Second Interval RMS

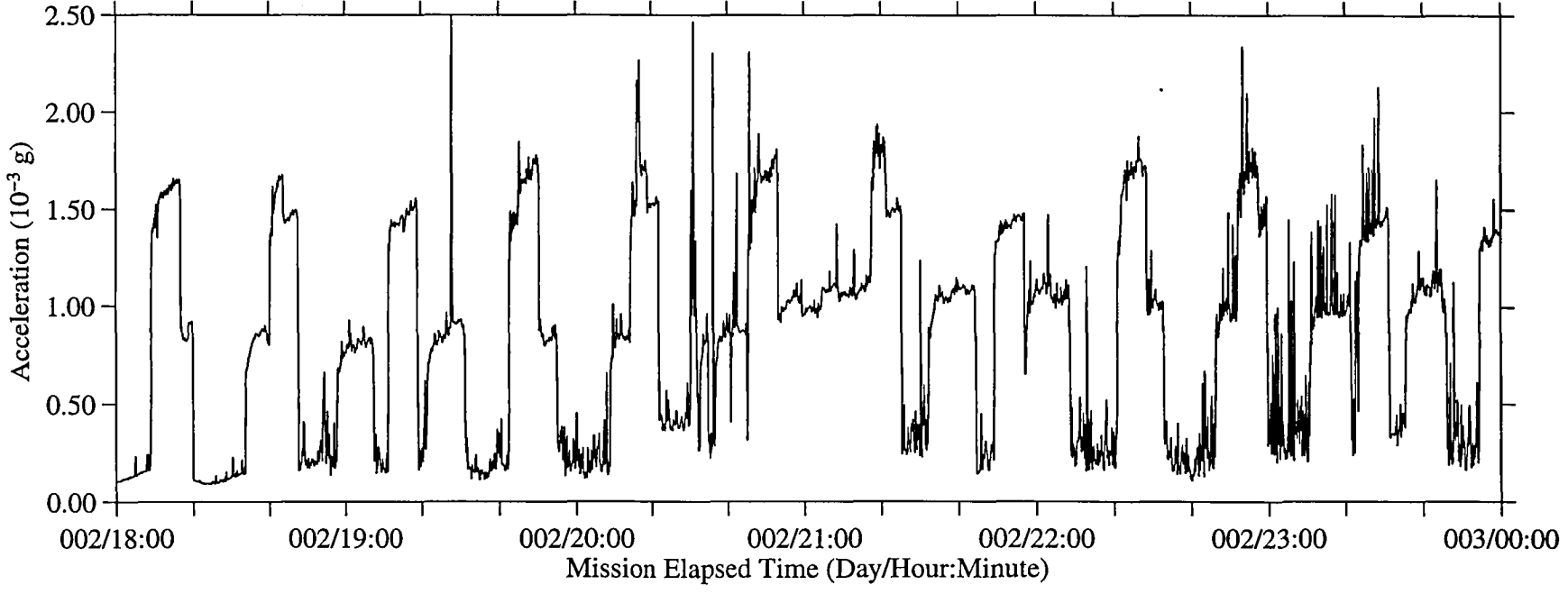

Figure 22: LMS, Head C (fc=25 Hz)

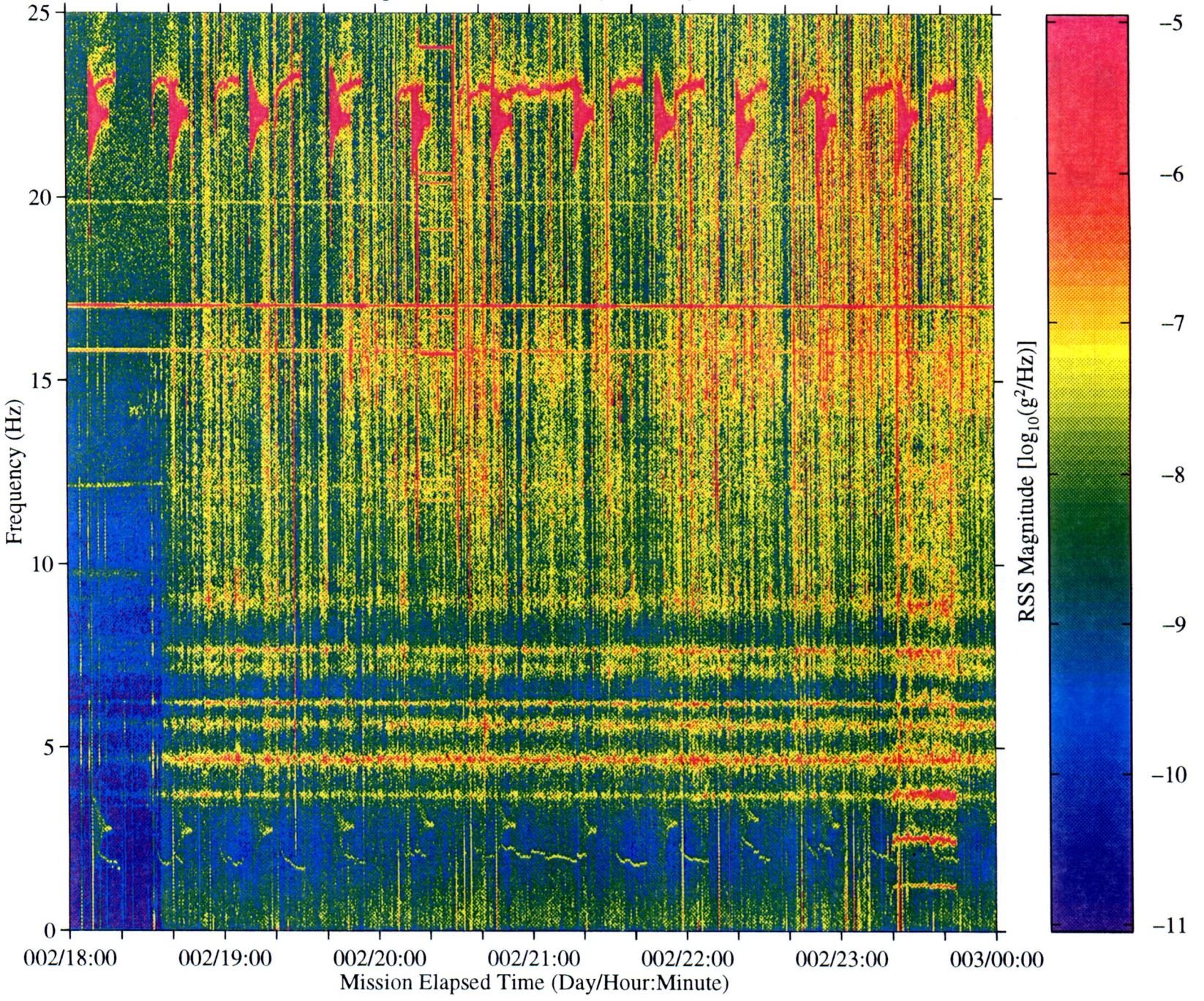

Figure 23a: LMS, Head C (fc=25 Hz), Ten Second Interval Average

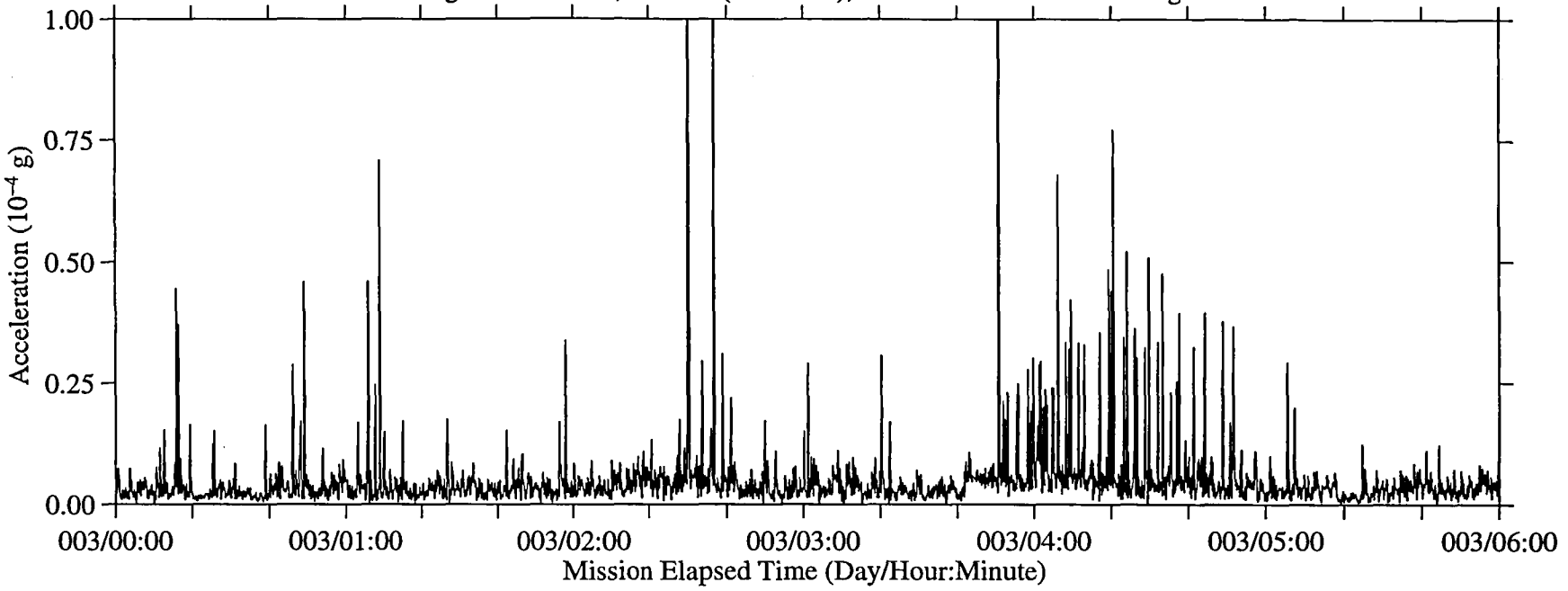

Figure 23b: LMS, Head C (fc=25 Hz), Ten Second Interval RMS

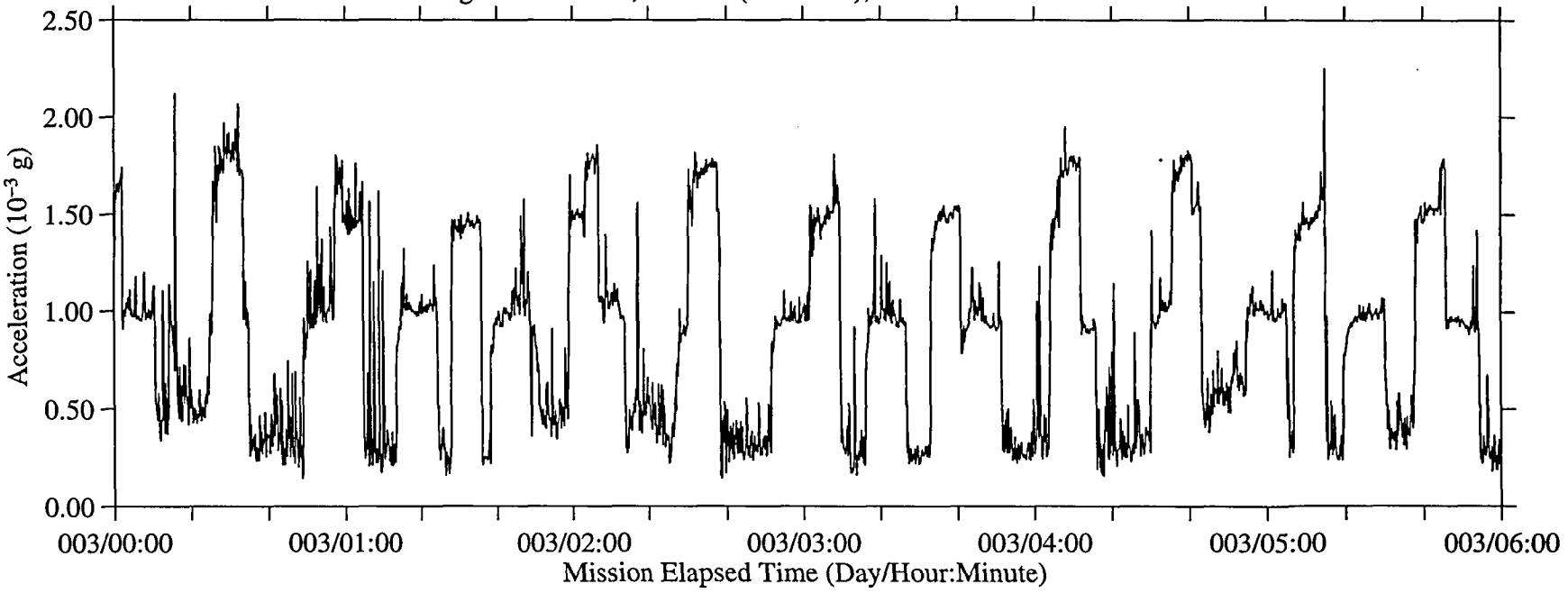

Figure 24: LMS, Head C (fc=25 Hz)

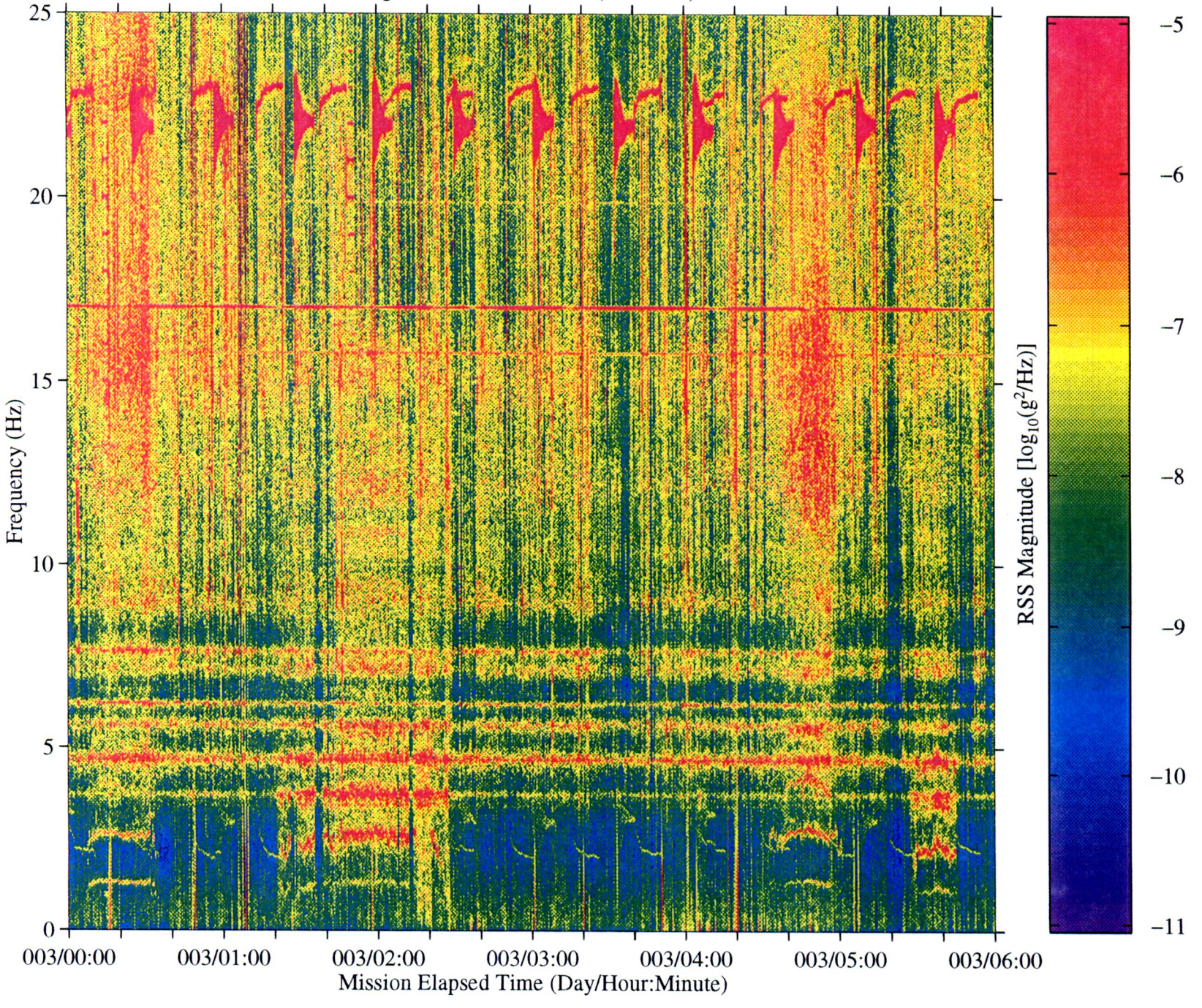

Figure 25a: LMS, Head C (fc=25 Hz), Ten Second Interval Average

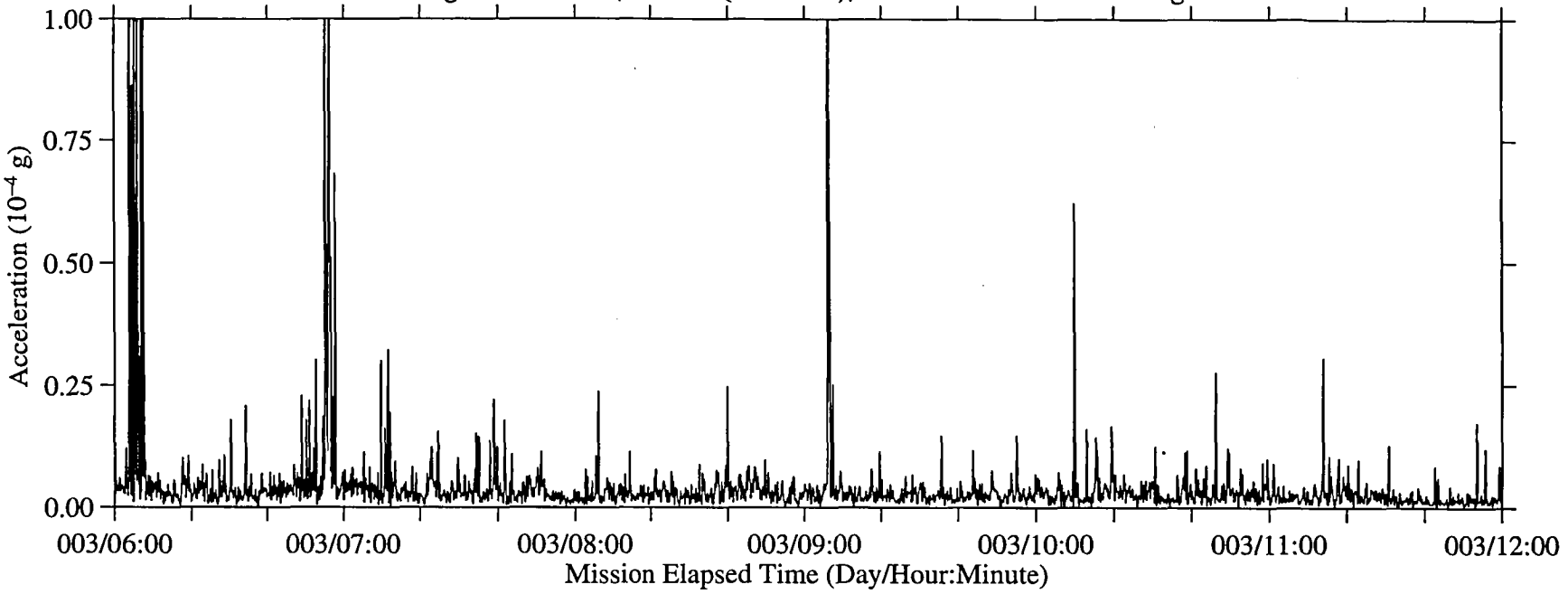

Figure 25b: LMS, Head C (fc=25 Hz), Ten Second Interval RMS

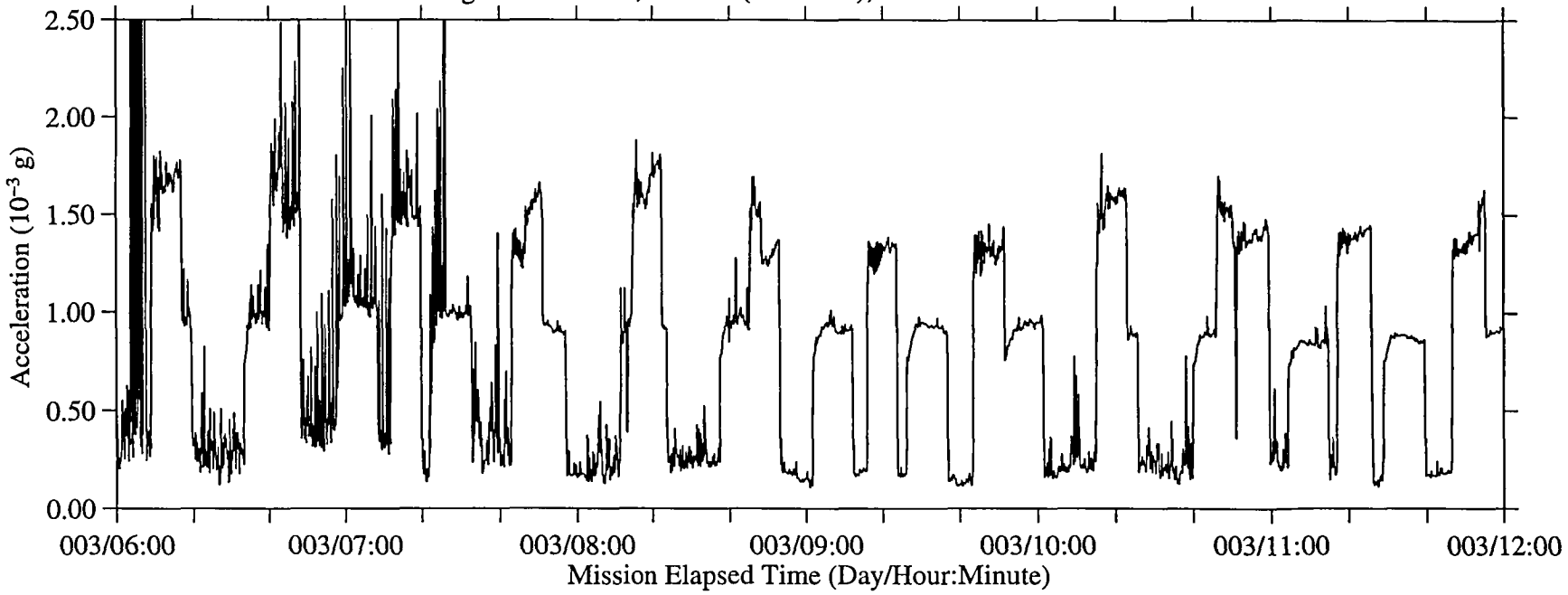

Figure 26: LMS, Head C (fc=25 Hz)

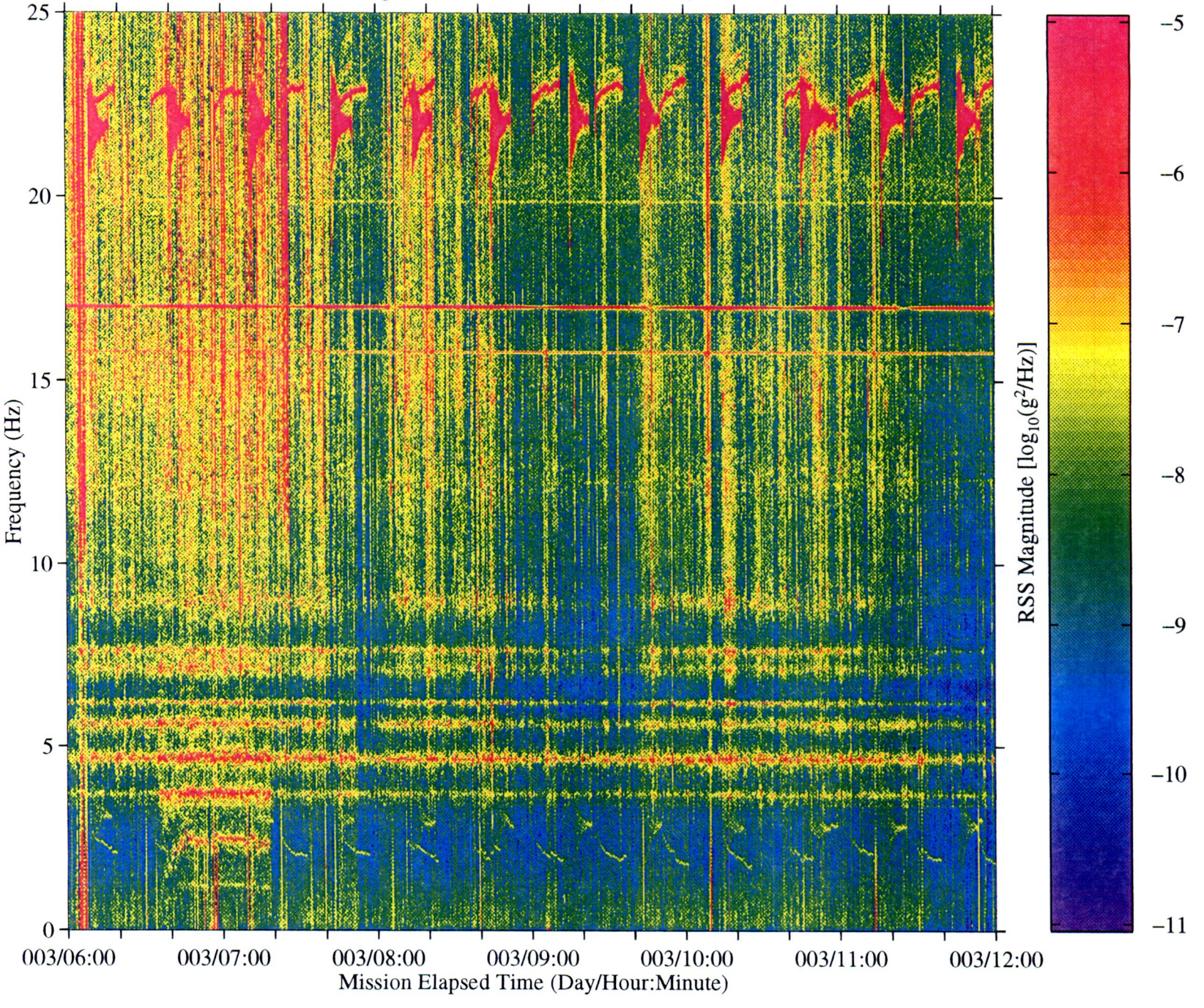

Figure 27a: LMS, Head C (fc=25 Hz), Ten Second Interval Average

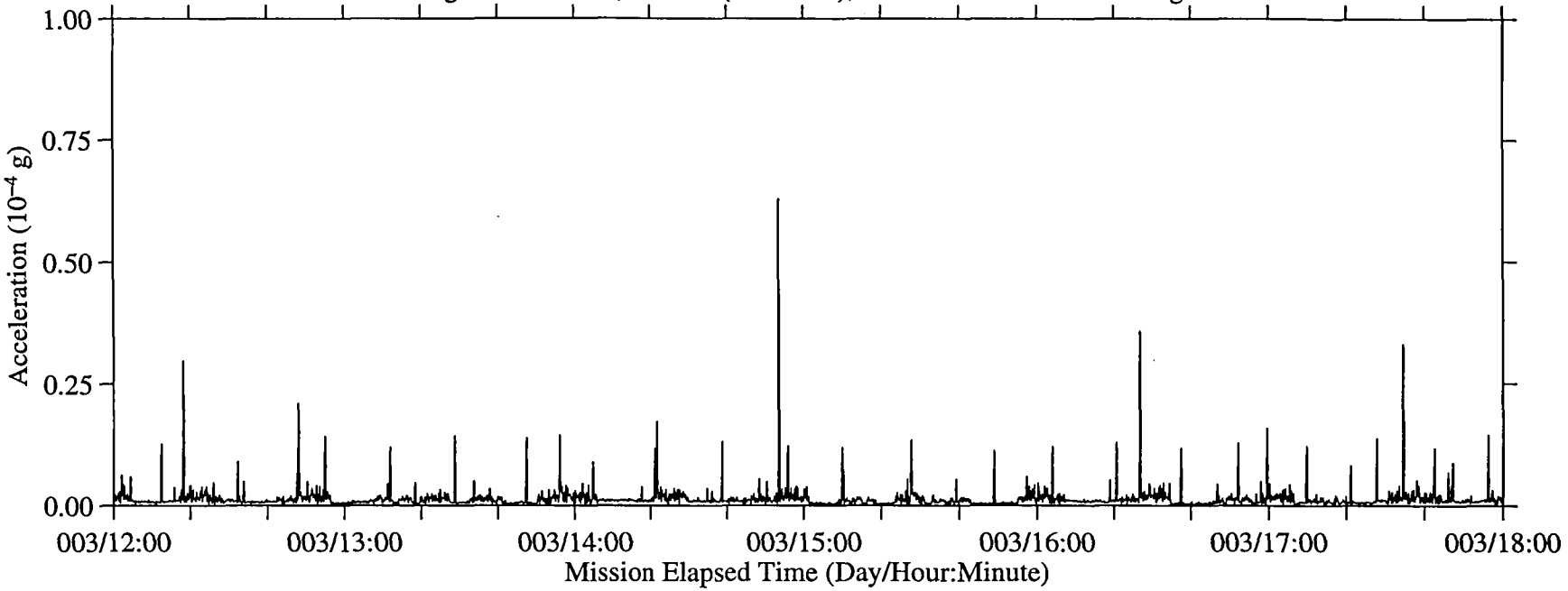

Figure 27b: LMS, Head C (fc=25 Hz), Ten Second Interval RMS

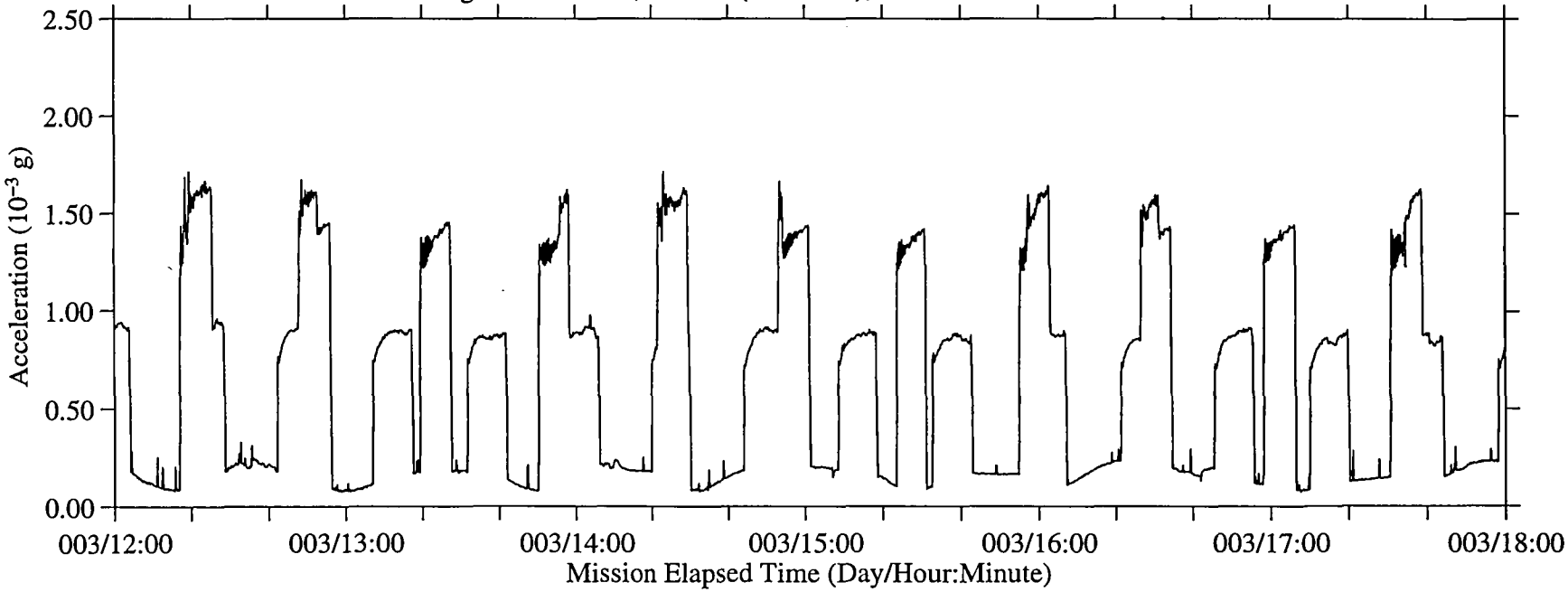

Figure 28: LMS, Head C (fc=25 Hz)

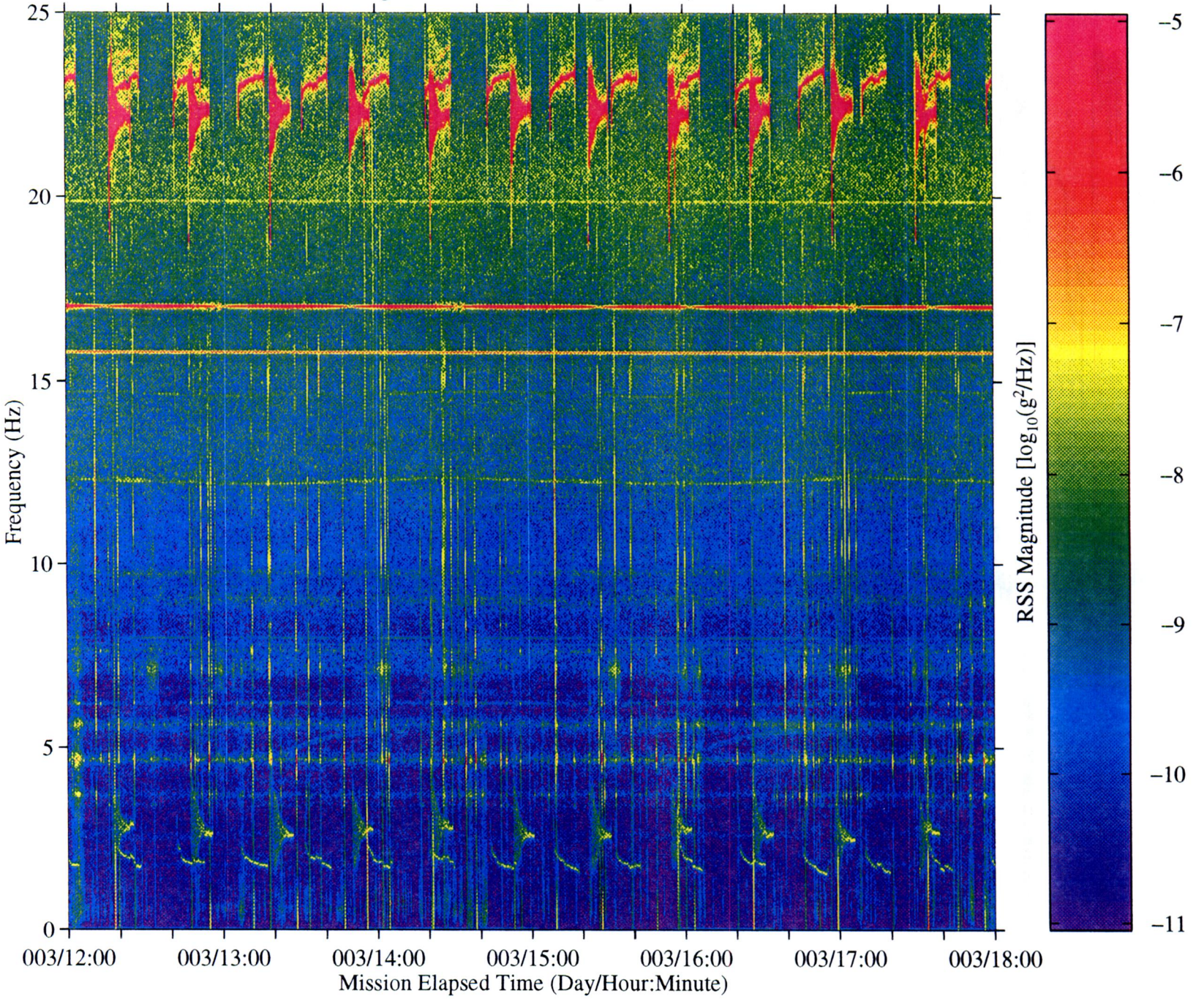

Figure 29a: LMS, Head C (fc=25 Hz), Ten Second Interval Average

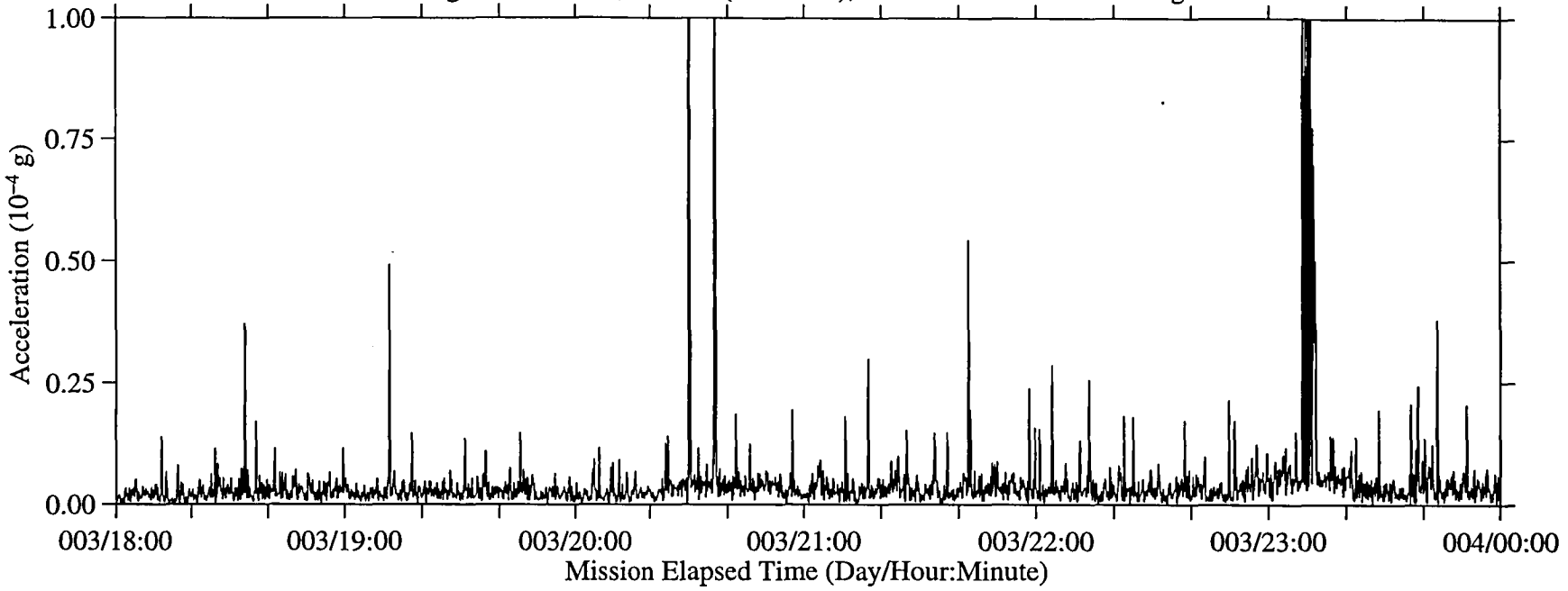

Figure 29b: LMS, Head C (fc=25 Hz), Ten Second Interval RMS

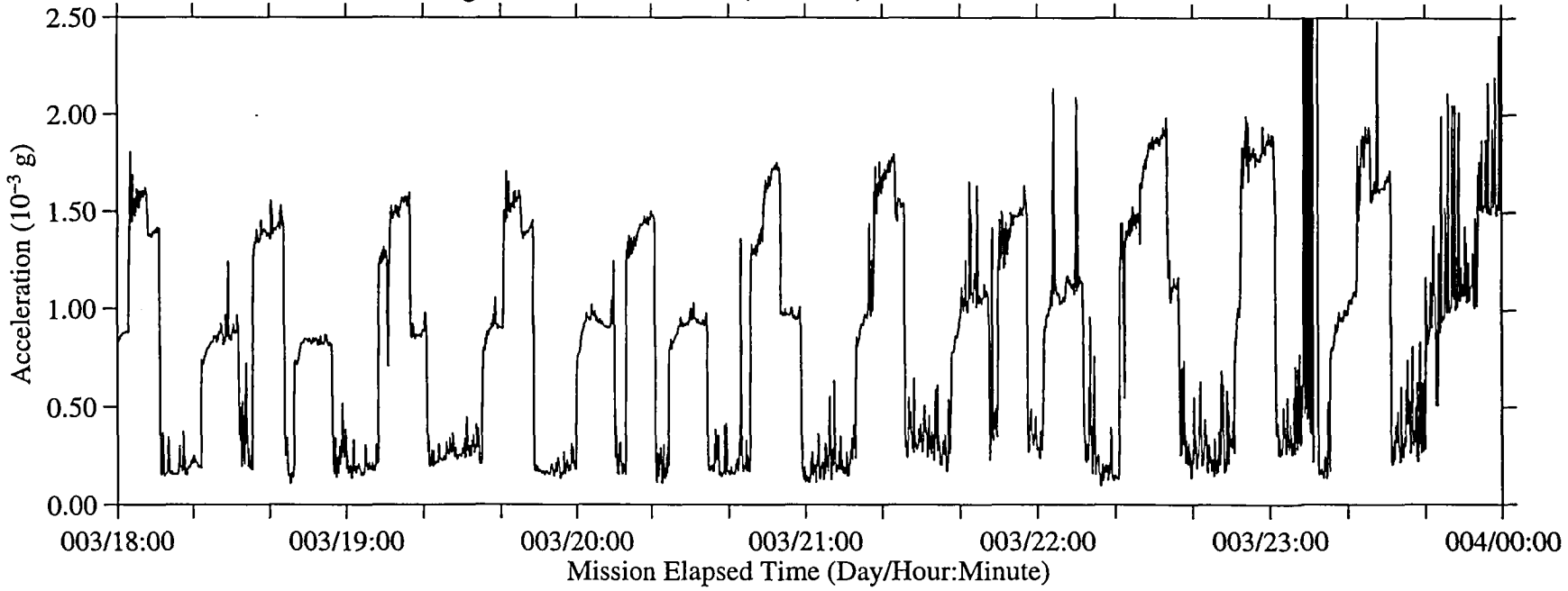

Figure 30: LMS, Head C (fc=25 Hz)

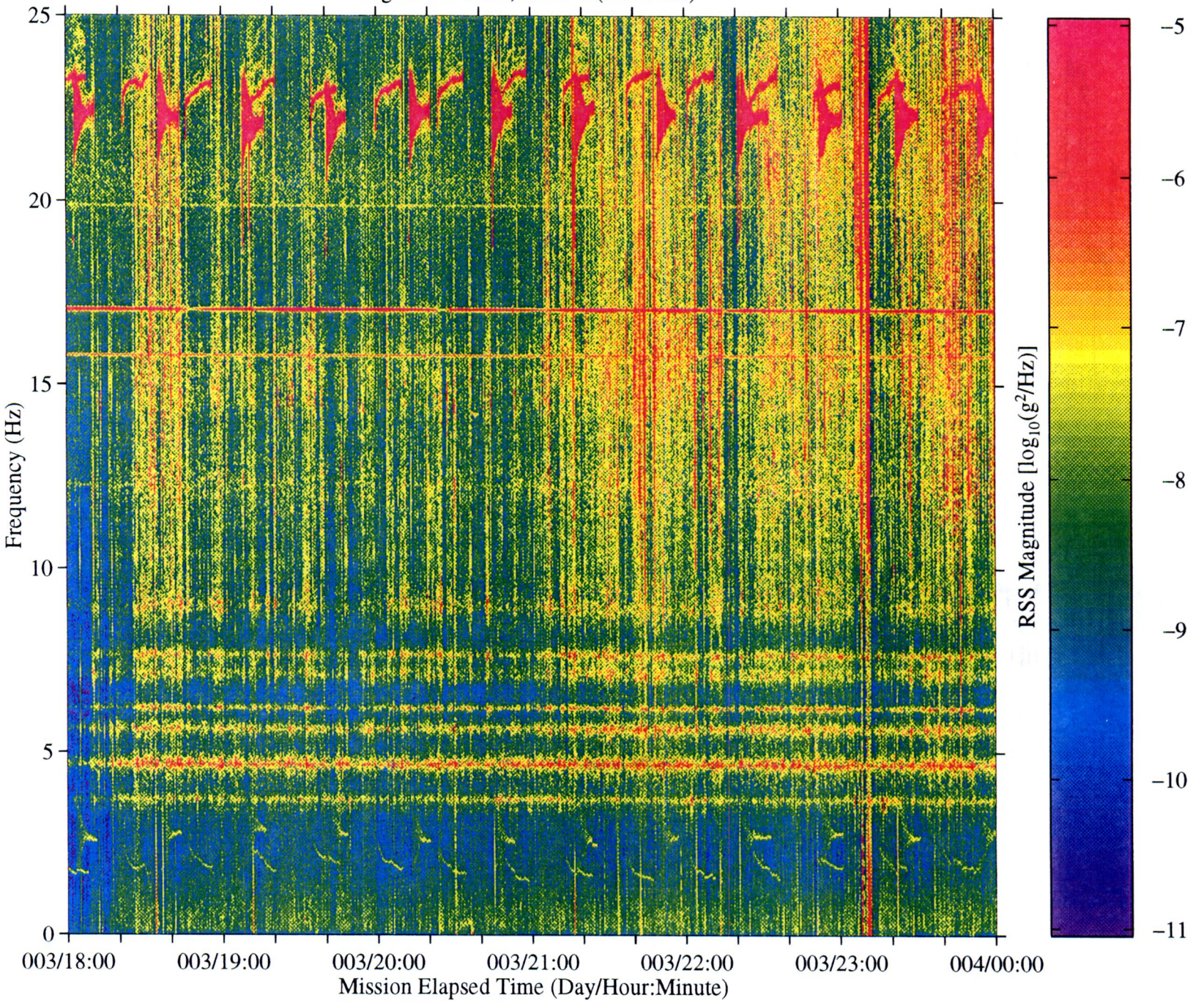

Figure 31a: LMS, Head C (fc=25 Hz), Ten Second Interval Average

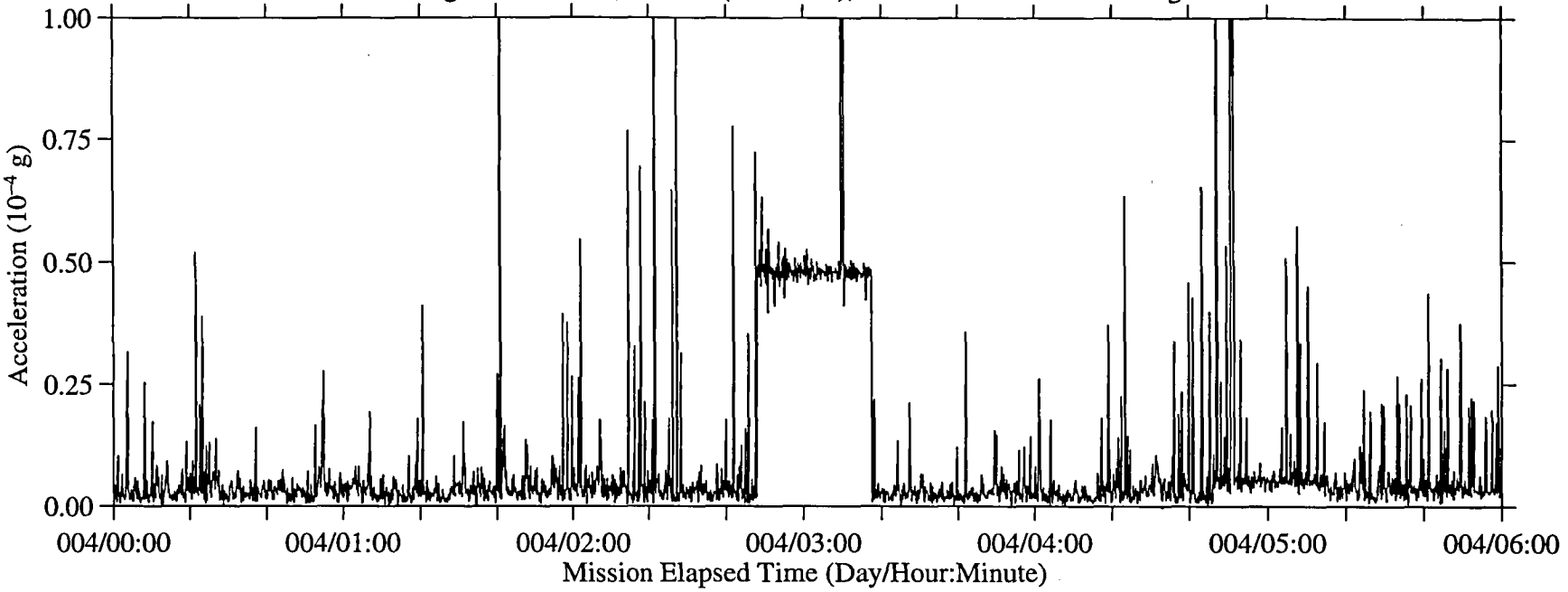

Figure 31b: LMS, Head C (fc=25 Hz), Ten Second Interval RMS

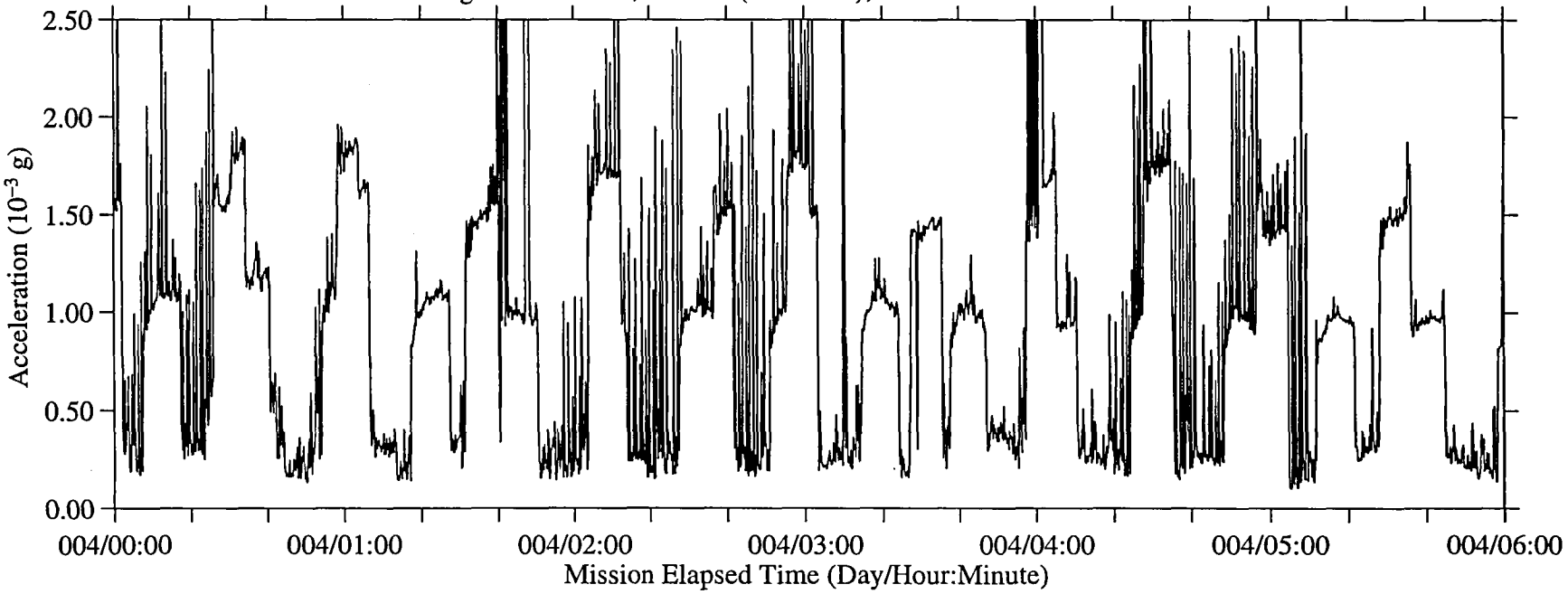

Figure 32: LMS, Head C (fc=25 Hz)

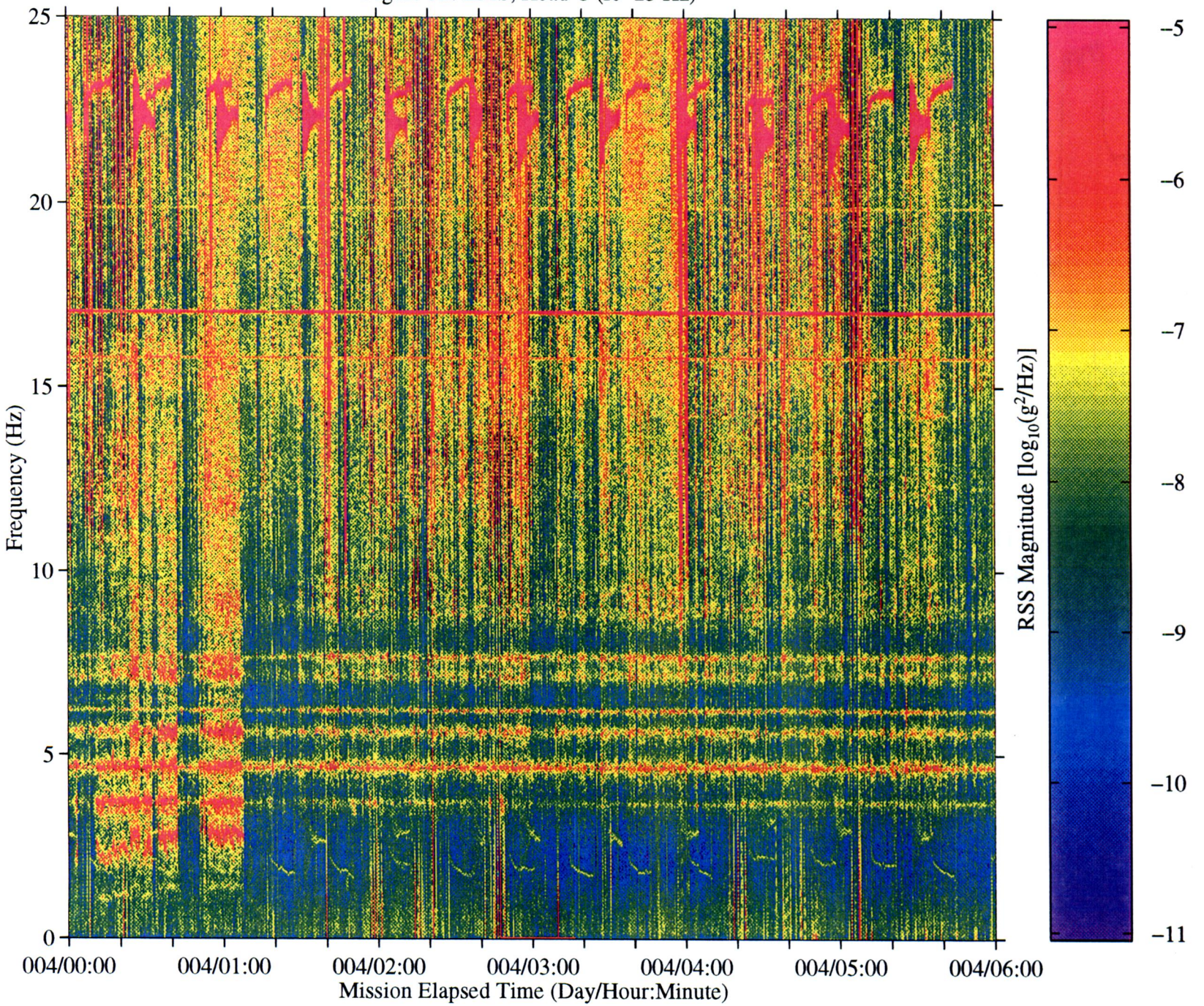

Figure 33a: LMS, Head C (fc=25 Hz), Ten Second Interval Average

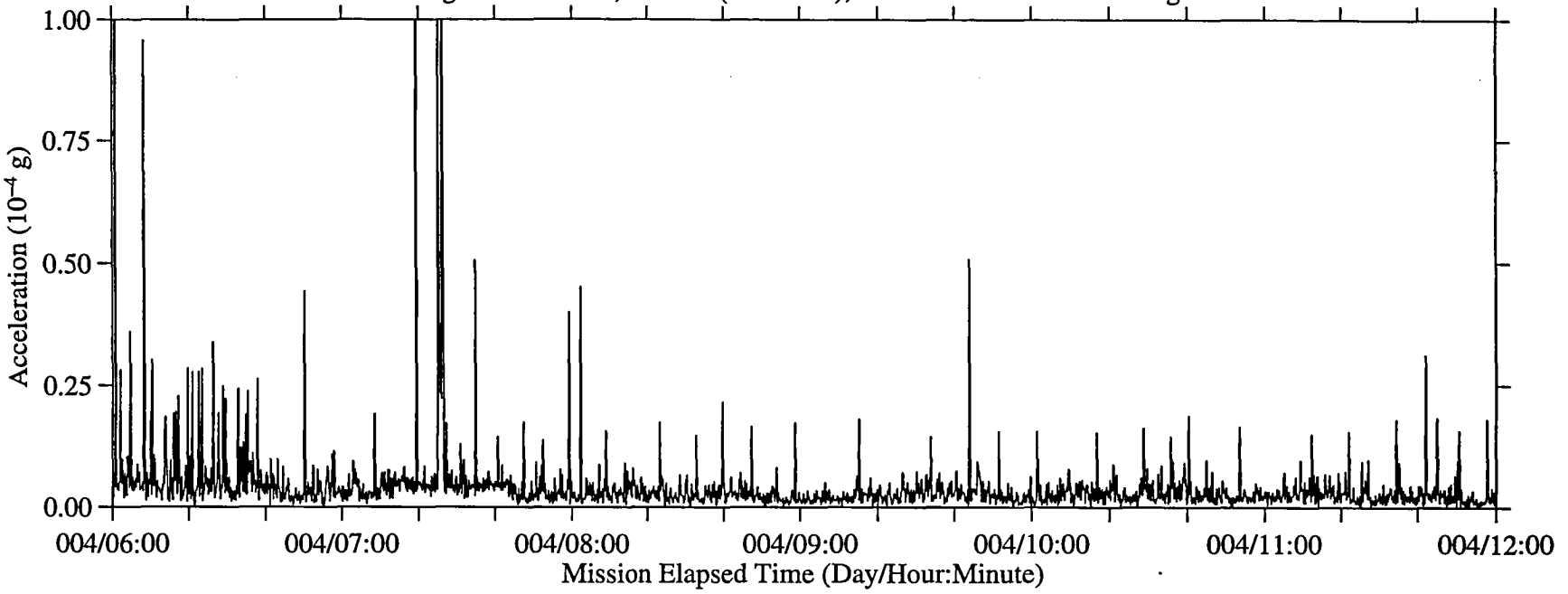

Figure 33b: LMS, Head C (fc=25 Hz), Ten Second Interval RMS

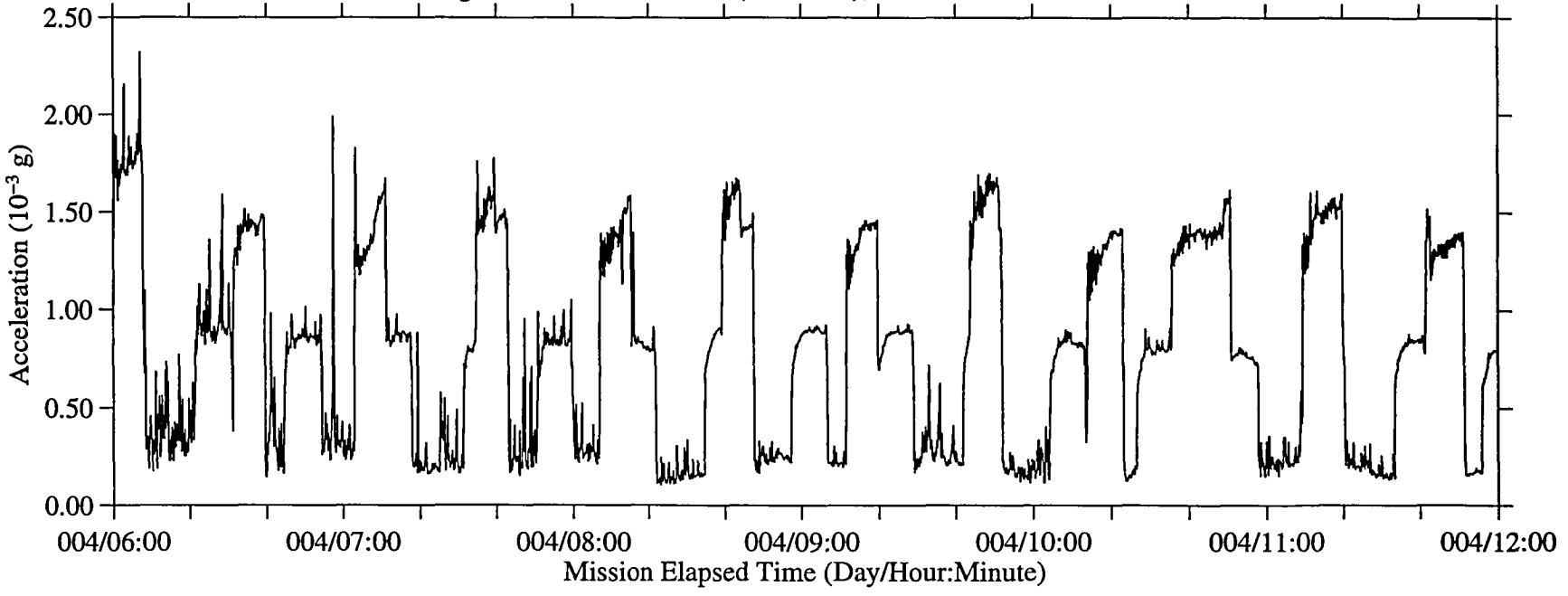

Figure 34: LMS, Head C (fc=25 Hz)

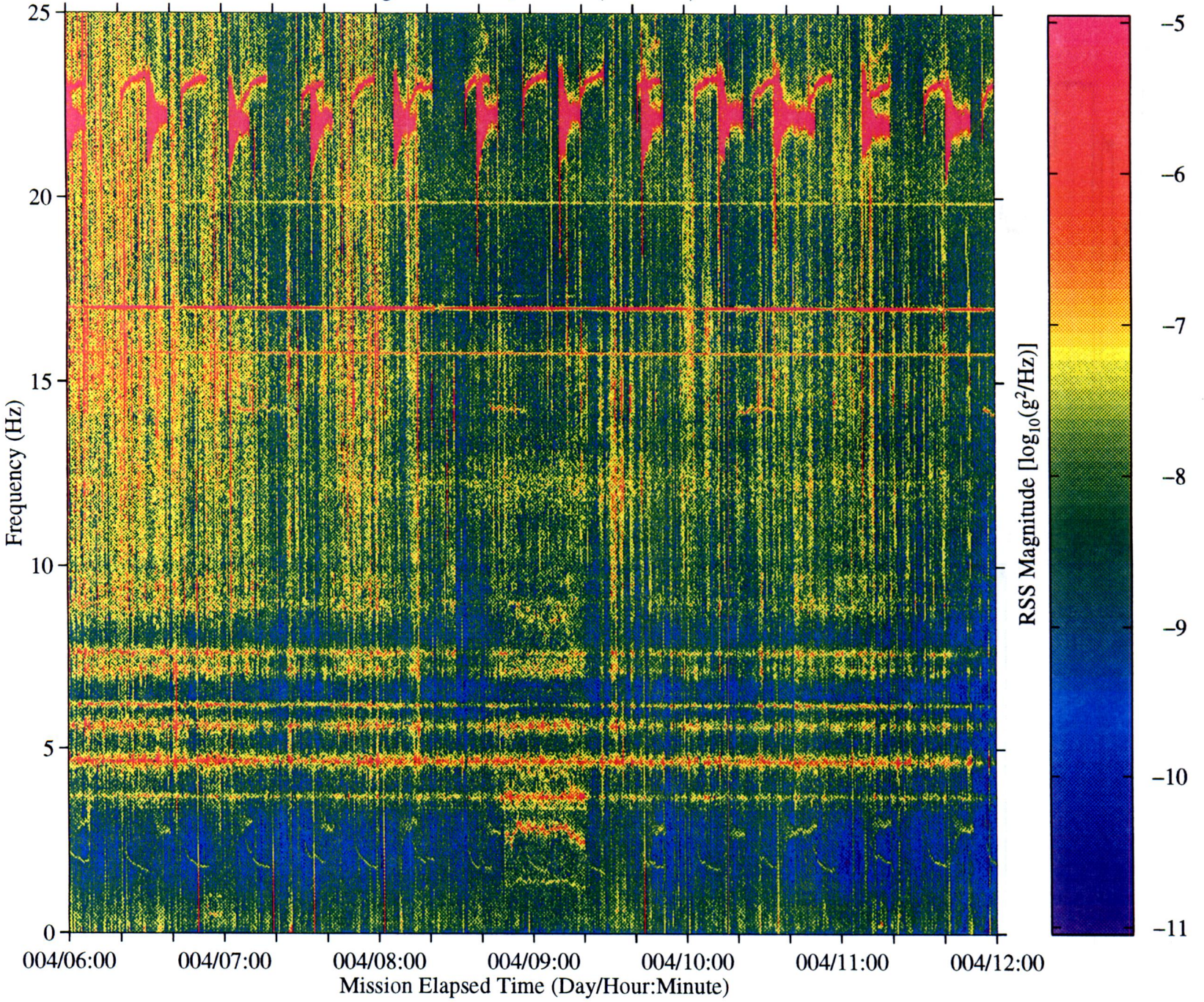

Figure 35a: LMS, Head C (fc=25 Hz), Ten Second Interval Average

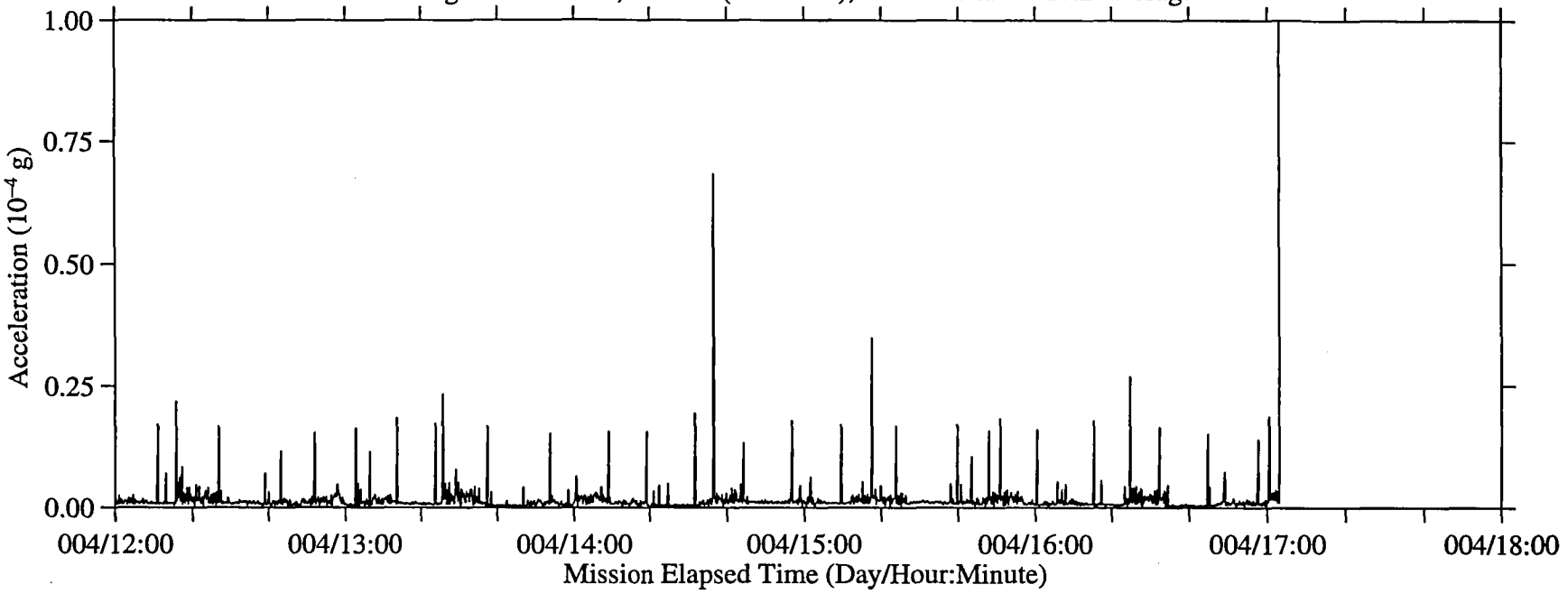

Figure 35b: LMS, Head C (fc=25 Hz), Ten Second Interval RMS

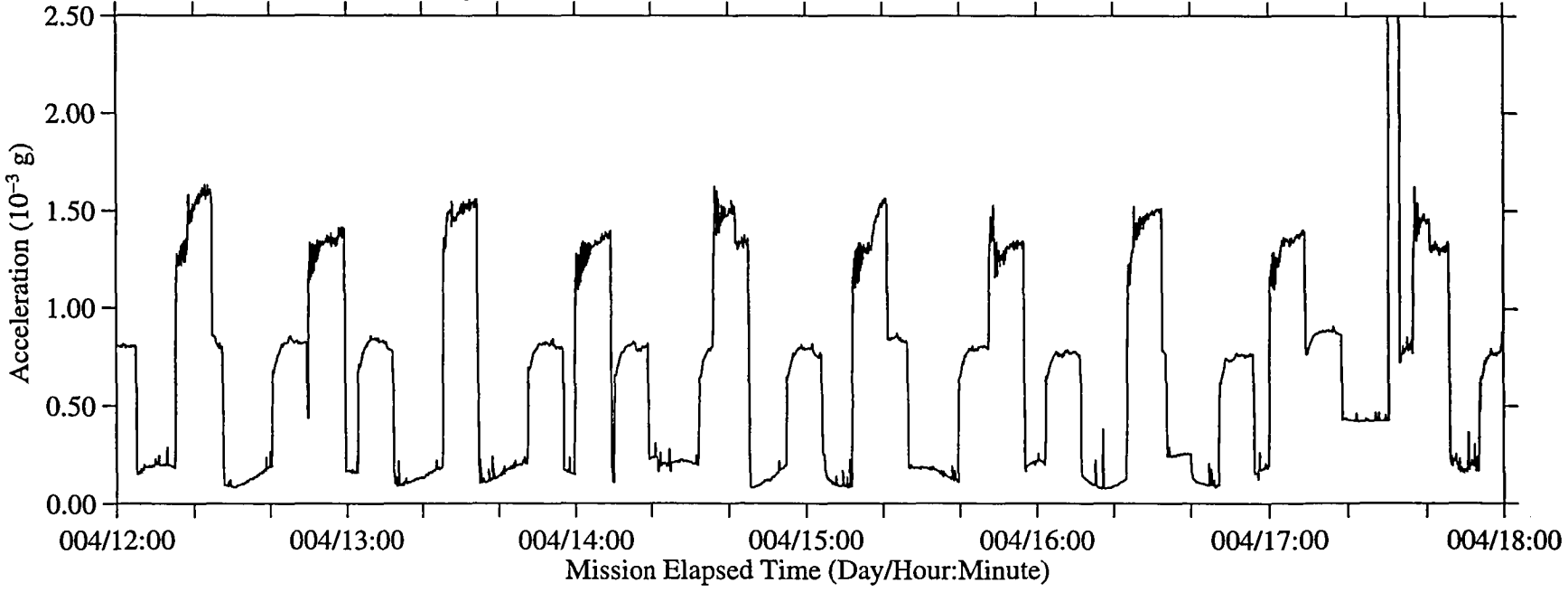

Figure 36: LMS, Head C (fc=25 Hz)

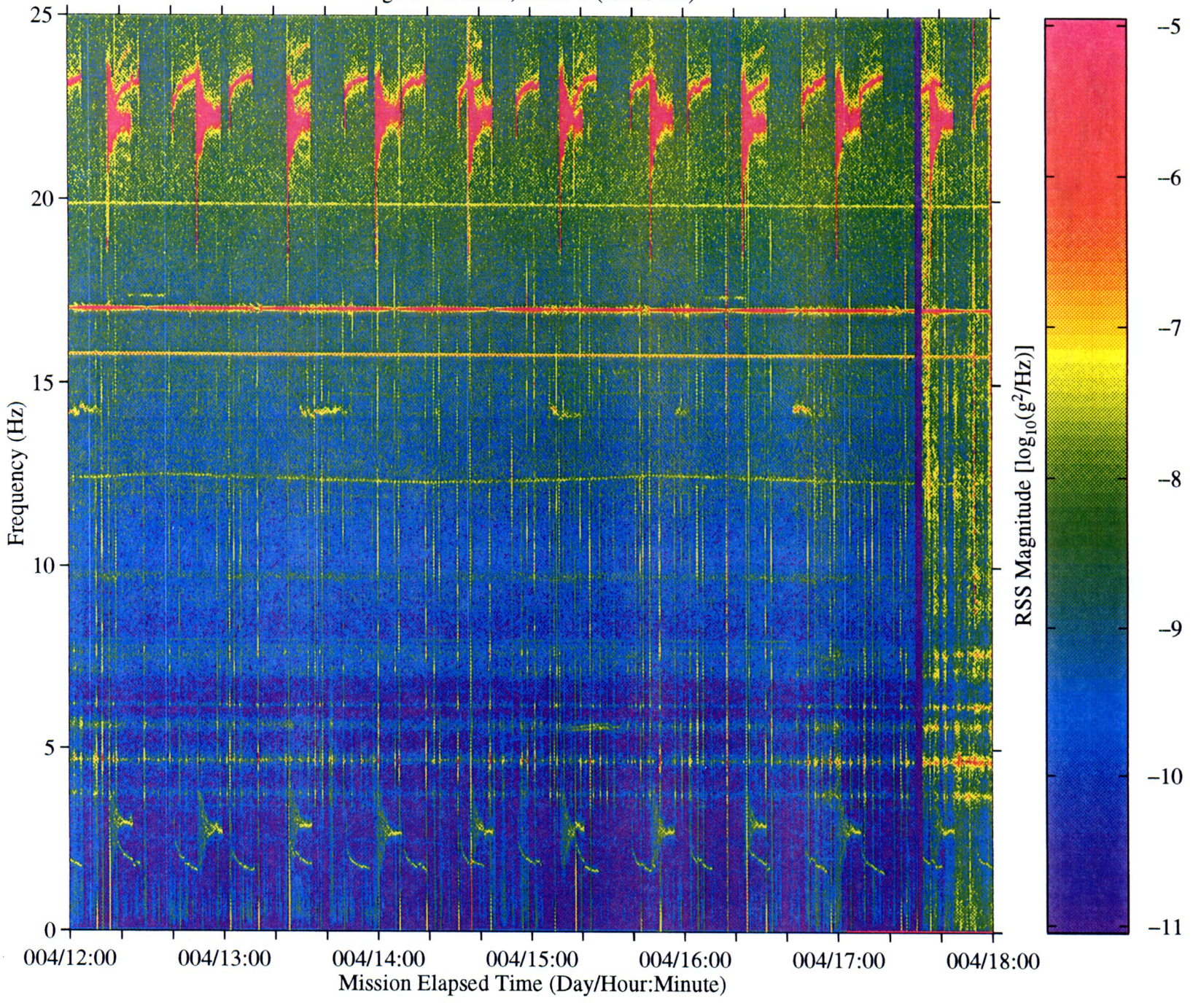

Figure 37a: LMS, Head C (fc=25 Hz), Ten Second Interval Average

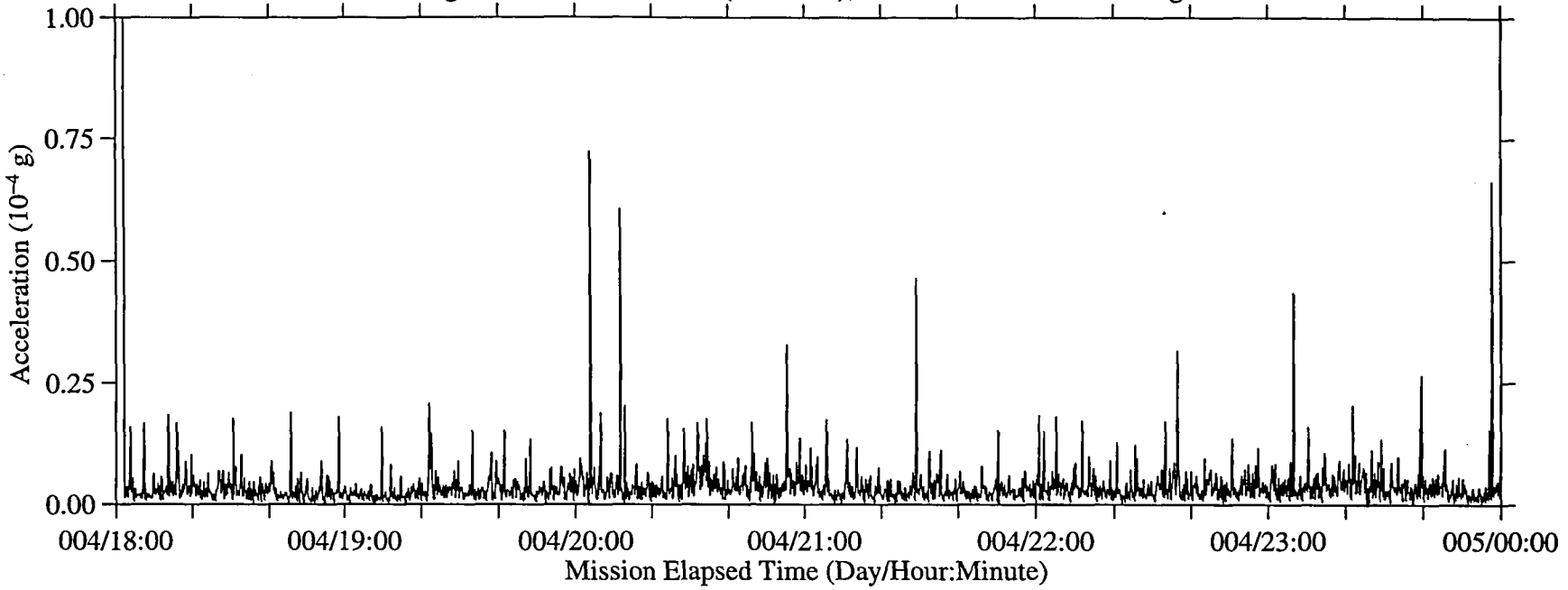

Figure 37b: LMS, Head C (fc=25 Hz), Ten Second Interval RMS

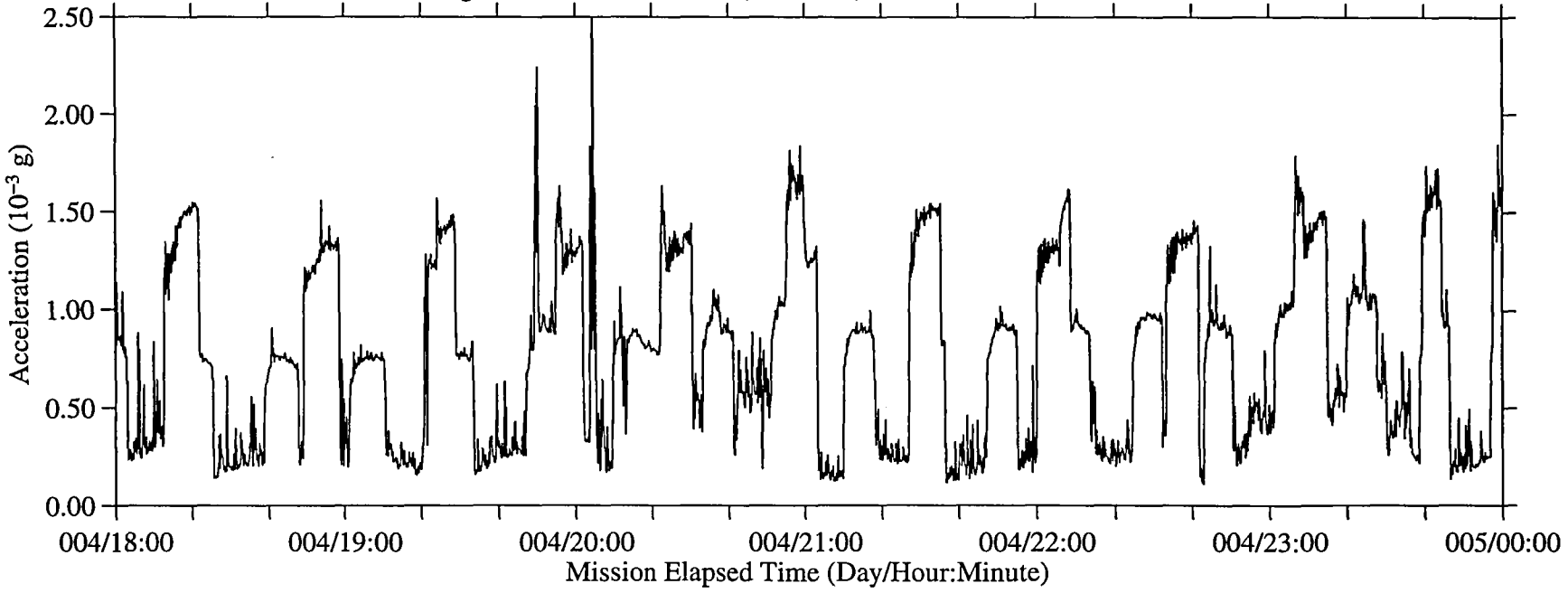

Figure 38: LMS, Head C (fc=25 Hz)

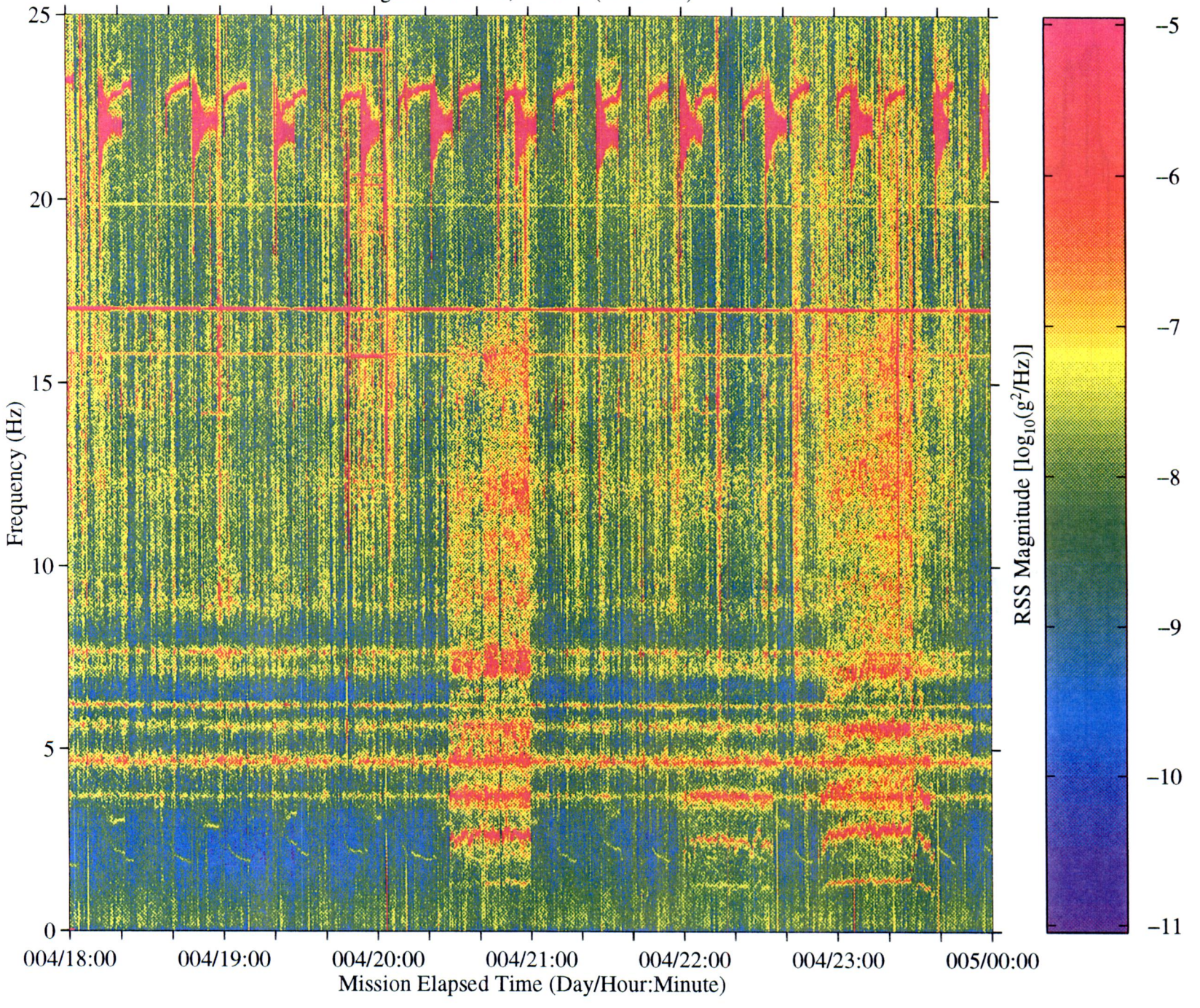

Figure 39a: LMS, Head C (fc=25 Hz), Ten Second Interval Average

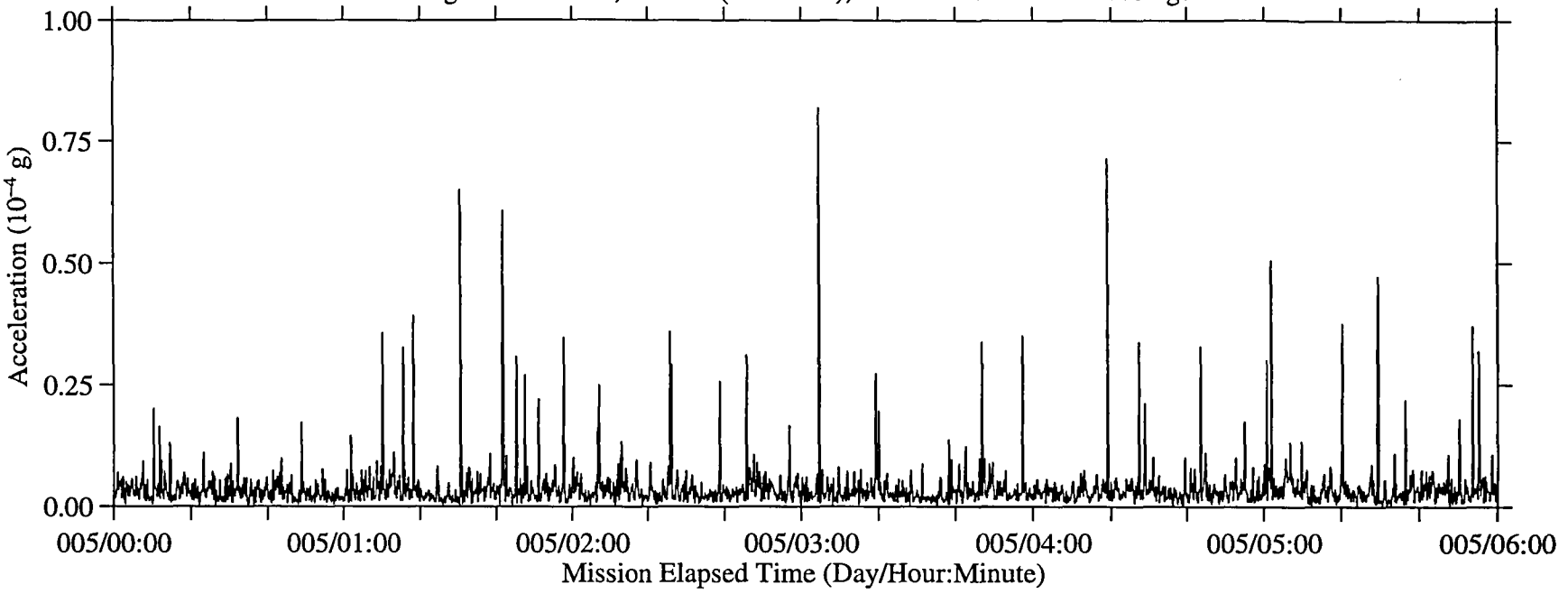

Figure 39b: LMS, Head C (fc=25 Hz), Ten Second Interval RMS

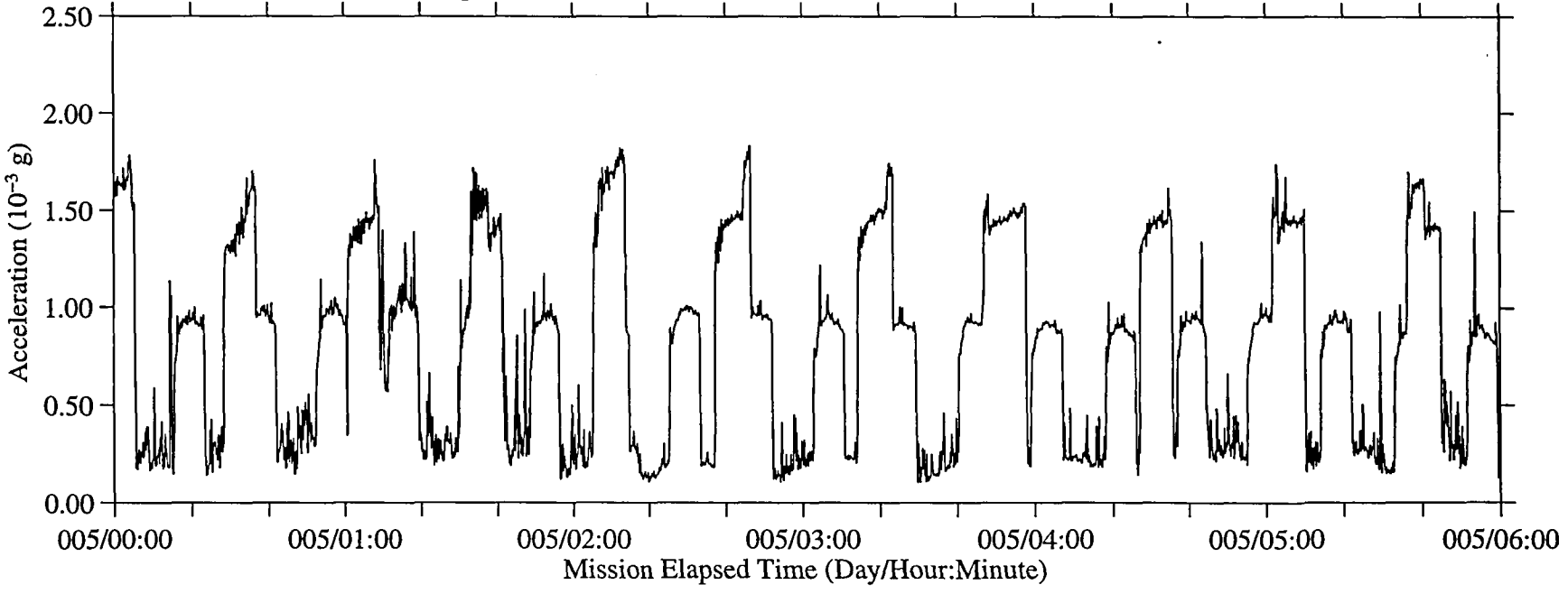

Figure 40: LMS, Head C (fc=25 Hz)

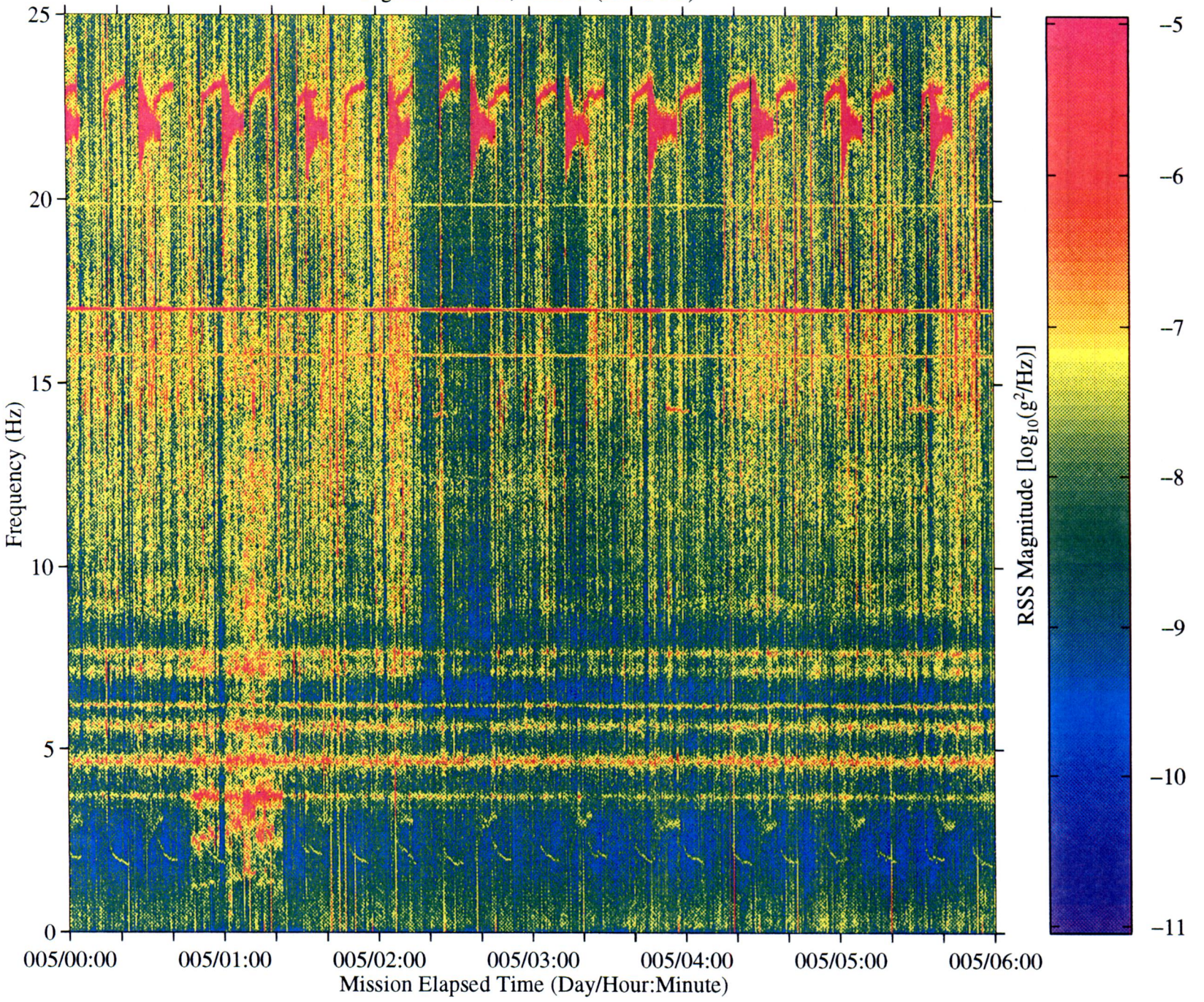

Figure 41a: LMS, Head C (fc=25 Hz), Ten Second Interval Average

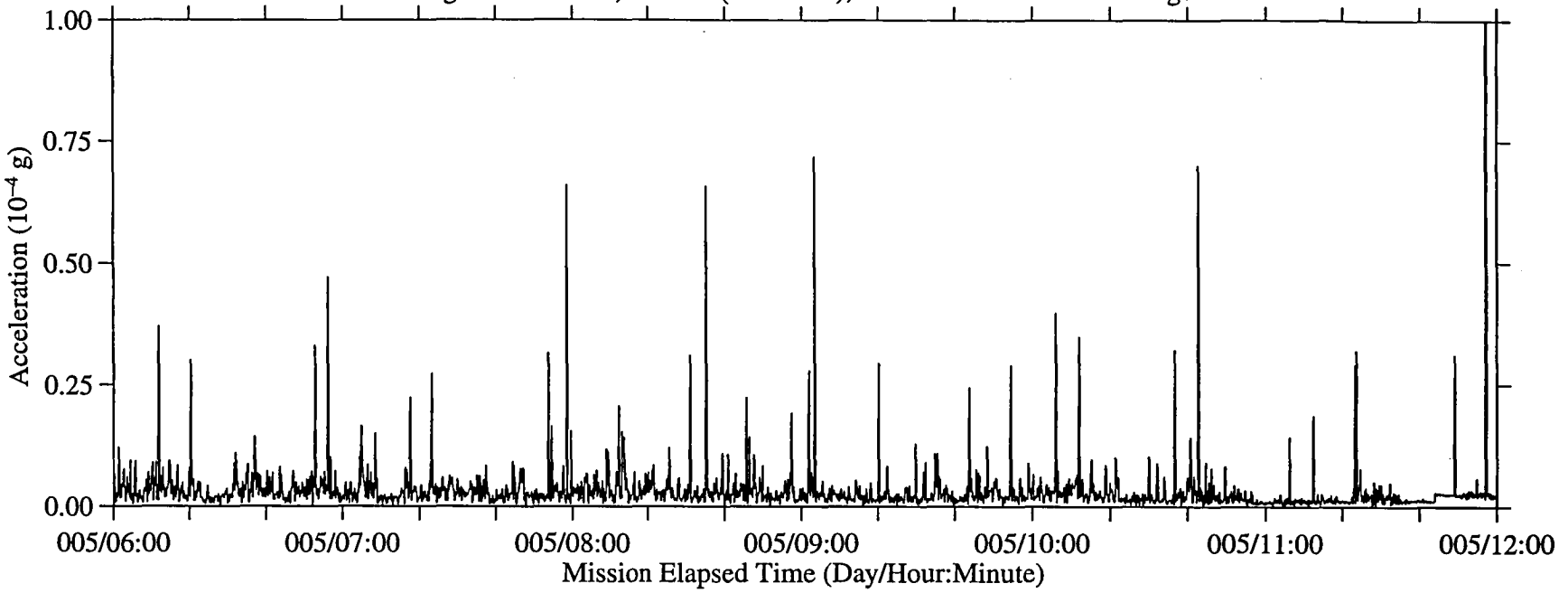

Figure 41b: LMS, Head C (fc=25 Hz), Ten Second Interval RMS

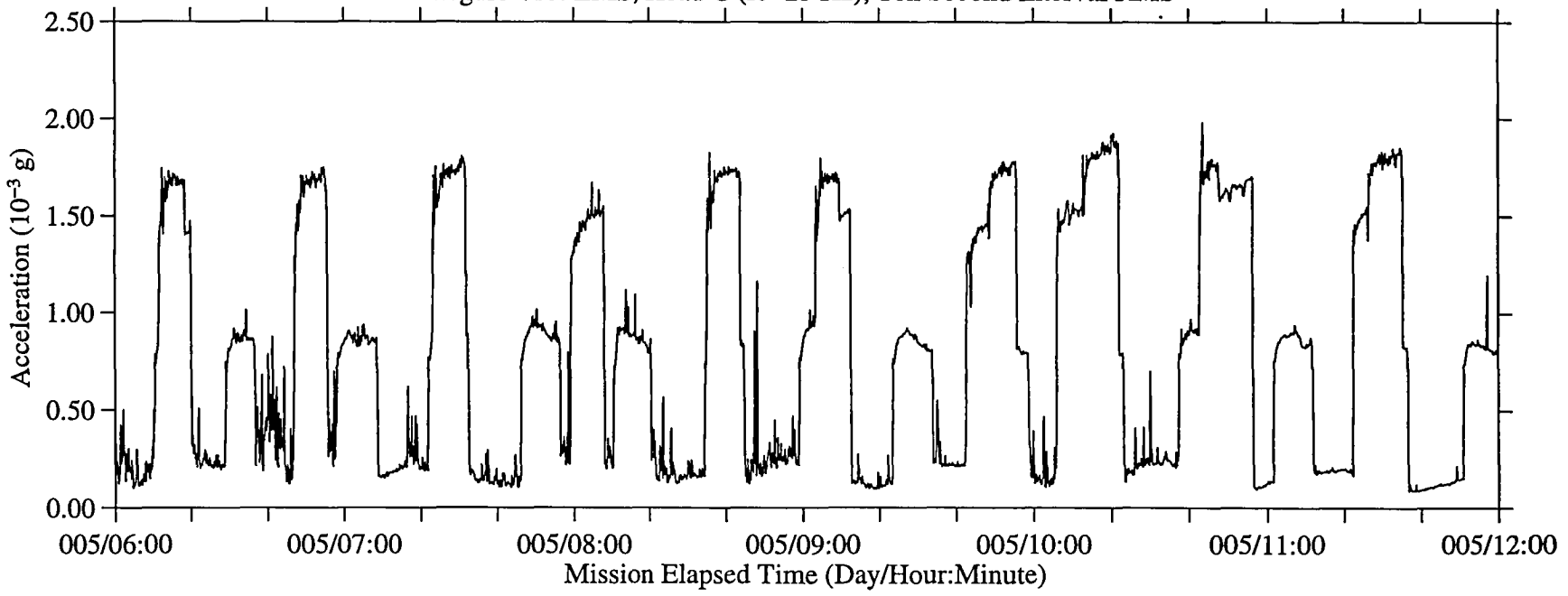

Figure 42: LMS, Head C (fc=25 Hz)

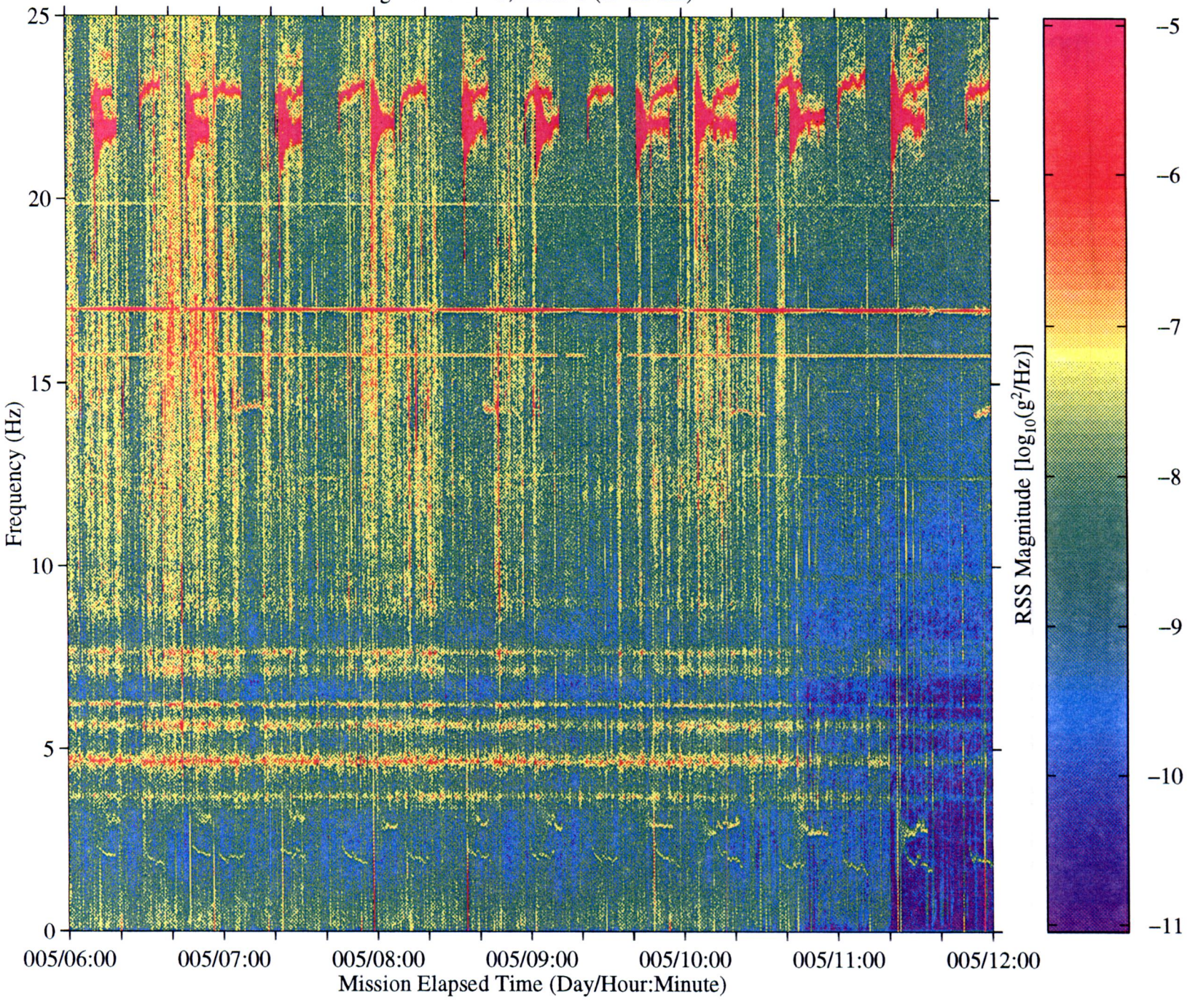

Figure 43a: LMS, Head C (fc=25 Hz), Ten Second Interval Average

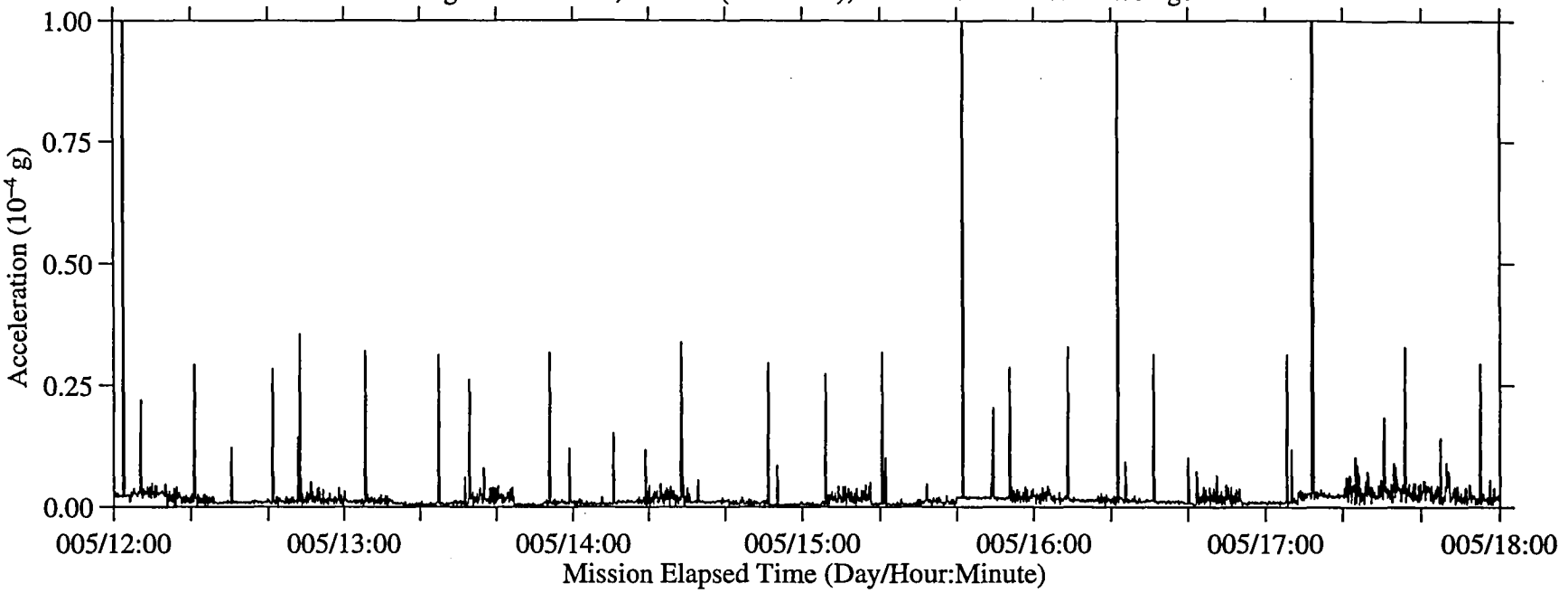

Figure 43b: LMS, Head C (fc=25 Hz), Ten Second Interval RMS

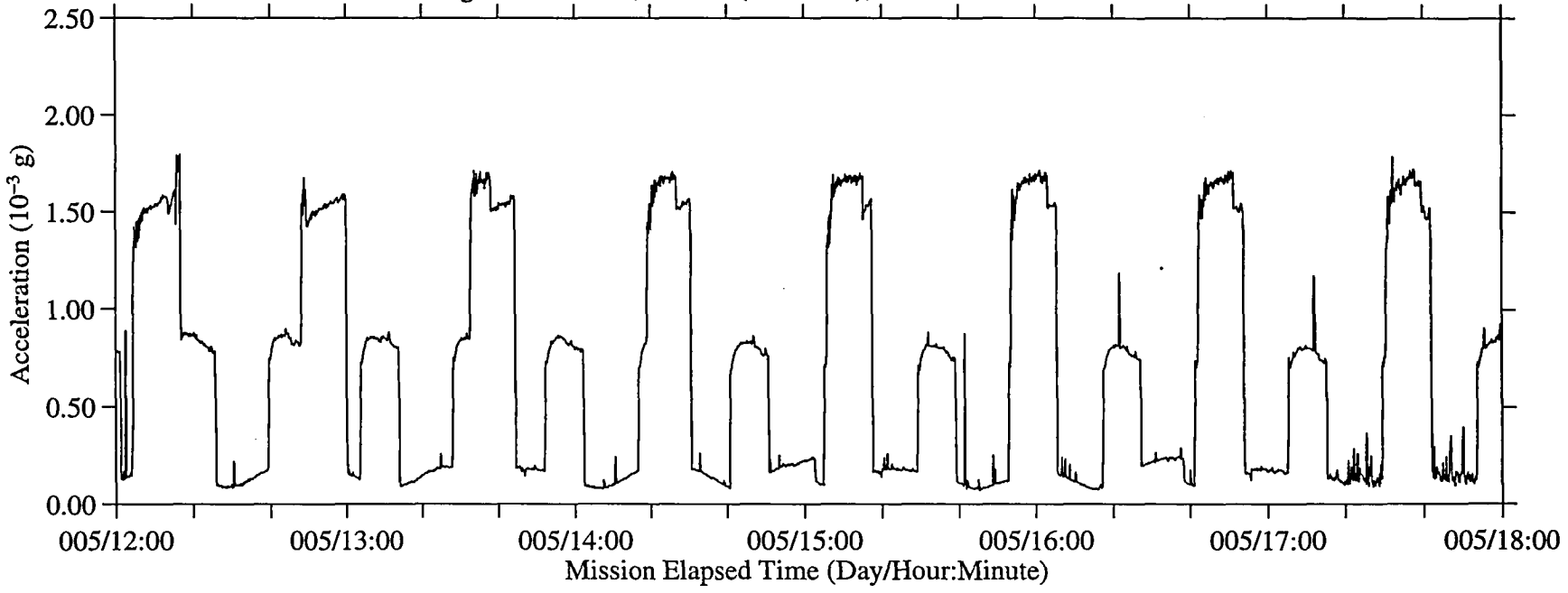

Figure 44: LMS, Head C (fc=25 Hz)

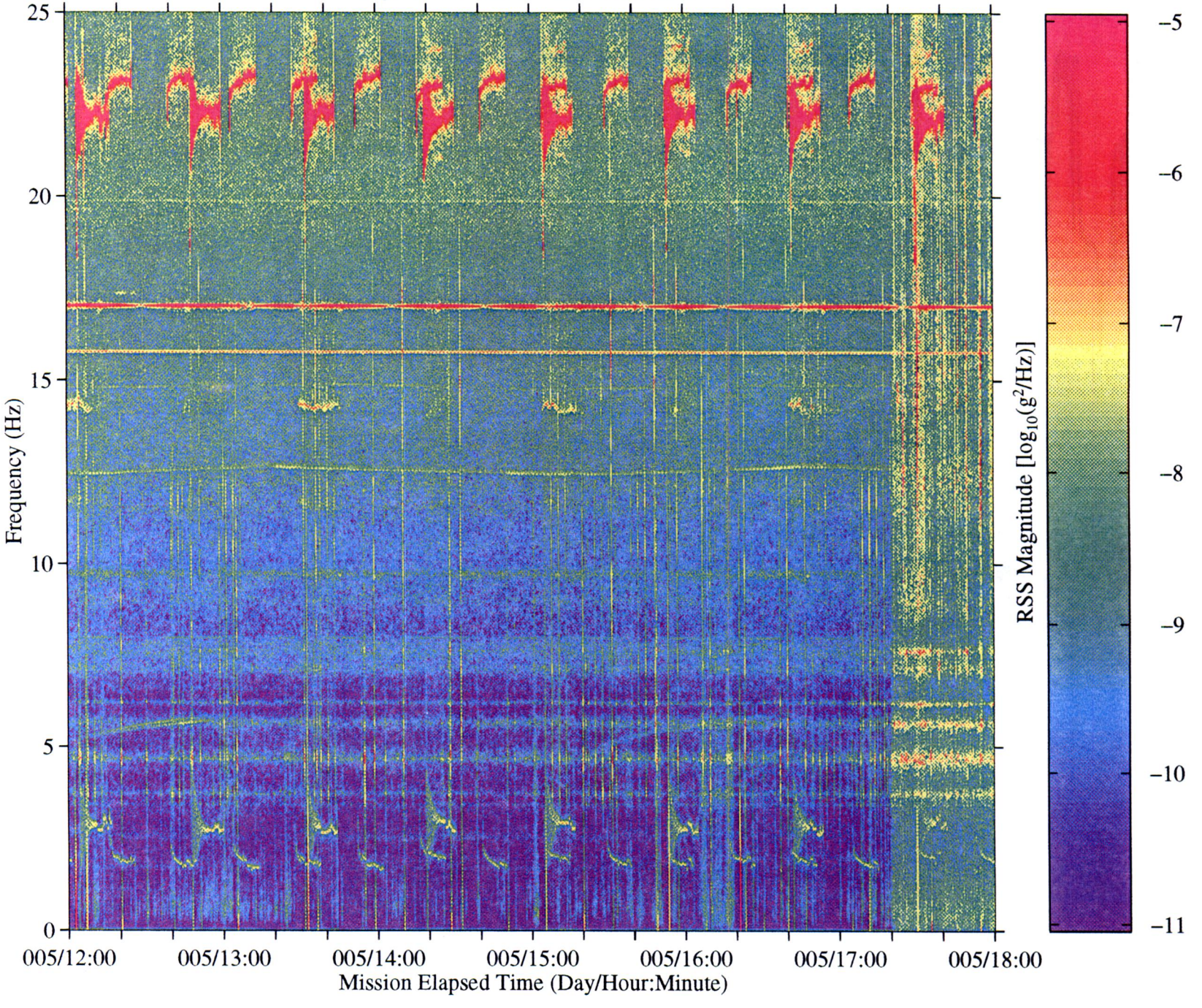

Figure 45a: LMS, Head C (fc=25 Hz), Ten Second Interval Average

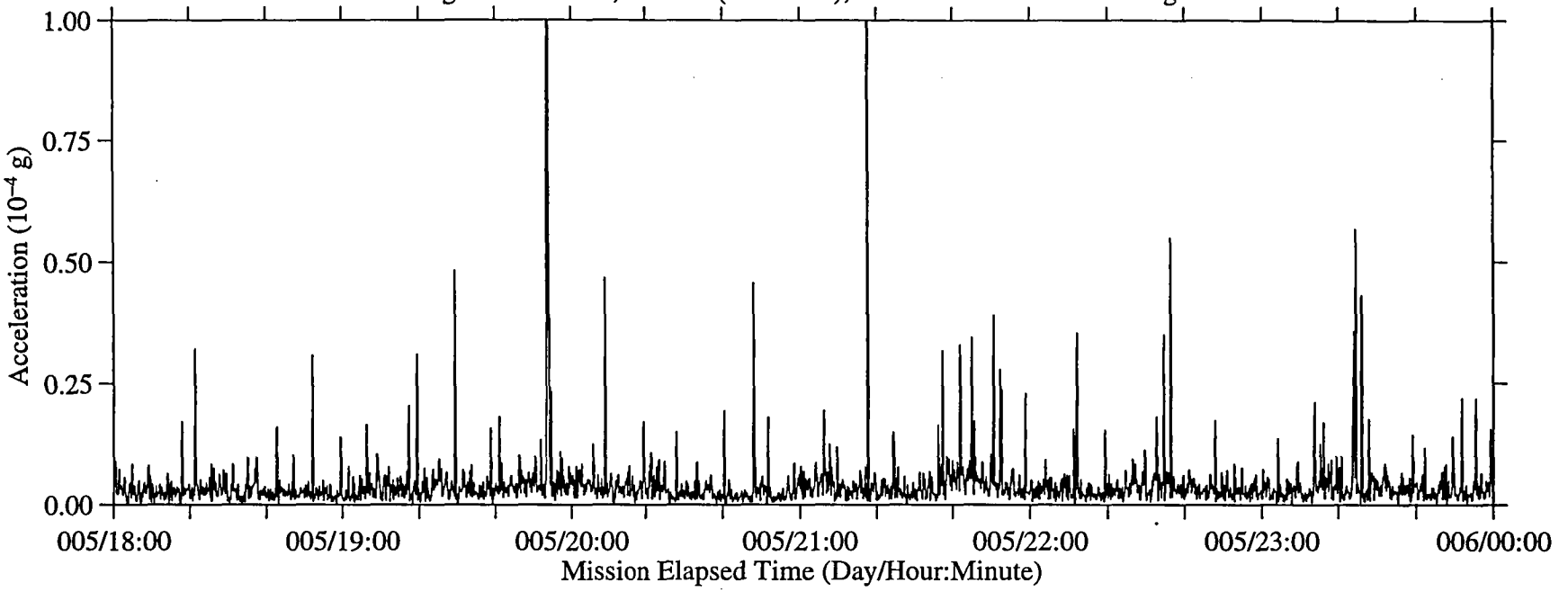

Figure 45b: LMS, Head C (fc=25 Hz), Ten Second Interval RMS

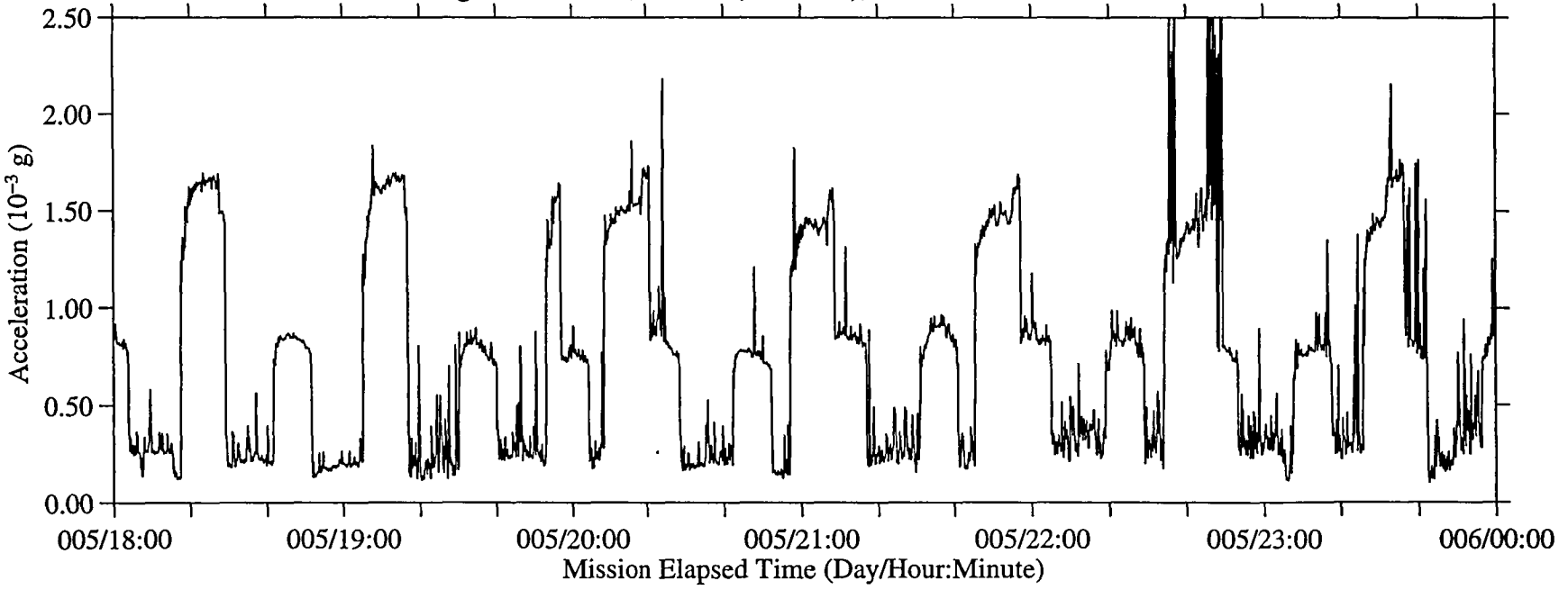

Figure 46: LMS, Head C (fc=25 Hz)

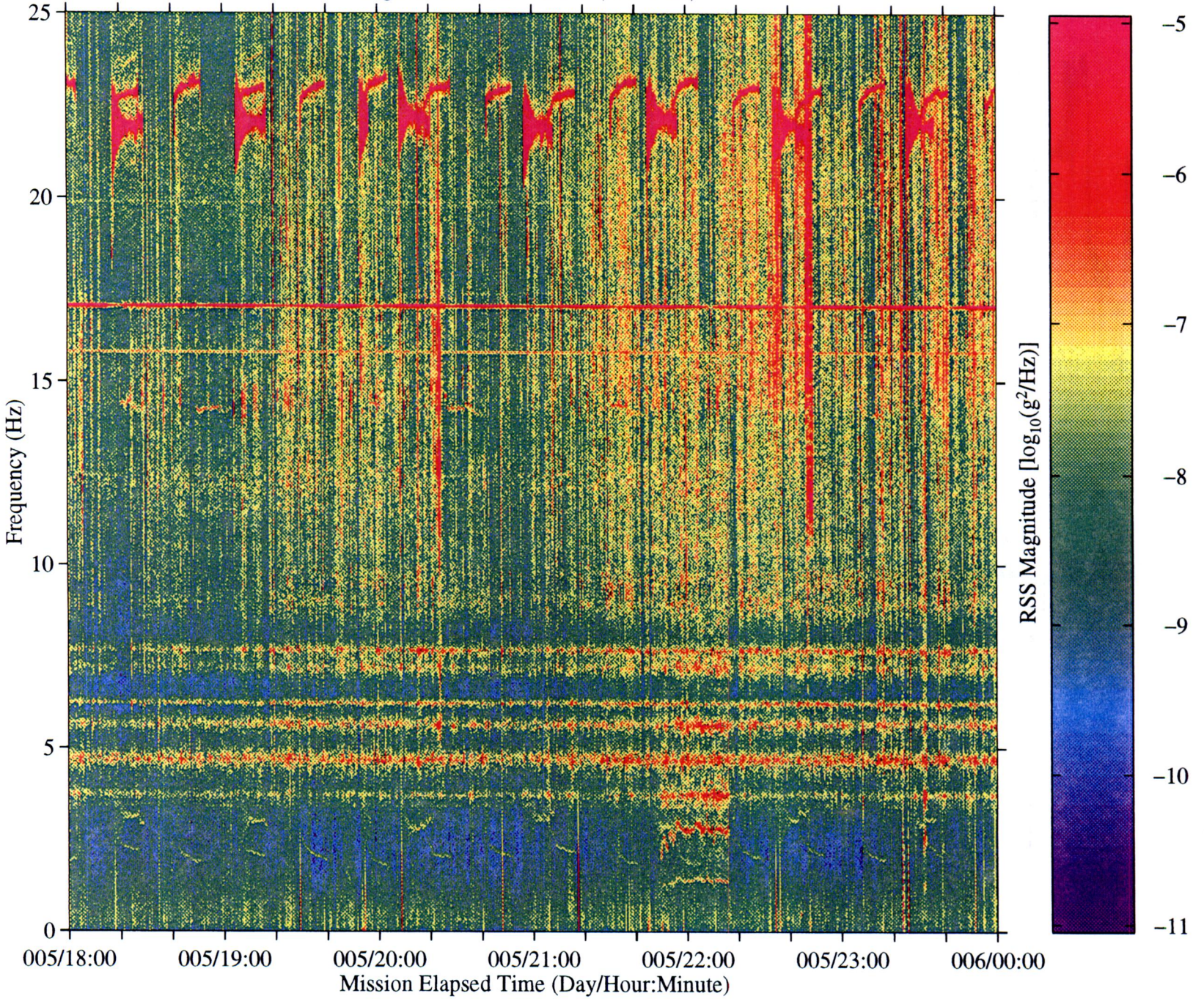

Figure 47a: LMS, Head C (fc=25 Hz), Ten Second Interval Average

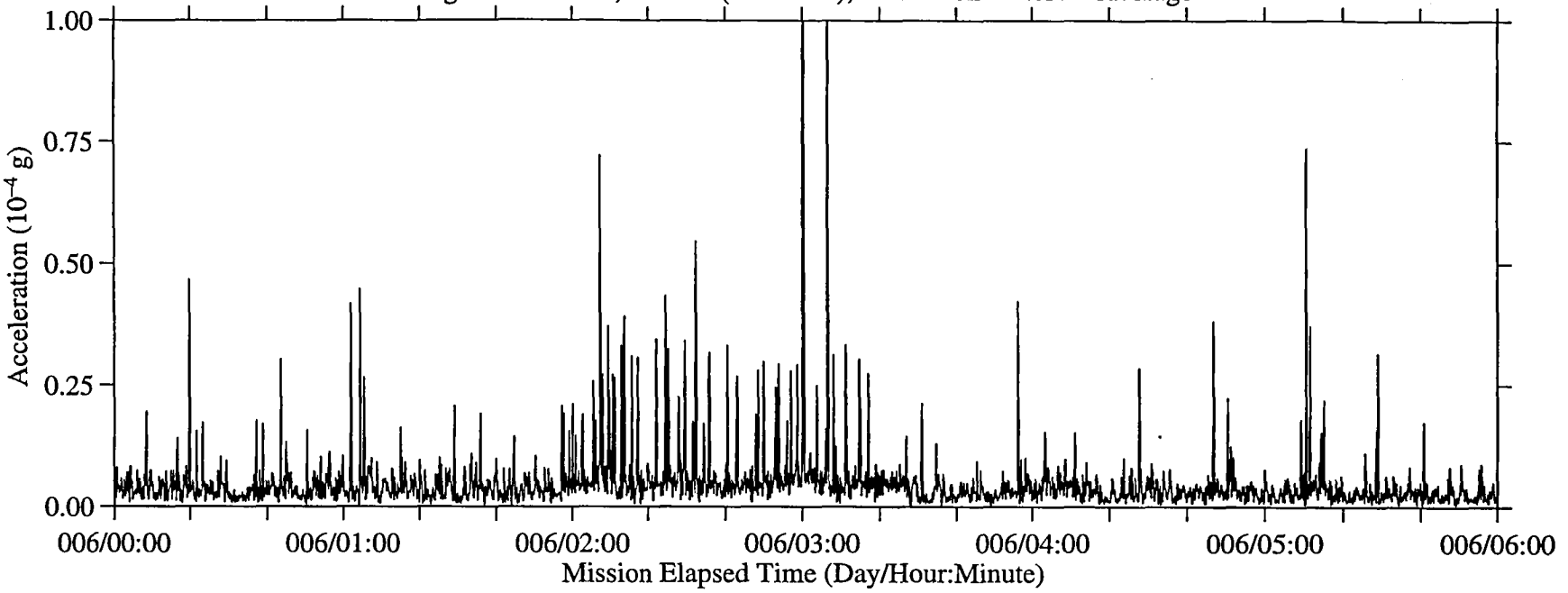

Figure 47b: LMS, Head C (fc=25 Hz), Ten Second Interval RMS

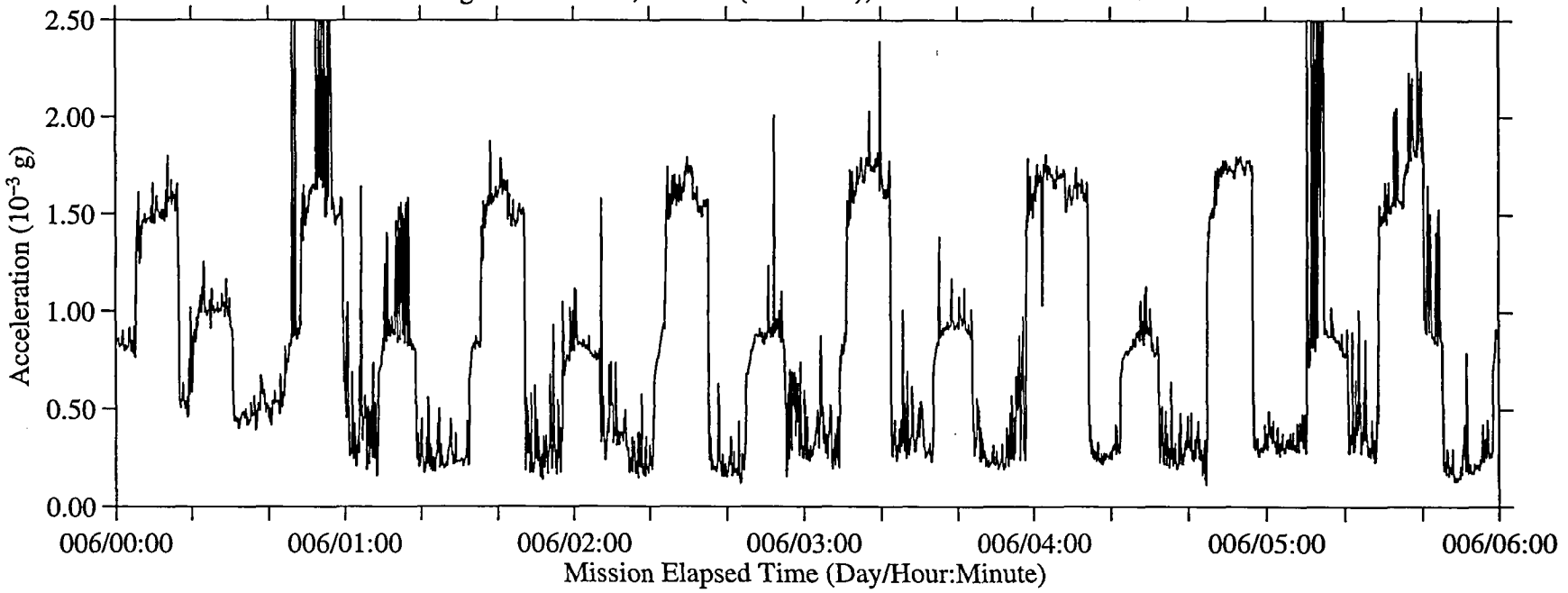

Figure 48: LMS, Head C (fc=25 Hz)

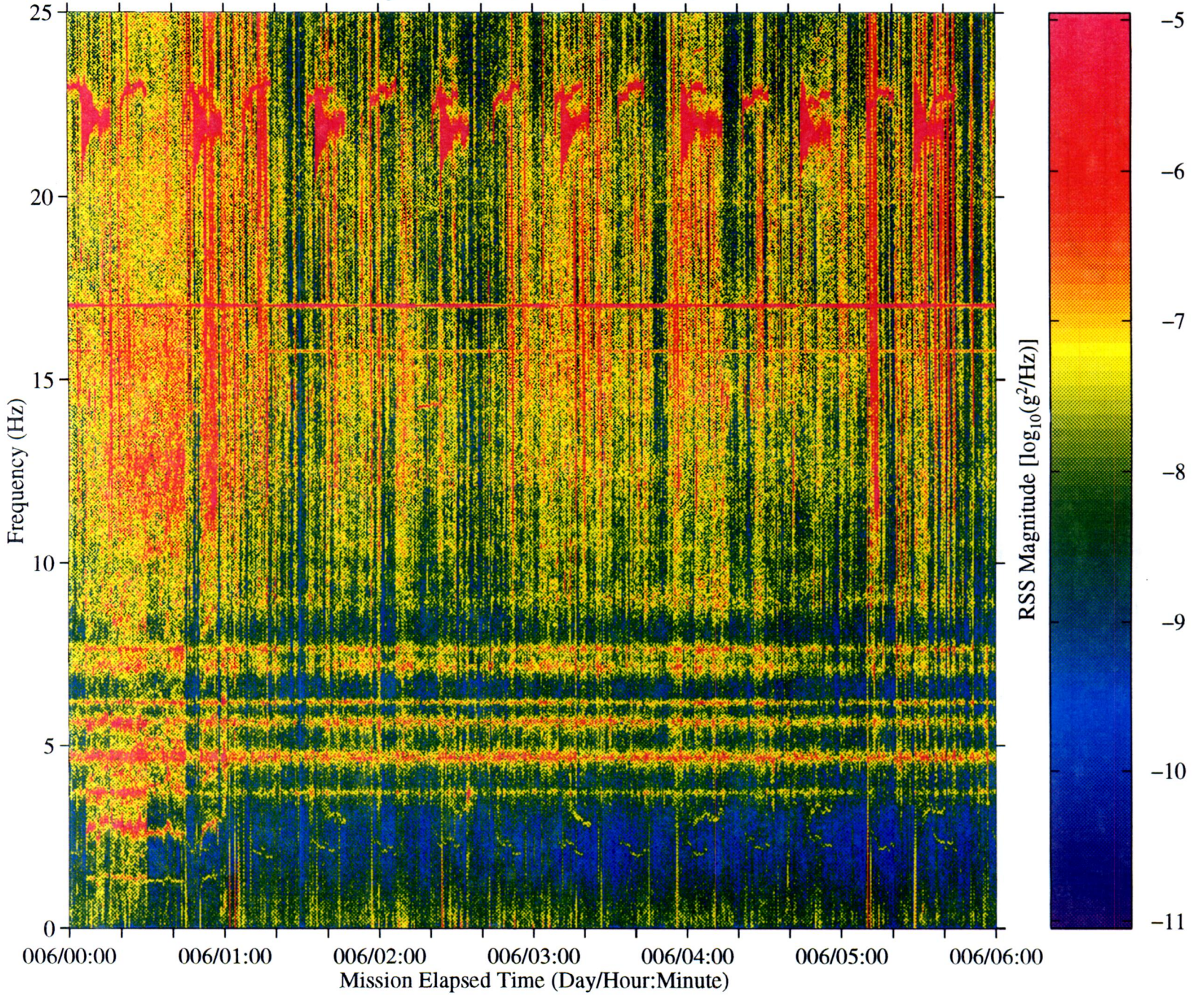

Figure 49a: LMS, Head C (fc=25 Hz), Ten Second Interval Average

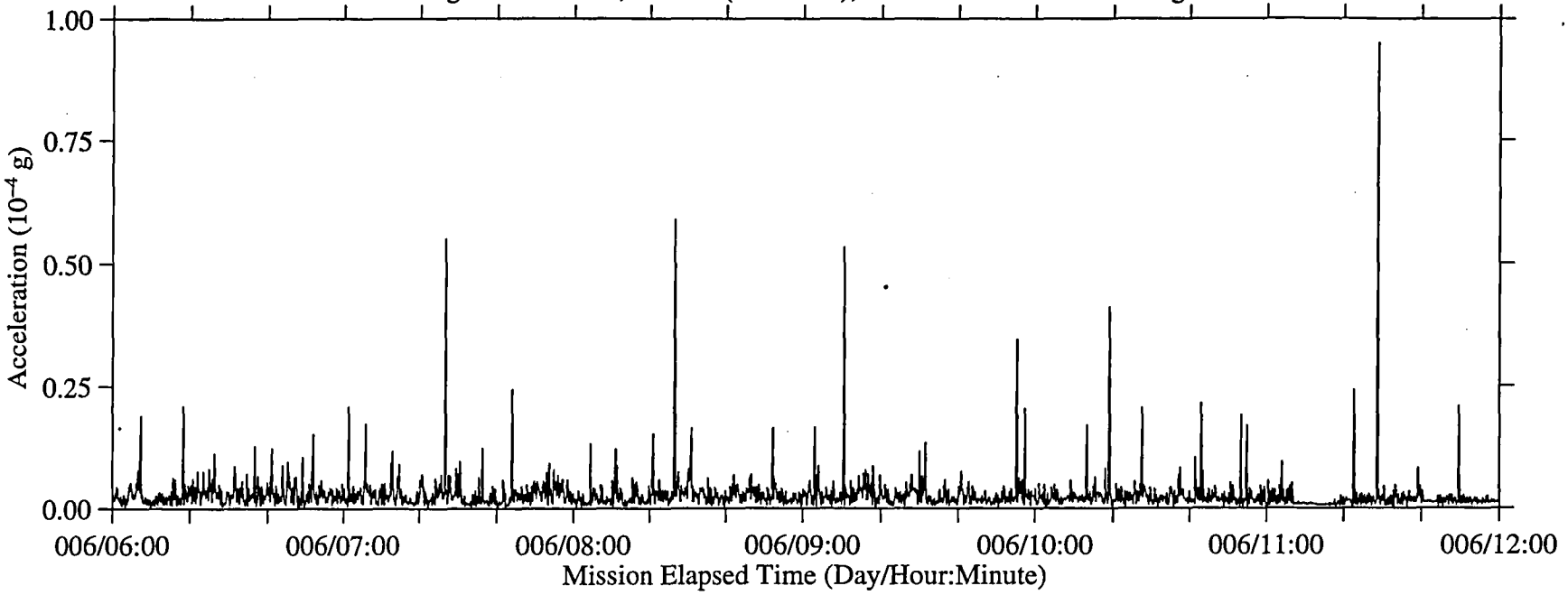

Figure 49b: LMS, Head C (fc=25 Hz), Ten Second Interval RMS

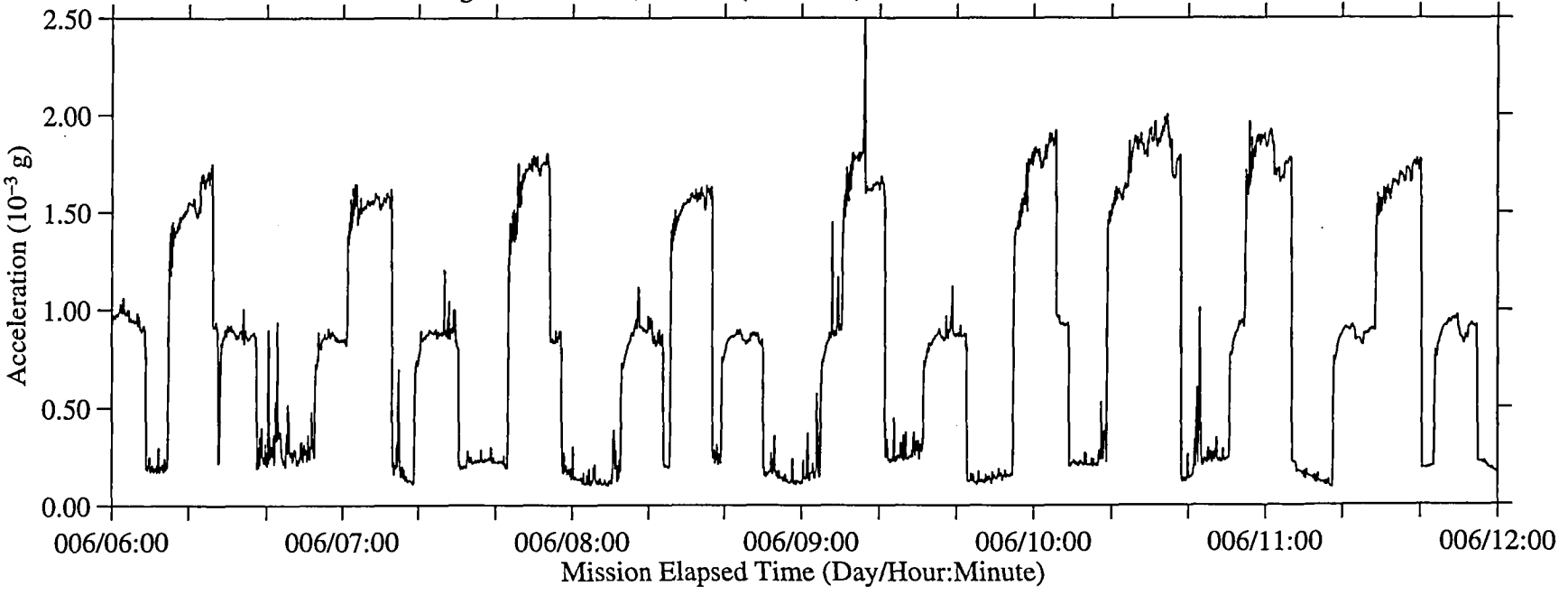

Figure 50: LMS, Head C (fc=25 Hz)

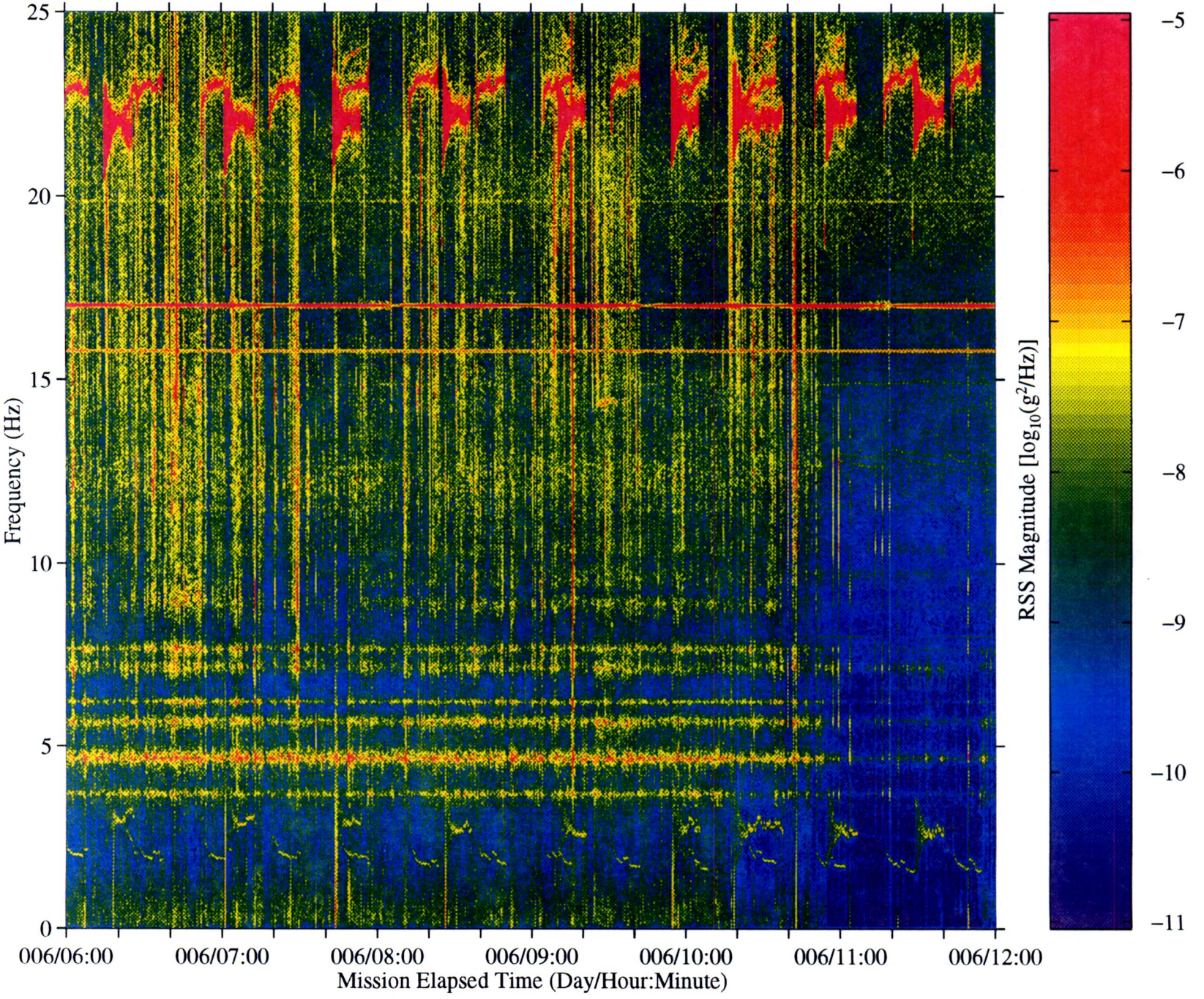

Figure 51a: LMS, Head C (fc=25 Hz), Ten Second Interval Average

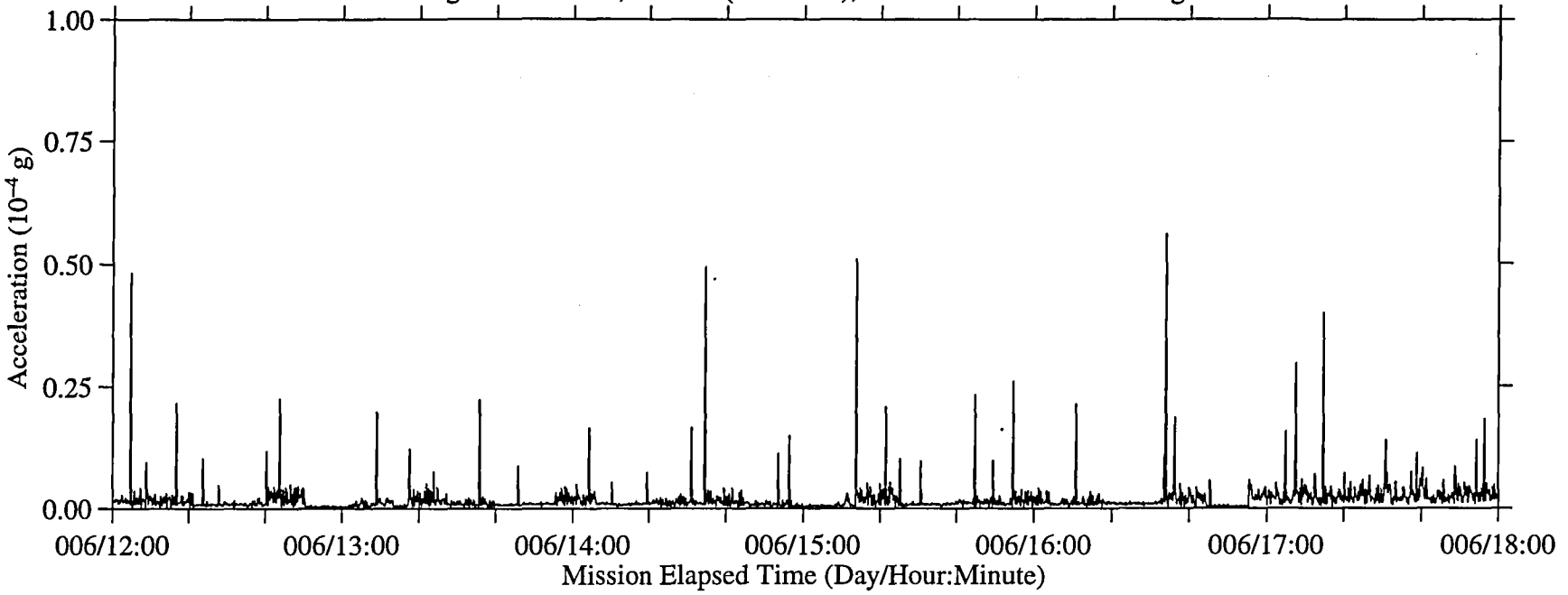

Figure 51b: LMS, Head C (fc=25 Hz), Ten Second Interval RMS

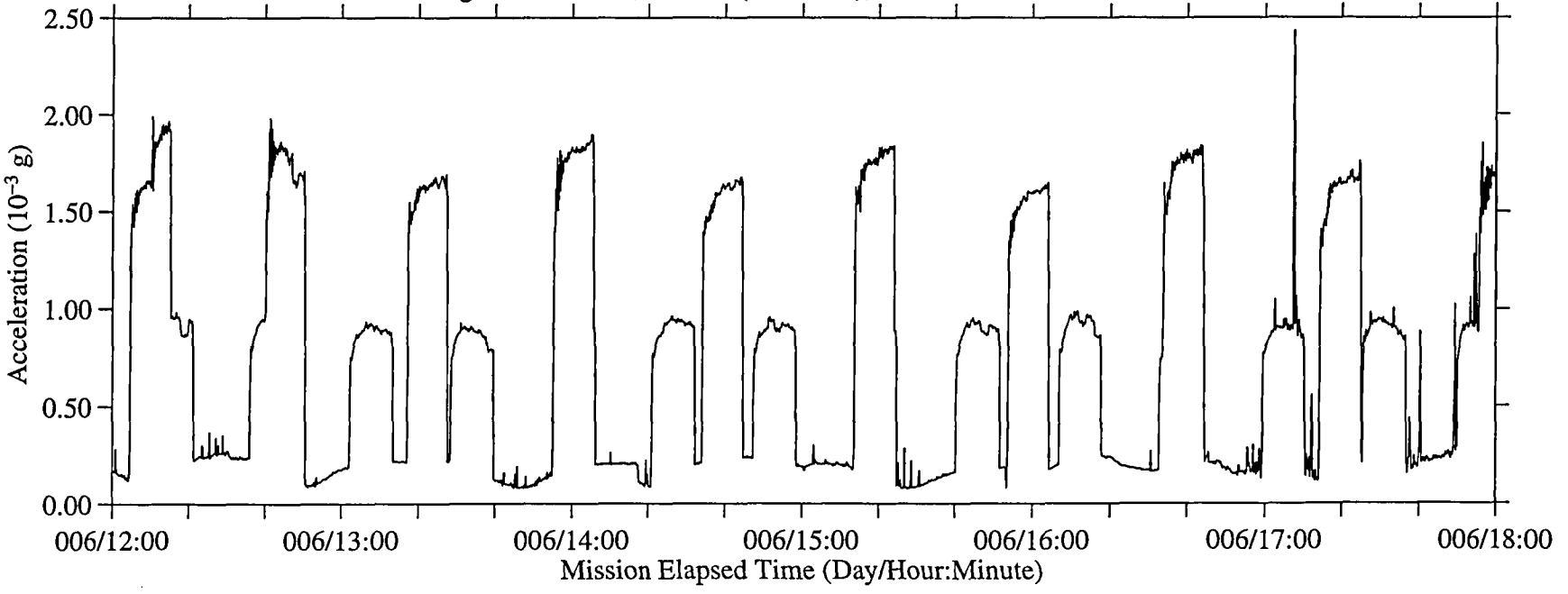

Figure 52: LMS, Head C (fc=25 Hz)

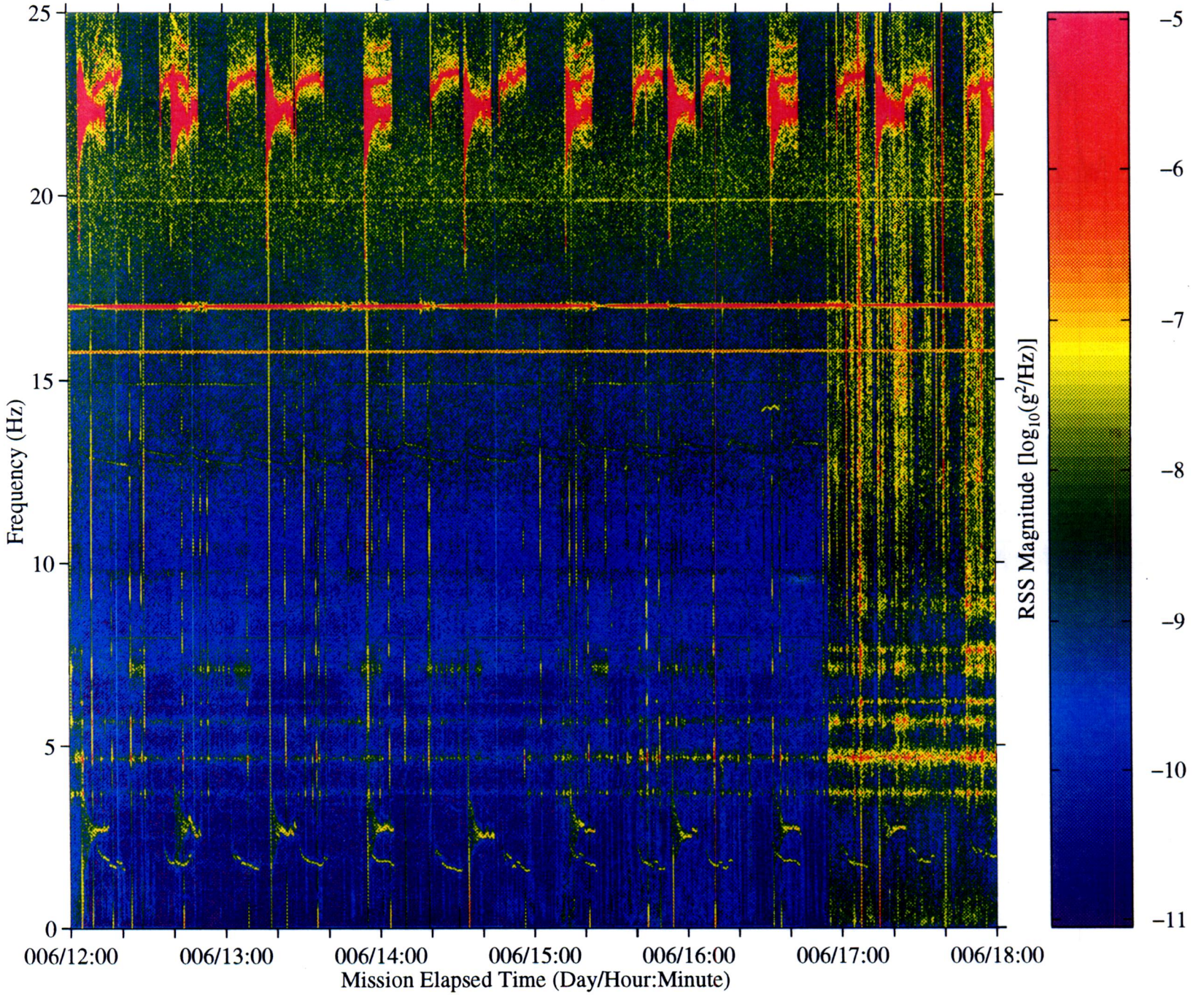

Figure 53a: LMS, Head C (fc=25 Hz), Ten Second Interval Average

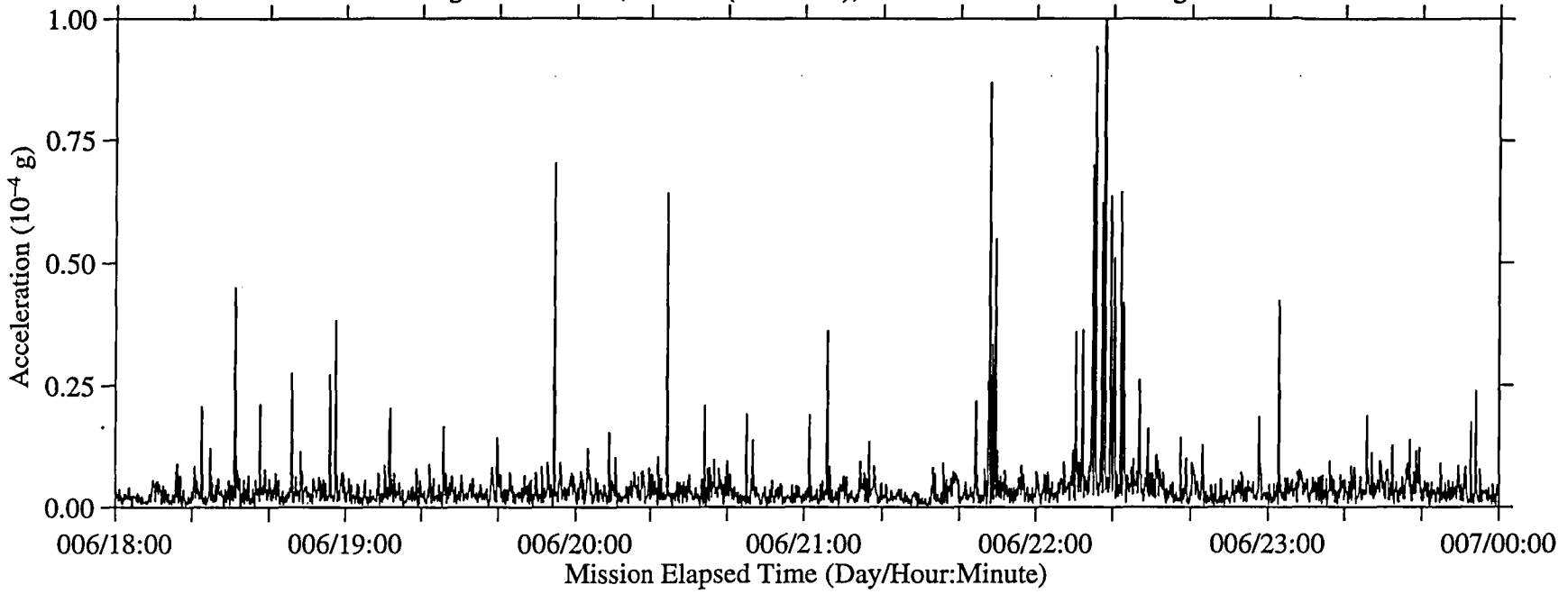

Figure 53b: LMS, Head C (fc=25 Hz), Ten Second Interval RMS

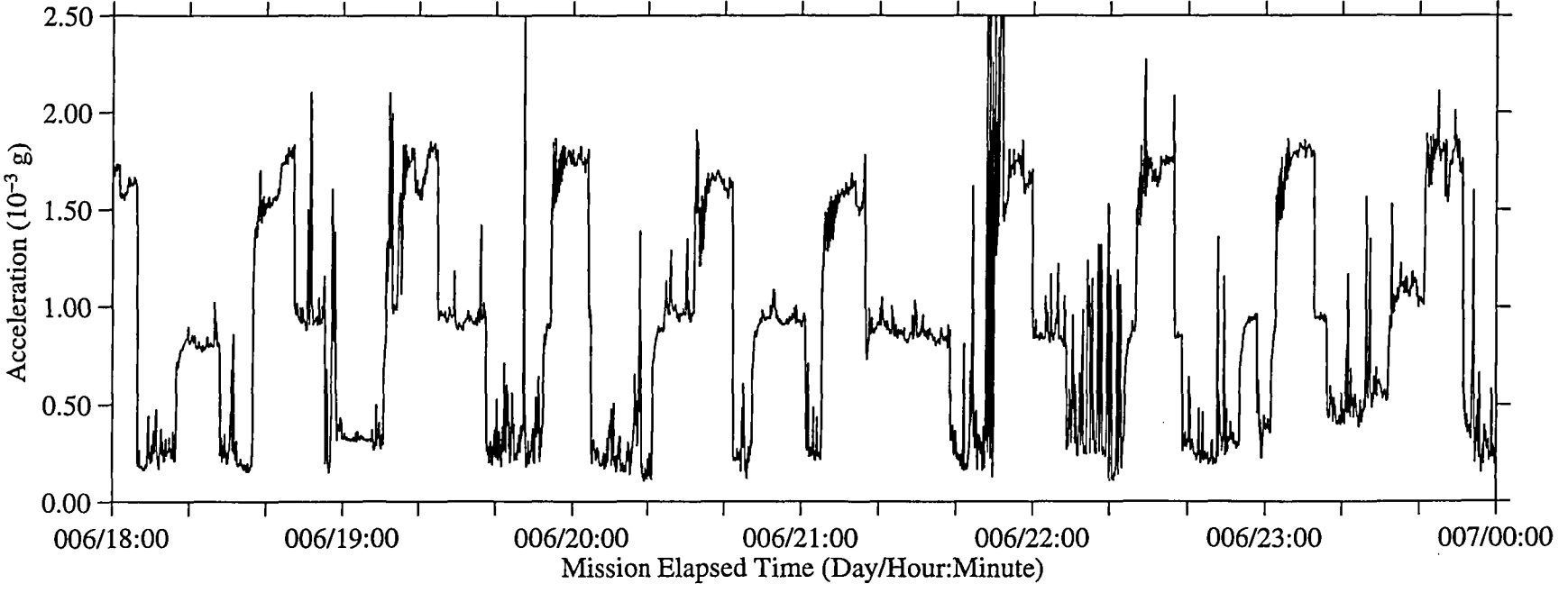

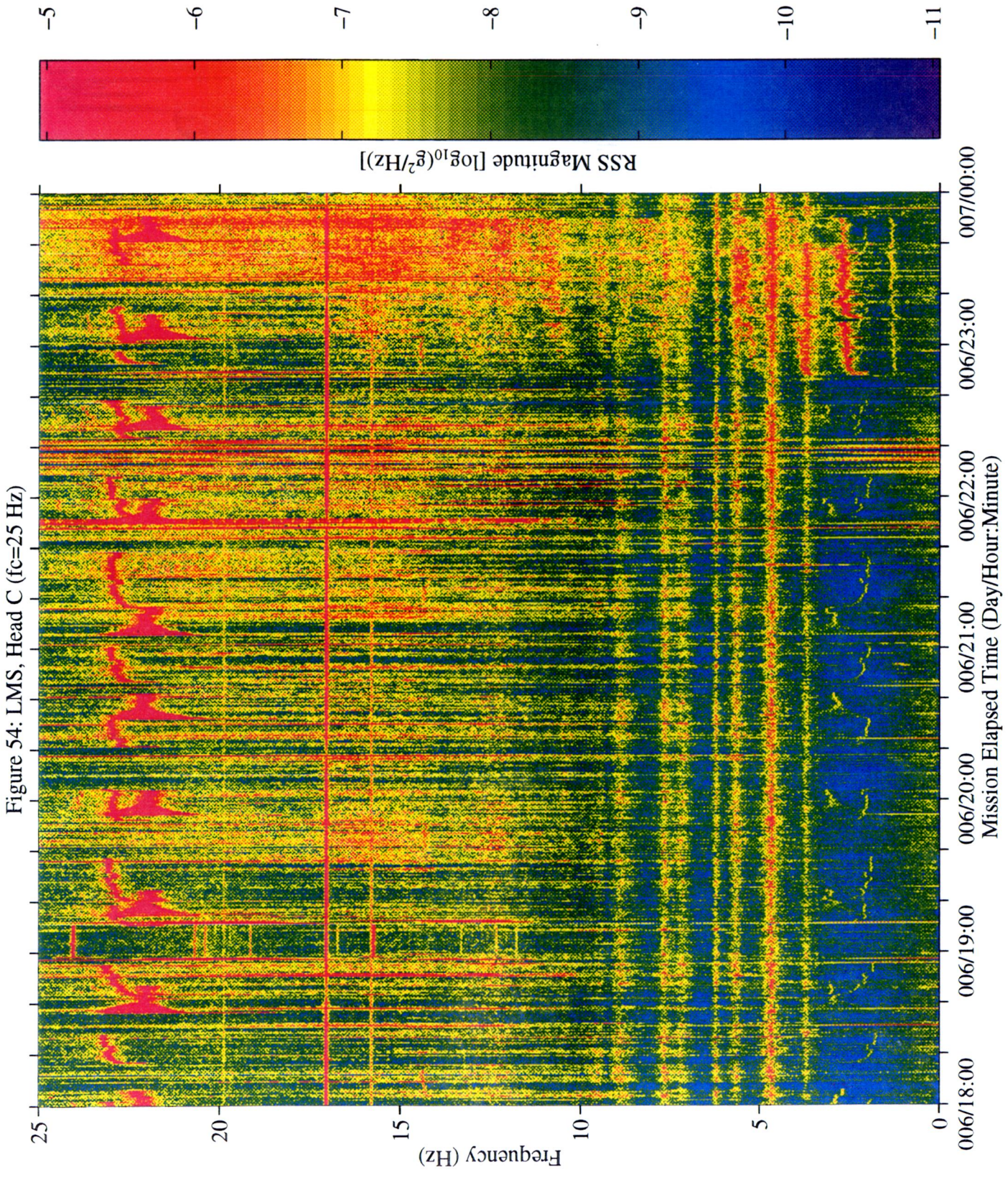

Figure 54: LMS, Head C (fc=25 Hz)

Figure 55a: LMS, Head C (fc=25 Hz), Ten Second Interval Average

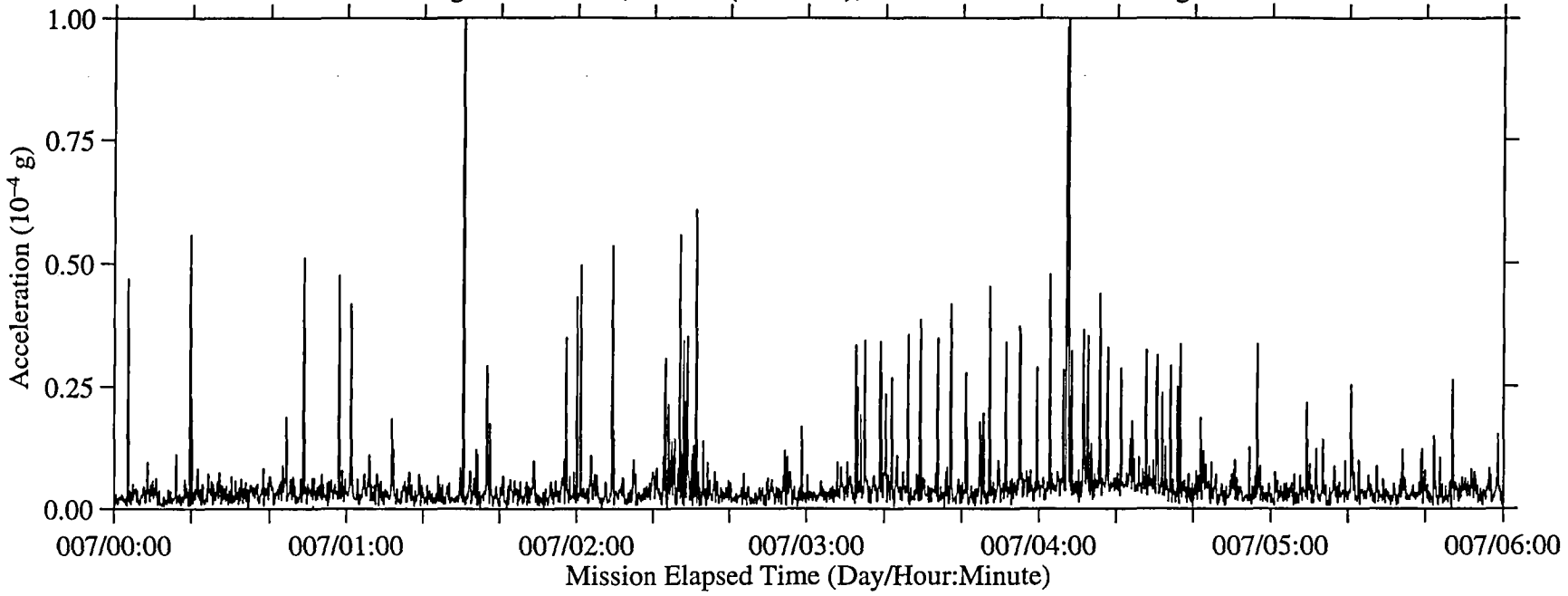

Figure 55b: LMS, Head C (fc=25 Hz), Ten Second Interval RMS

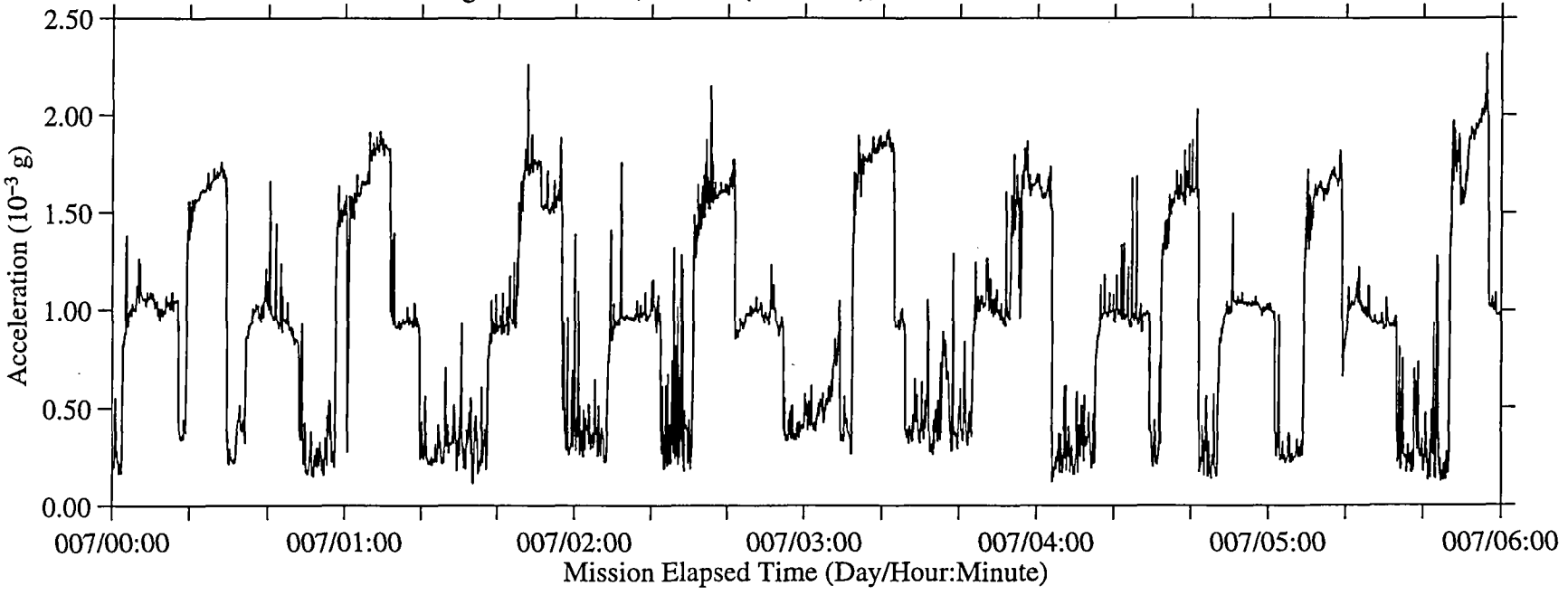

Figure 56: LMS, Head C (fc=25 Hz)

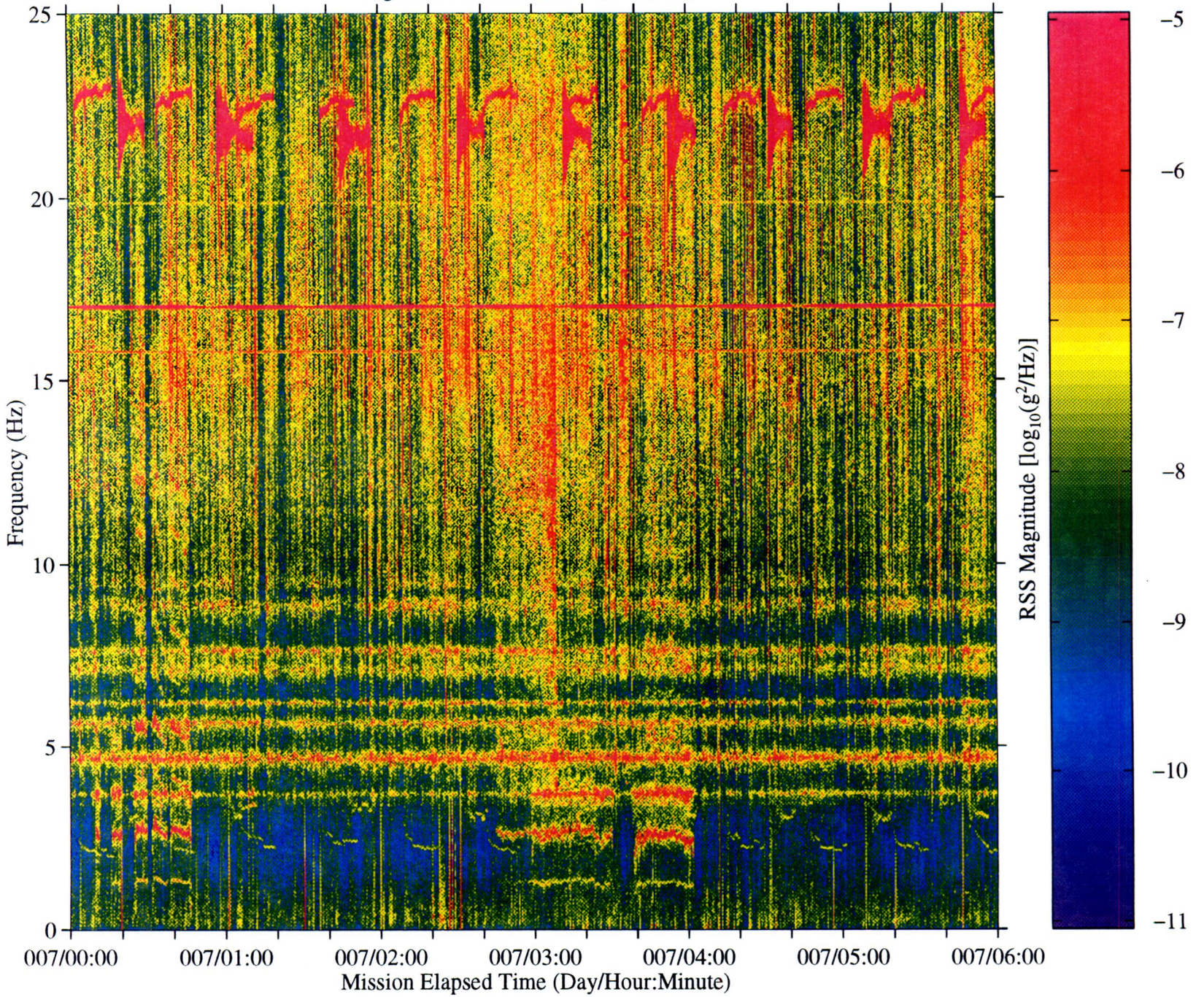

Figure 57a: LMS, Head C (fc=25 Hz), Ten Second Interval Average

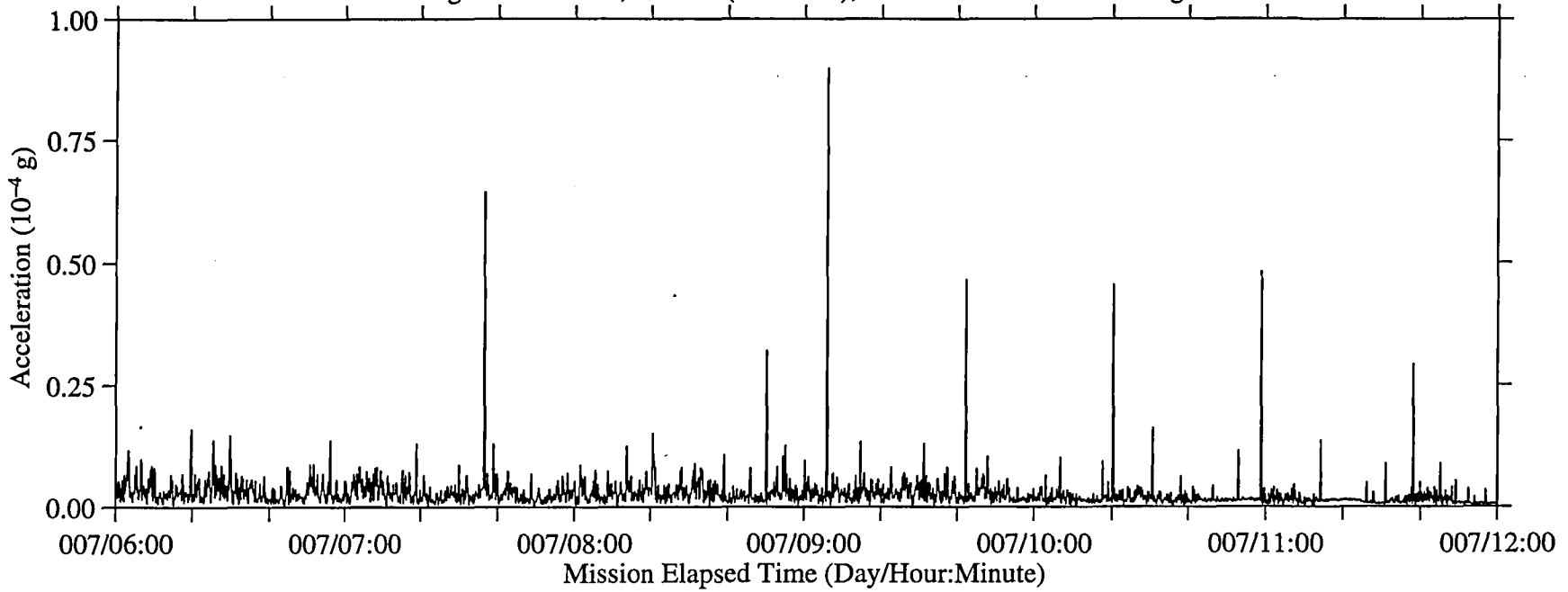

Figure 57b: LMS, Head C (fc=25 Hz), Ten Second Interval RMS

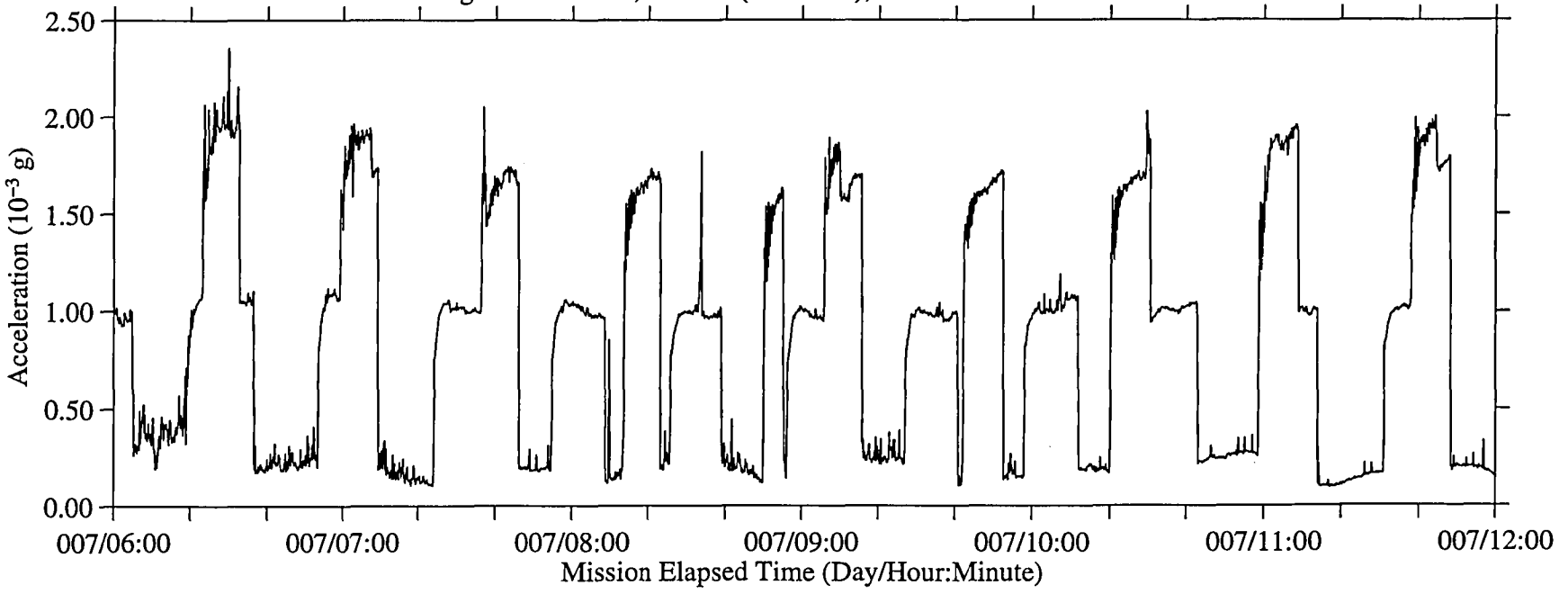

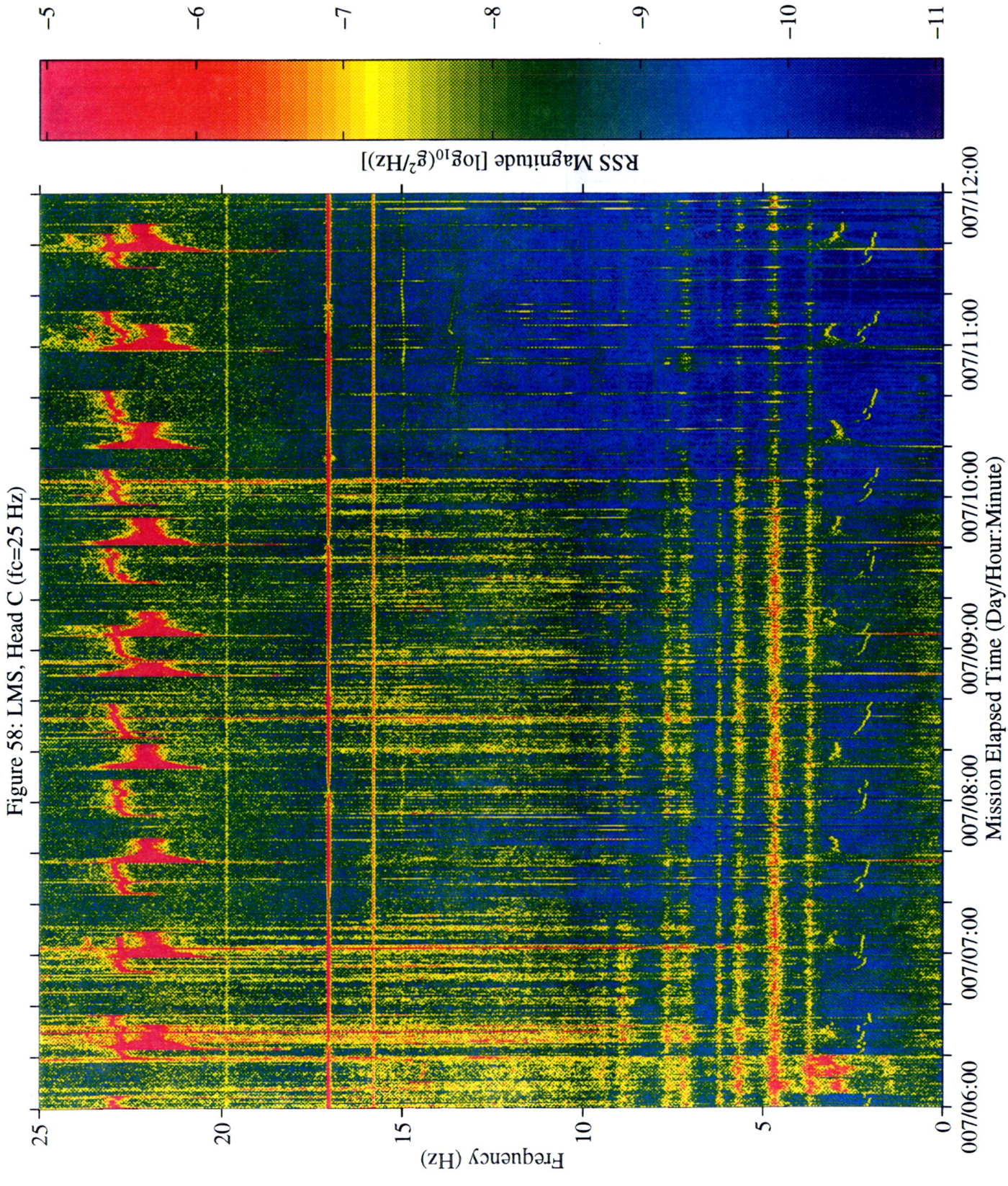

Figure 58: LMS, Head C (fc=25 Hz)

Figure 59a: LMS, Head C (fc=25 Hz), Ten Second Interval Average

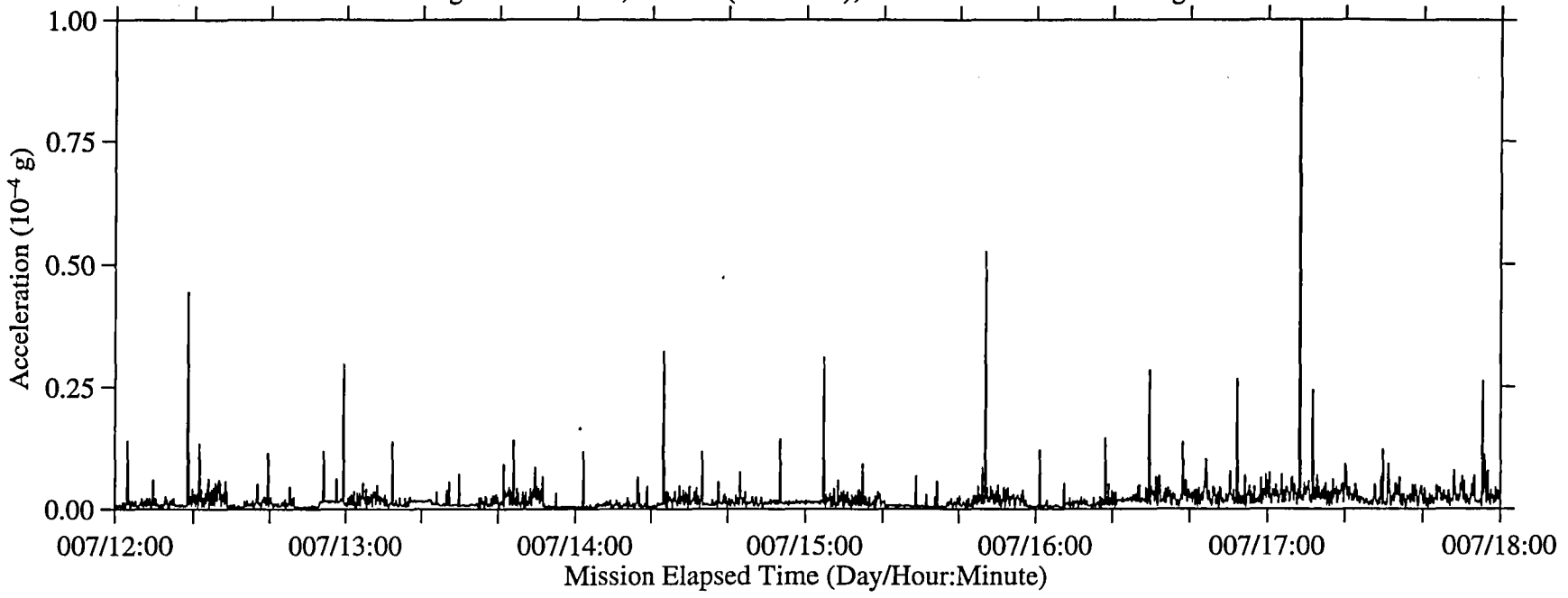

Figure 59b: LMS, Head C (fc=25 Hz), Ten Second Interval RMS

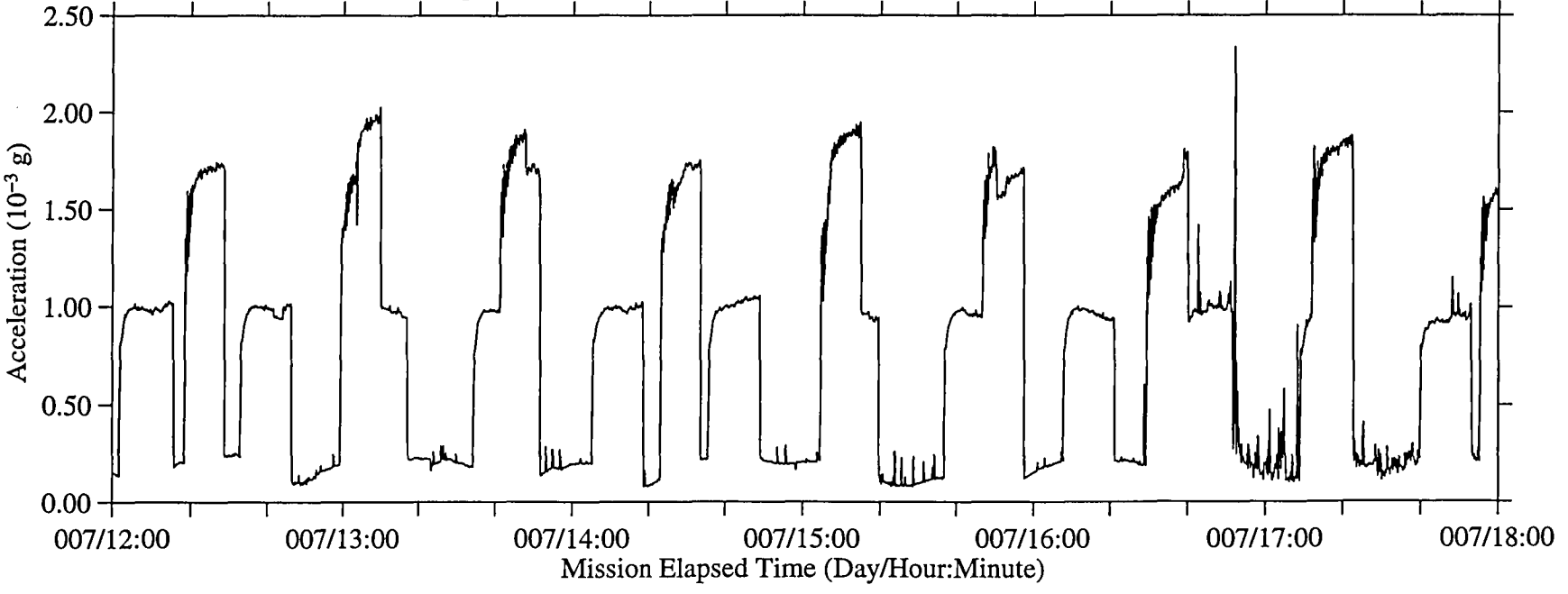

Figure 60: LMS, Head C (fc=25 Hz)

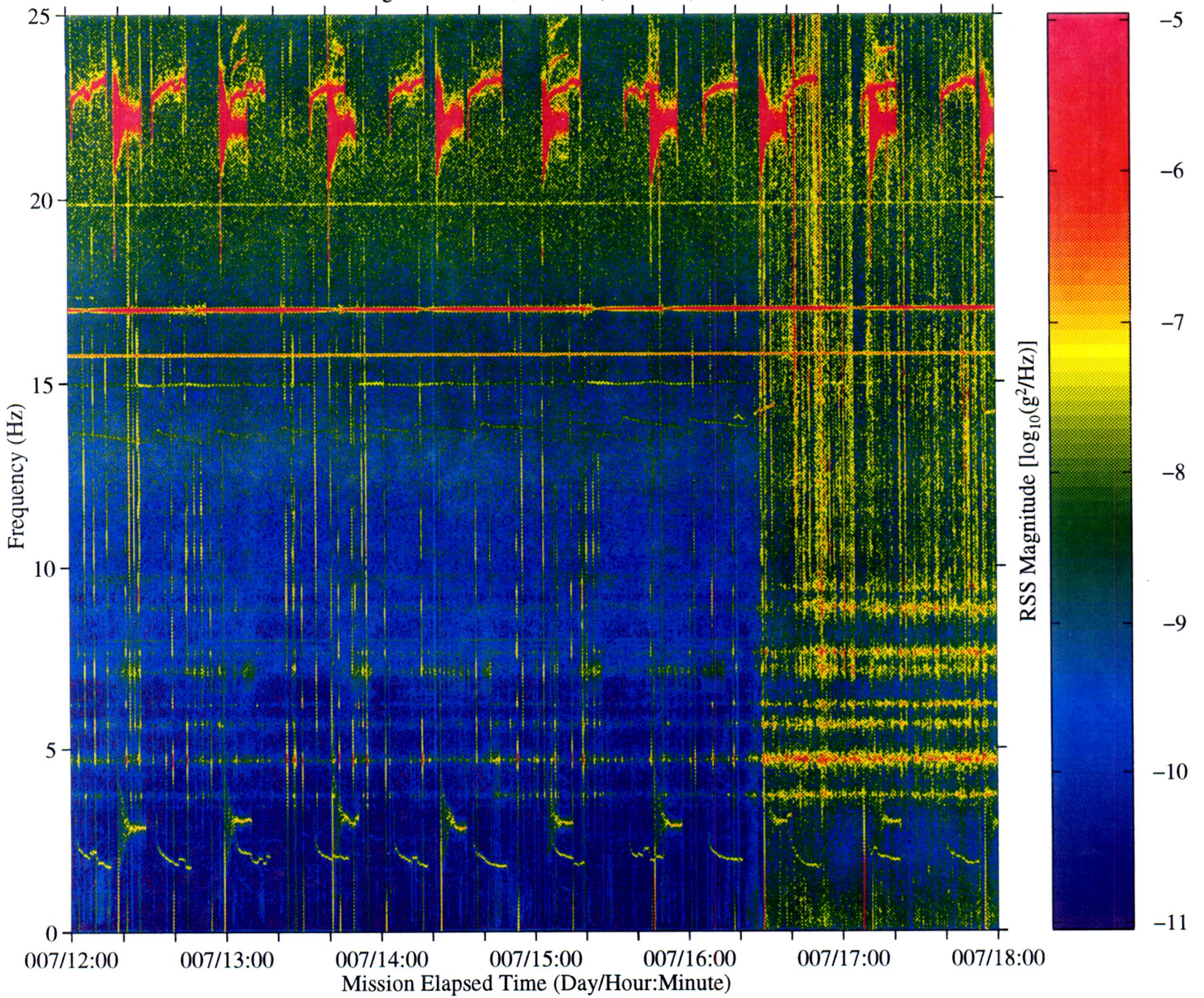

Figure 61a: LMS, Head C (fc=25 Hz), Ten Second Interval Average

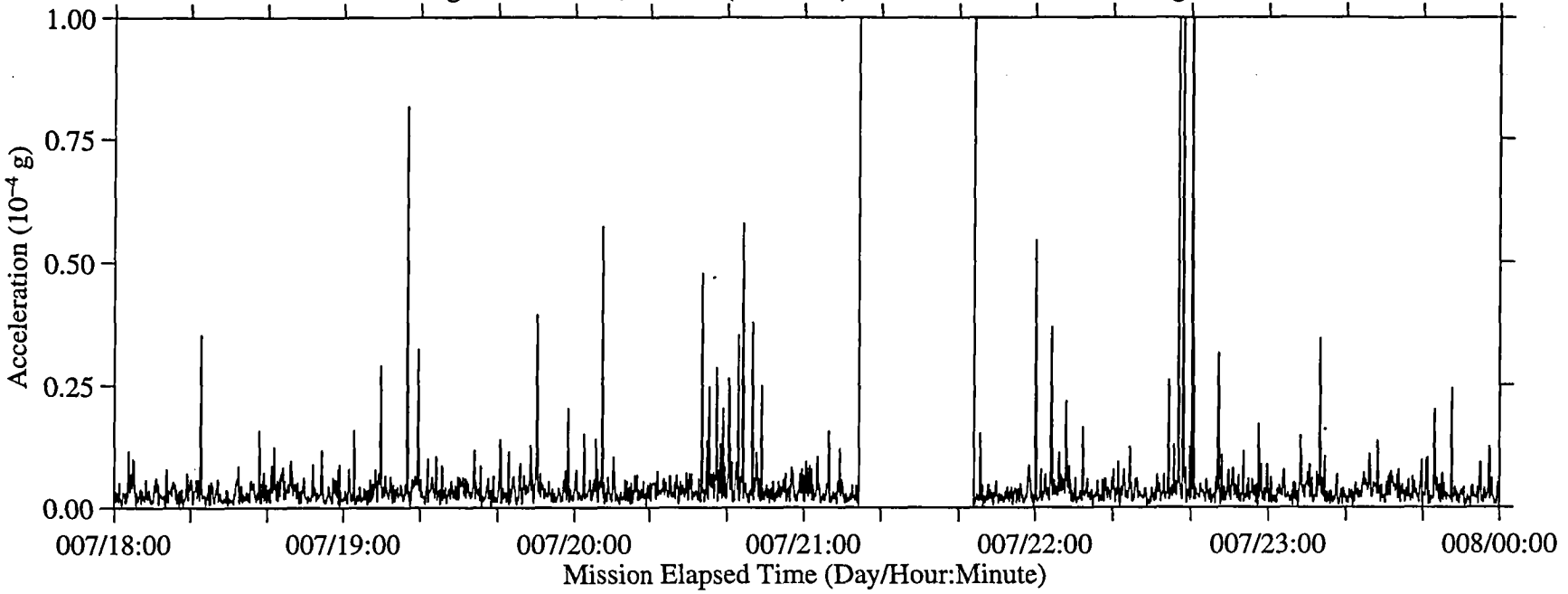

Figure 61b: LMS, Head C (fc=25 Hz), Ten Second Interval RMS

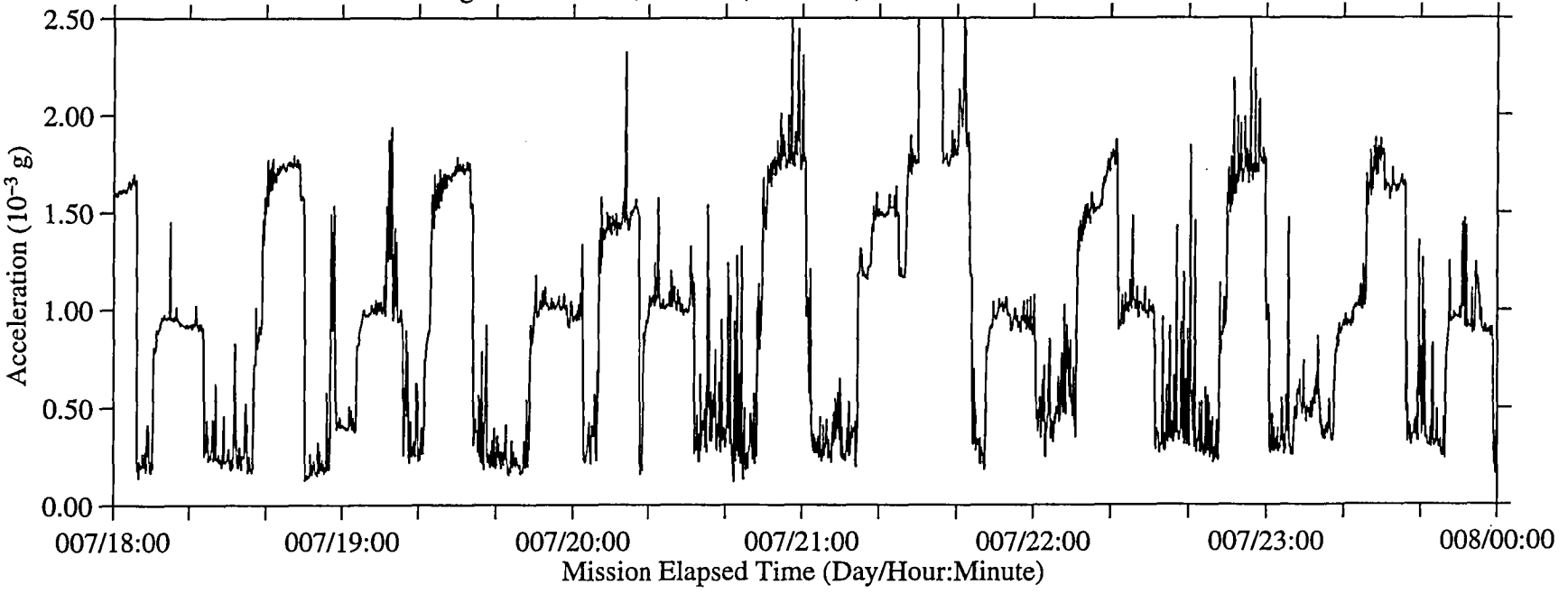

Figure 62: LMS, Head C (fc=25 Hz)

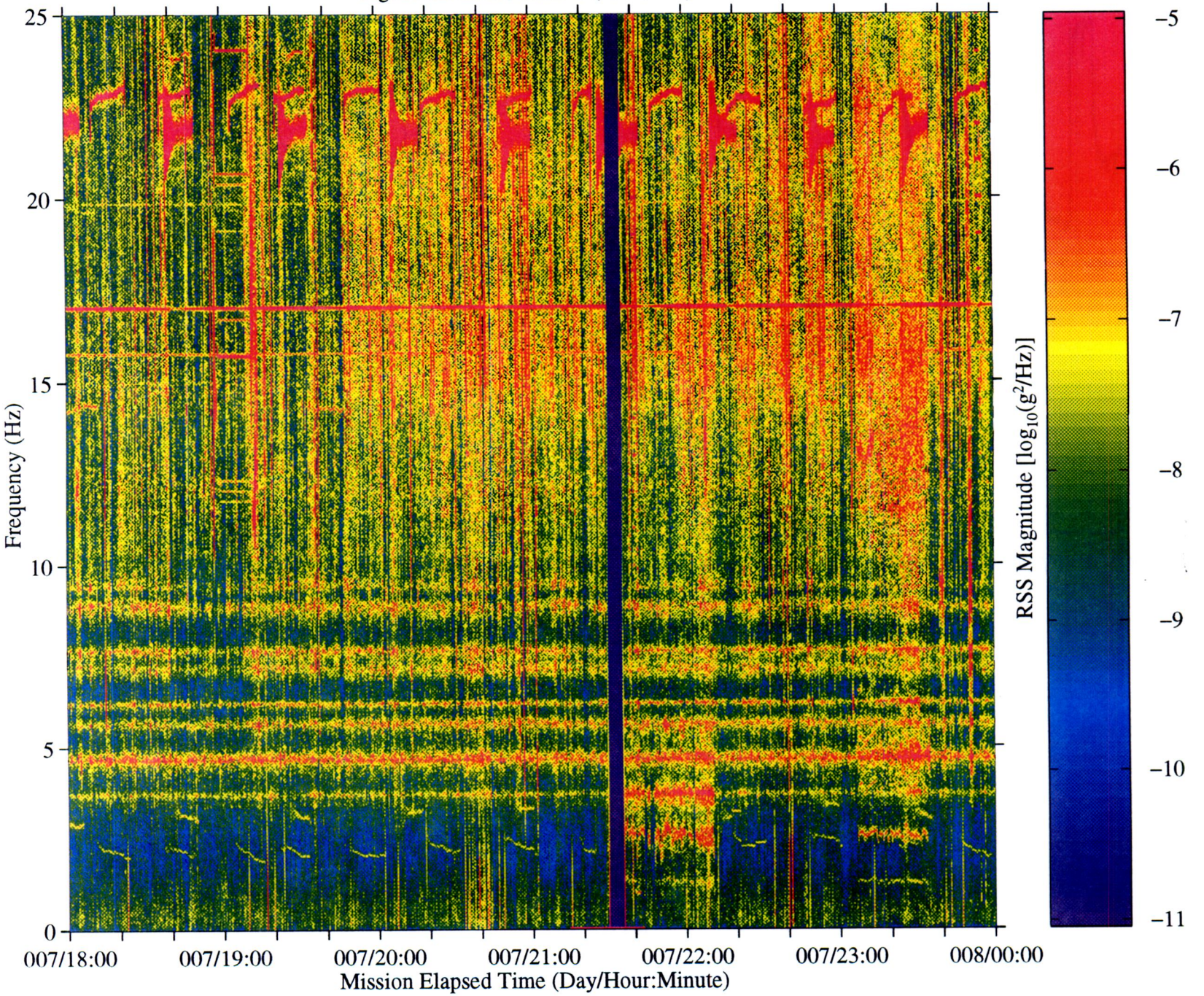

Figure 63a: LMS, Head C (fc=25 Hz), Ten Second Interval Average

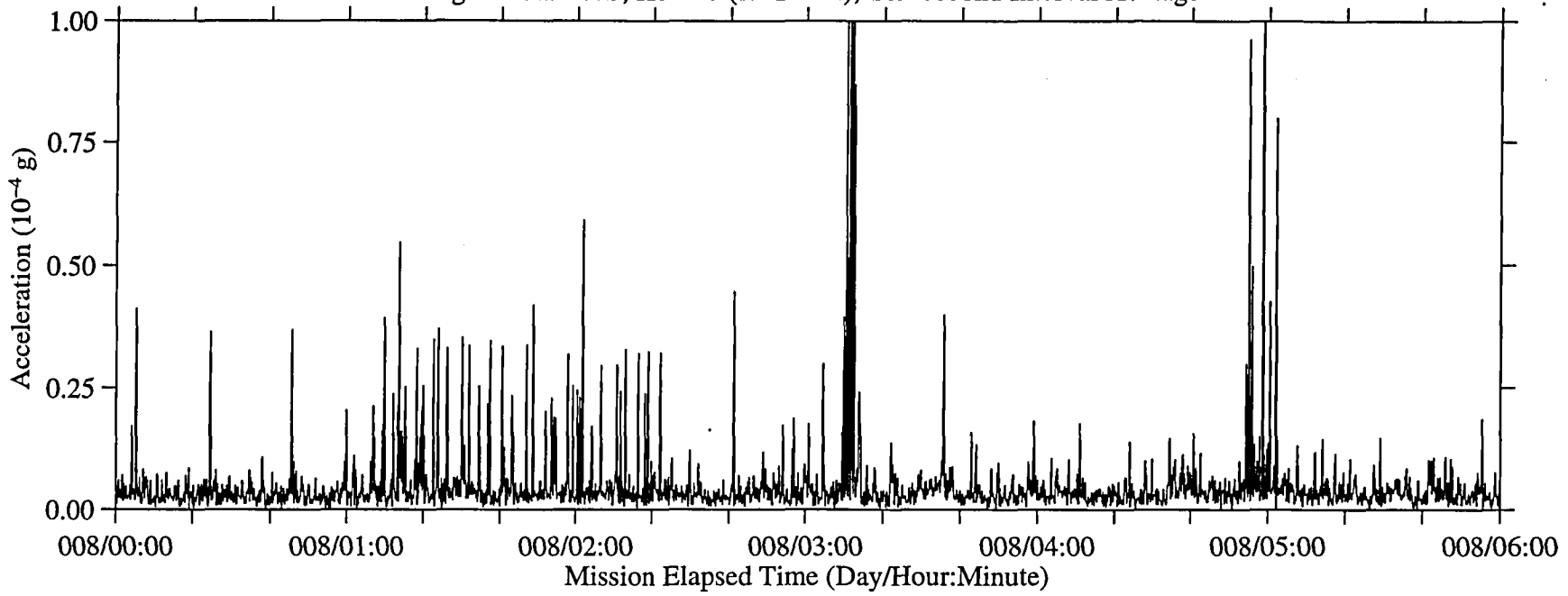

Figure 63b: LMS, Head C (fc=25 Hz), Ten Second Interval RMS

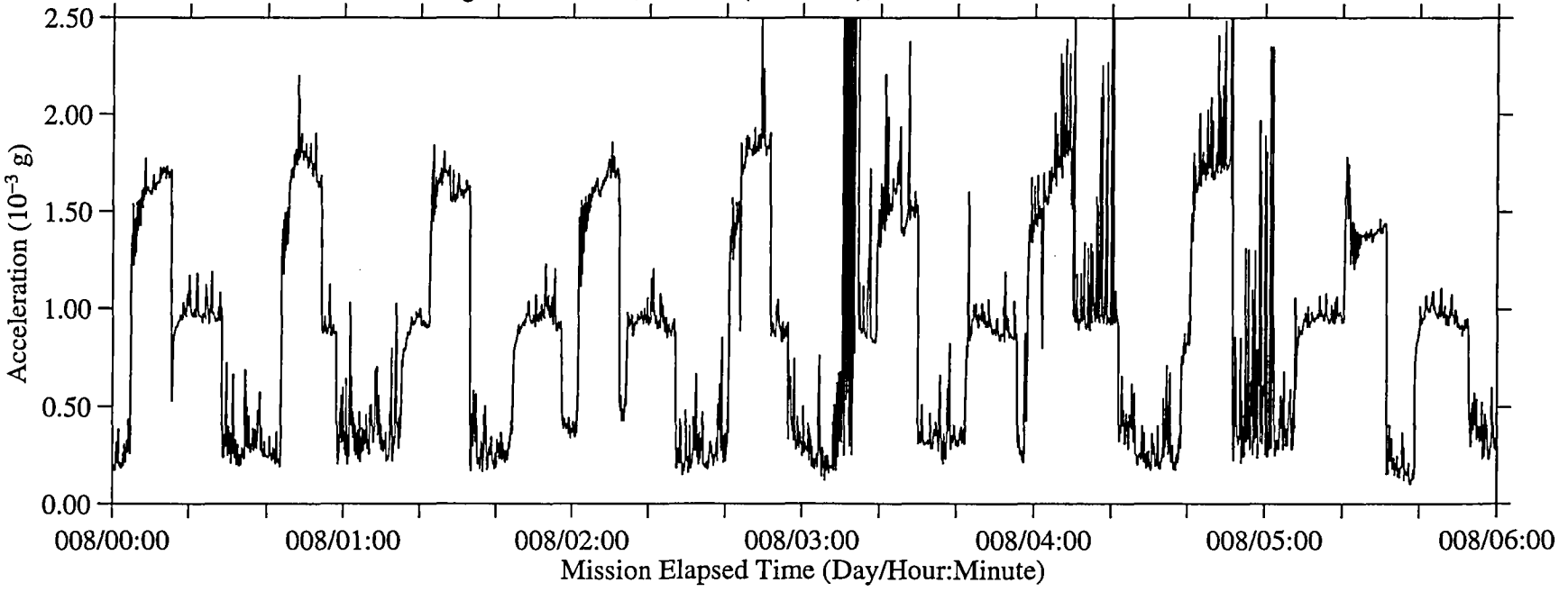

Figure 64: LMS, Head C (fc=25 Hz)

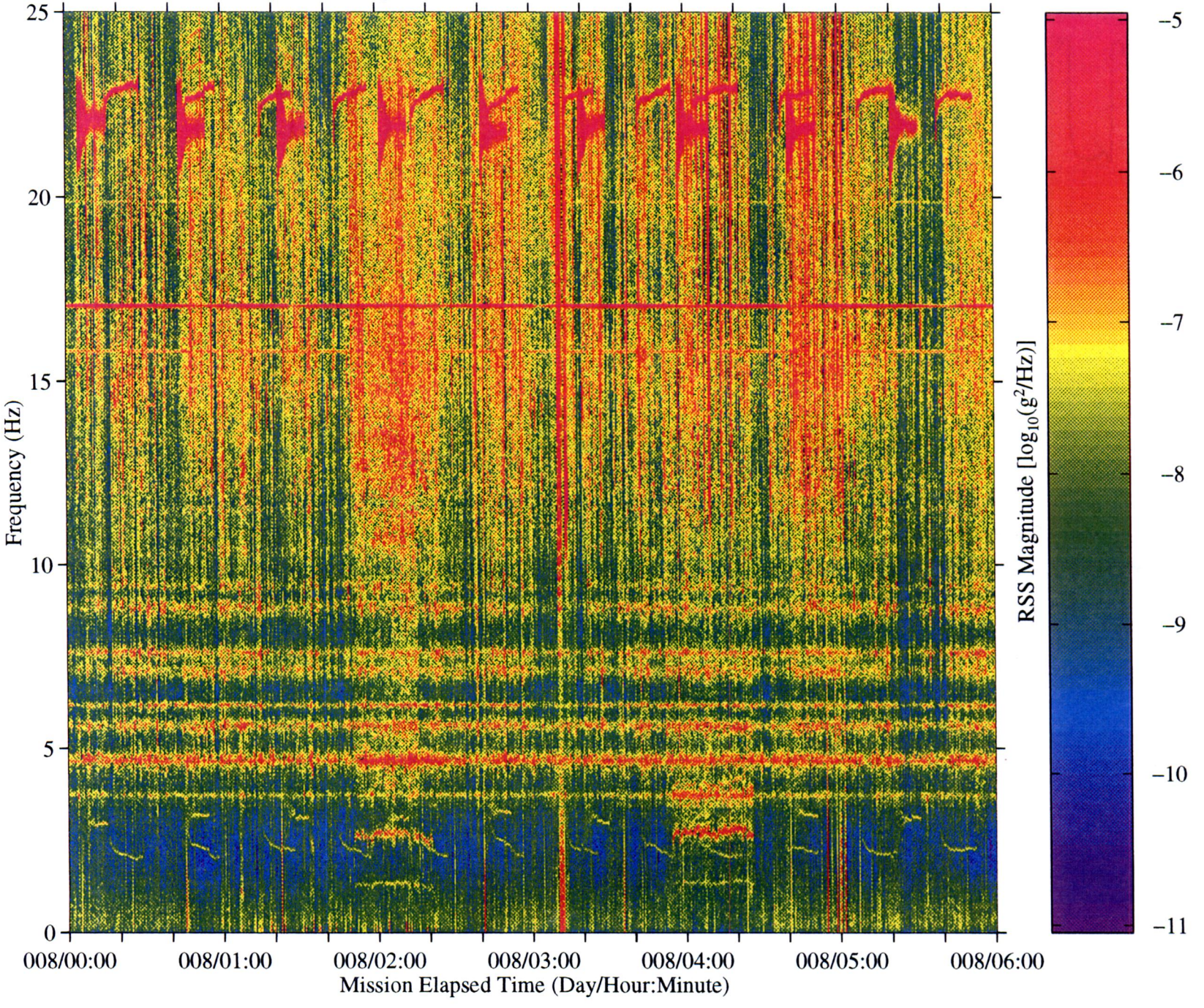

Figure 65a: LMS, Head C (fc=25 Hz), Ten Second Interval Average

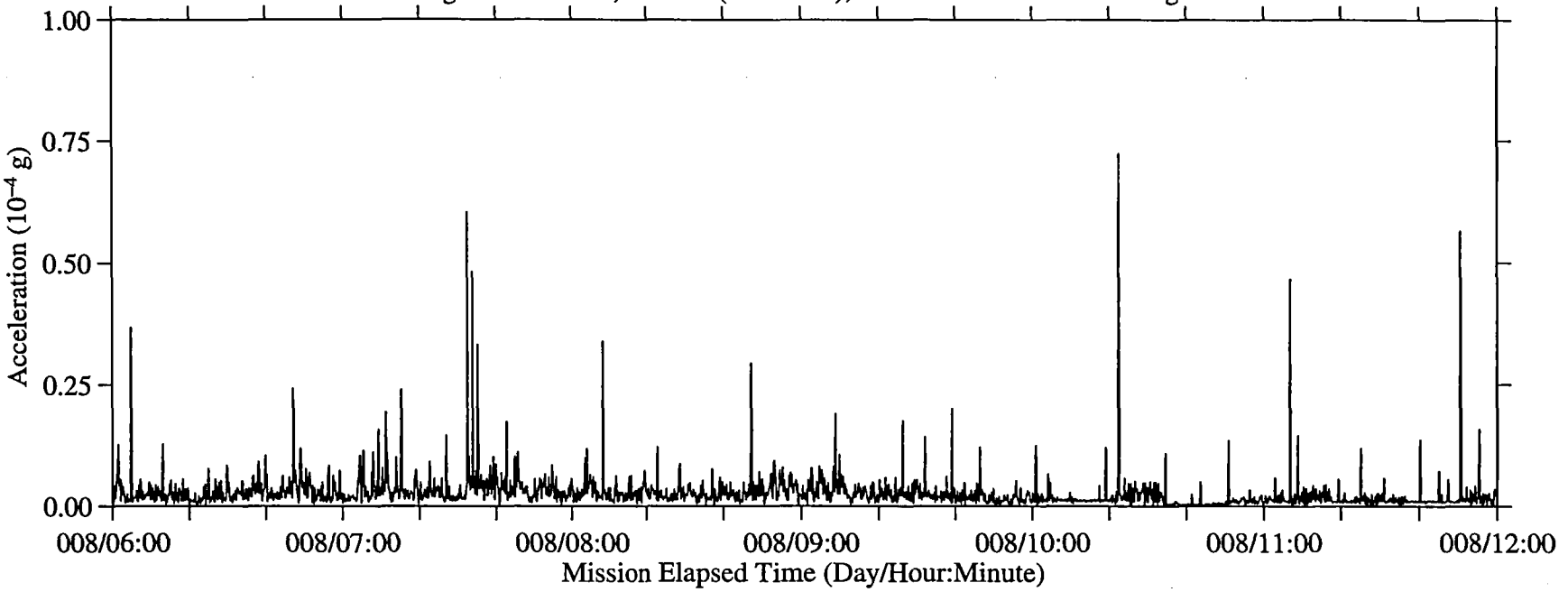

Figure 65b: LMS, Head C (fc=25 Hz), Ten Second Interval RMS

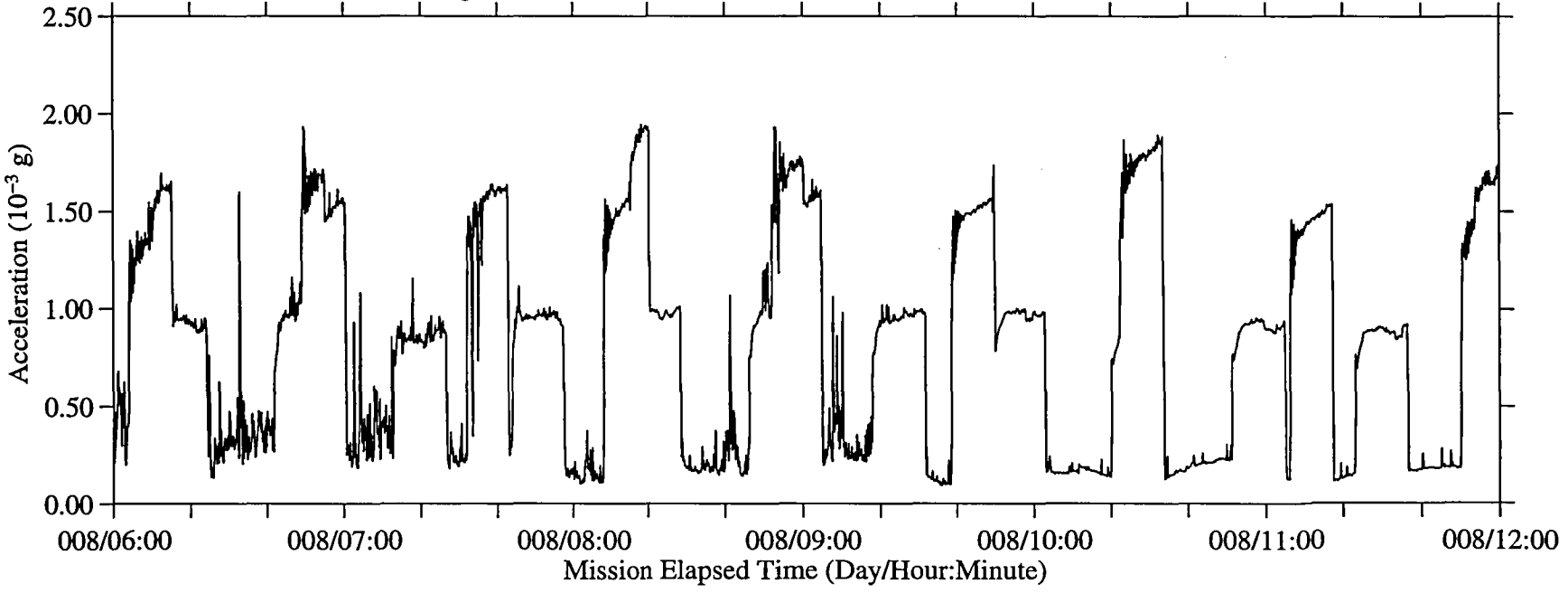

Figure 66: LMS, Head C (fc=25 Hz)

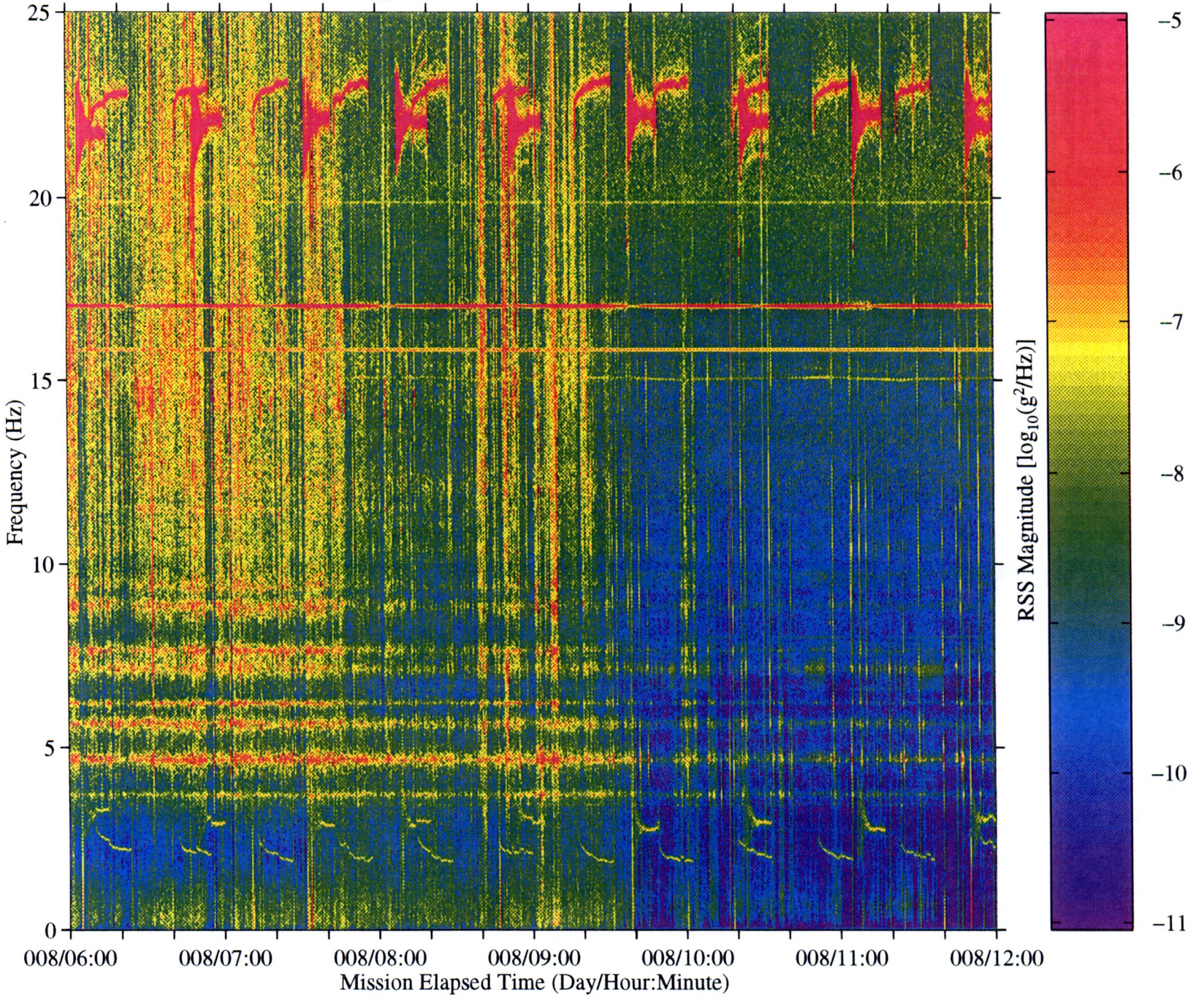

Figure 67a: LMS, Head C (fc=25 Hz), Ten Second Interval Average

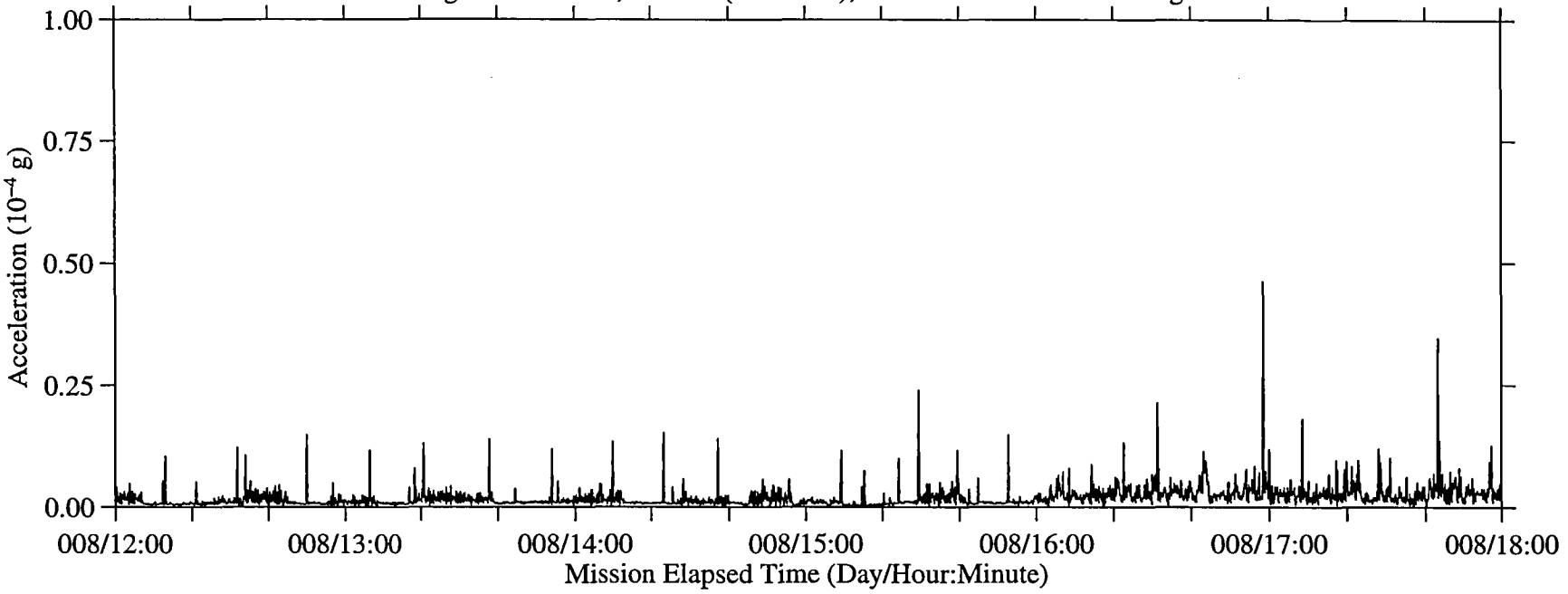

Figure 67b: LMS, Head C (fc=25 Hz), Ten Second Interval RMS

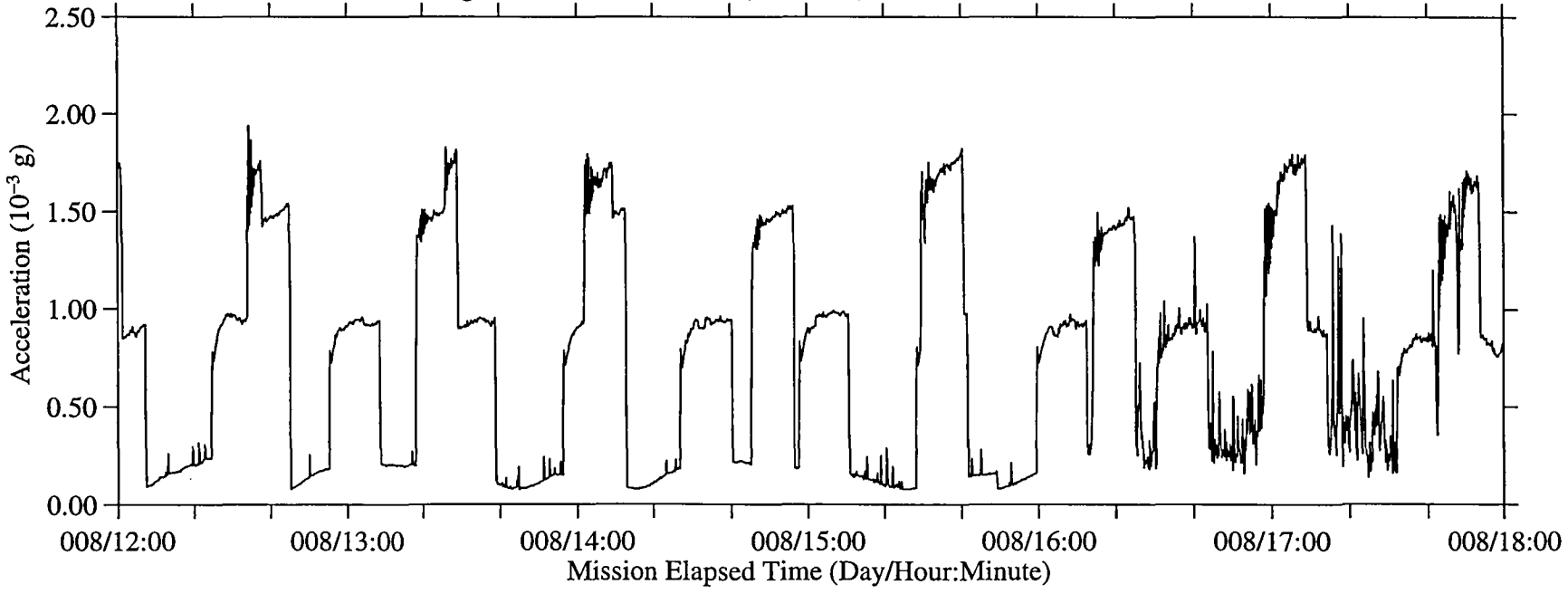

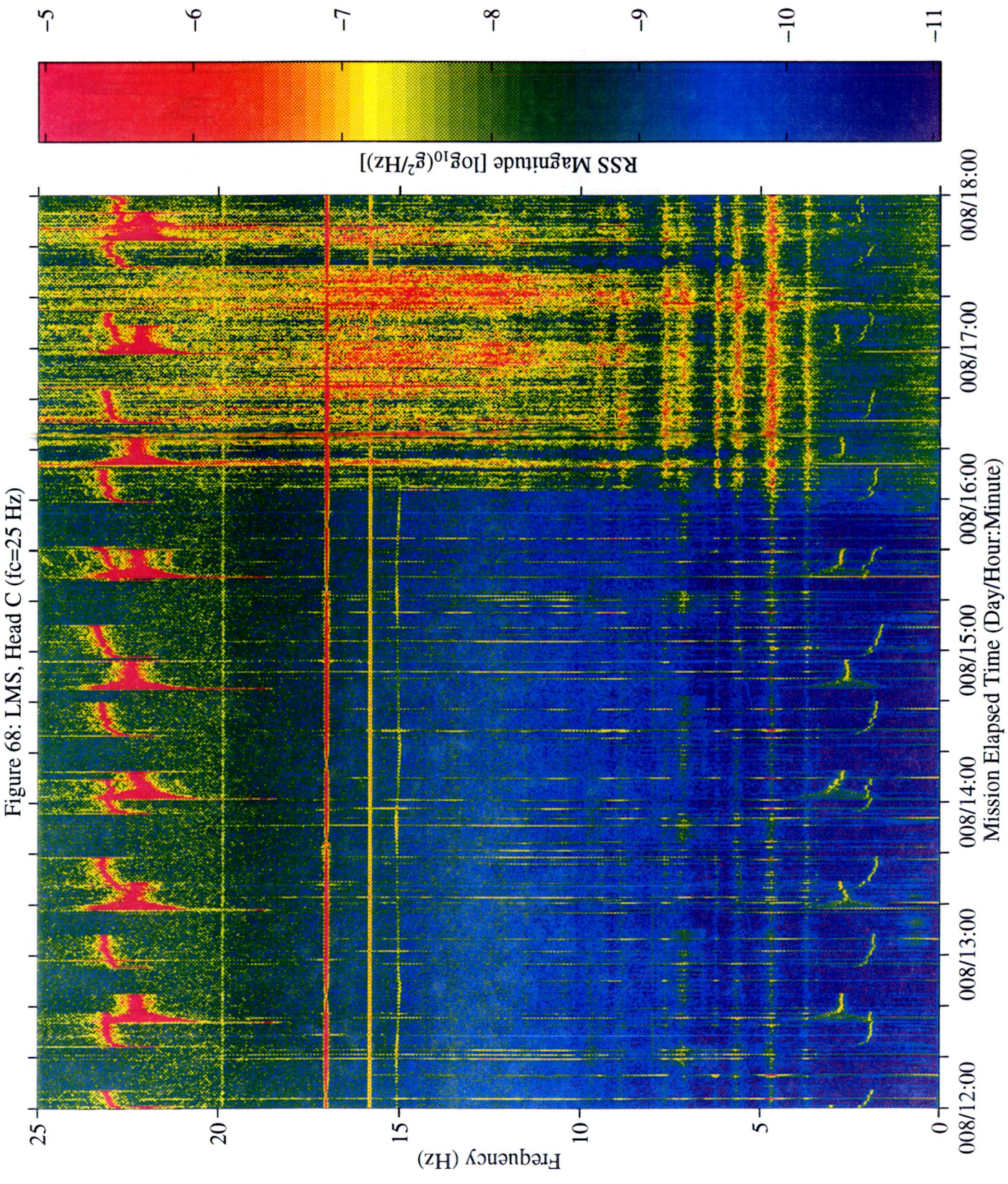

Figure 68: LMS, Head C (fc=25 Hz)

Figure 69a: LMS, Head C (fc=25 Hz), Ten Second Interval Average

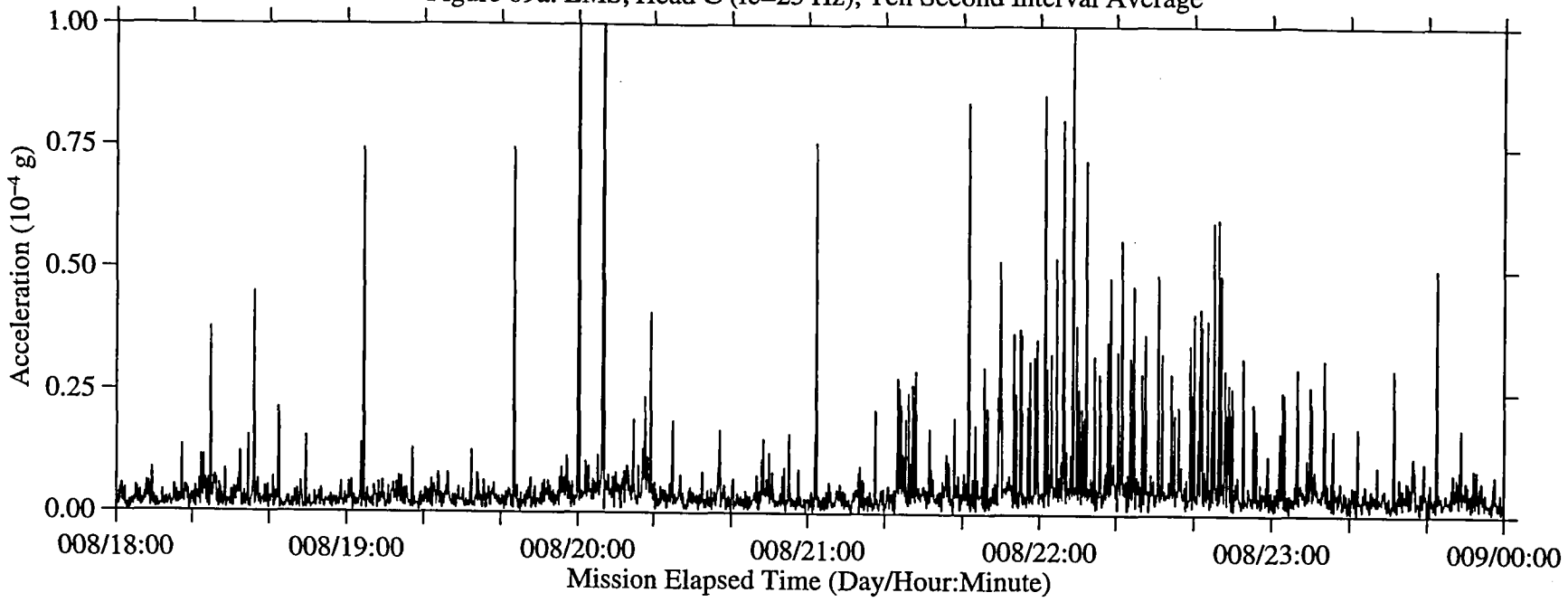

Figure 69b: LMS, Head C (fc=25 Hz), Ten Second Interval RMS

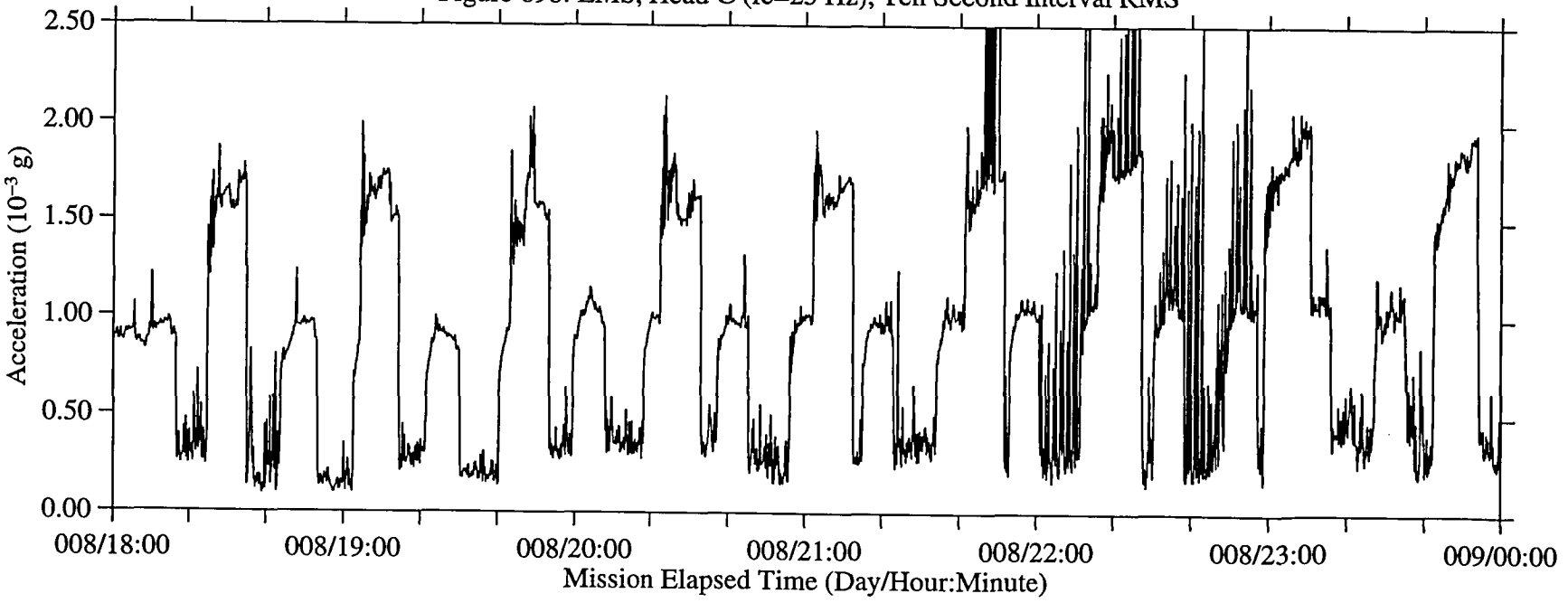

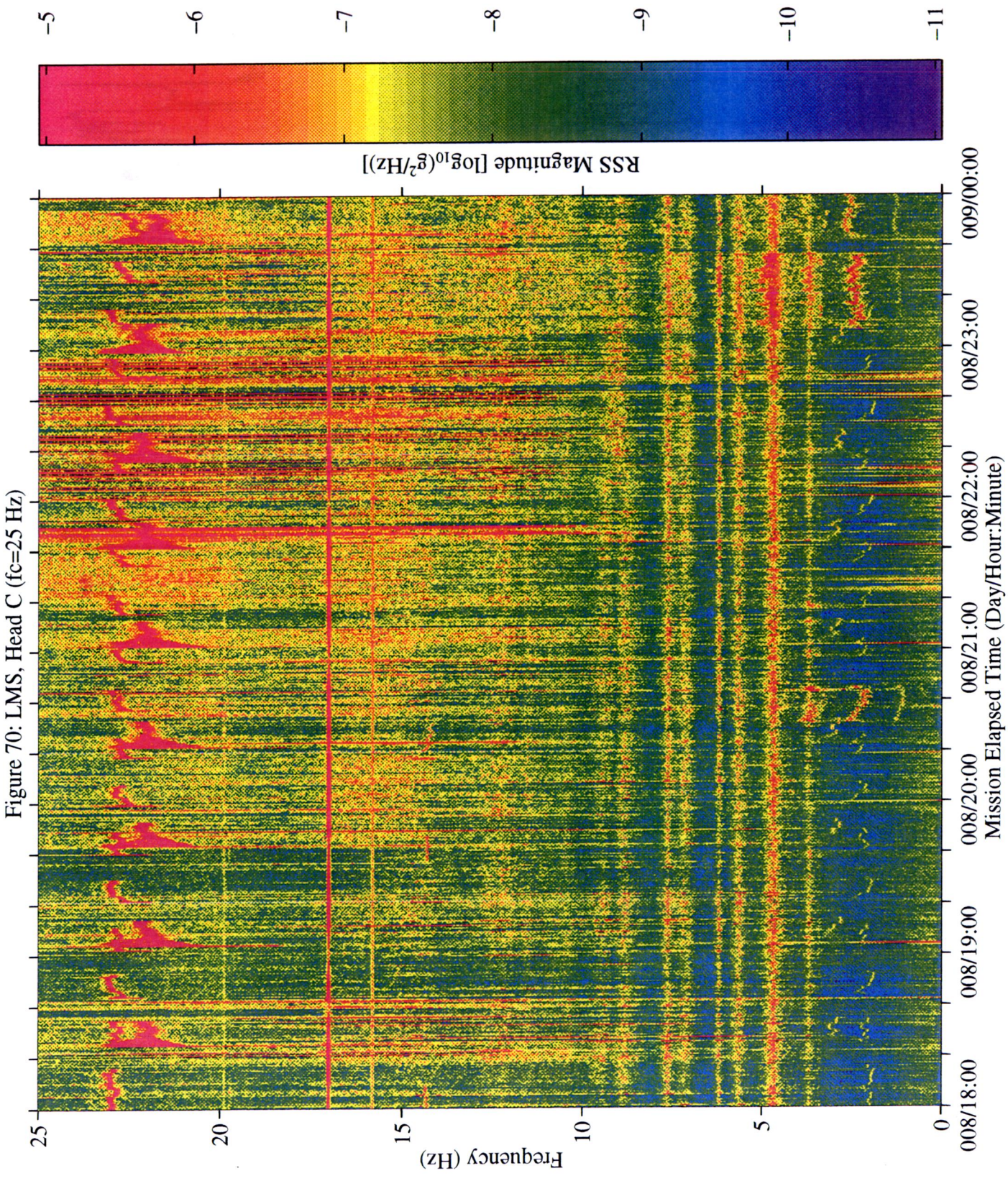

Figure 70: LMS, Head C (fc=25 Hz)

Figure 71a: LMS, Head C (fc=25 Hz), Ten Second Interval Average

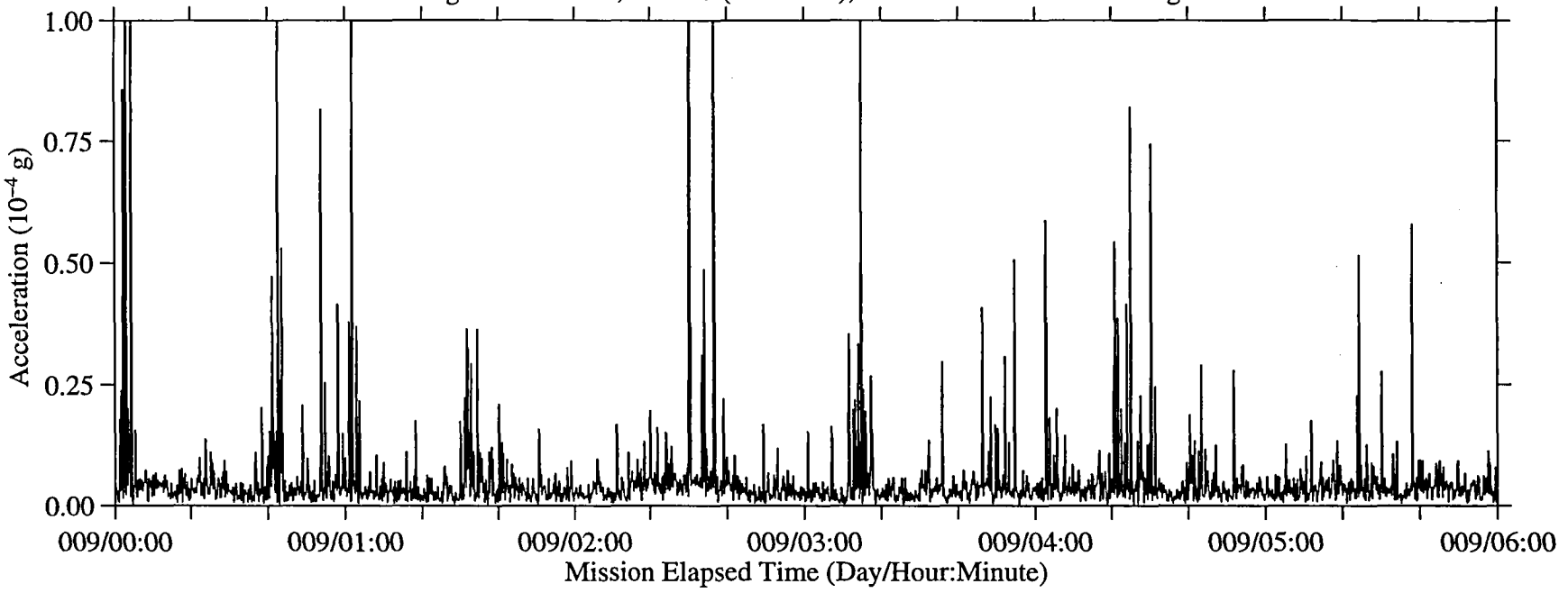

Figure 71b: LMS, Head C (fc=25 Hz), Ten Second Interval RMS

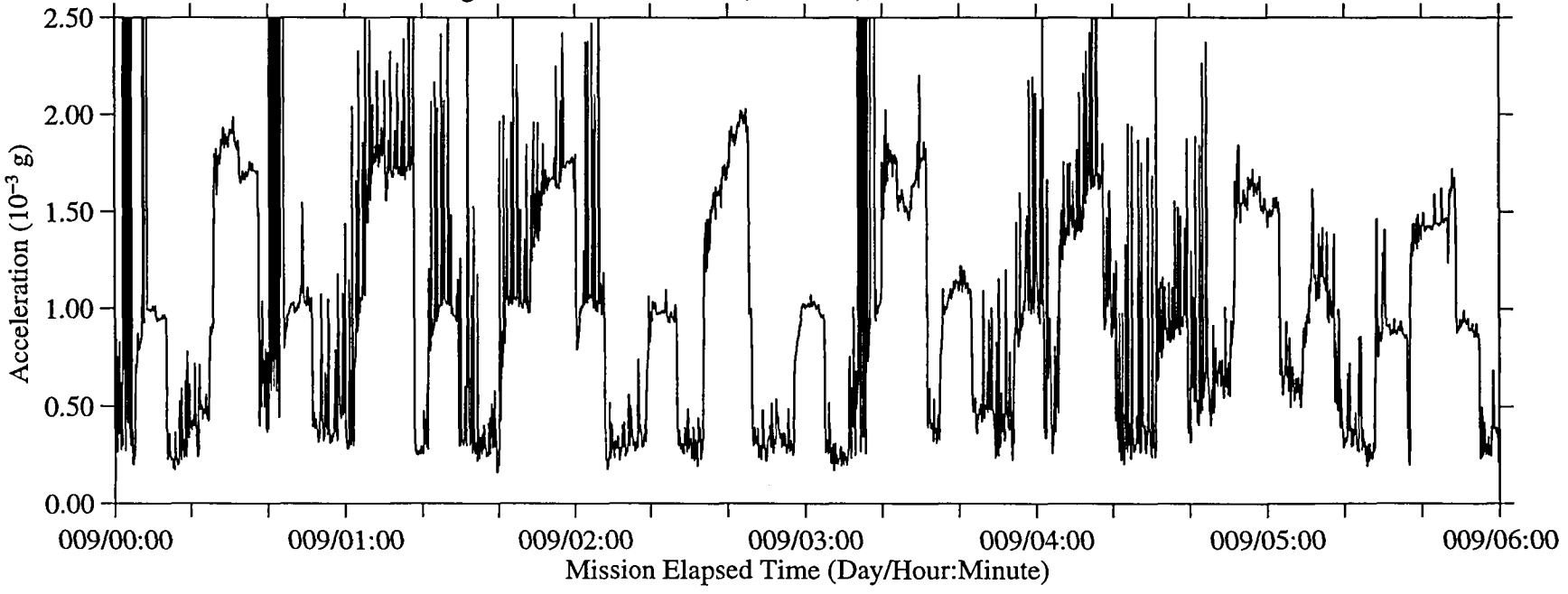

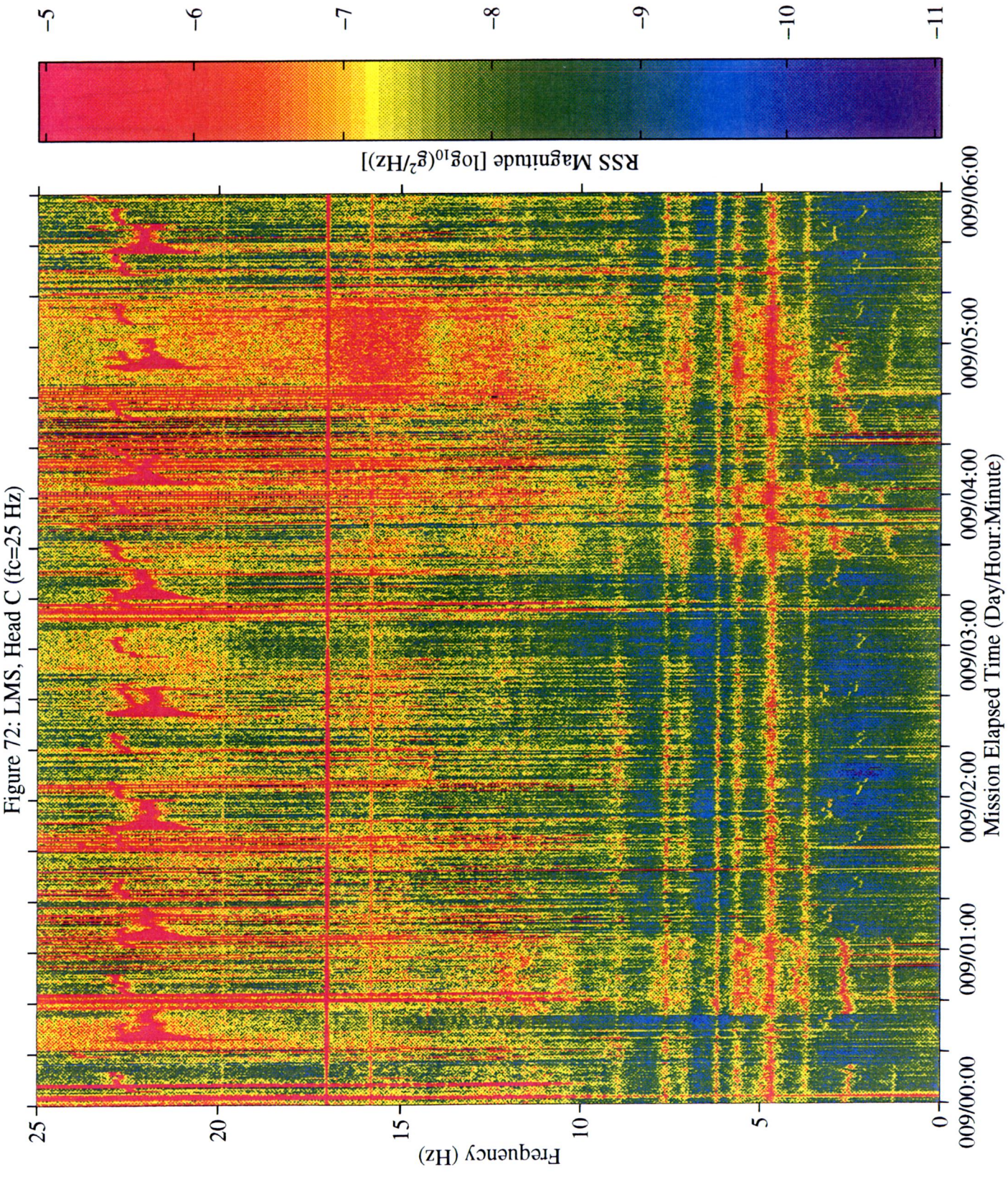

Figure 72: LMS, Head C (fc=25 Hz)

Figure 73a: LMS, Head C (fc=25 Hz), Ten Second Interval Average

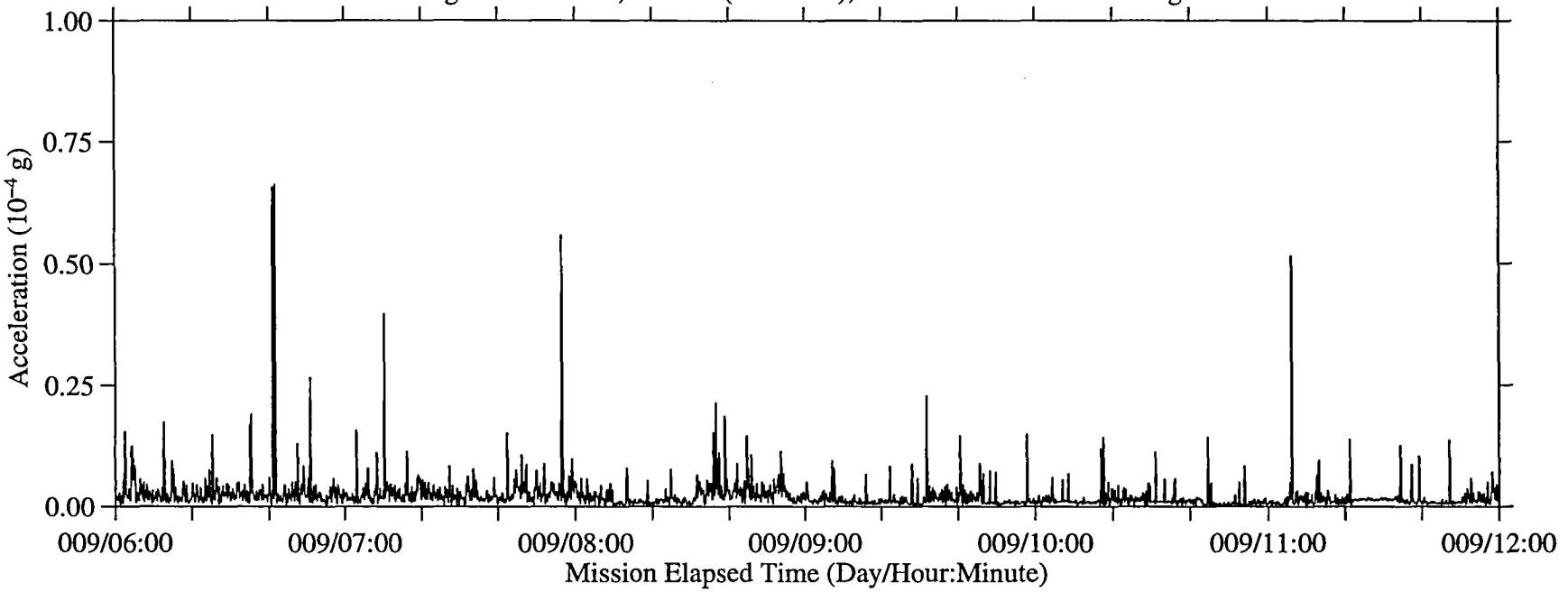

Figure 73b: LMS, Head C (fc=25 Hz), Ten Second Interval RMS

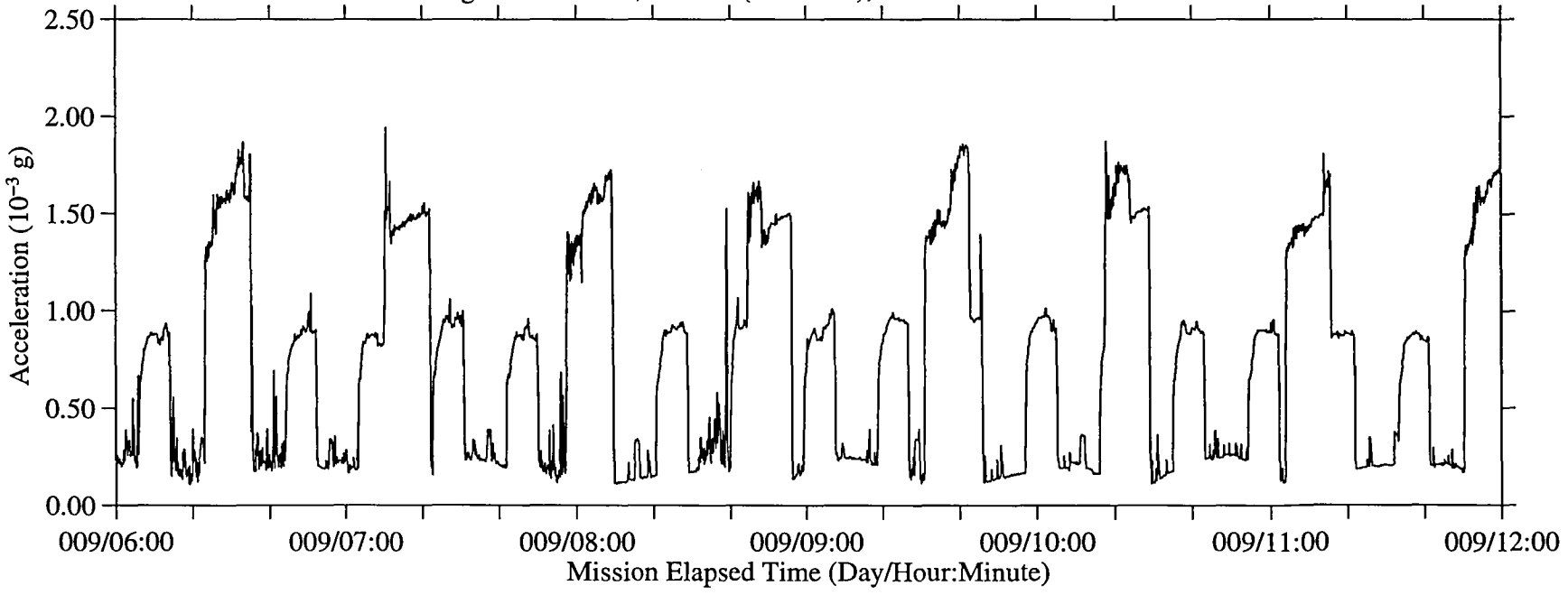

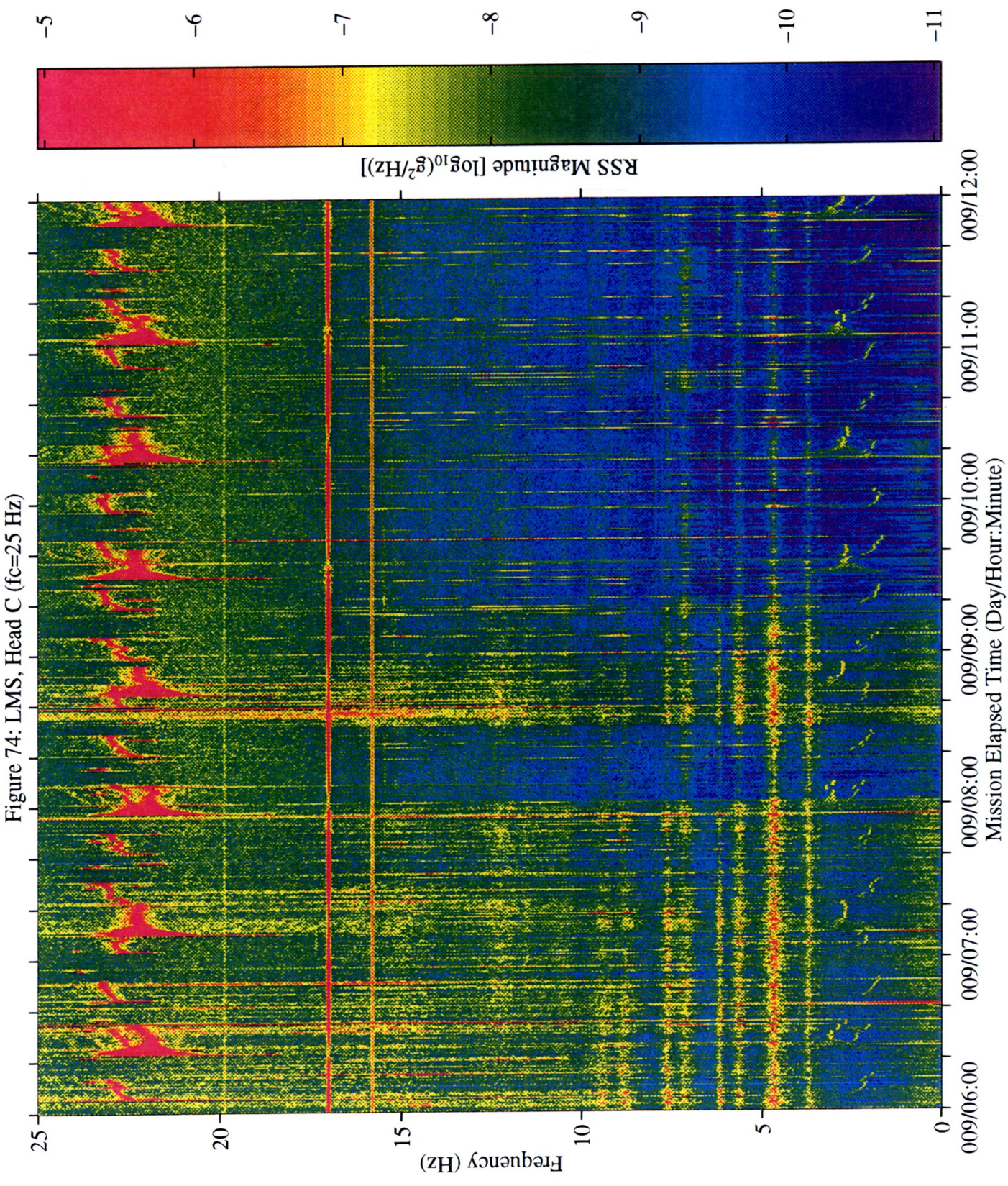

Figure 74: LMS, Head C (fc=25 Hz)

Figure 75a: LMS, Head C (fc=25 Hz), Ten Second Interval Average

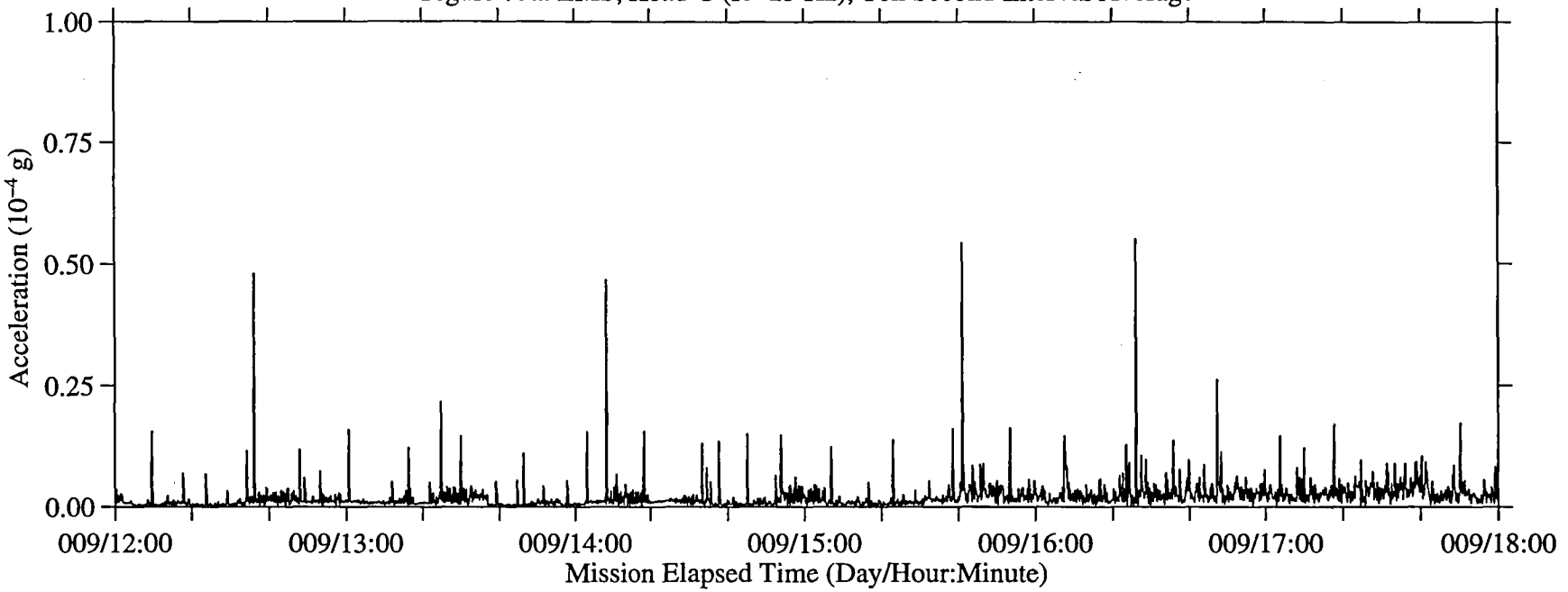

Figure 75b: LMS, Head C (fc=25 Hz), Ten Second Interval RMS

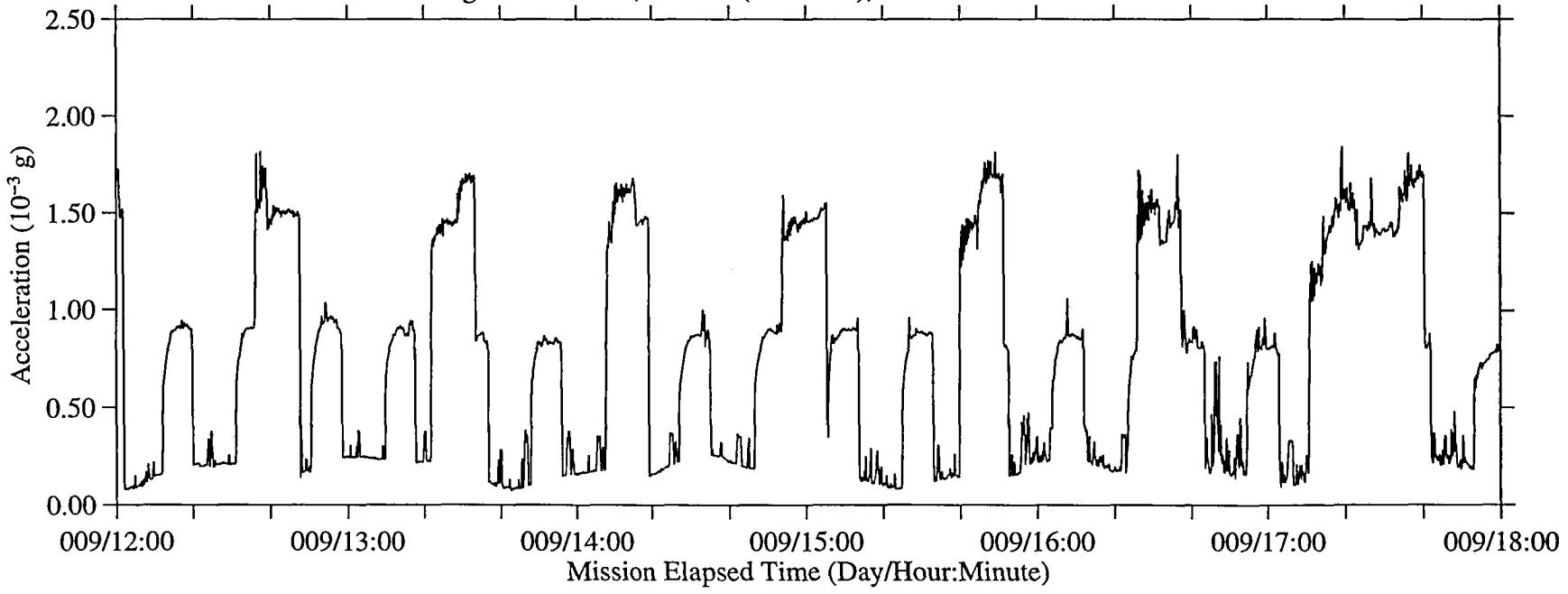

Figure 76: LMS, Head C (fc=25 Hz)

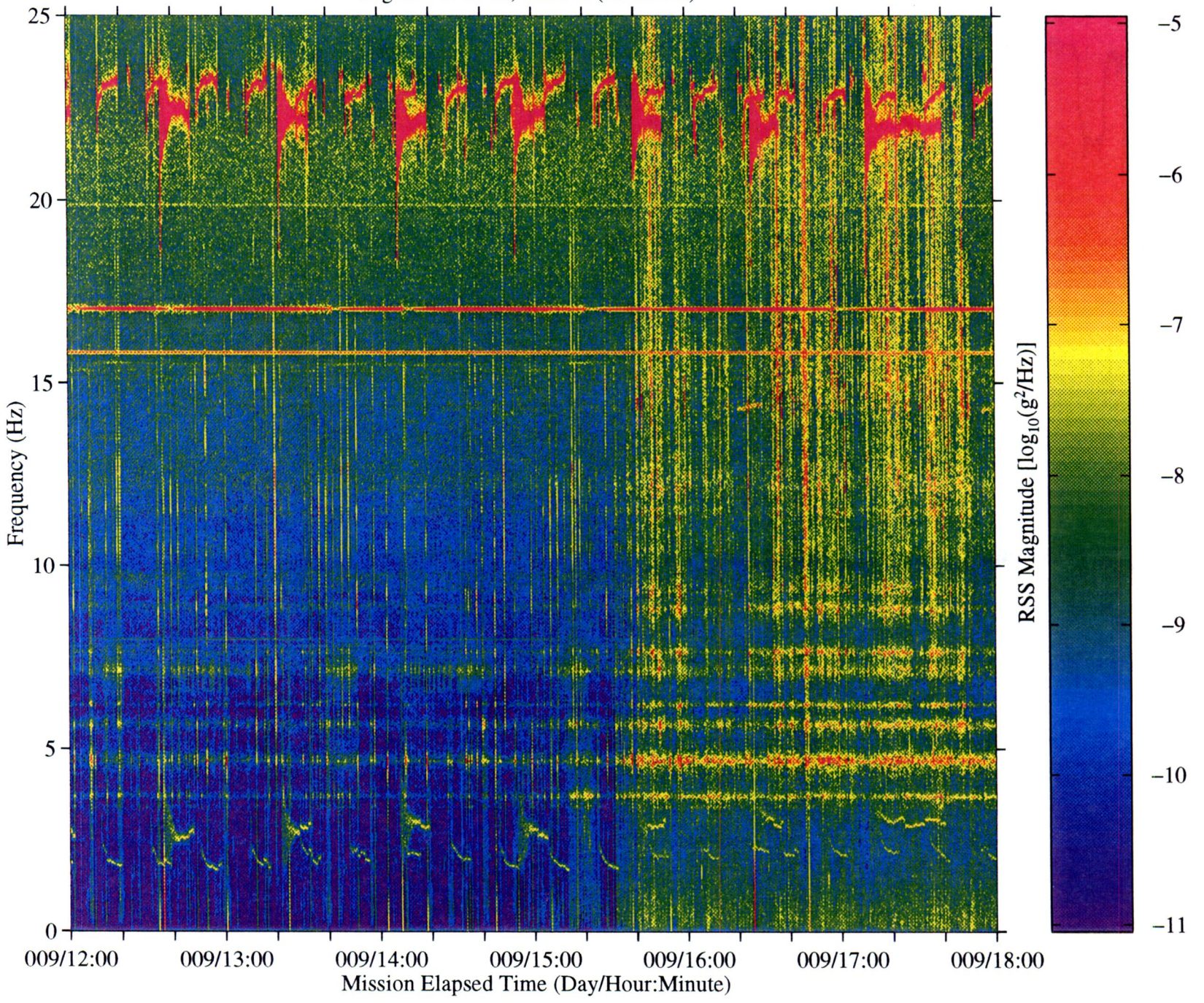

Figure 77a: LMS, Head C (fc=25 Hz), Ten Second Interval Average

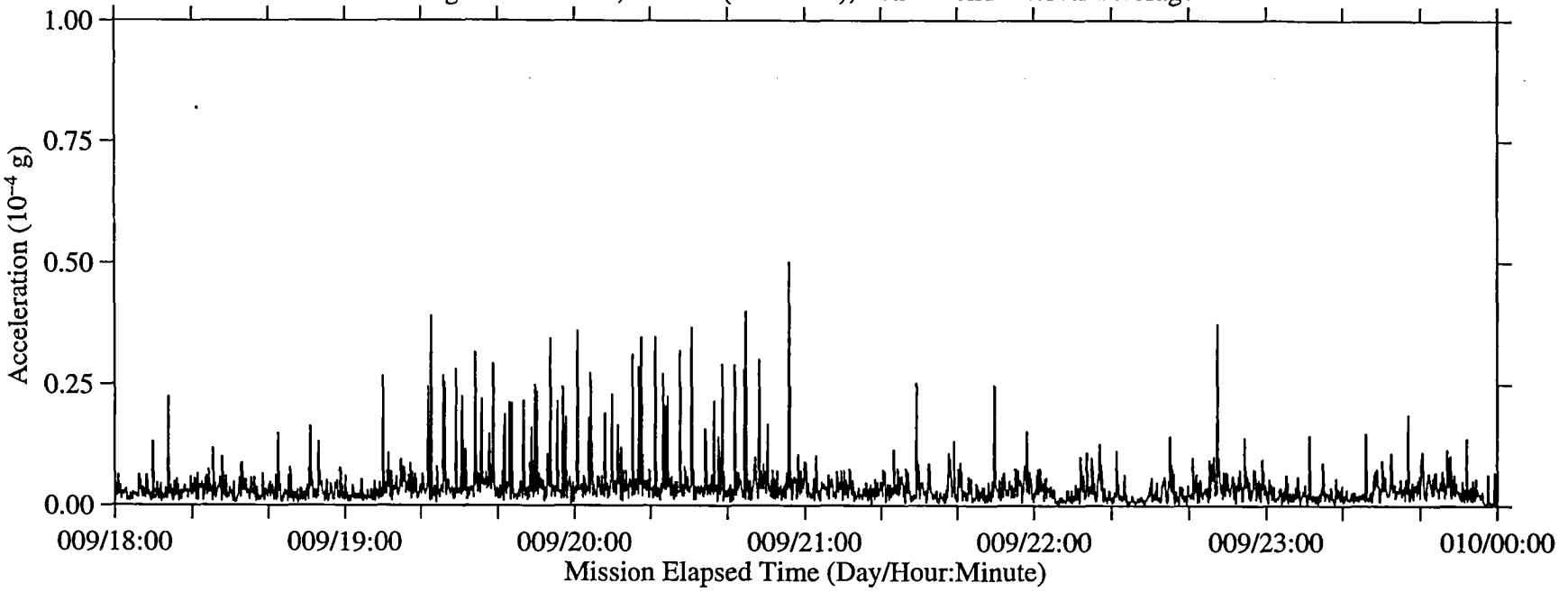

Figure 77b: LMS, Head C (fc=25 Hz), Ten Second Interval RMS

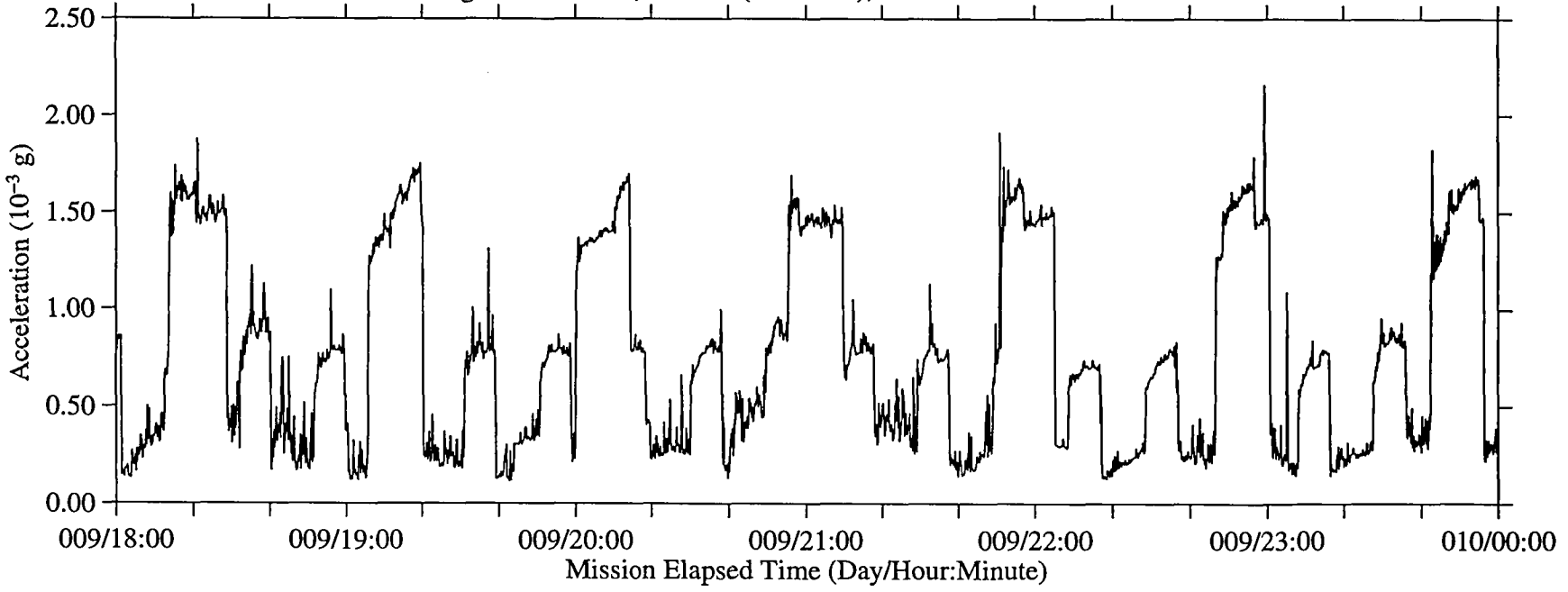

Figure 78: LMS, Head C (fc=25 Hz)

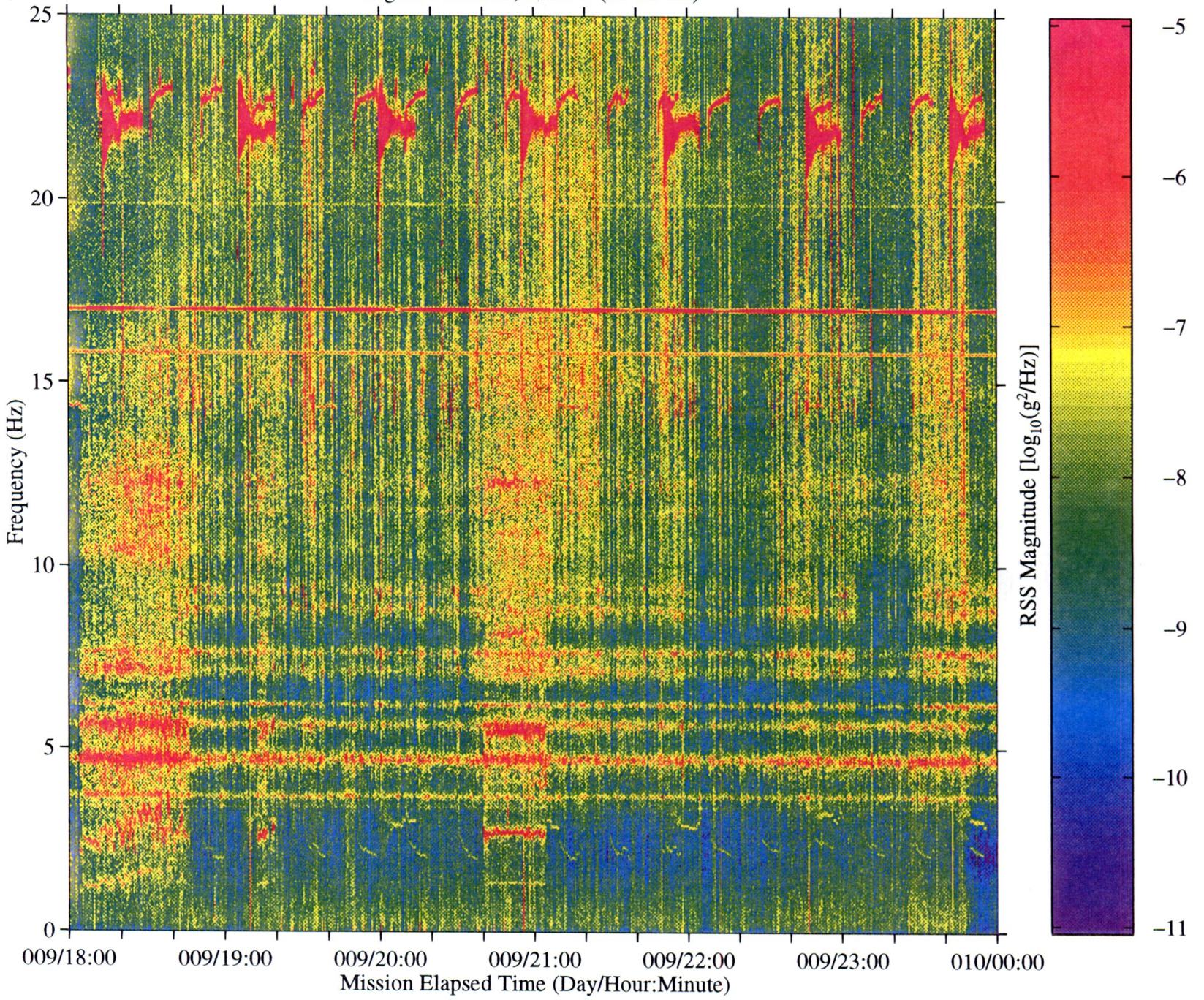

Figure 79a: LMS, Head C (fc=25 Hz), Ten Second Interval Average

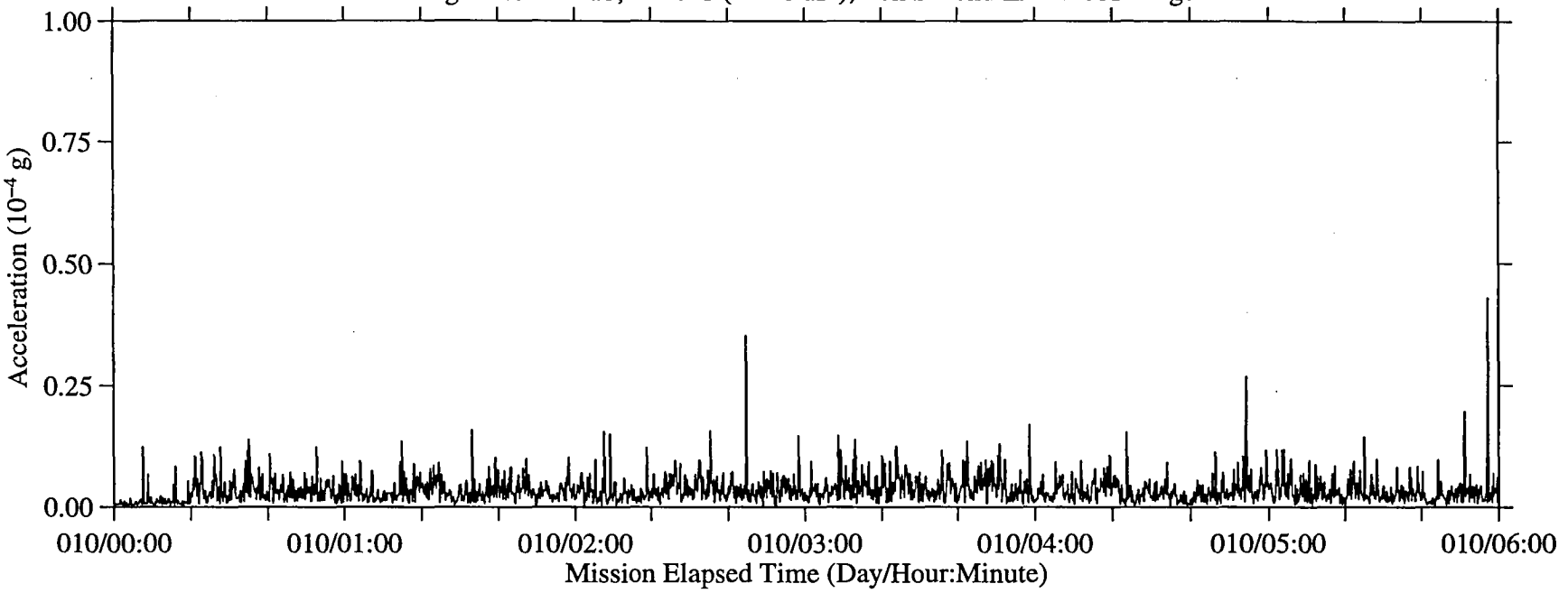

Figure 79b: LMS, Head C (fc=25 Hz), Ten Second Interval RMS

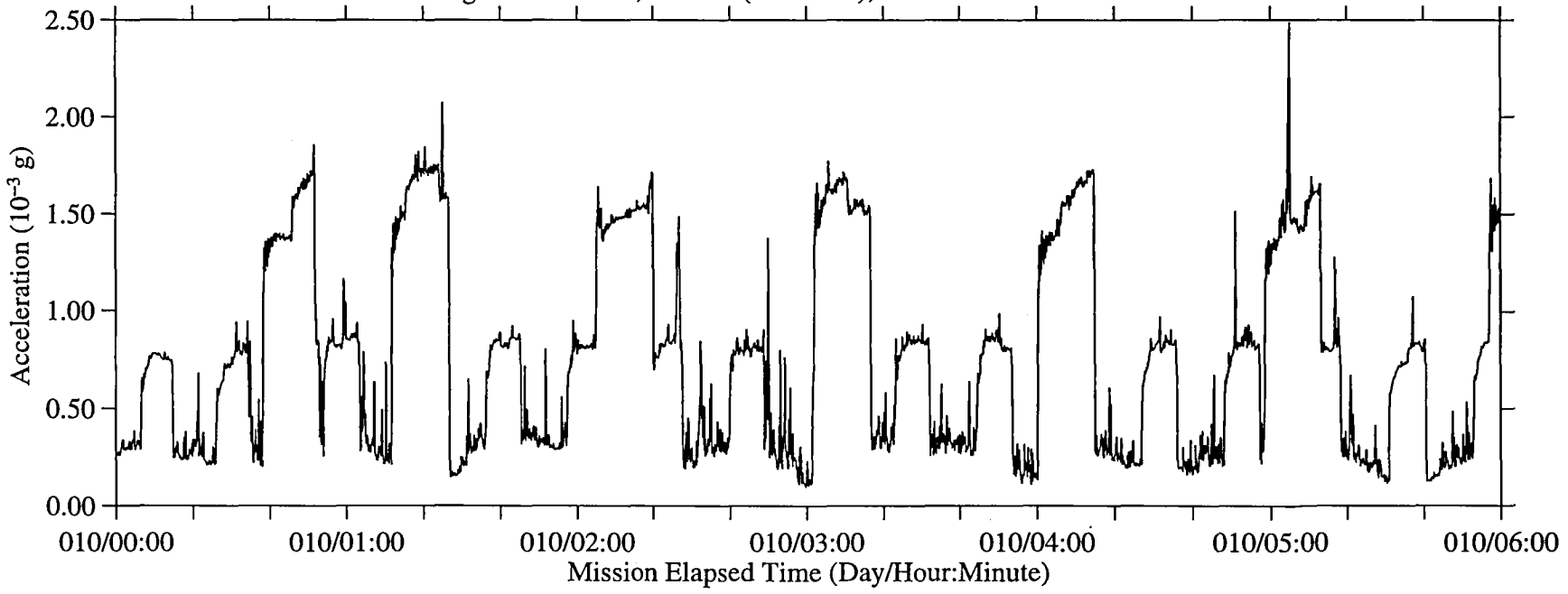

Figure 80: LMS, Head C (fc=25 Hz)

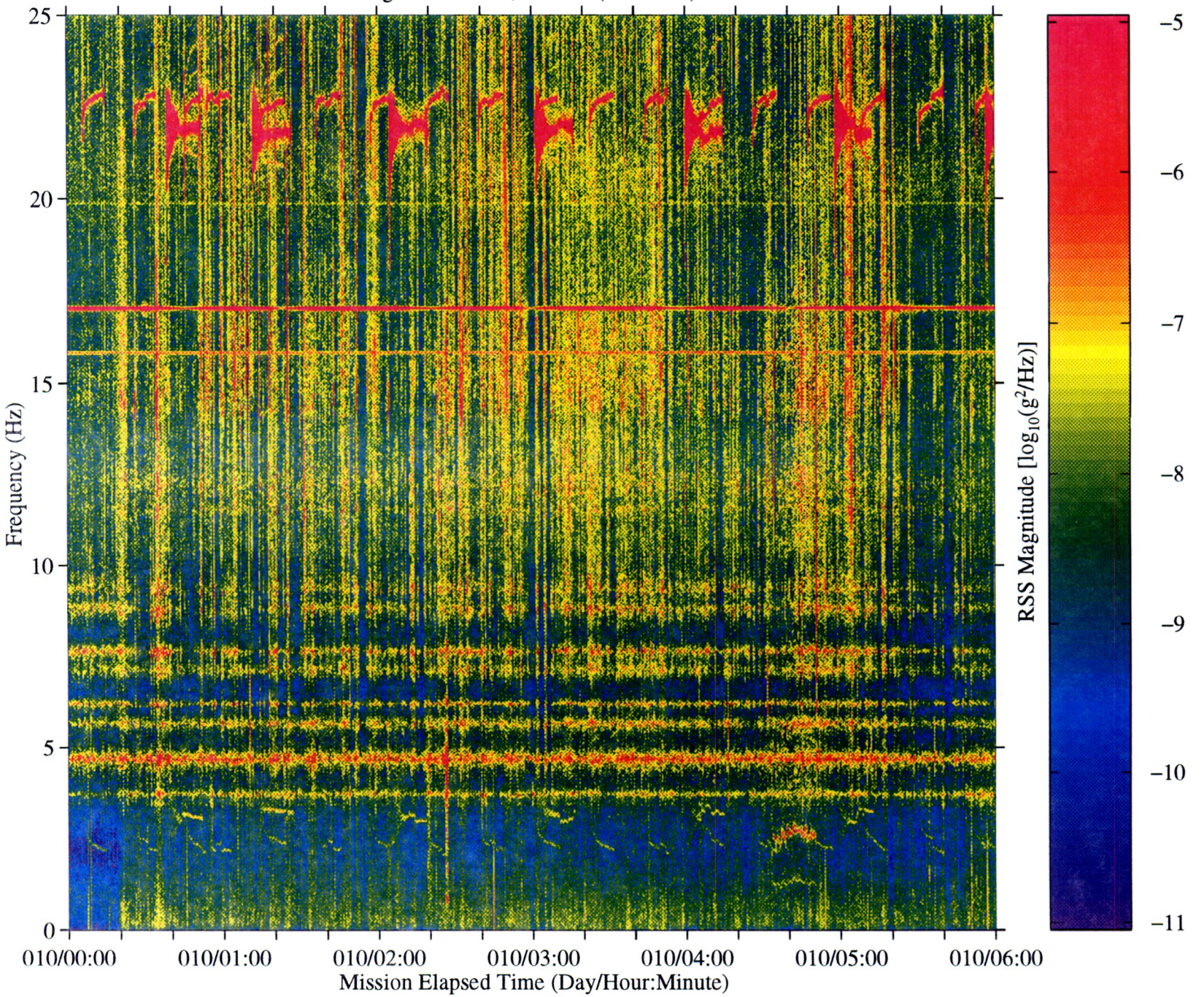

Figure 81a: LMS, Head C (fc=25 Hz), Ten Second Interval Average

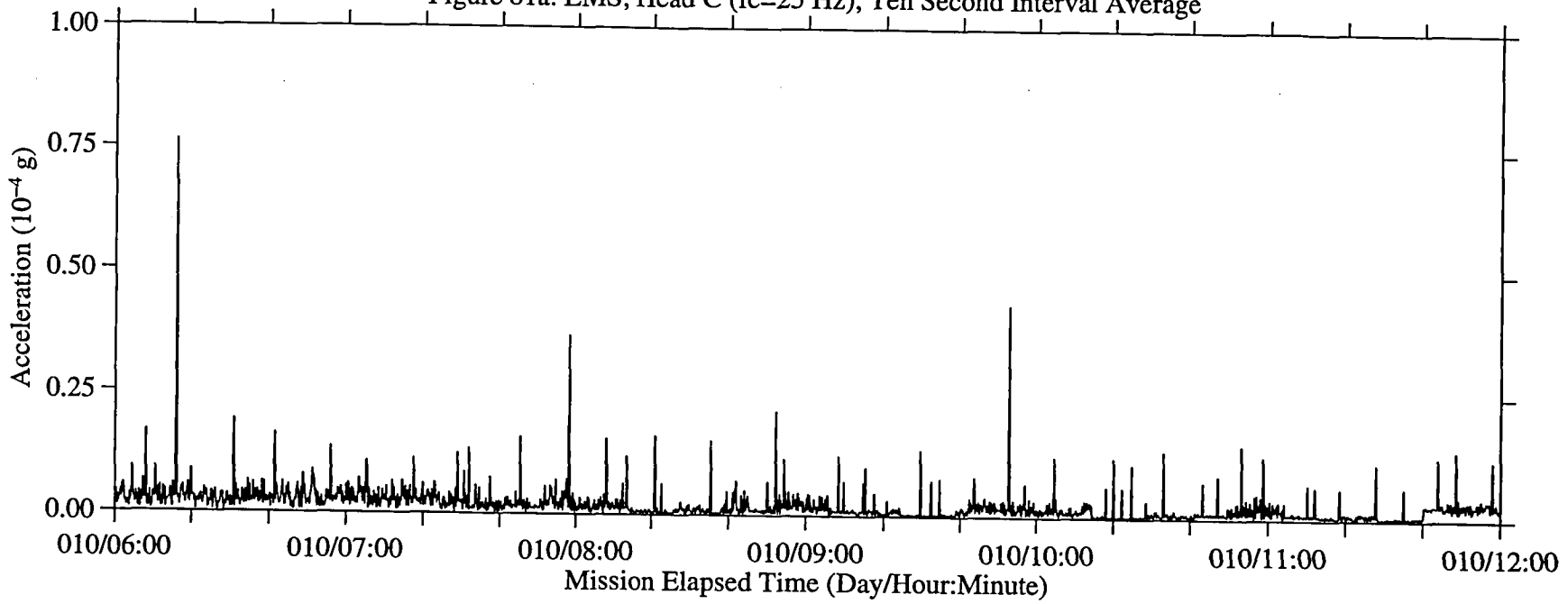

Figure 81b: LMS, Head C (fc=25 Hz), Ten Second Interval RMS

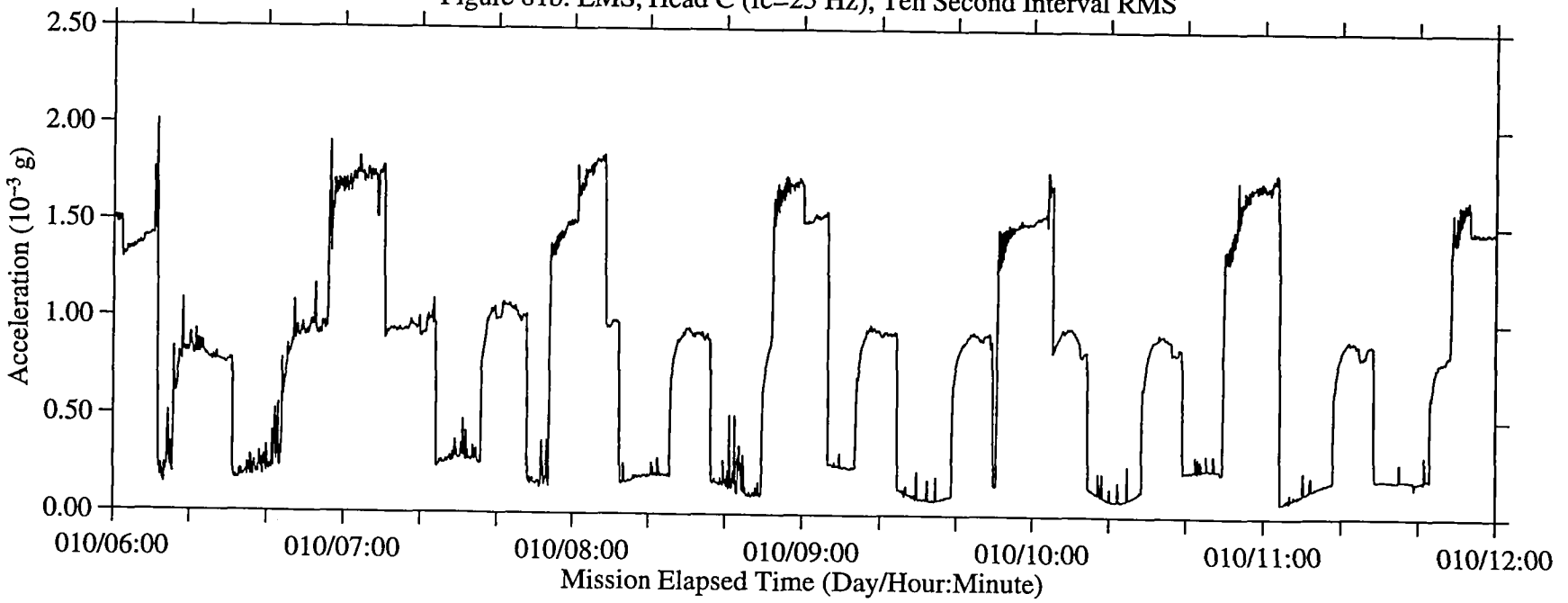

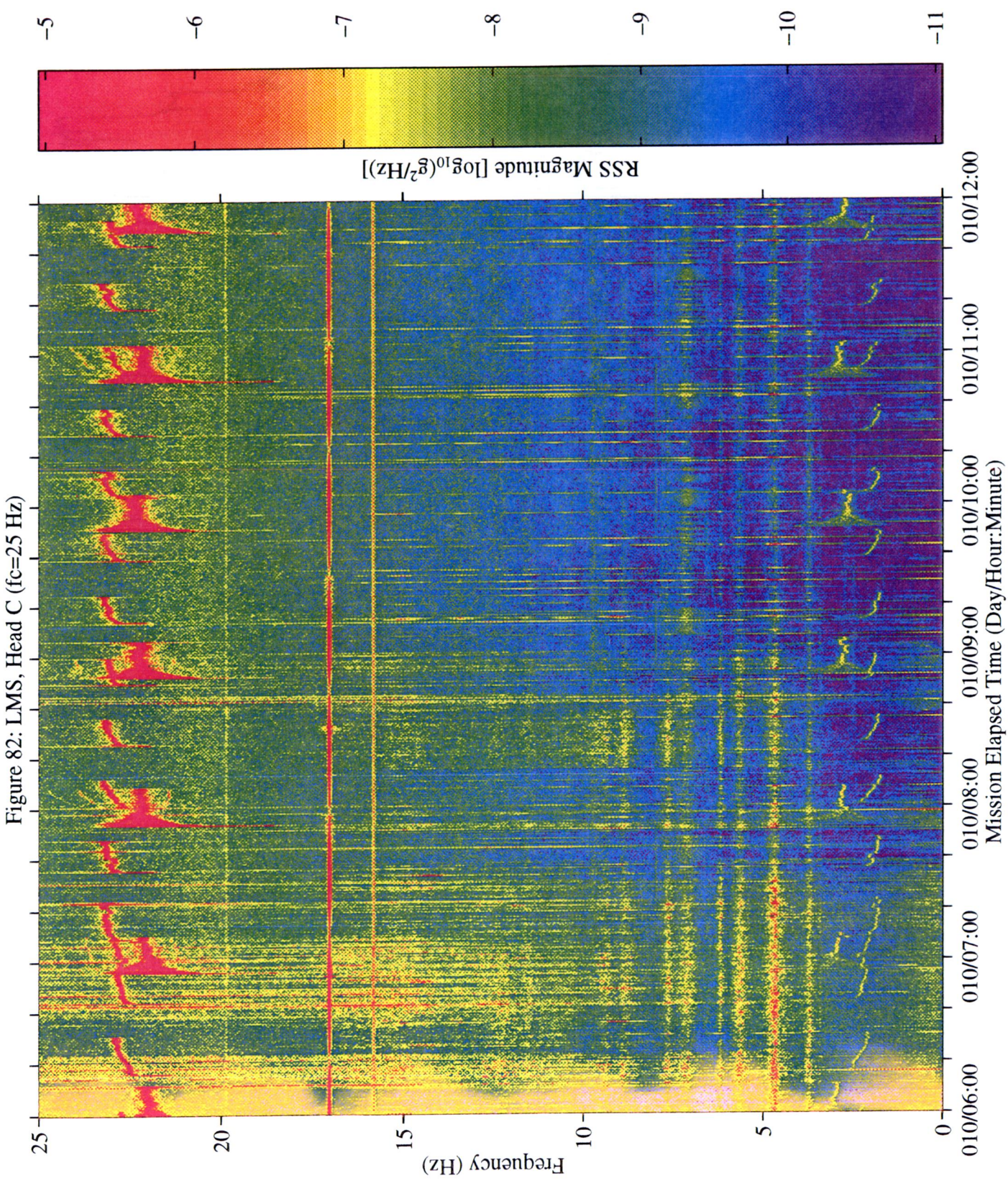

Figure 82: LMS, Head C (fc=25 Hz)

Figure 83a: LMS, Head C (fc=25 Hz), Ten Second Interval Average

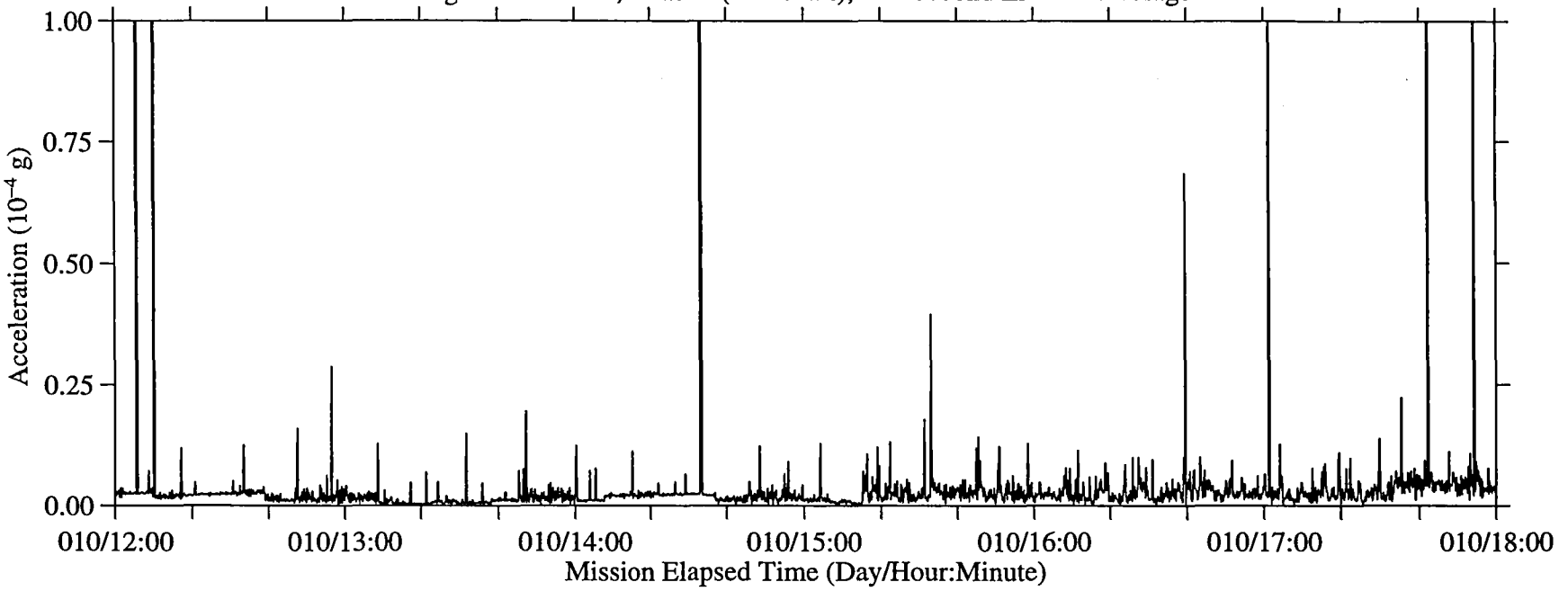

Figure 83b: LMS, Head C (fc=25 Hz), Ten Second Interval RMS

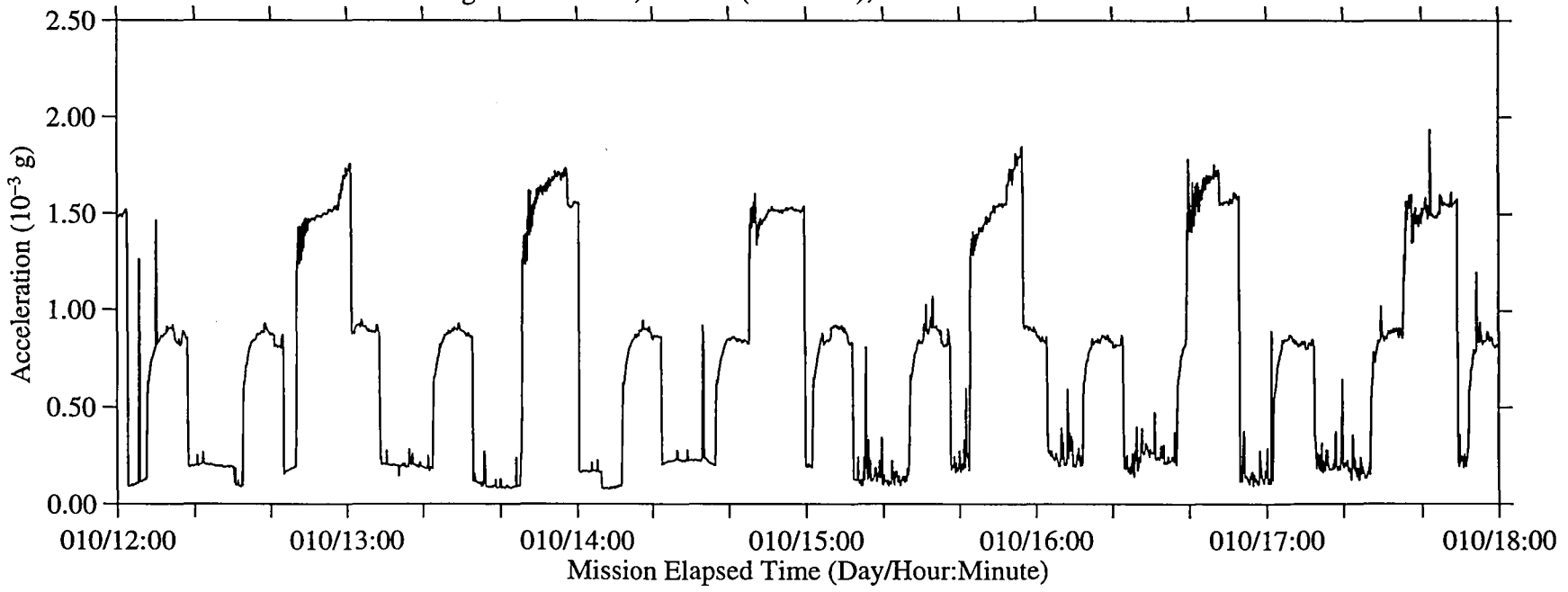

Figure 84: LMS, Head C (fc=25 Hz)

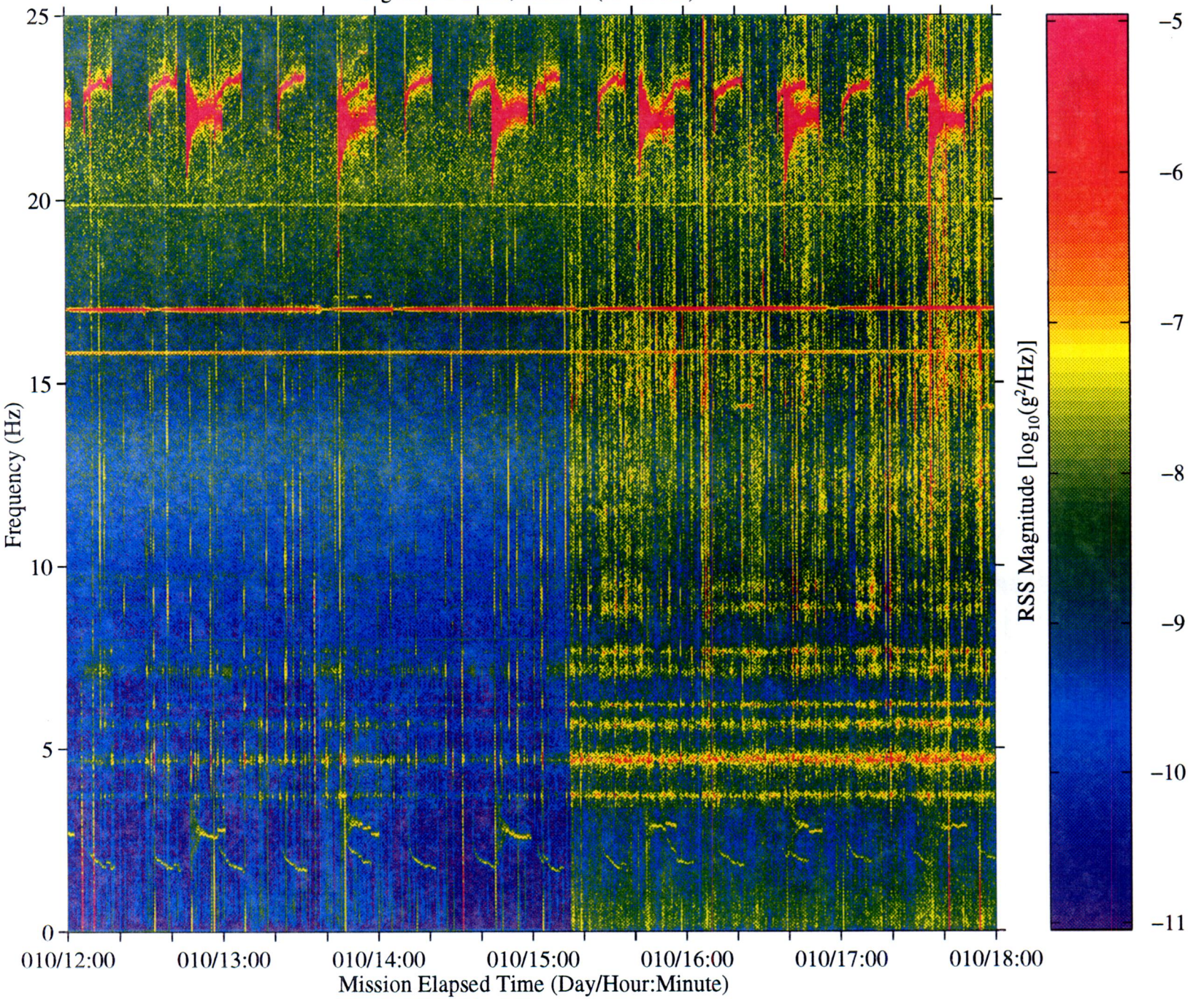

Figure 85a: LMS, Head C (fc=25 Hz), Ten Second Interval Average

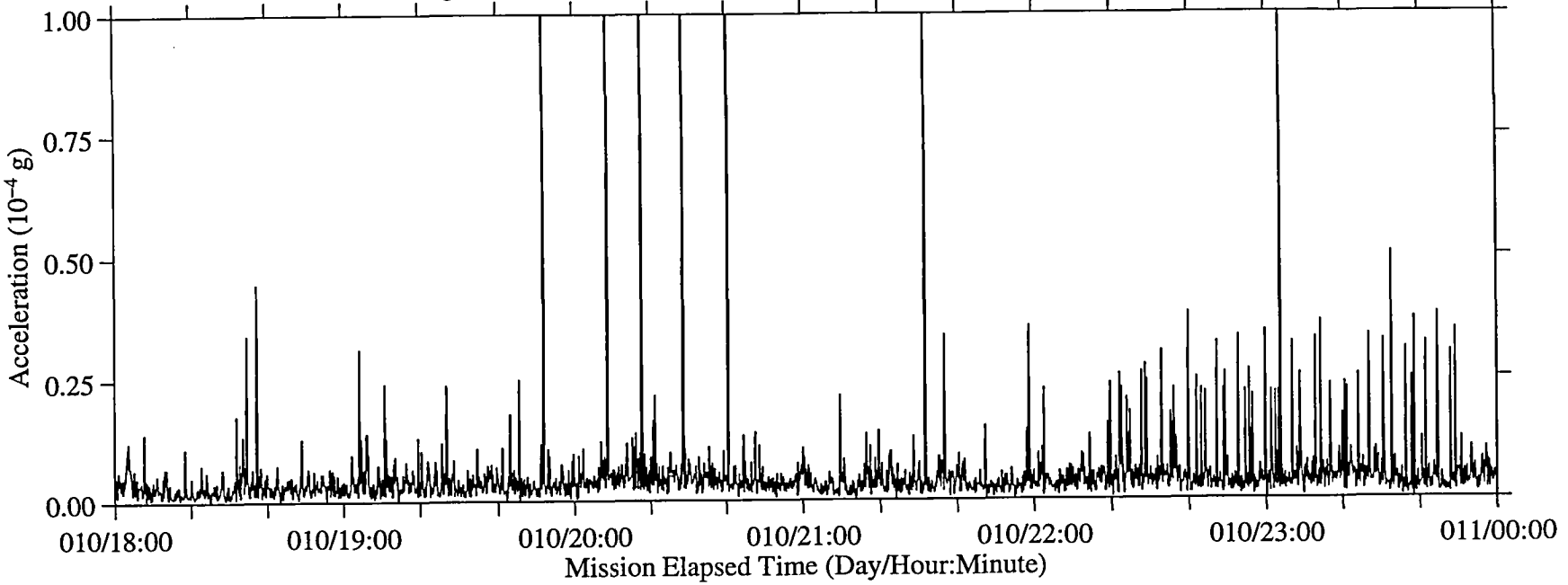

Figure 85b: LMS, Head C (fc=25 Hz), Ten Second Interval RMS

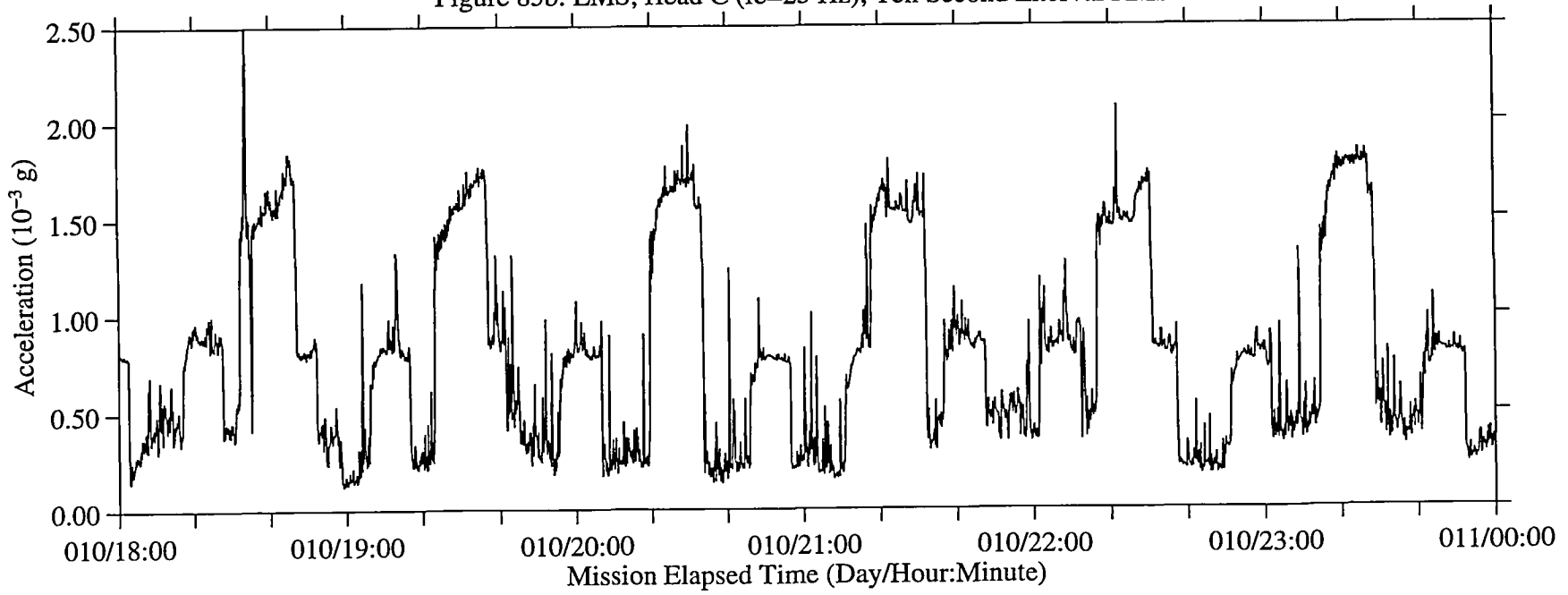

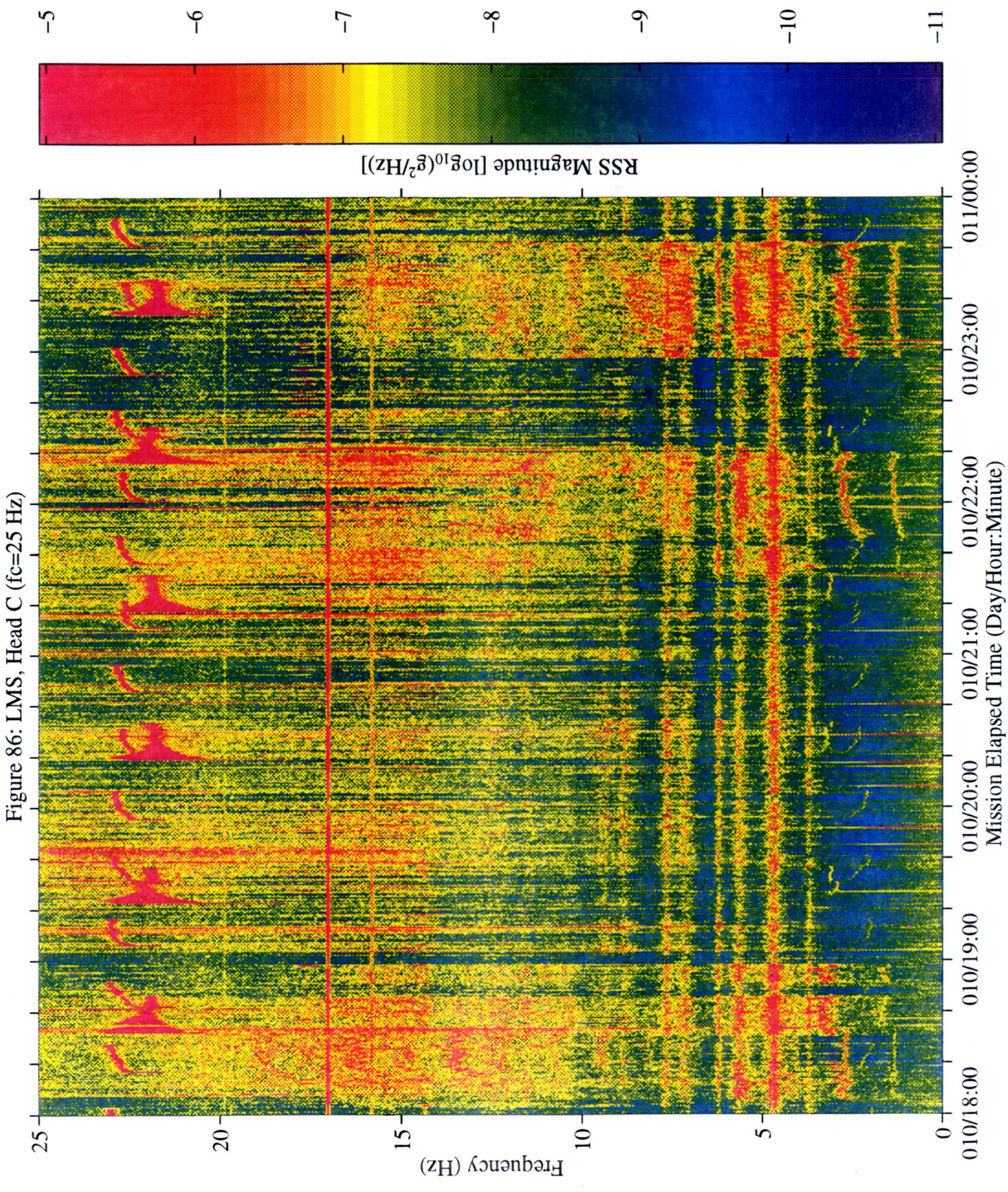

Figure 86: LMS, Head C (fc=25 Hz)

Figure 87a: LMS, Head C (fc=25 Hz), Ten Second Interval Average

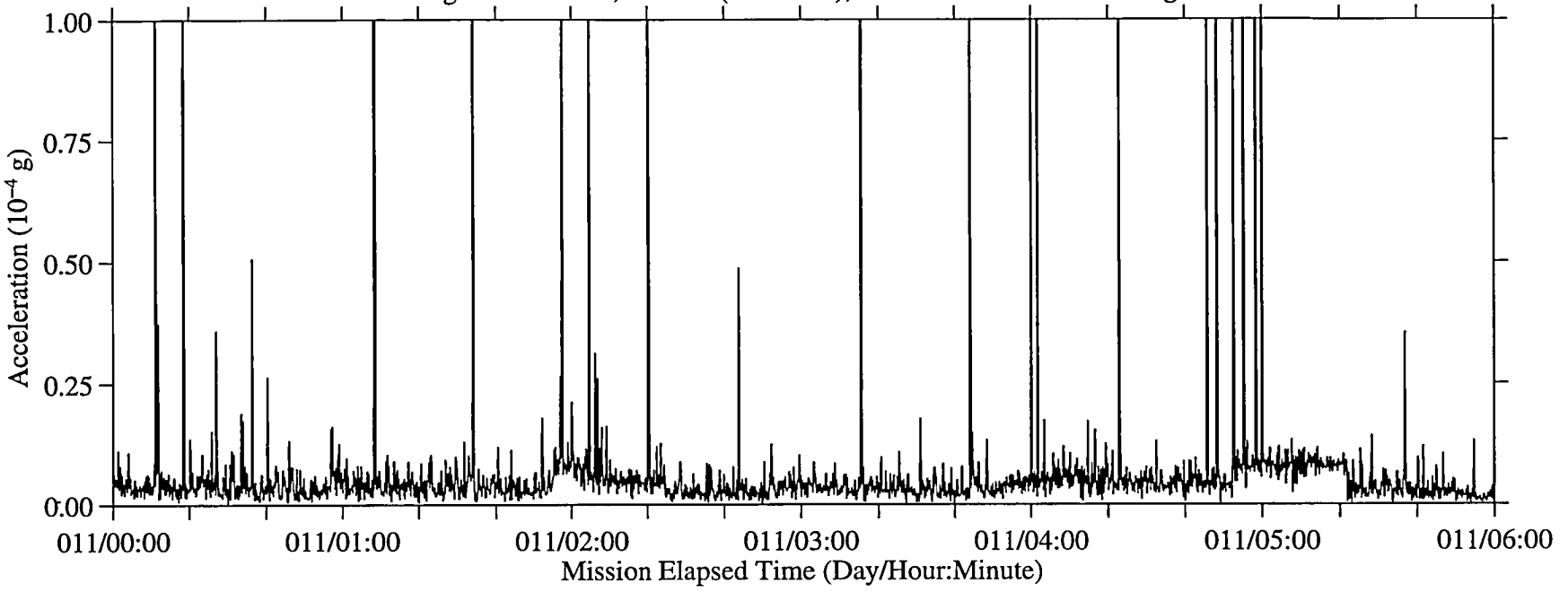

Figure 87b: LMS, Head C (fc=25 Hz), Ten Second Interval RMS

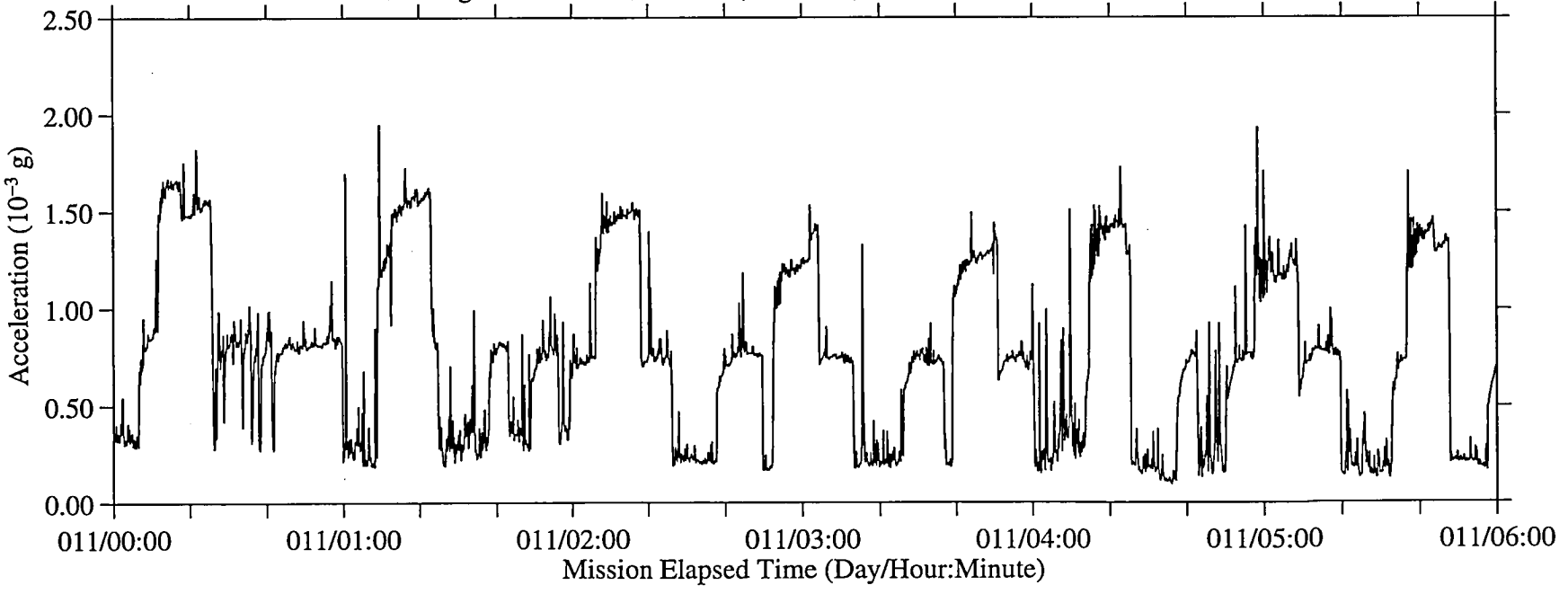

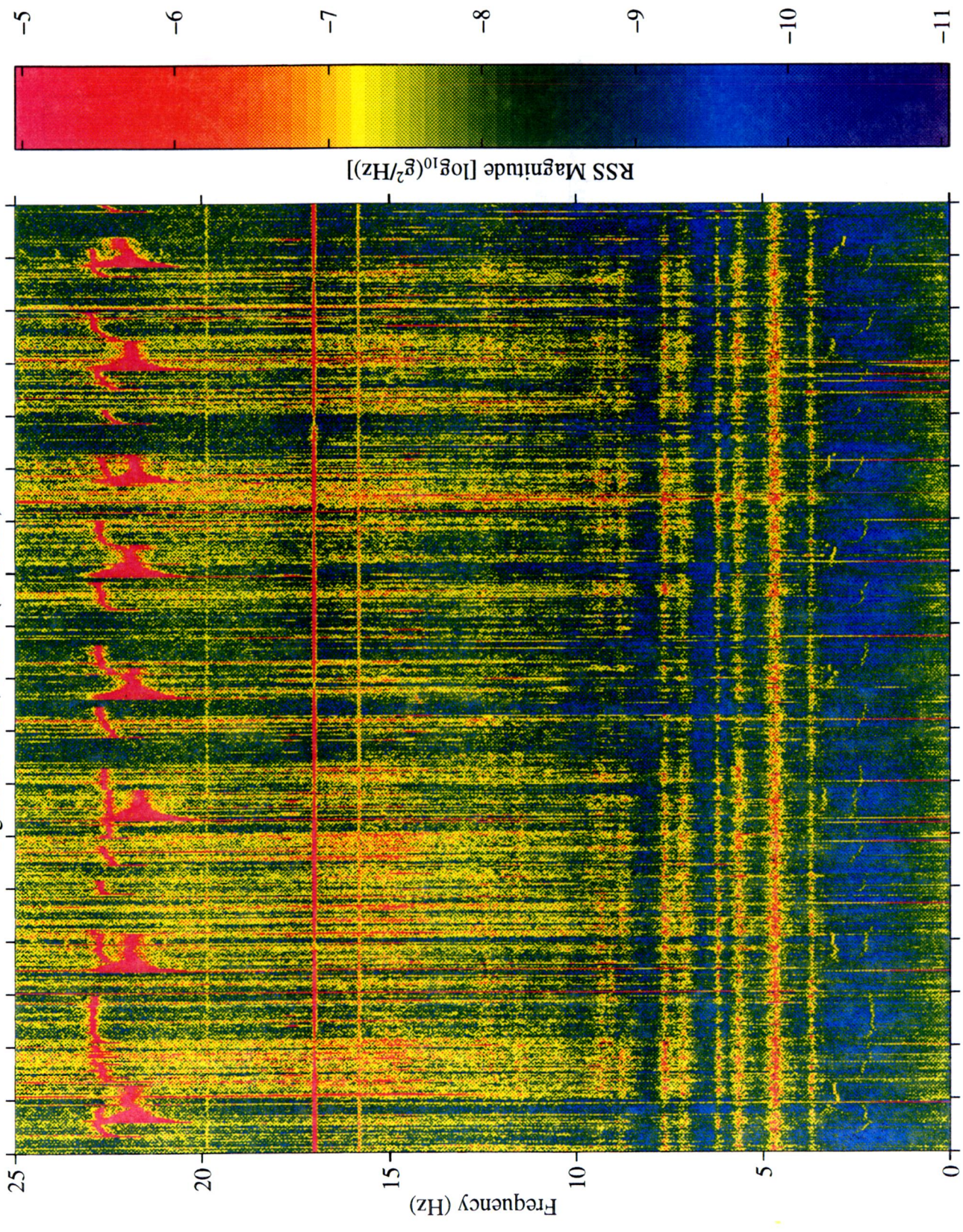

Figure 88: LMS, Head C (fc=25 Hz)

Figure 89a: LMS, Head C (fc=25 Hz), Ten Second Interval Average

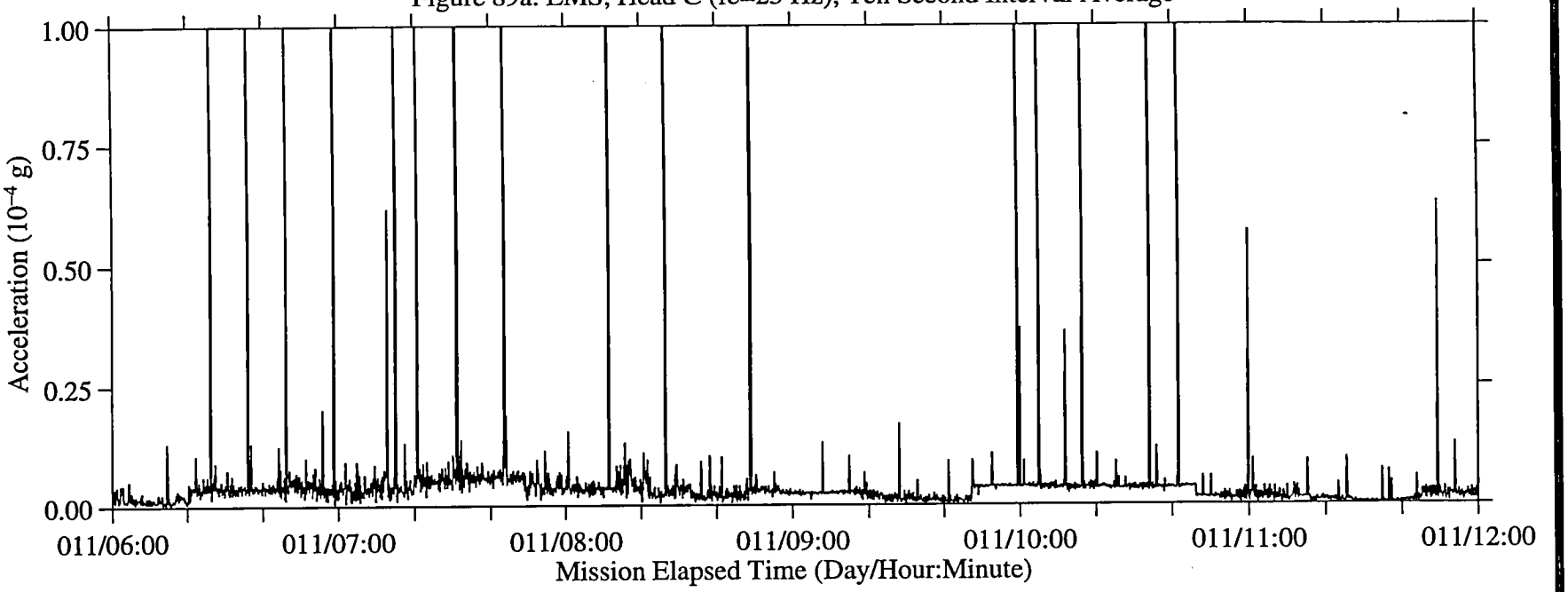

Figure 89b: LMS, Head C (fc=25 Hz), Ten Second Interval RMS

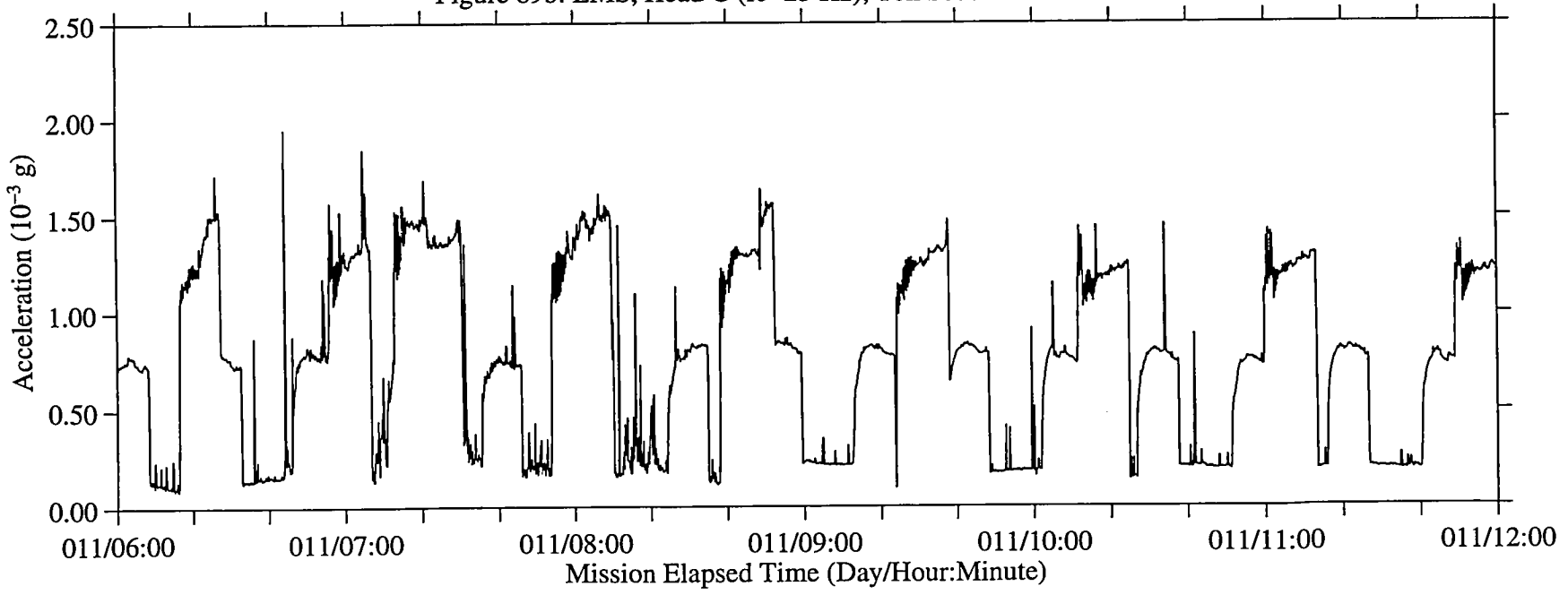

Figure 90: LMS, Head C (fc=25 Hz)

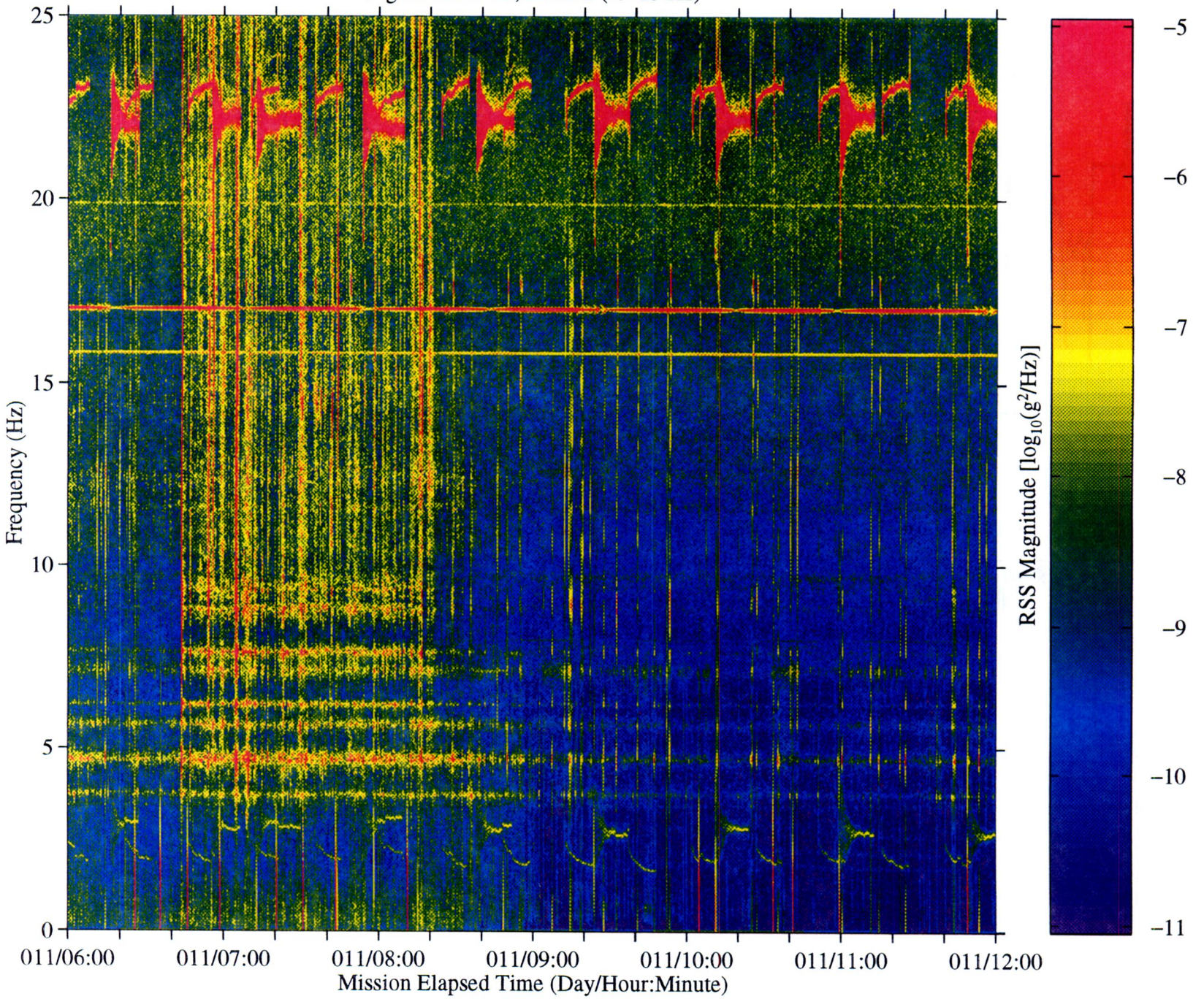

Figure 91a: LMS, Head C (fc=25 Hz), Ten Second Interval Average

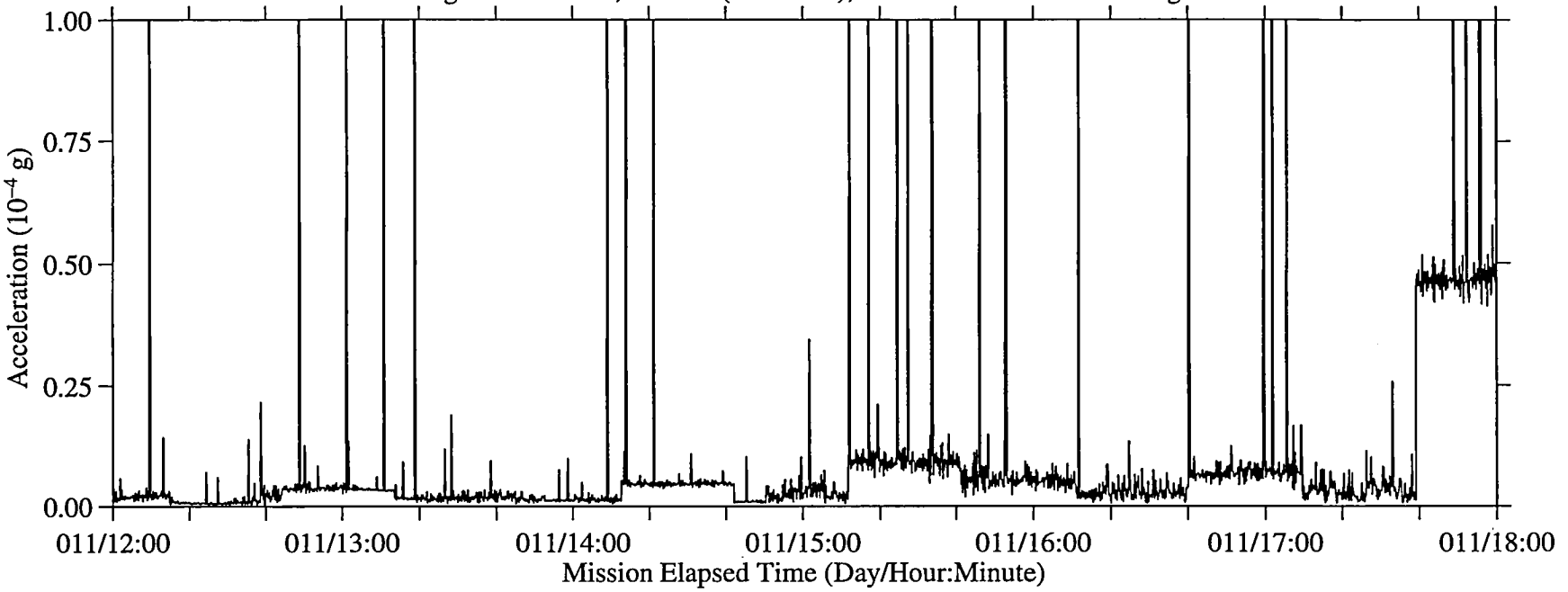

Figure 91b: LMS, Head C (fc=25 Hz), Ten Second Interval RMS

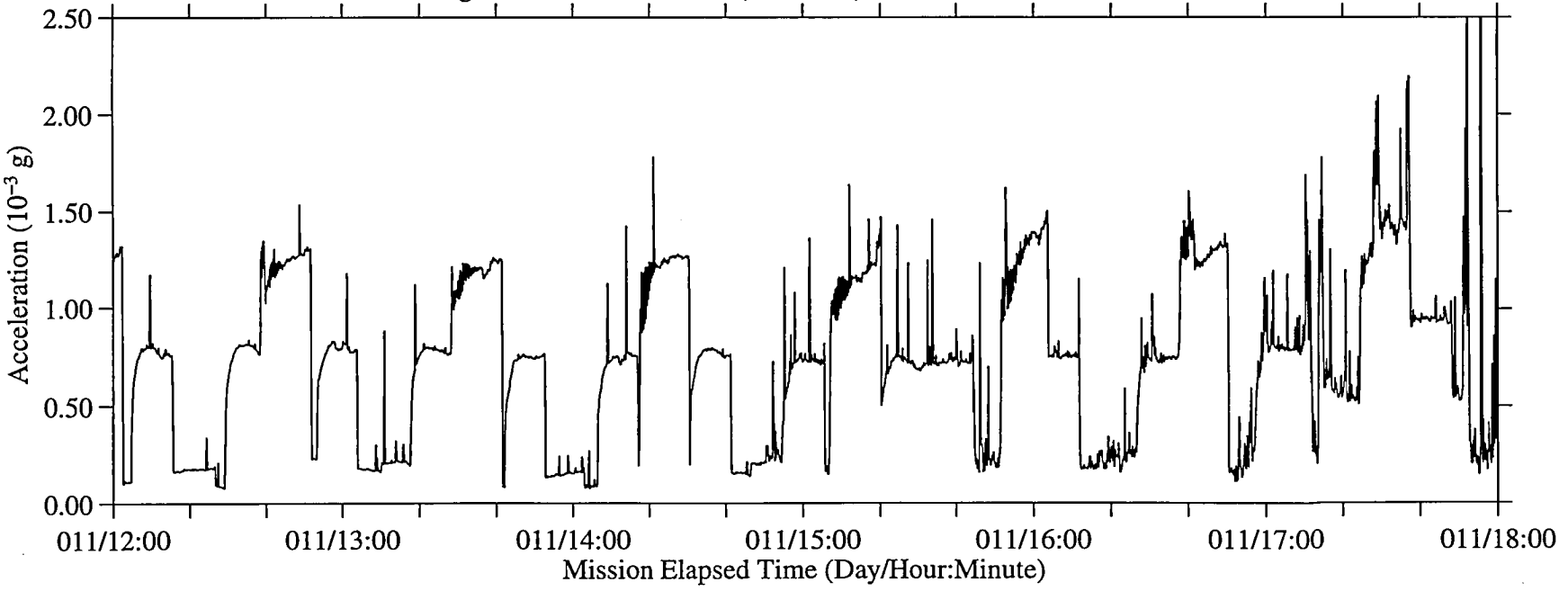

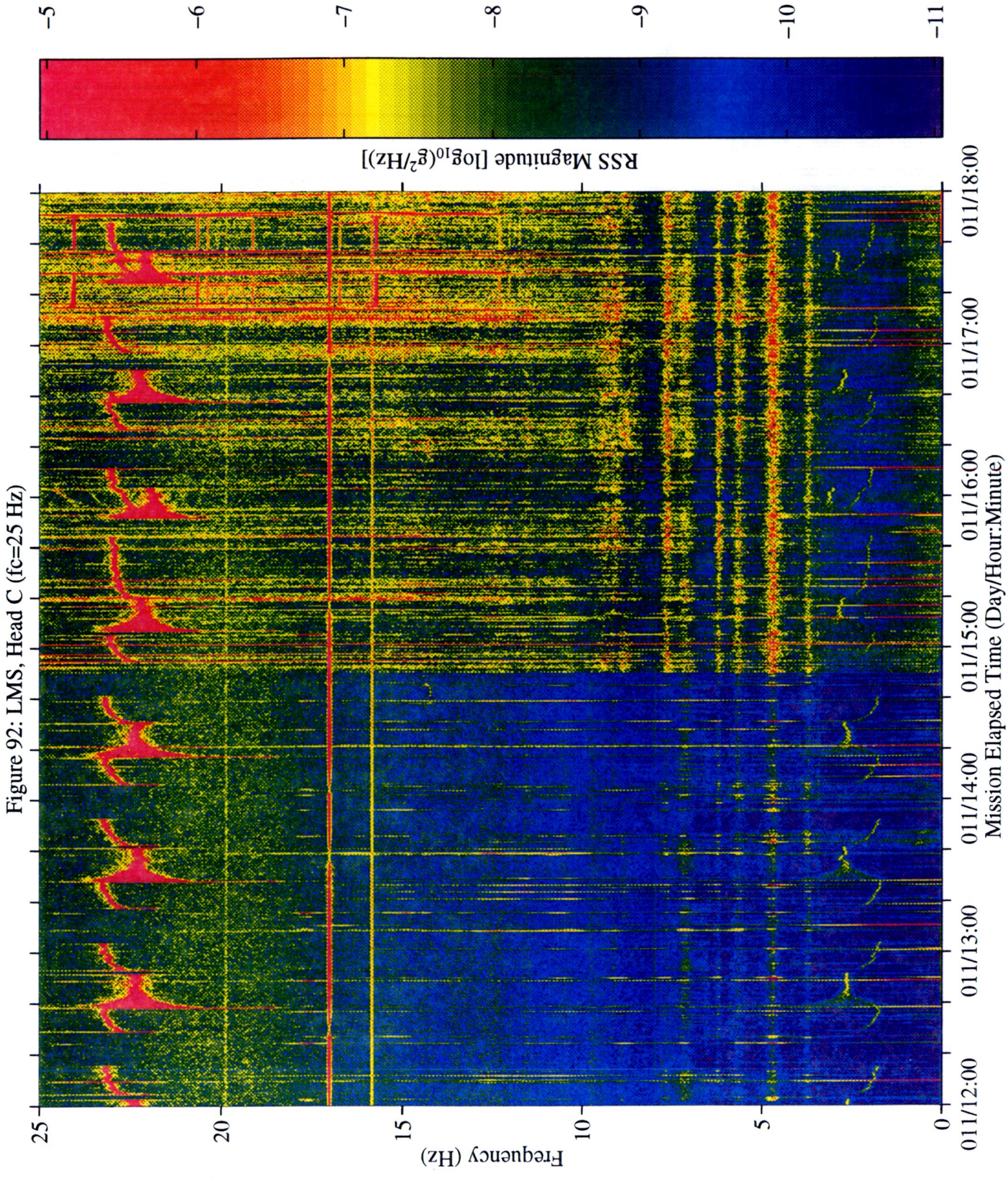

Figure 92: LMS, Head C (fc=25 Hz)

Figure 93a: LMS, Head C (fc=25 Hz), Ten Second Interval Average

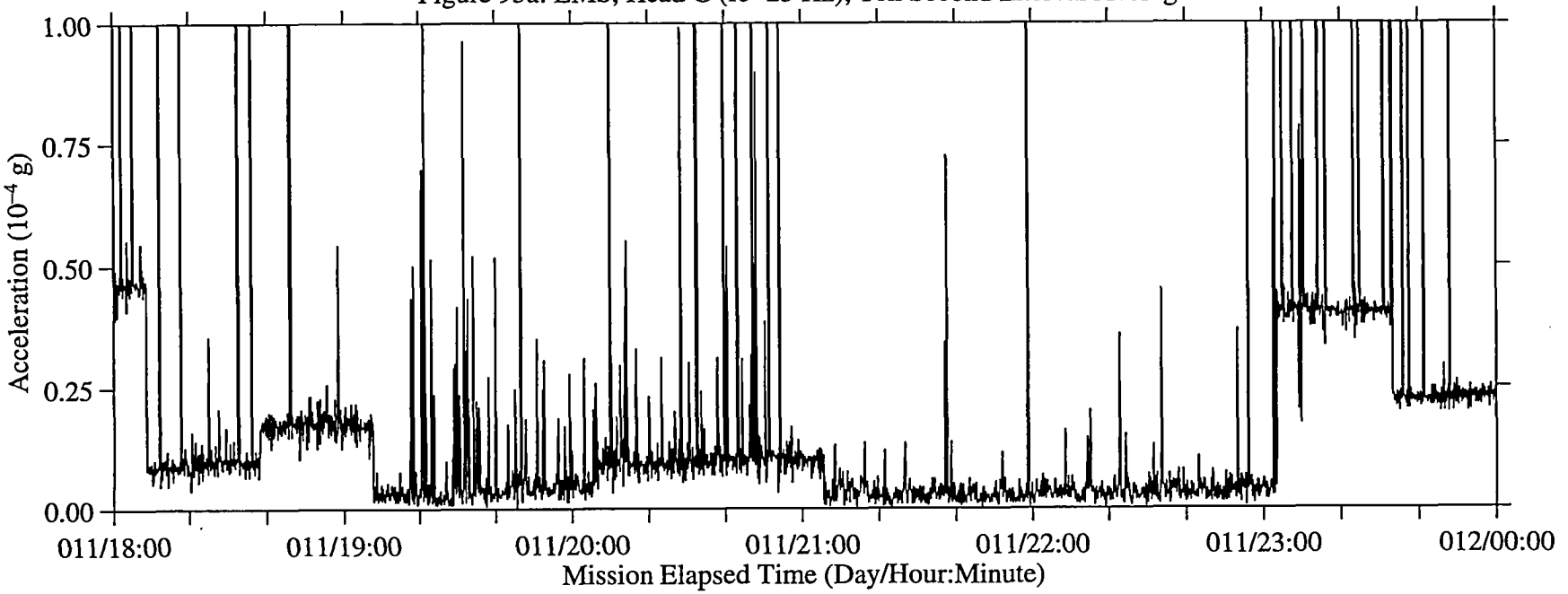

Figure 93b: LMS, Head C (fc=25 Hz), Ten Second Interval RMS

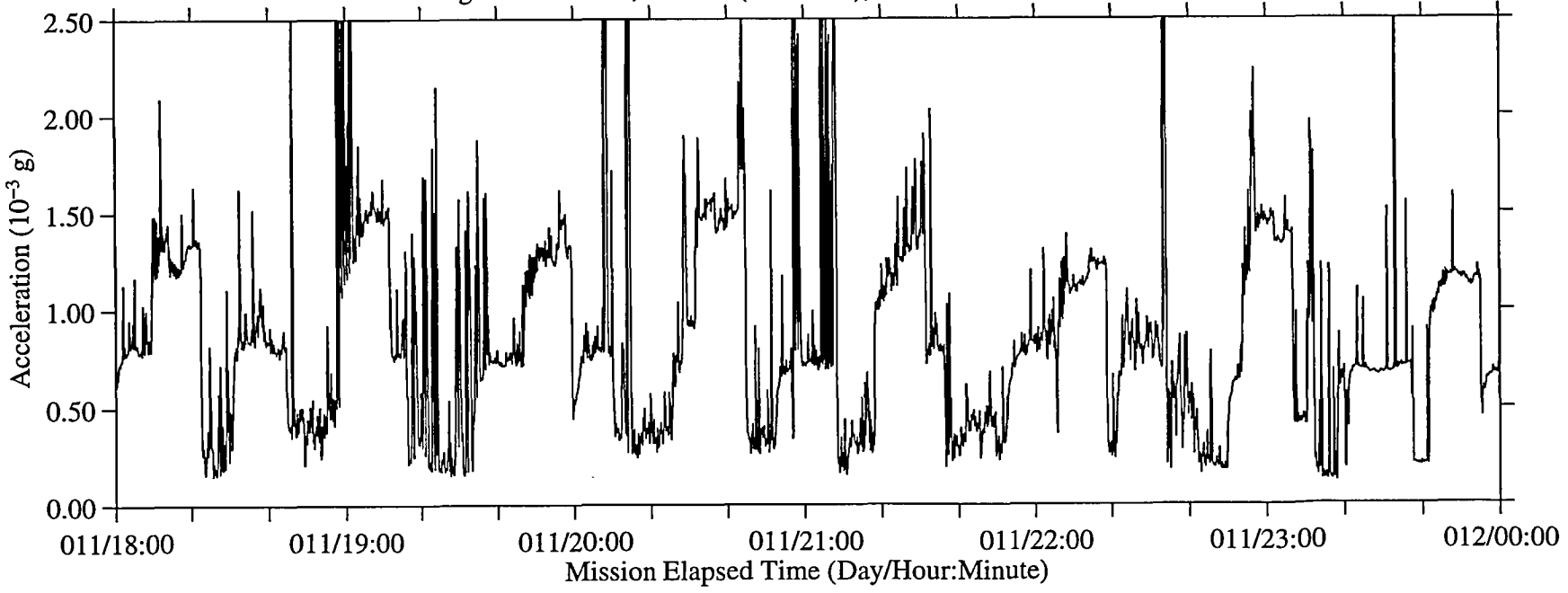

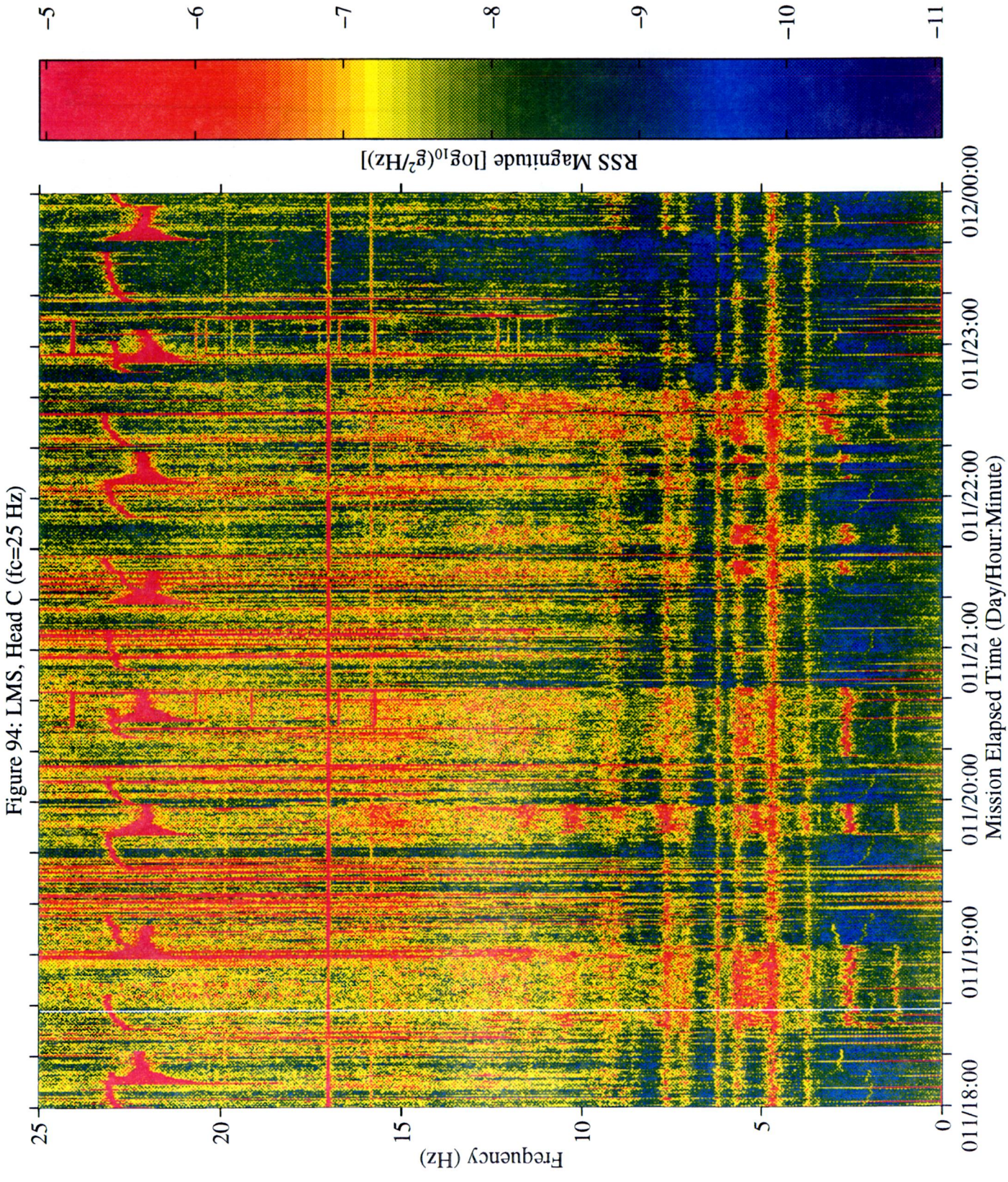

Figure 94: LMS, Head C (fc=25 Hz)

Figure 95a: LMS, Head C (fc=25 Hz), Ten Second Interval Average

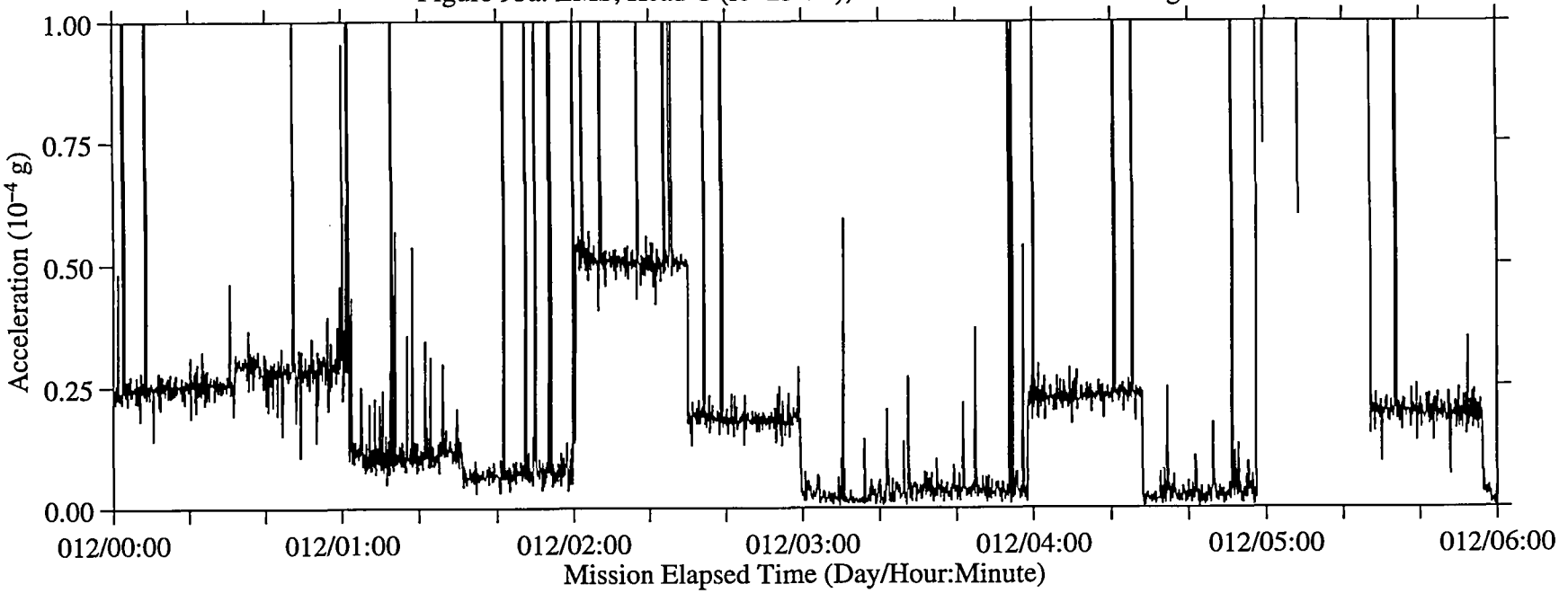

Figure 95b: LMS, Head C (fc=25 Hz), Ten Second Interval RMS

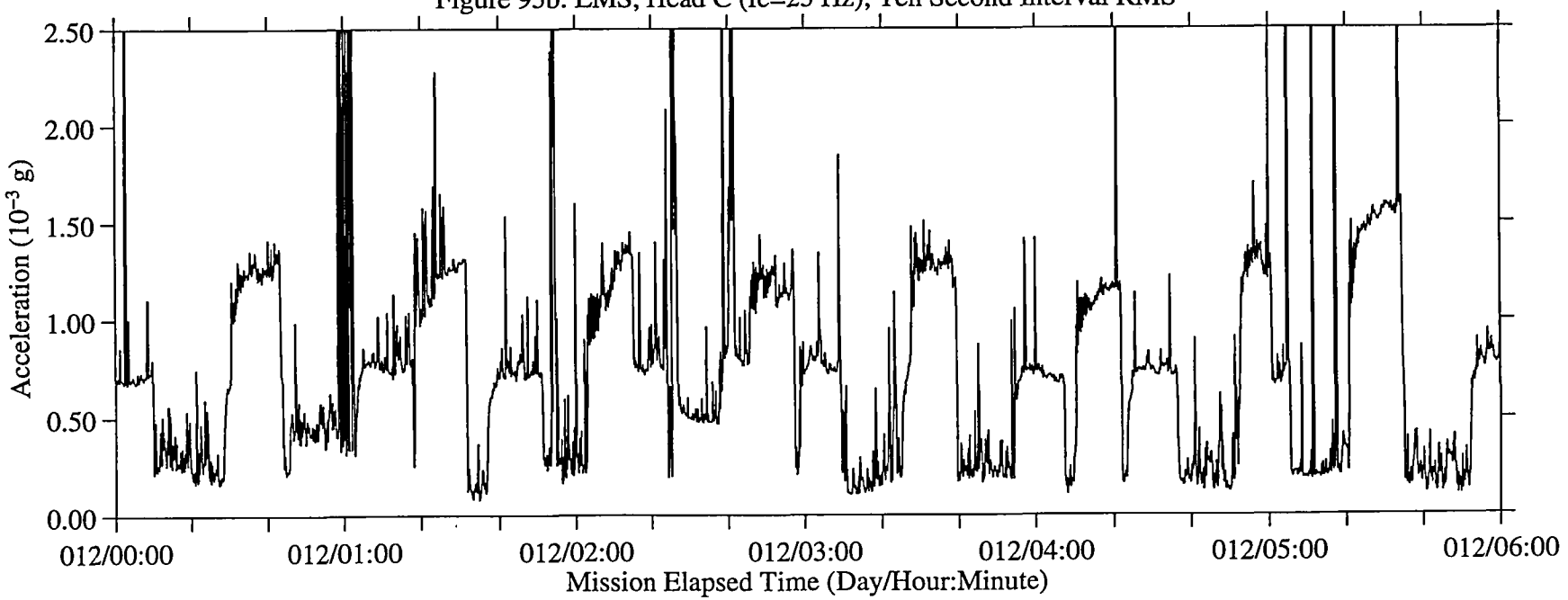

Figure 96: LMS, Head C (fc=25 Hz)

Figure 97a: LMS, Head C (fc=25 Hz), Ten Second Interval Average

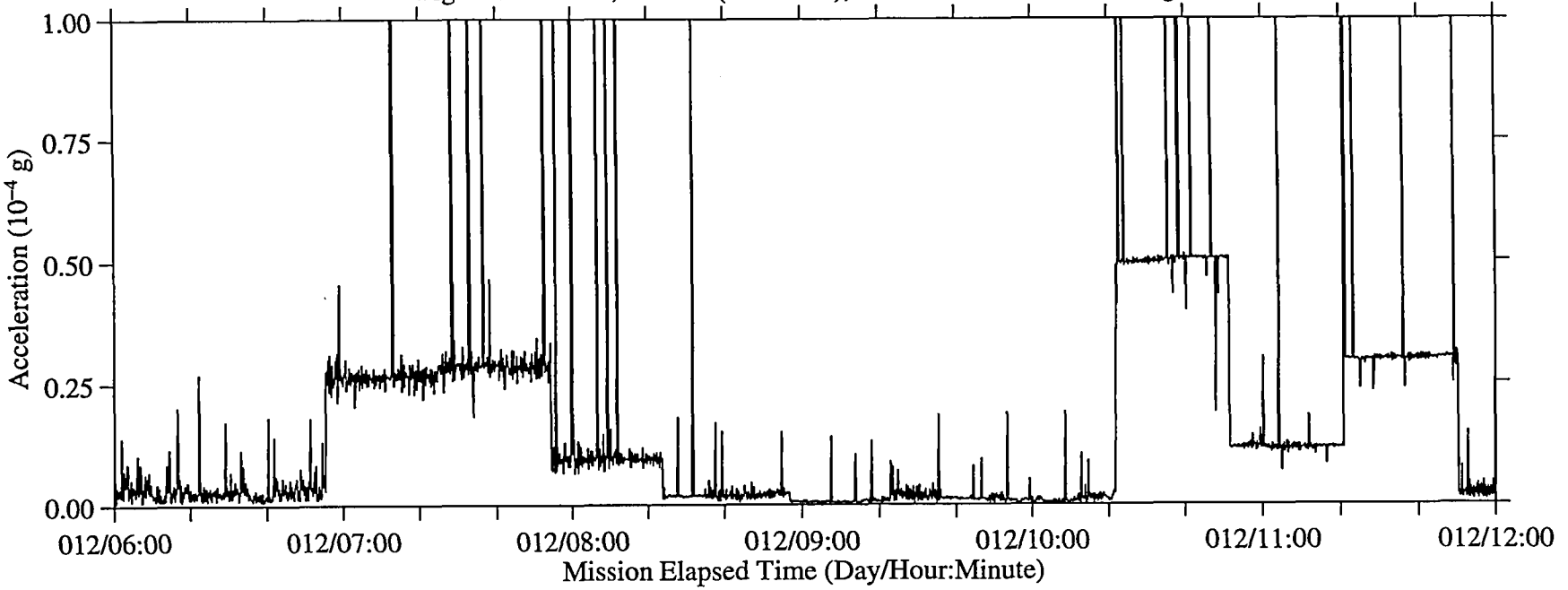

Figure 97b: LMS, Head C (fc=25 Hz), Ten Second Interval RMS

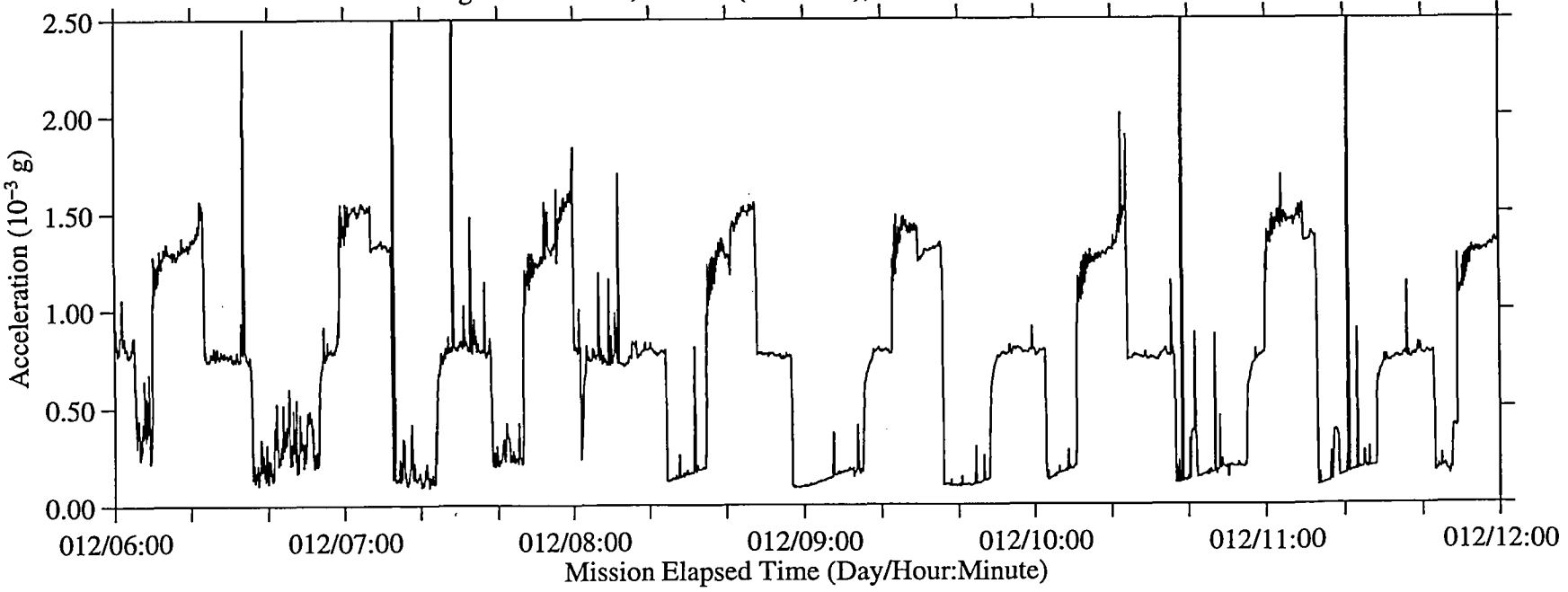

Figure 98: LMS, Head C (fc=25 Hz)

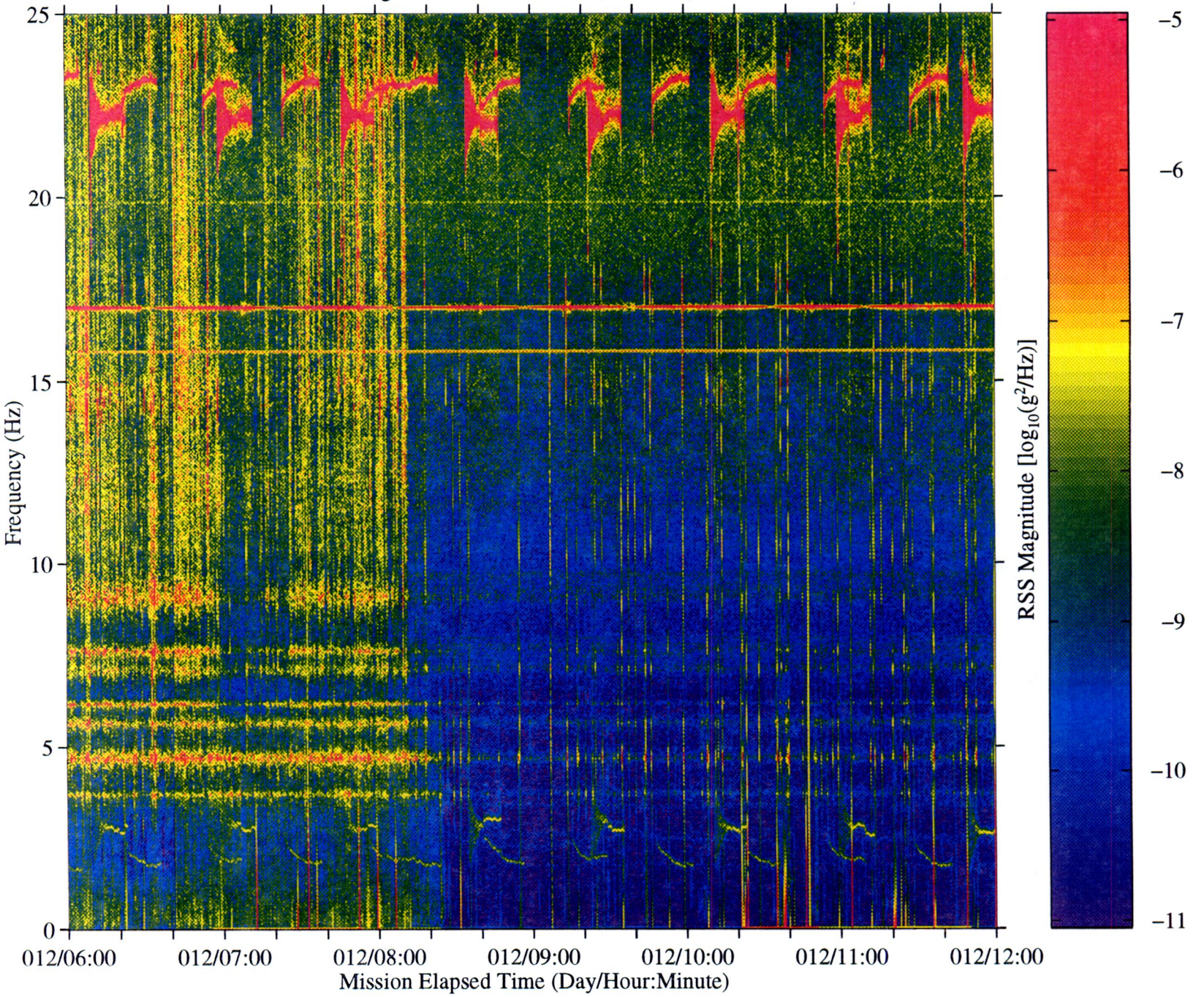

Figure 99a: LMS, Head C (fc=25 Hz), Ten Second Interval Average

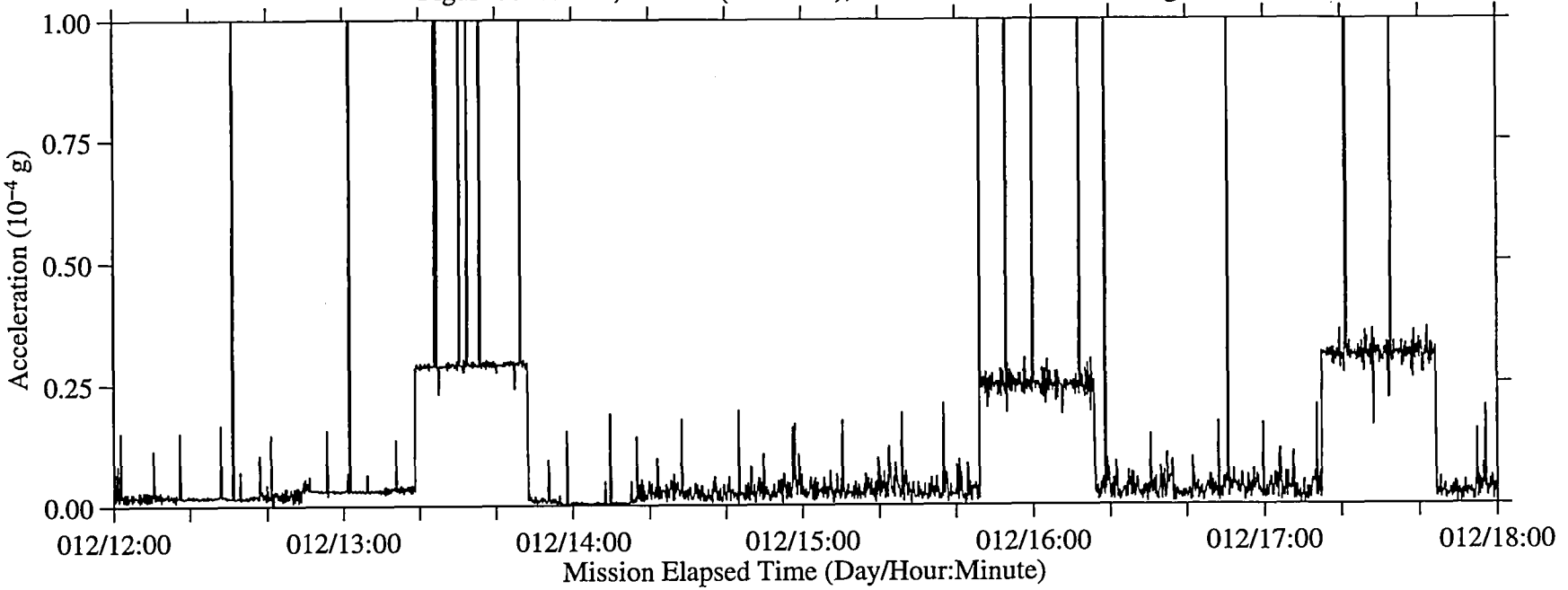

Figure 99b: LMS, Head C (fc=25 Hz), Ten Second Interval RMS

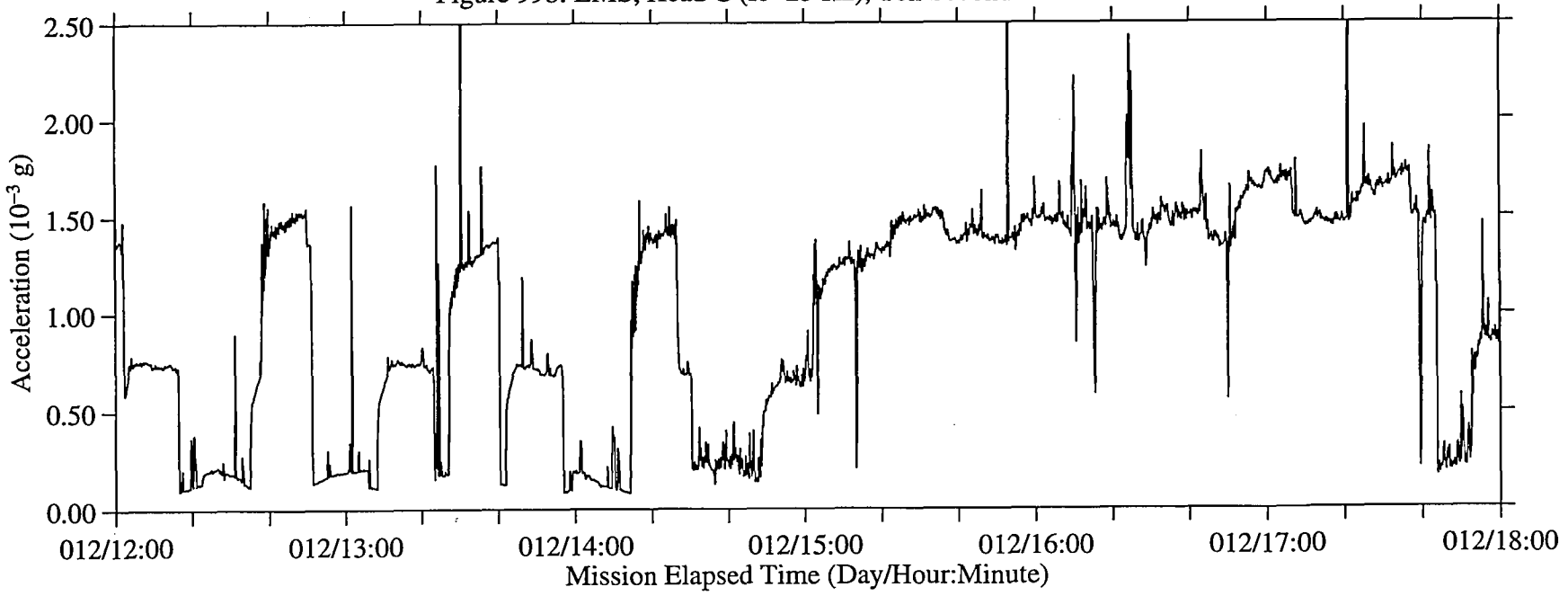

Figure 100: LMS, Head C (fc=25 Hz)

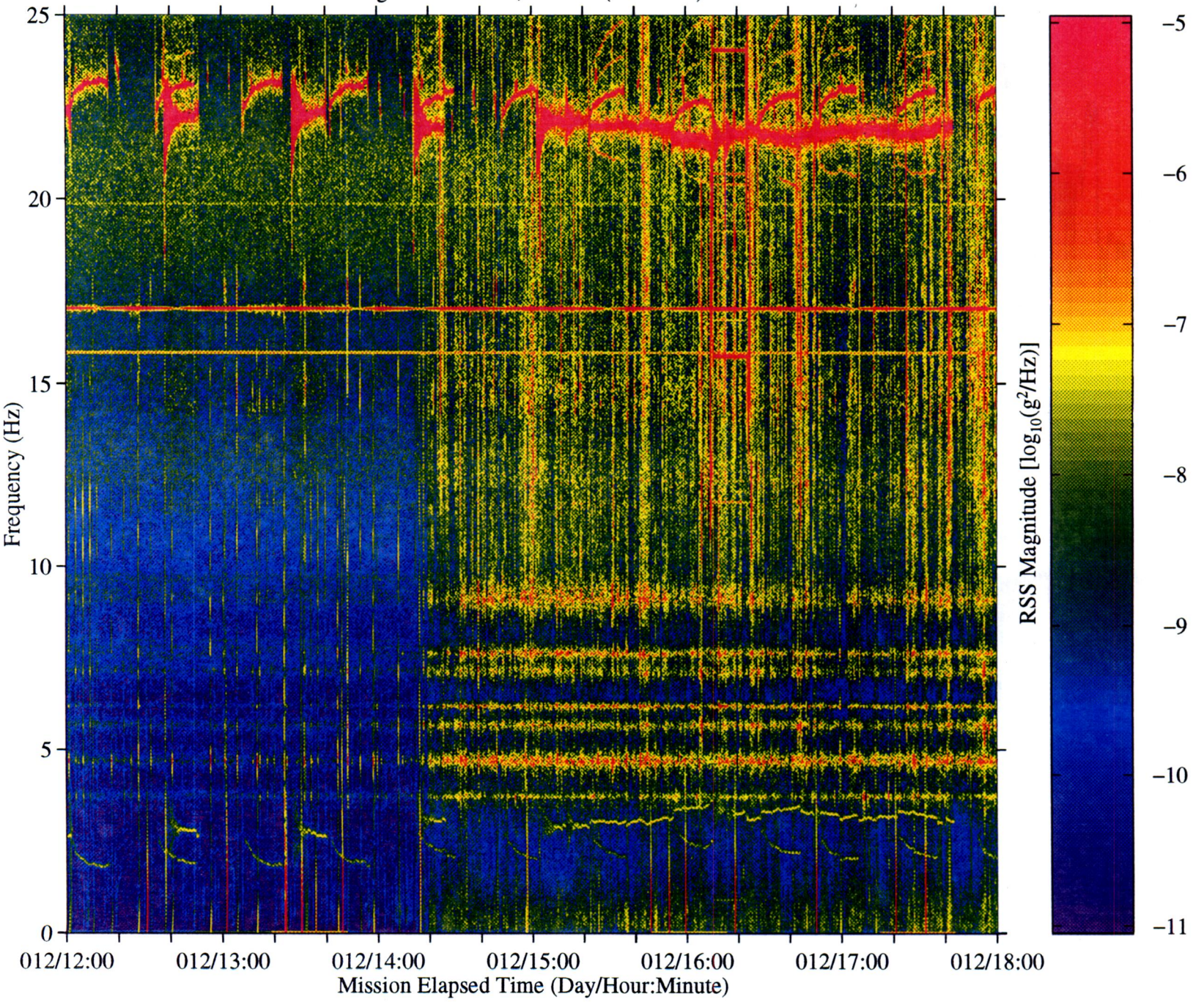

Figure 101a: LMS, Head C (fc=25 Hz), Ten Second Interval Average

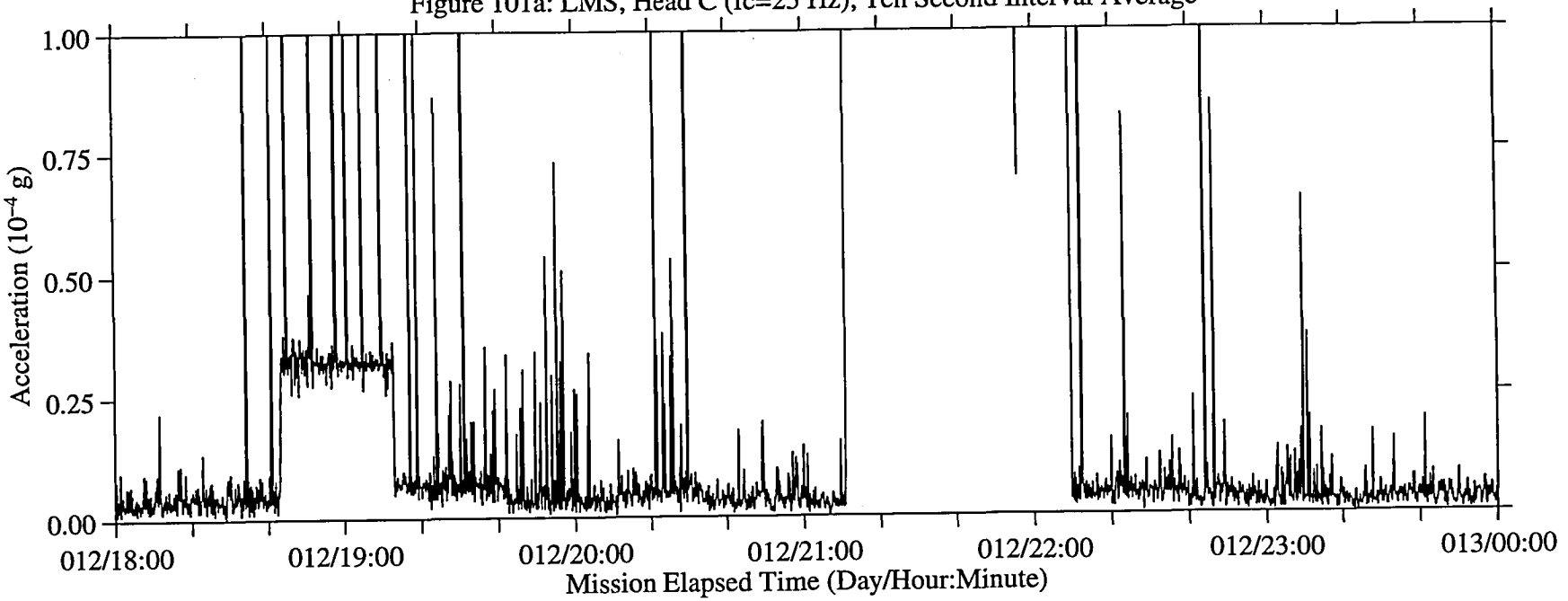

Figure 101b: LMS, Head C (fc=25 Hz), Ten Second Interval RMS

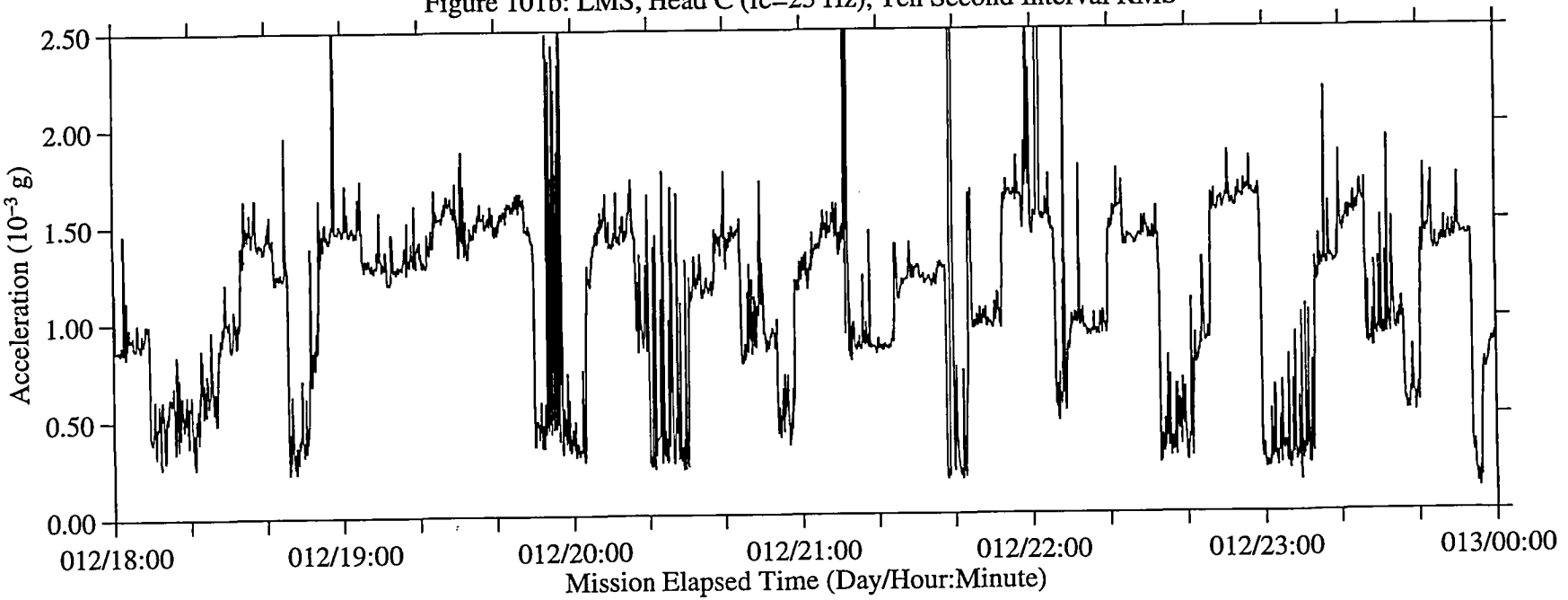

Figure 102: LMS, Head C (fc=25 Hz)

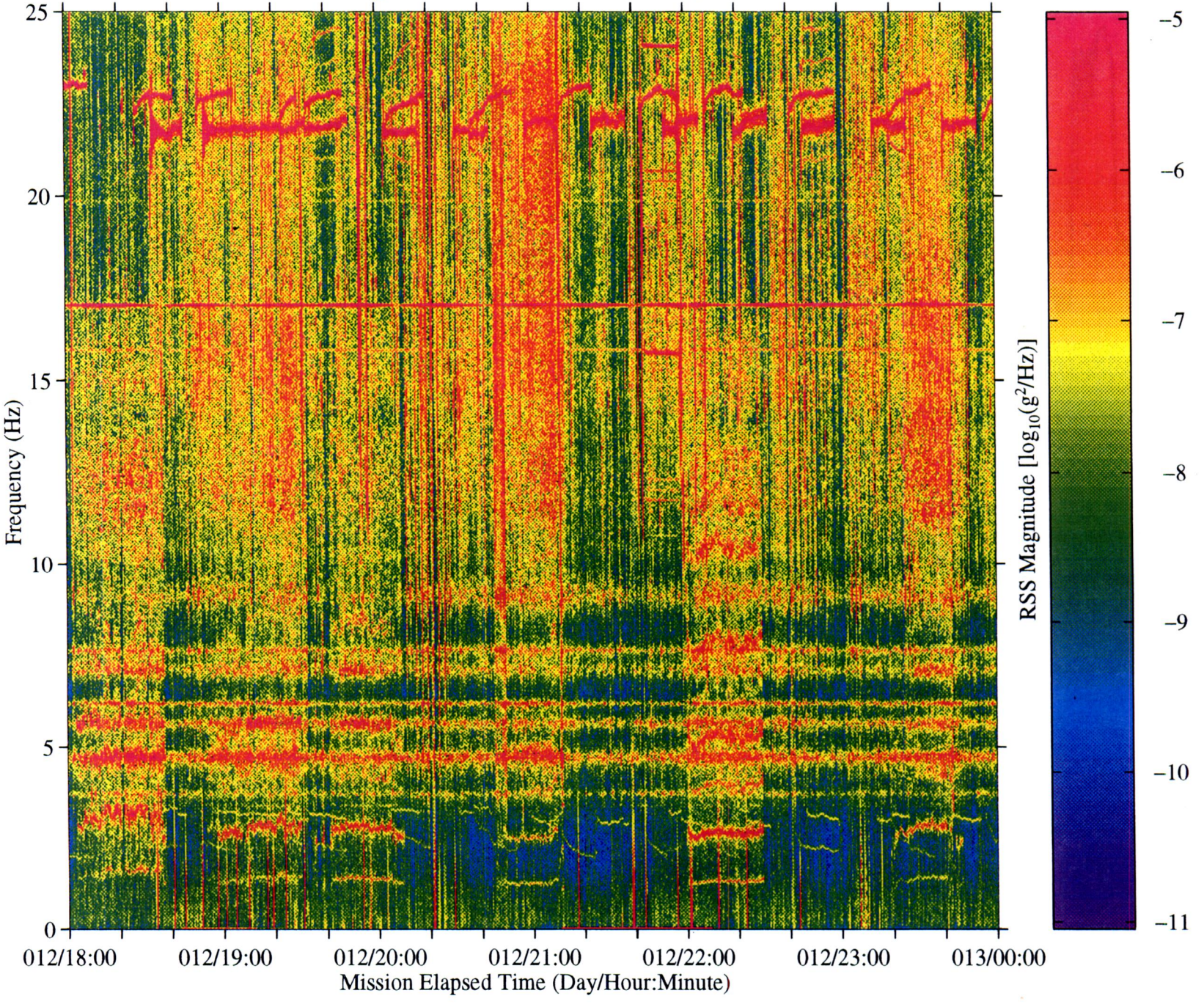

Figure 103a: LMS, Head C (fc=25 Hz), Ten Second Interval Average

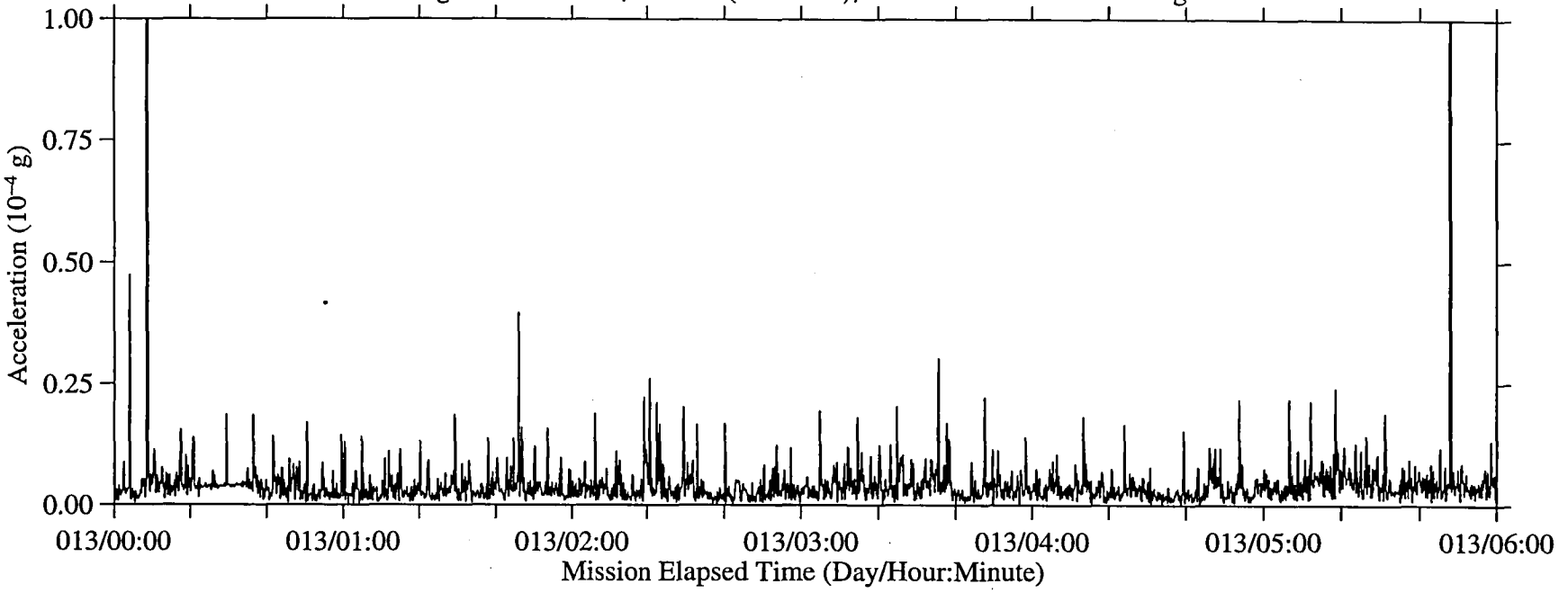

Figure 103b: LMS, Head C (fc=25 Hz), Ten Second Interval RMS

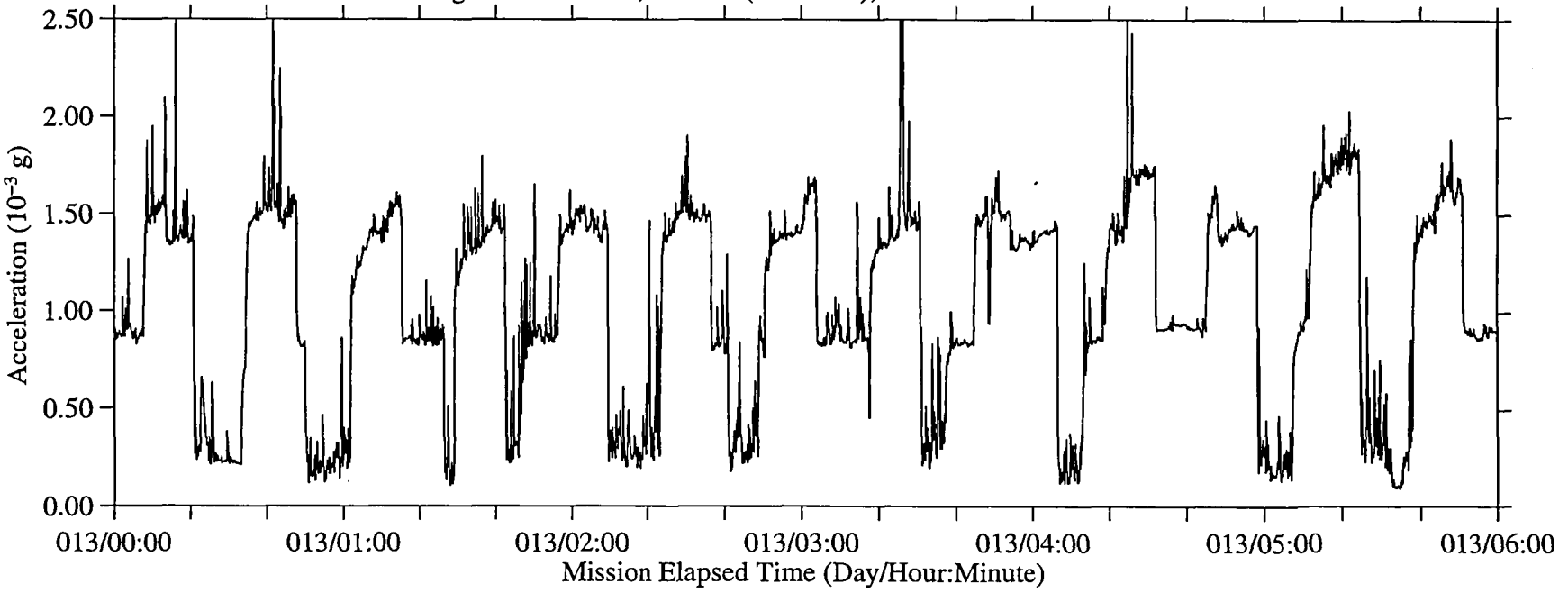

Figure 104: LMS, Head C (fc=25 Hz)

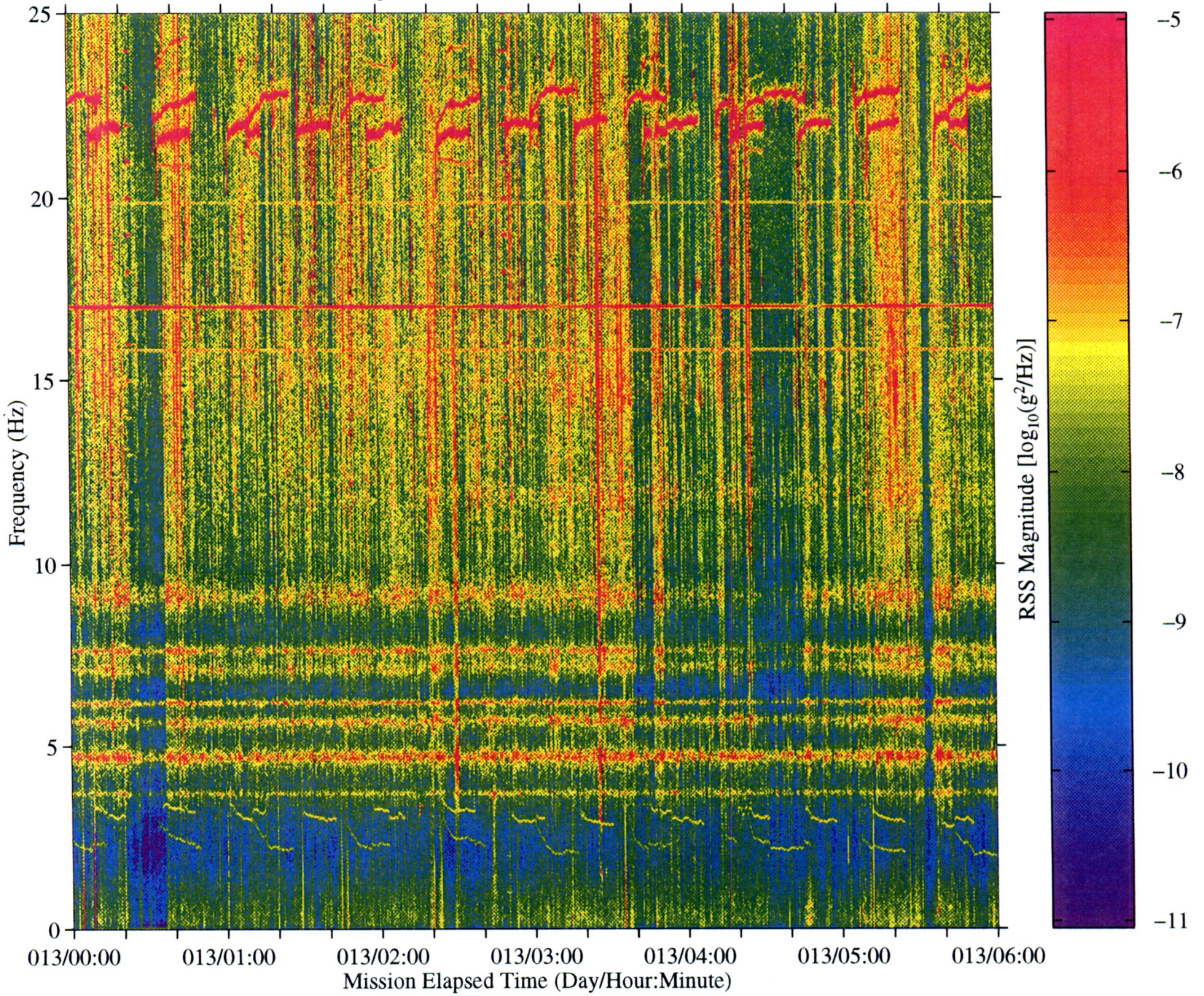

Figure 105a: LMS, Head C (fc=25 Hz), Ten Second Interval Average

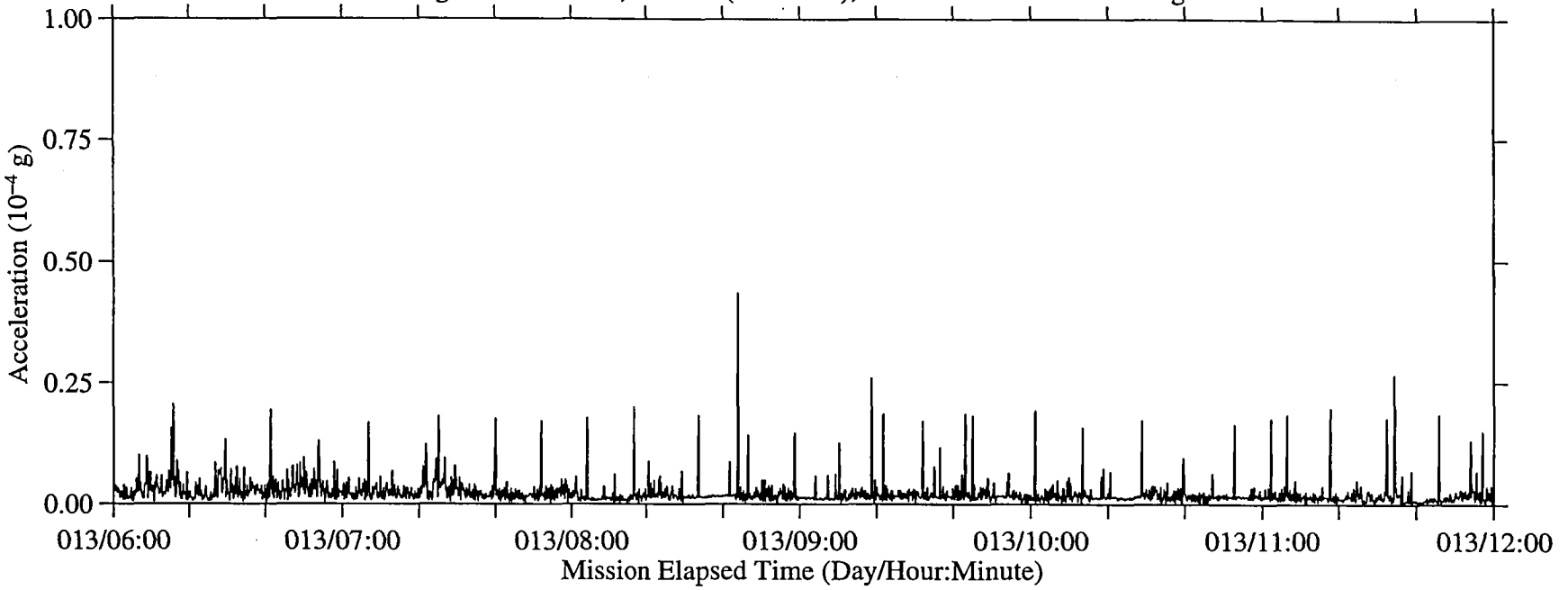

Figure 105b: LMS, Head C (fc=25 Hz), Ten Second Interval RMS

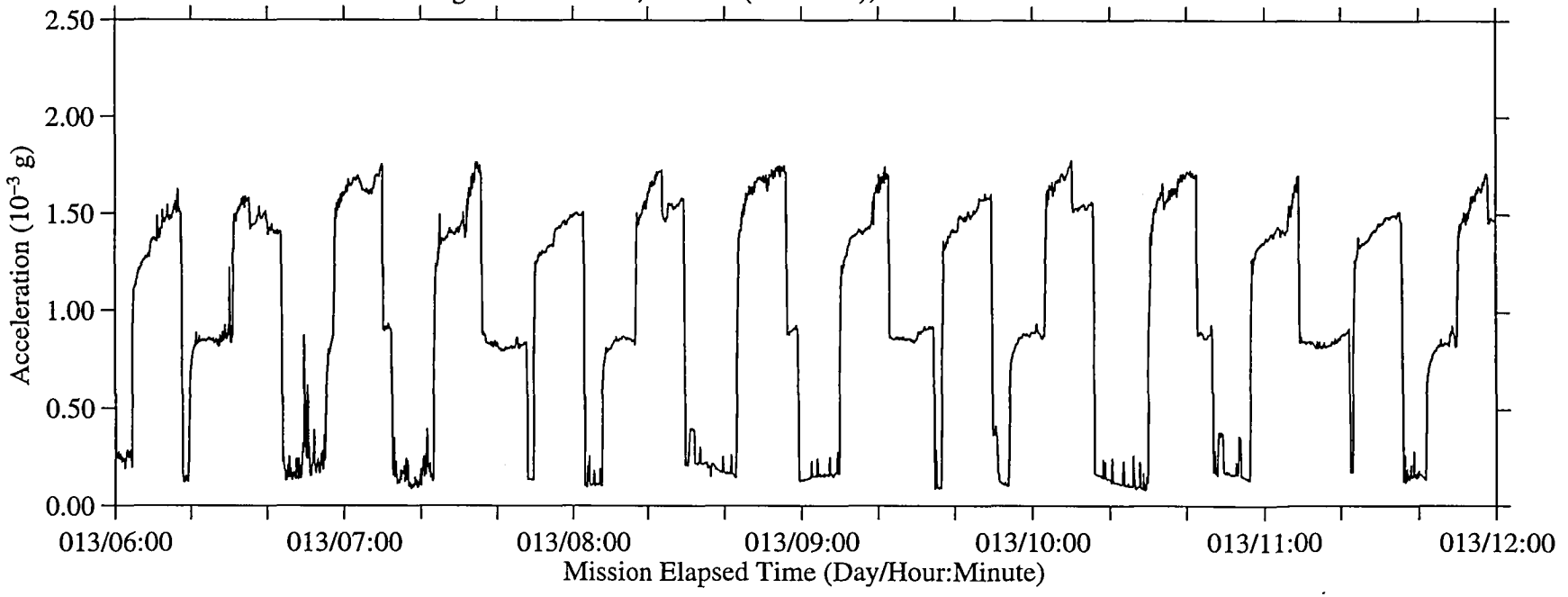

Figure 106: LMS, Head C (fc=25 Hz)

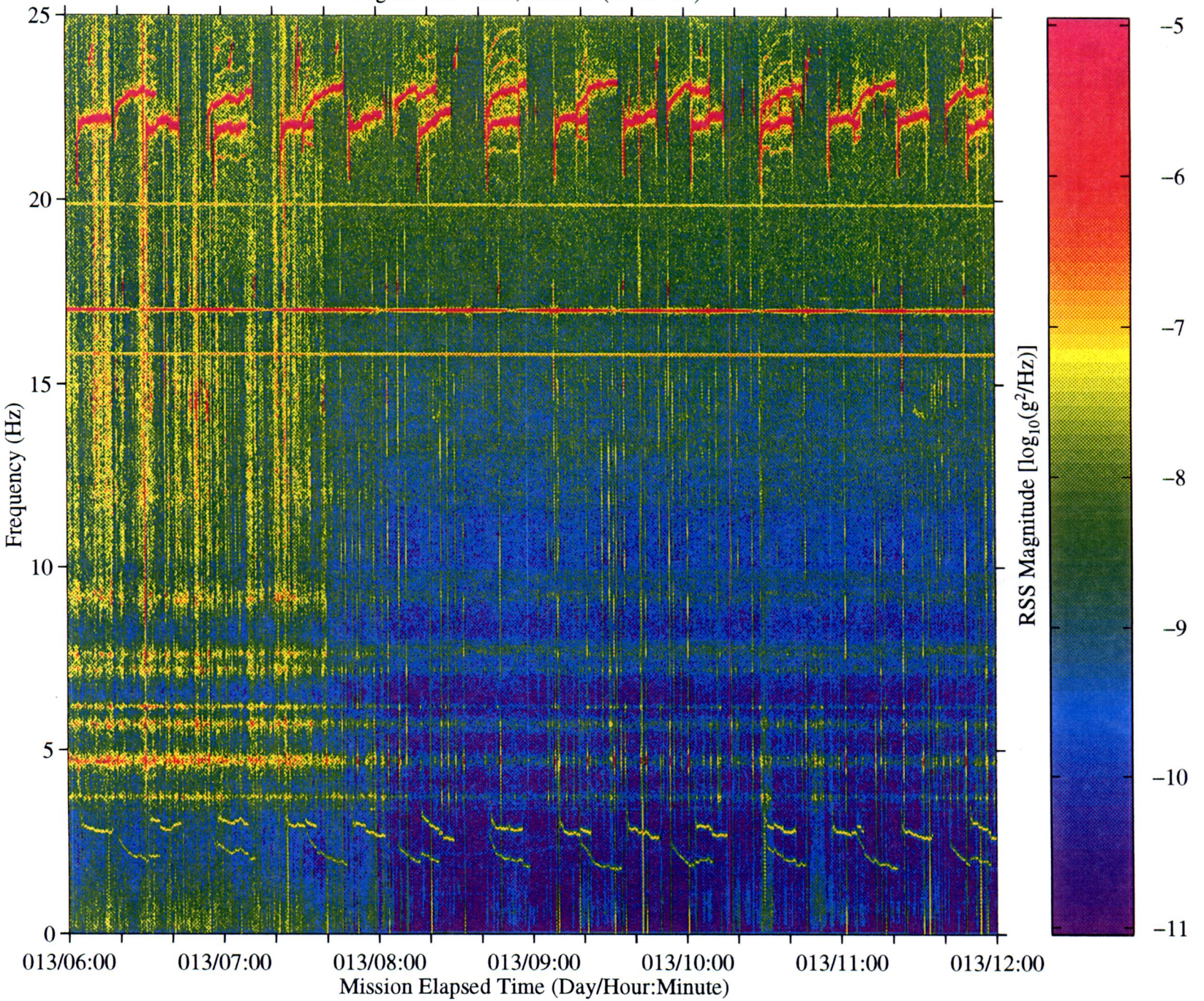

Figure 107a: LMS, Head C (fc=25 Hz), Ten Second Interval Average

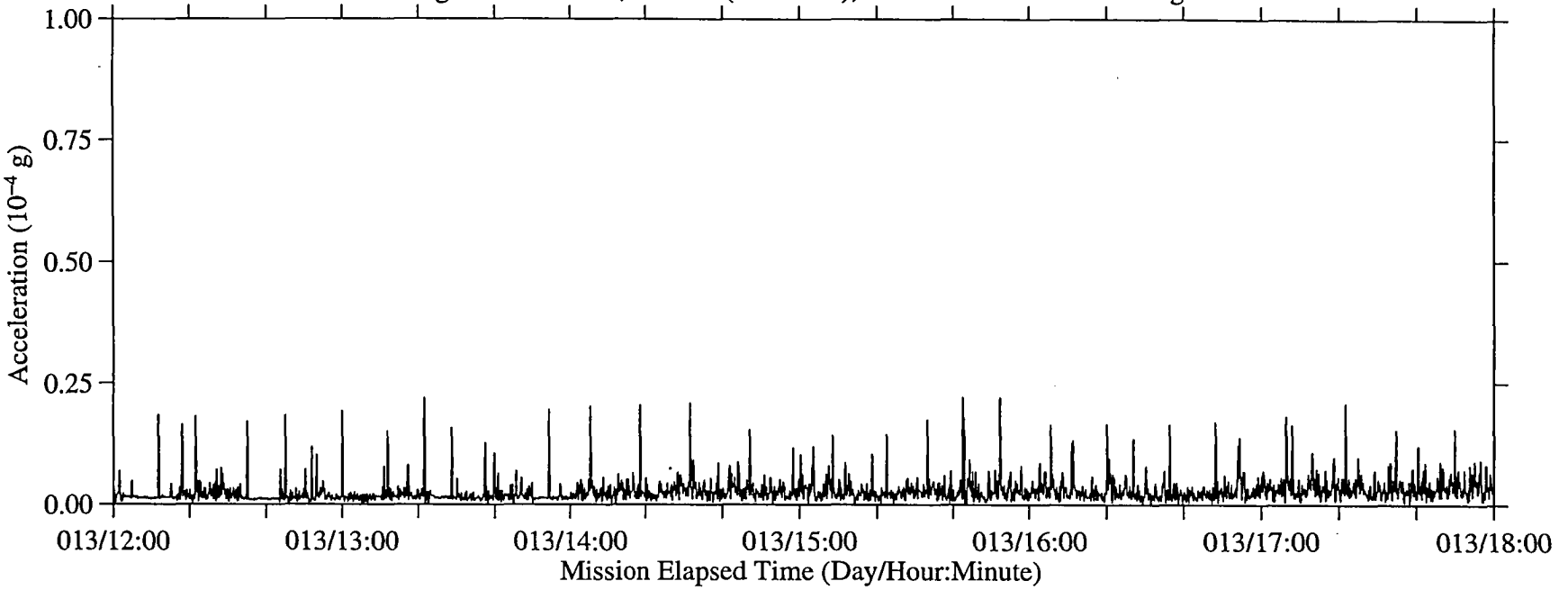

Figure 107b: LMS, Head C (fc=25 Hz), Ten Second Interval RMS

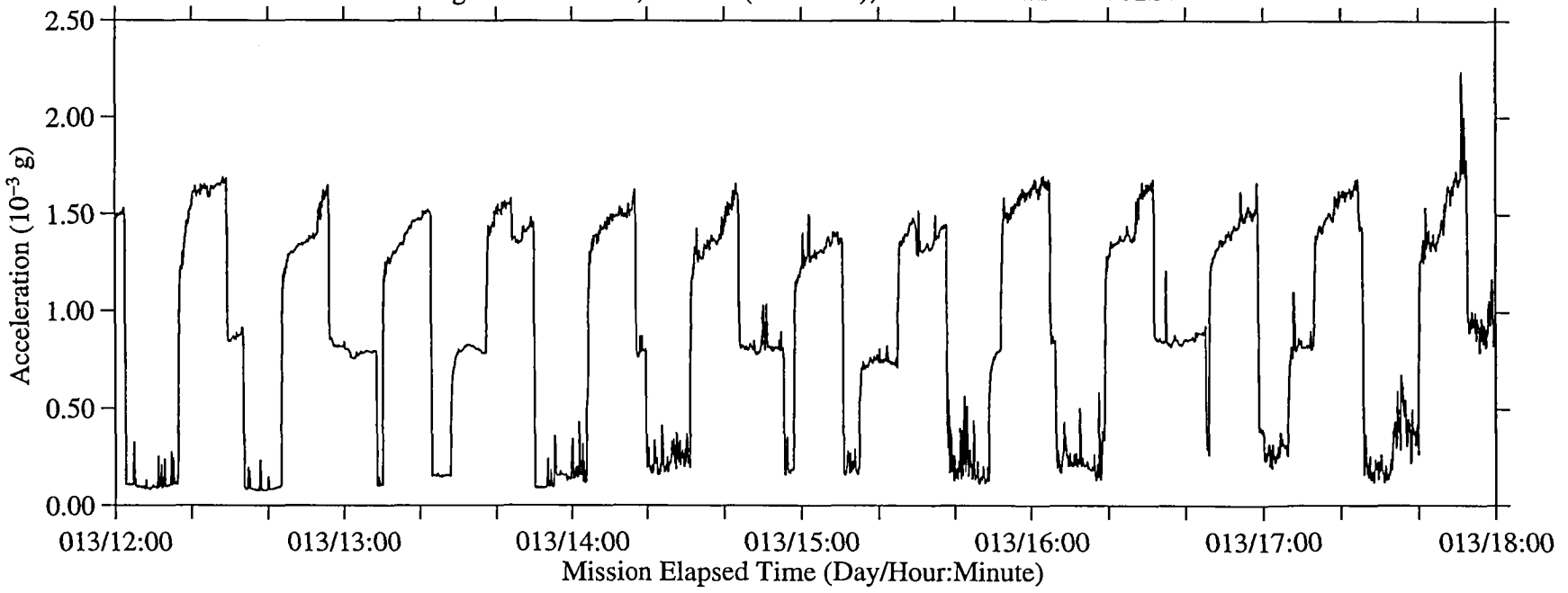

Figure 108: LMS, Head C (fc=25 Hz)

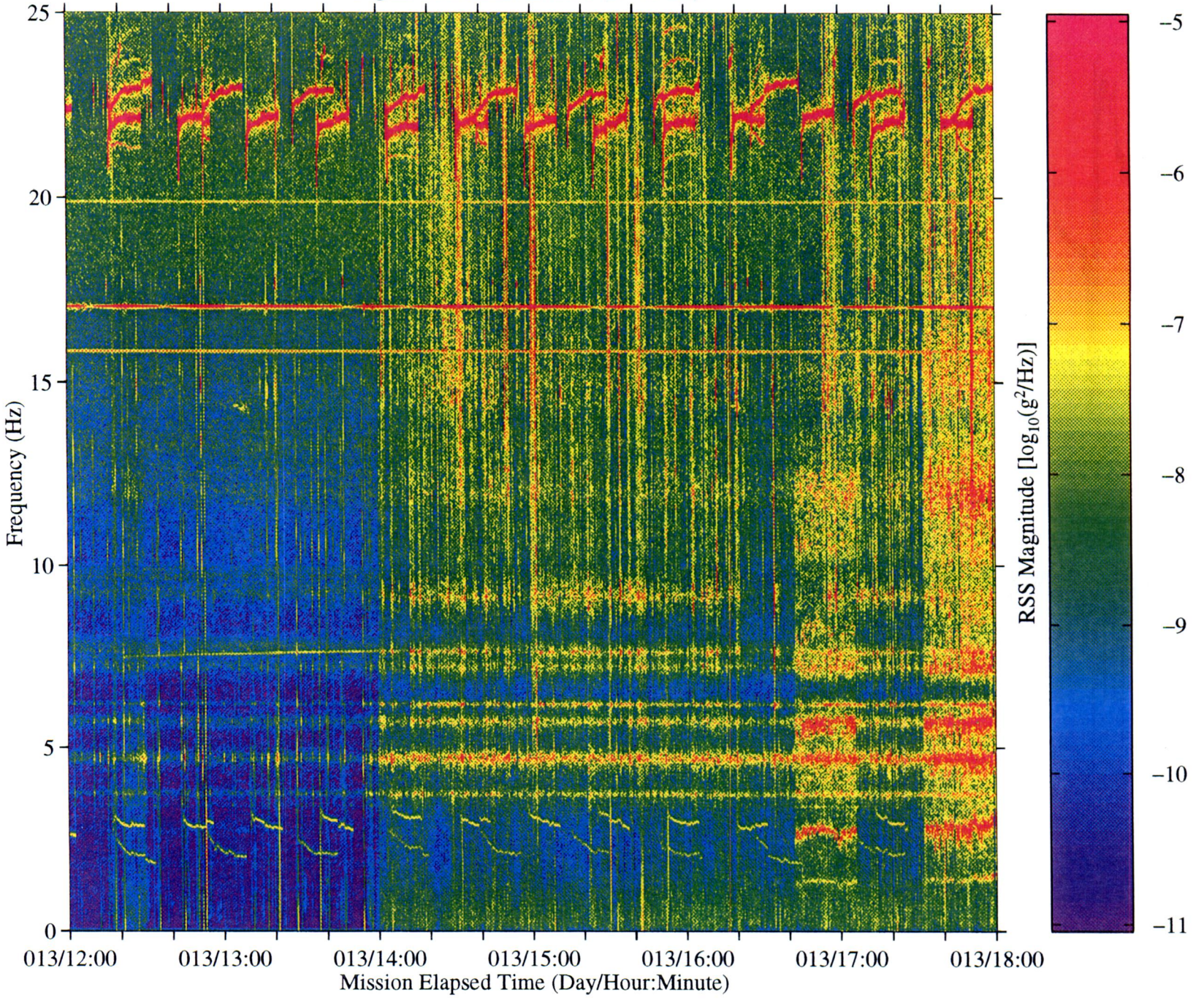

Figure 109a: LMS, Head C (fc=25 Hz), Ten Second Interval Average

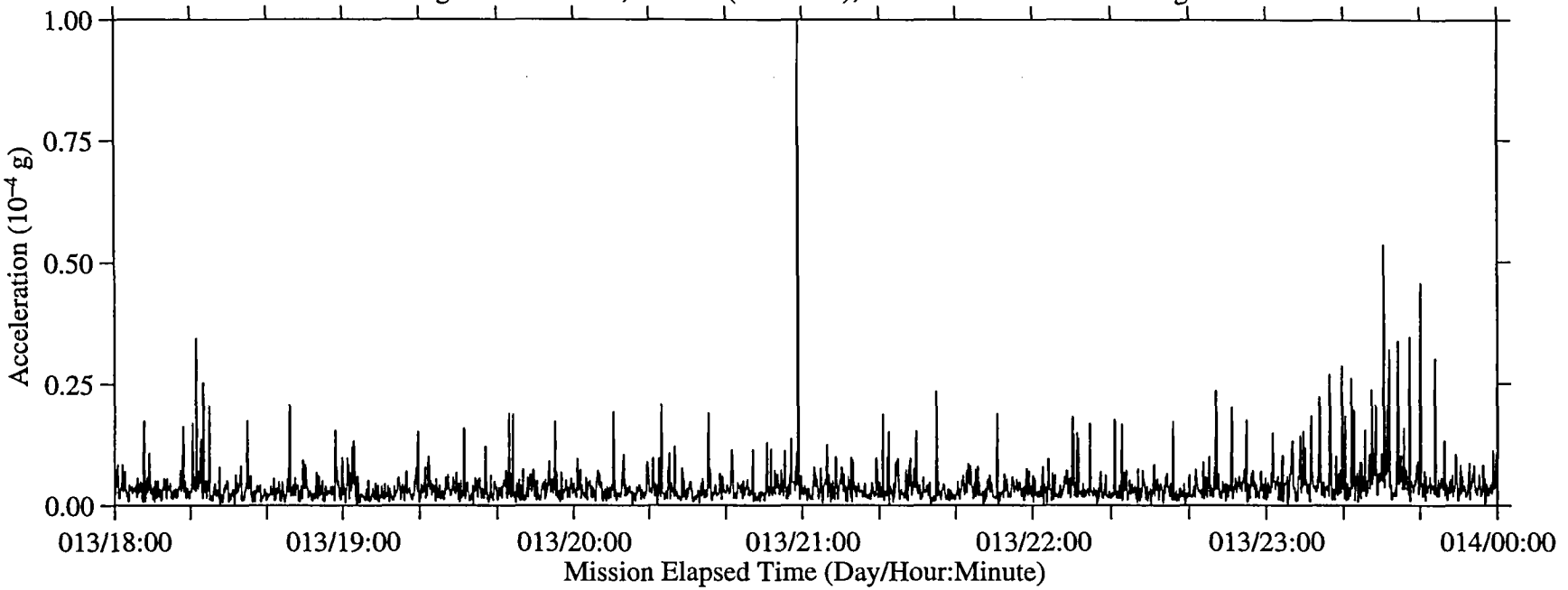

Figure 109b: LMS, Head C (fc=25 Hz), Ten Second Interval RMS

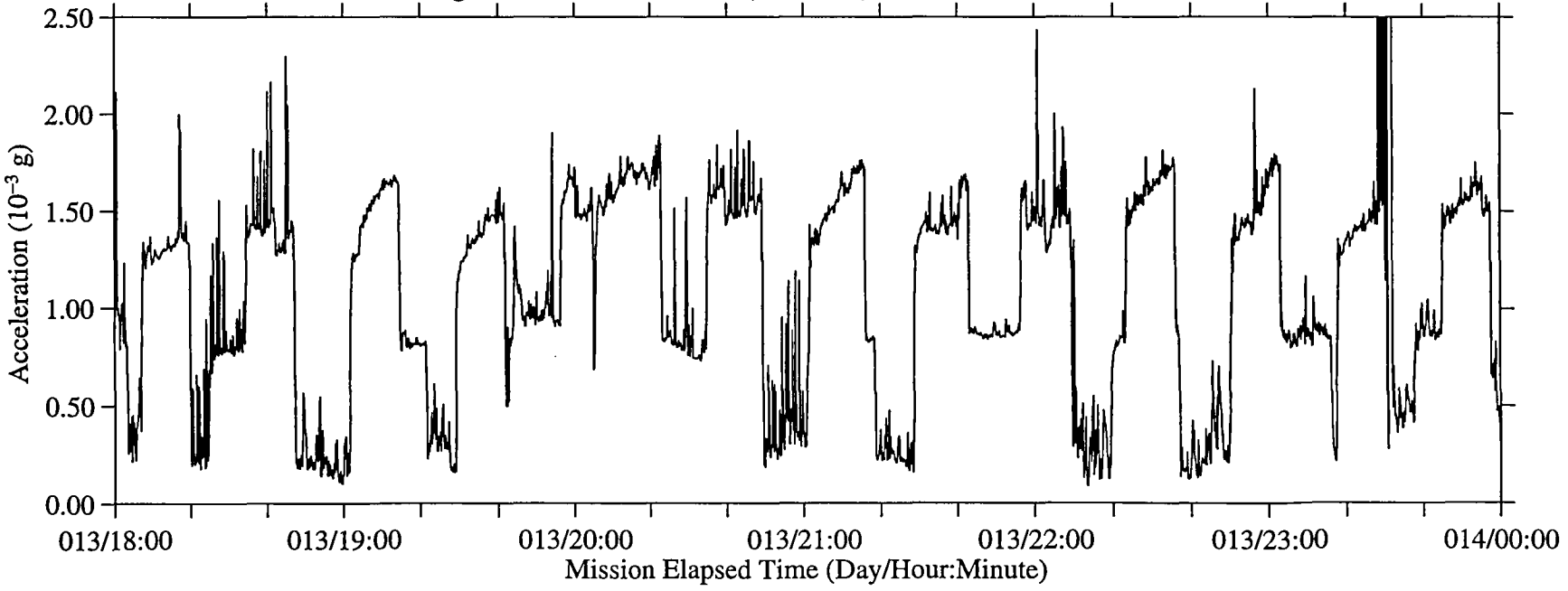

Figure 110: LMS, Head C (fc=25 Hz)

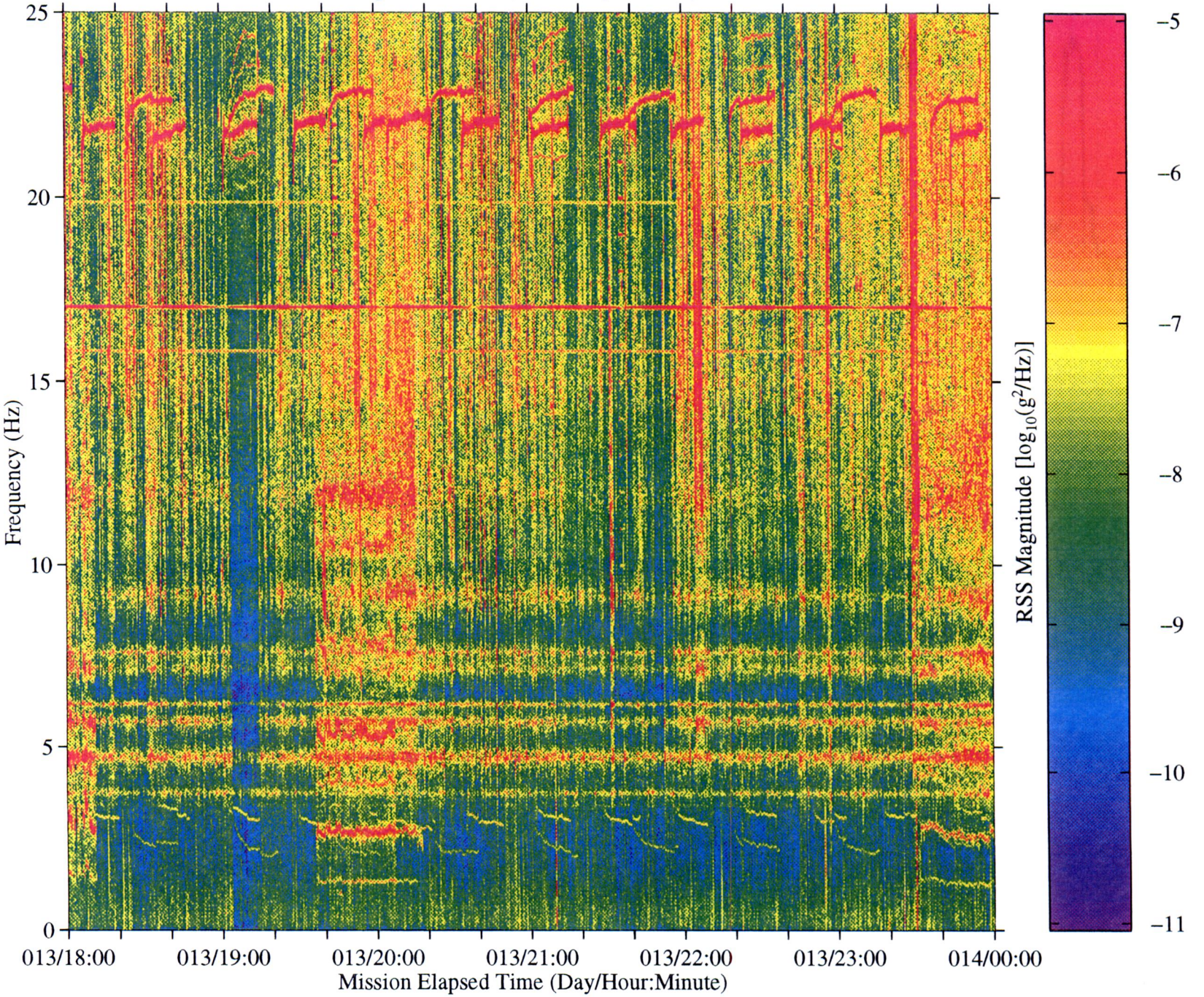

Figure 111a: LMS, Head C (fc=25 Hz), Ten Second Interval Average

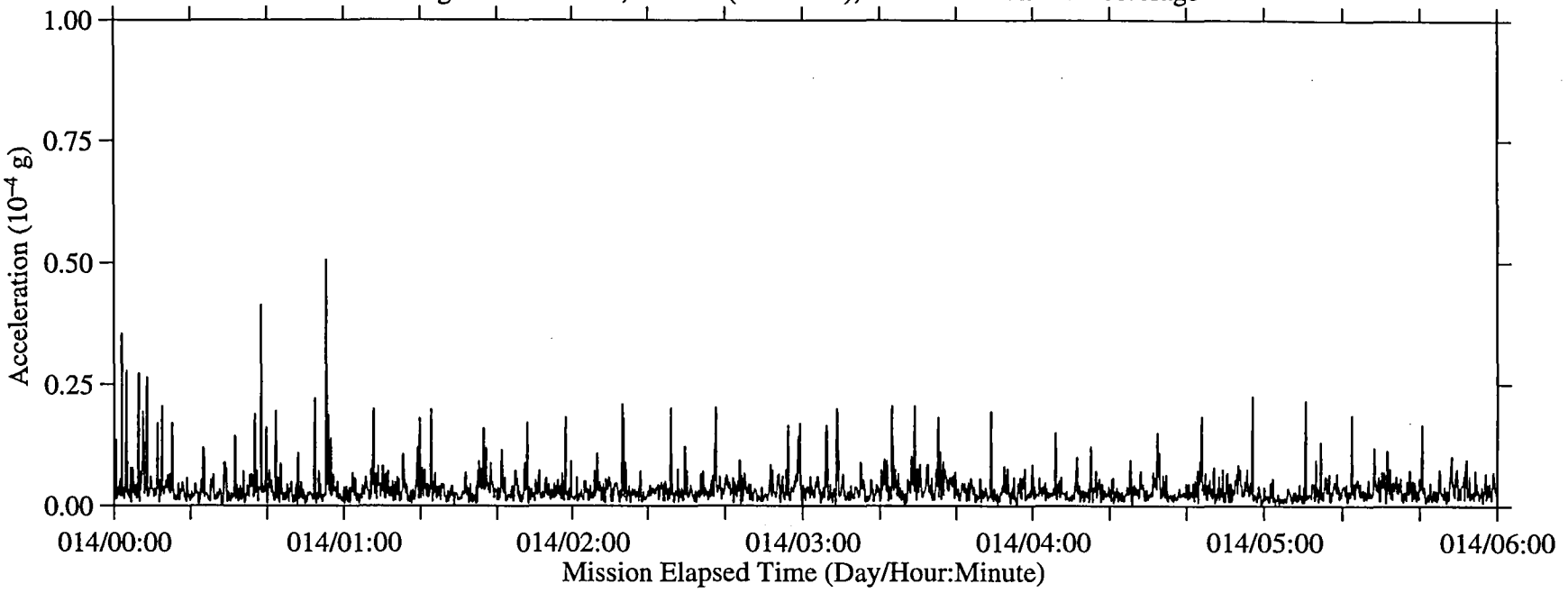

Figure 111b: LMS, Head C (fc=25 Hz), Ten Second Interval RMS

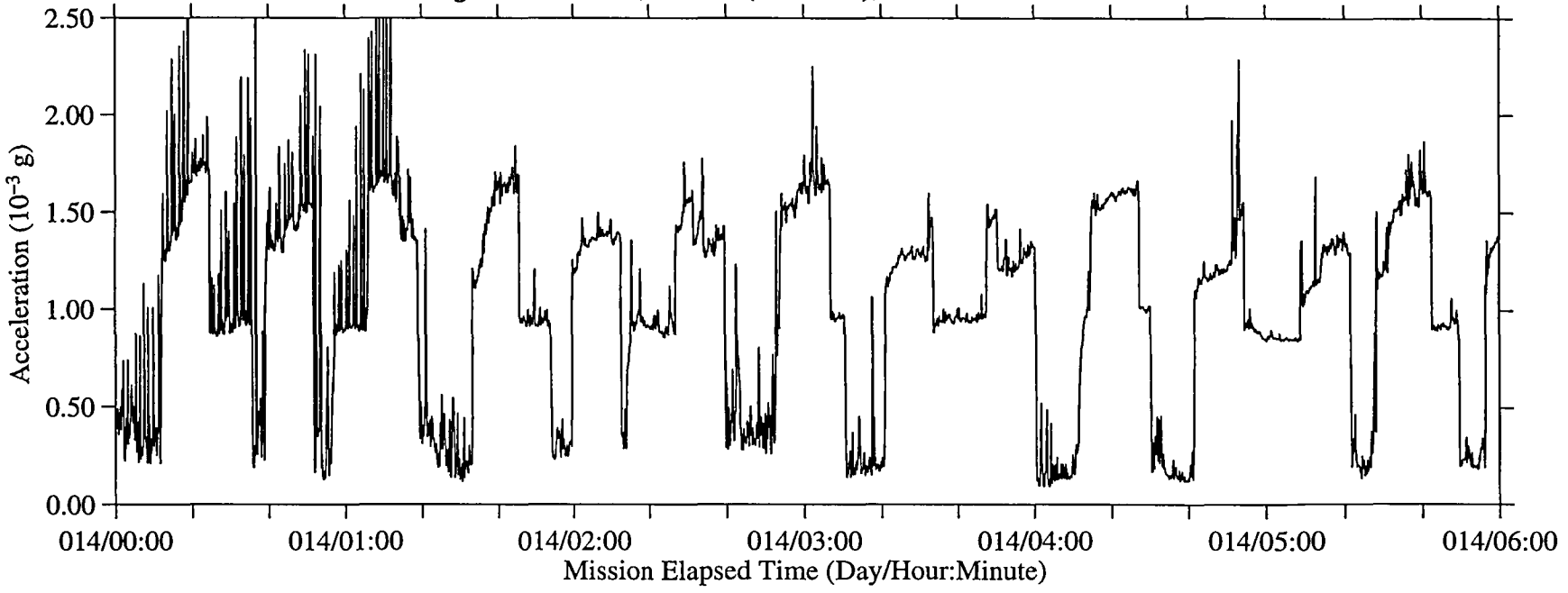

Figure 112: LMS, Head C (fc=25 Hz)

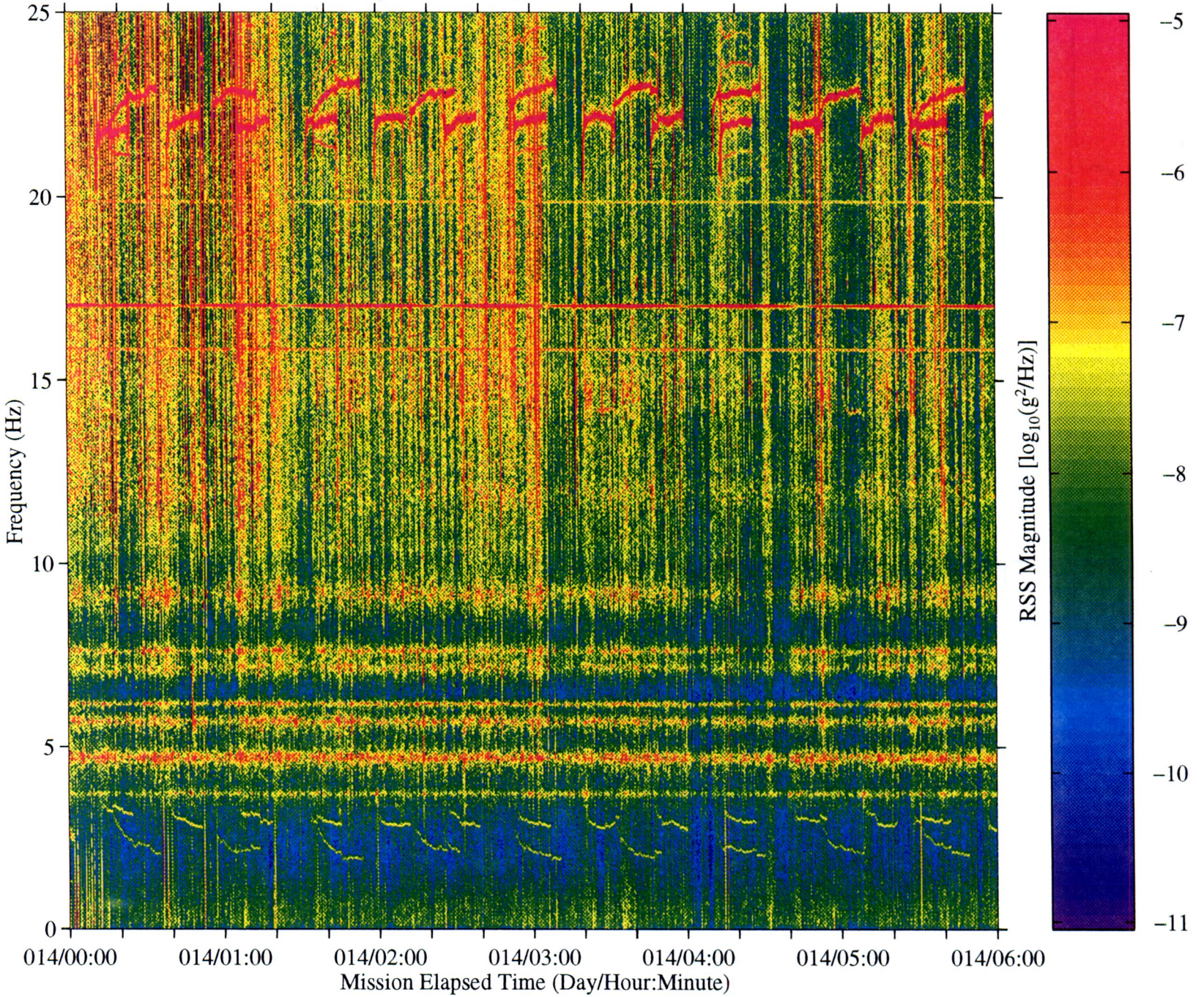

Figure 113a: LMS, Head C (fc=25 Hz), Ten Second Interval Average

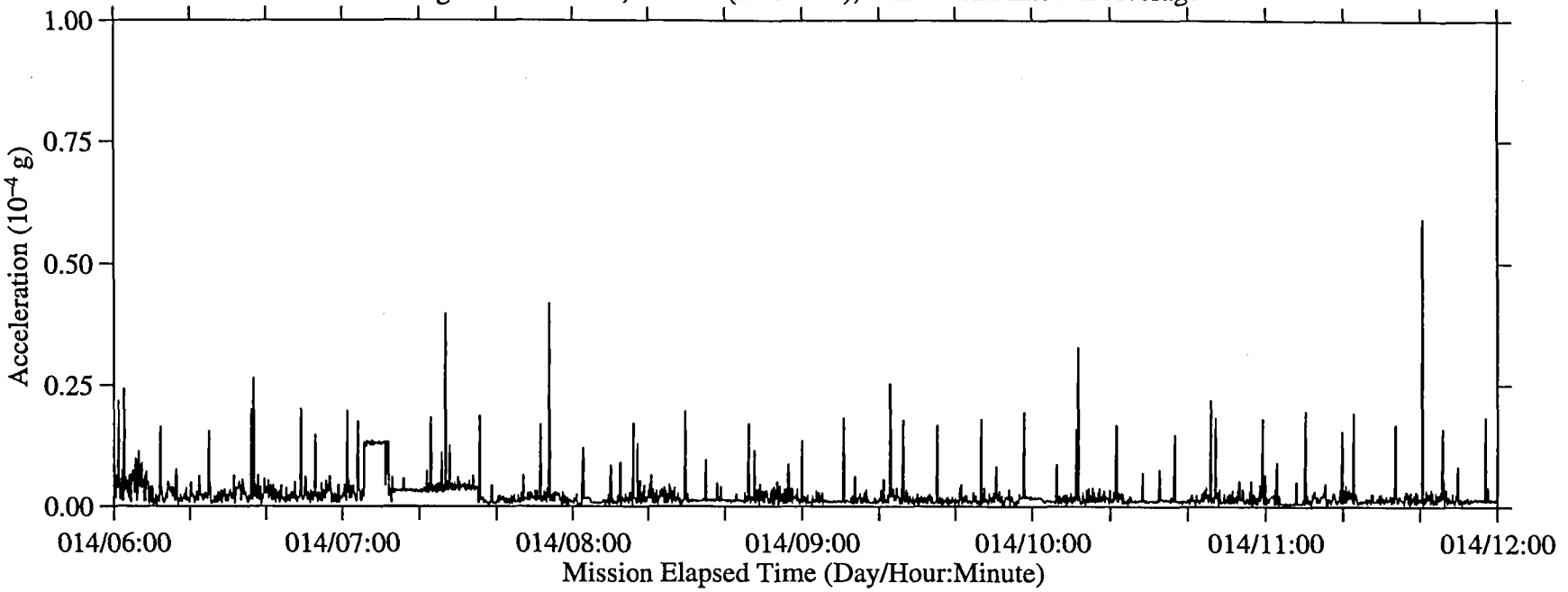

Figure 113b: LMS, Head C (fc=25 Hz), Ten Second Interval RMS

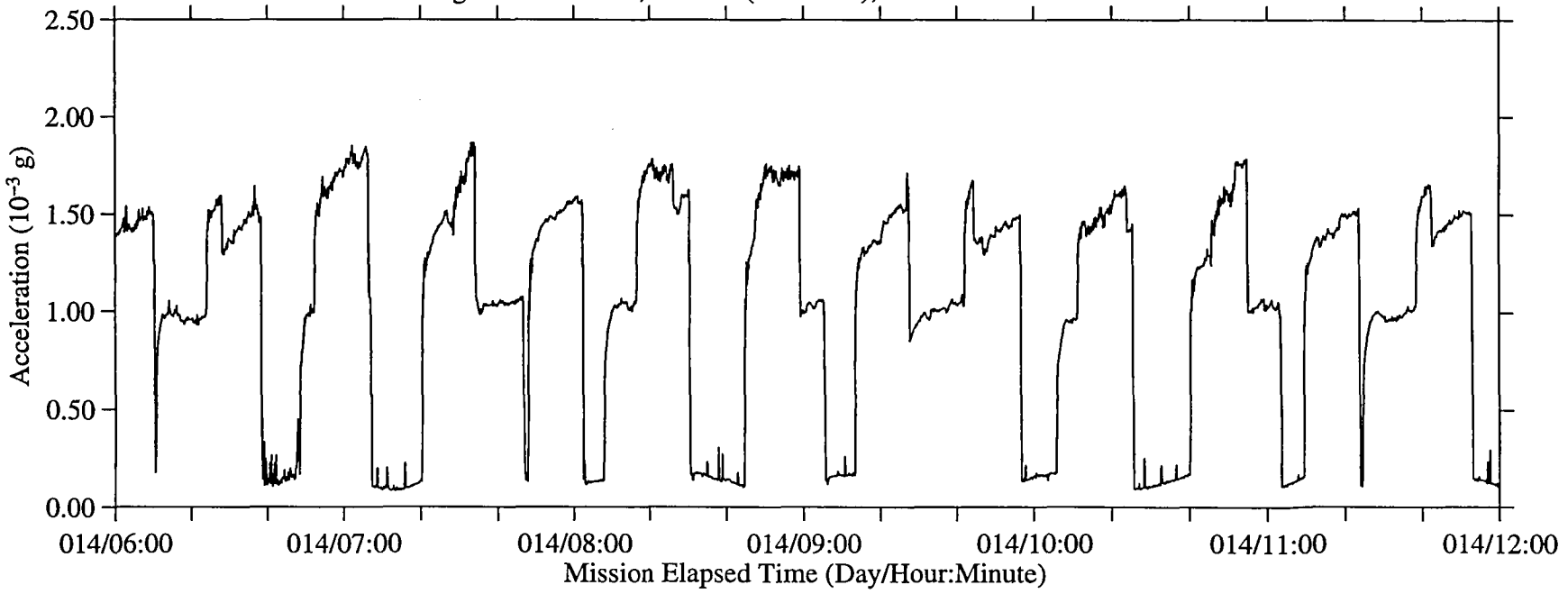

Figure 114: LMS, Head C (fc=25 Hz)

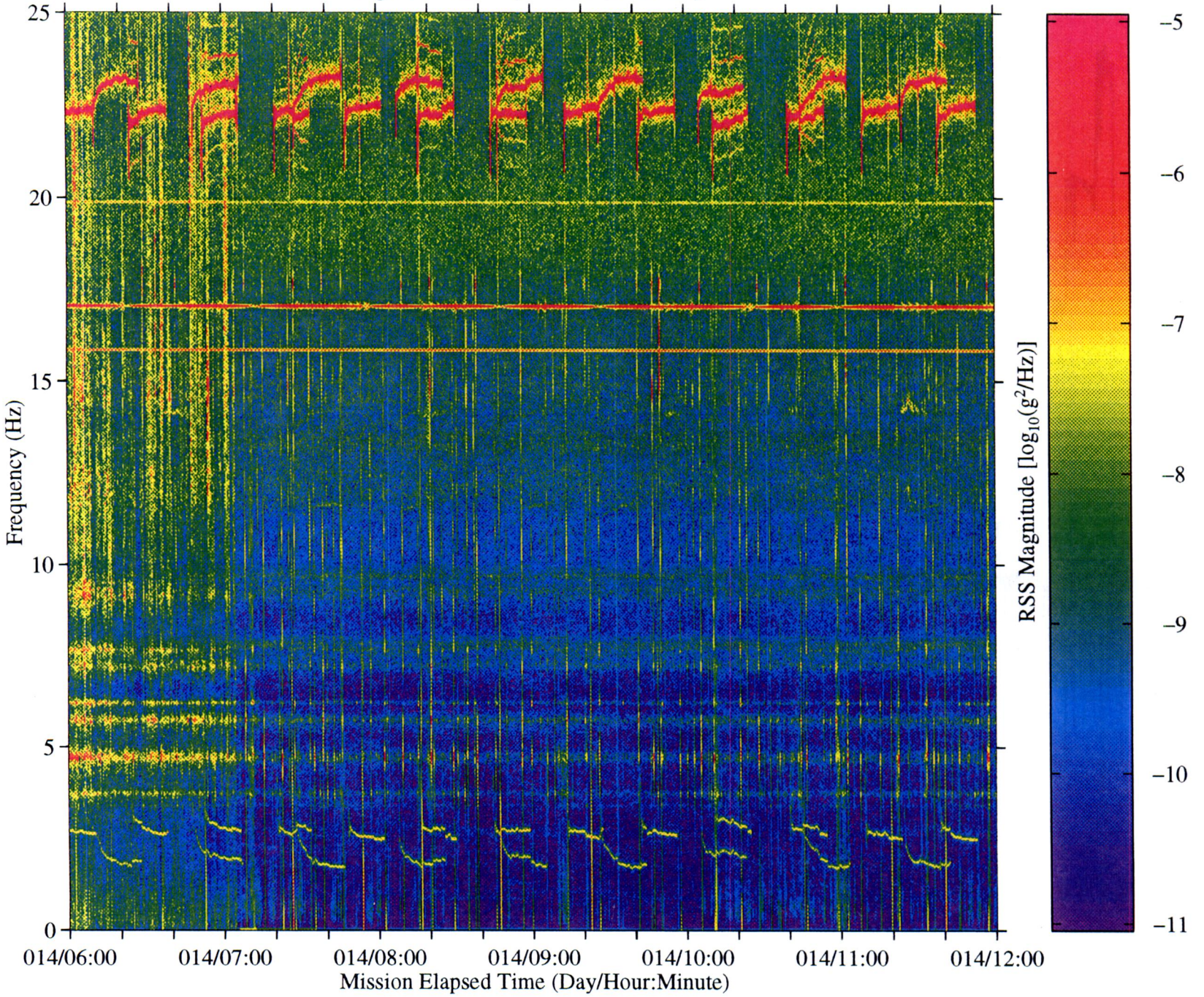

Figure 115a: LMS, Head C (fc=25 Hz), Ten Second Interval Average

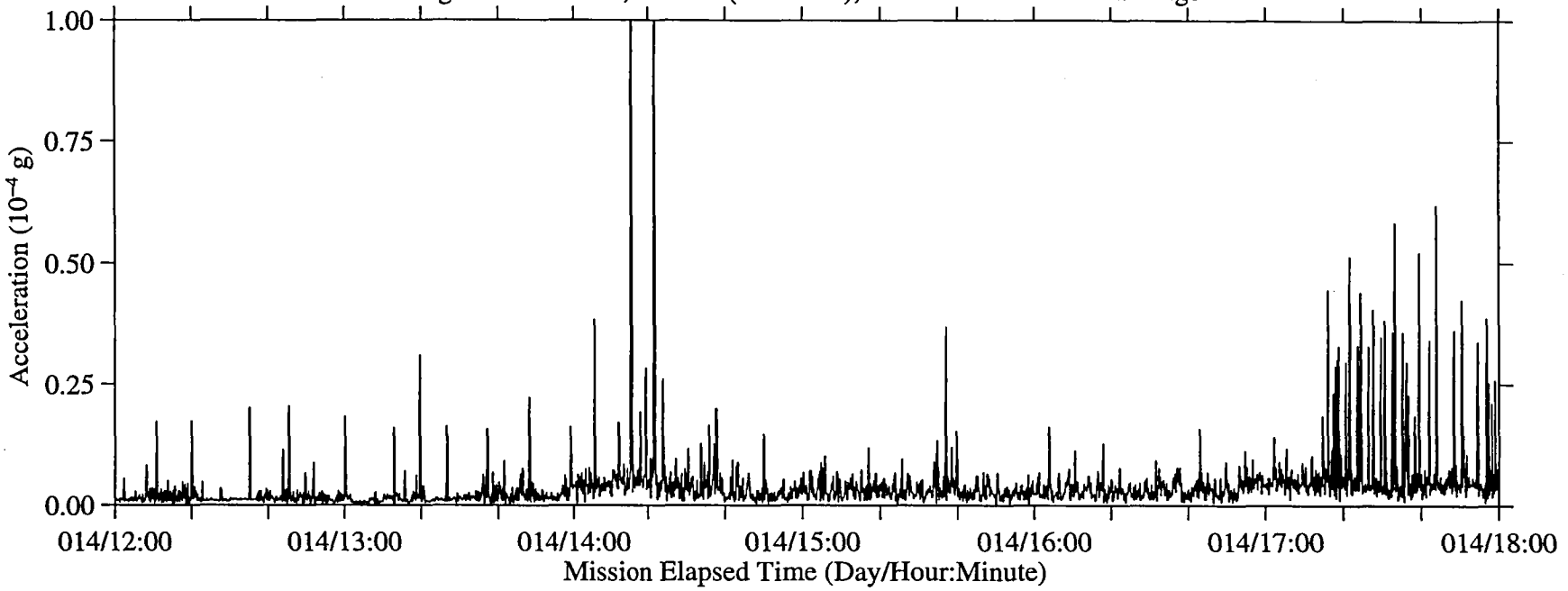

Figure 115b: LMS, Head C (fc=25 Hz), Ten Second Interval RMS

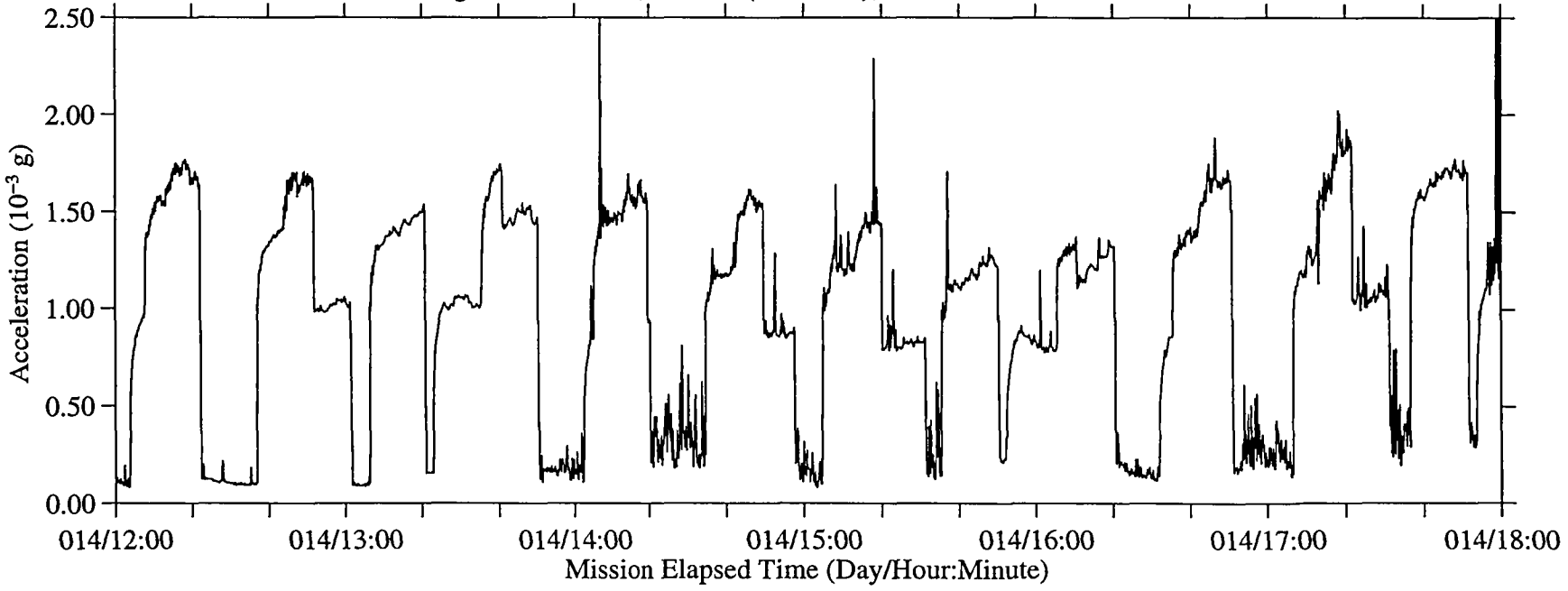

Figure 116: LMS, Head C (fc=25 Hz)

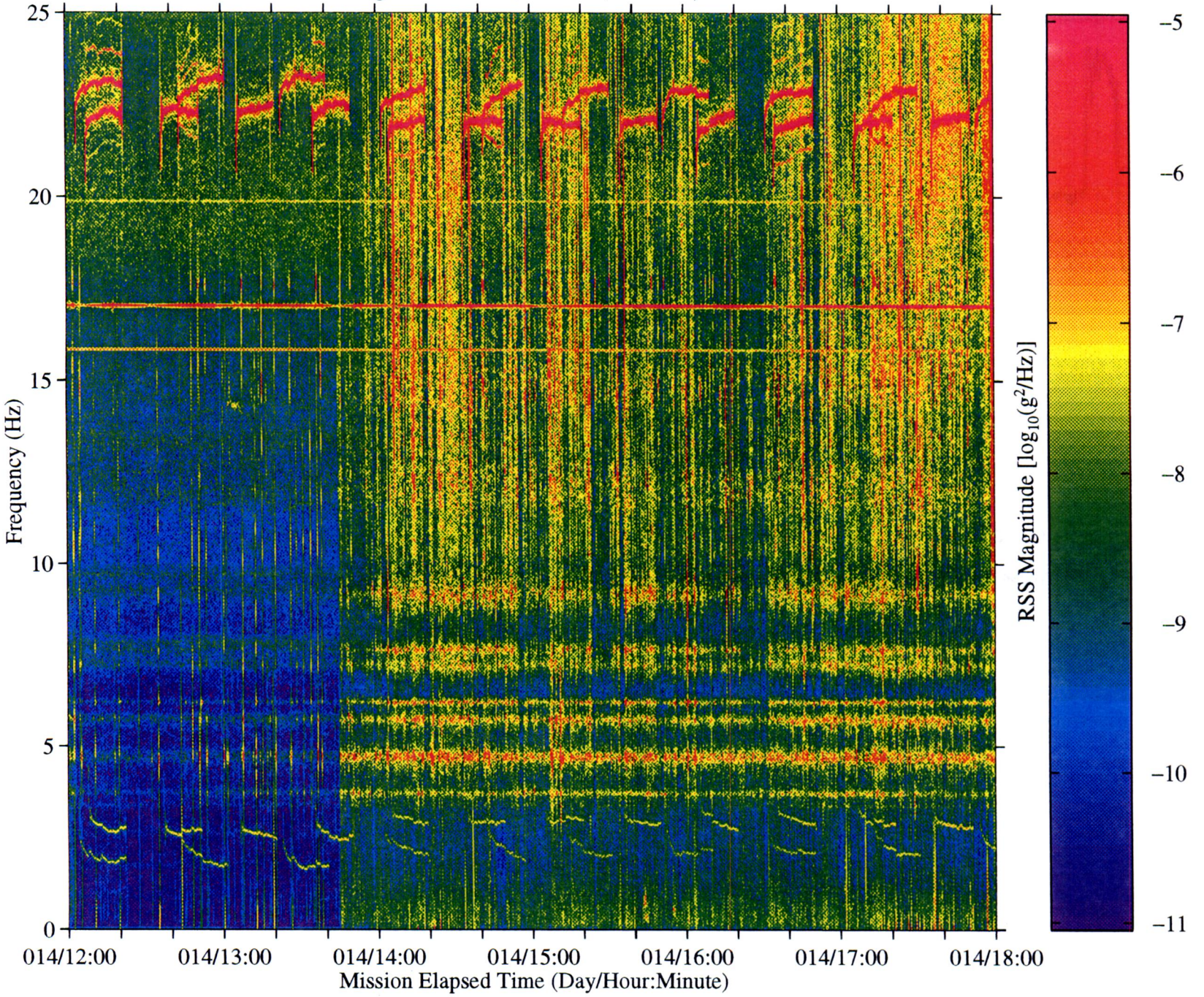

Figure 117a: LMS, Head C (fc=25 Hz), Ten Second Interval Average

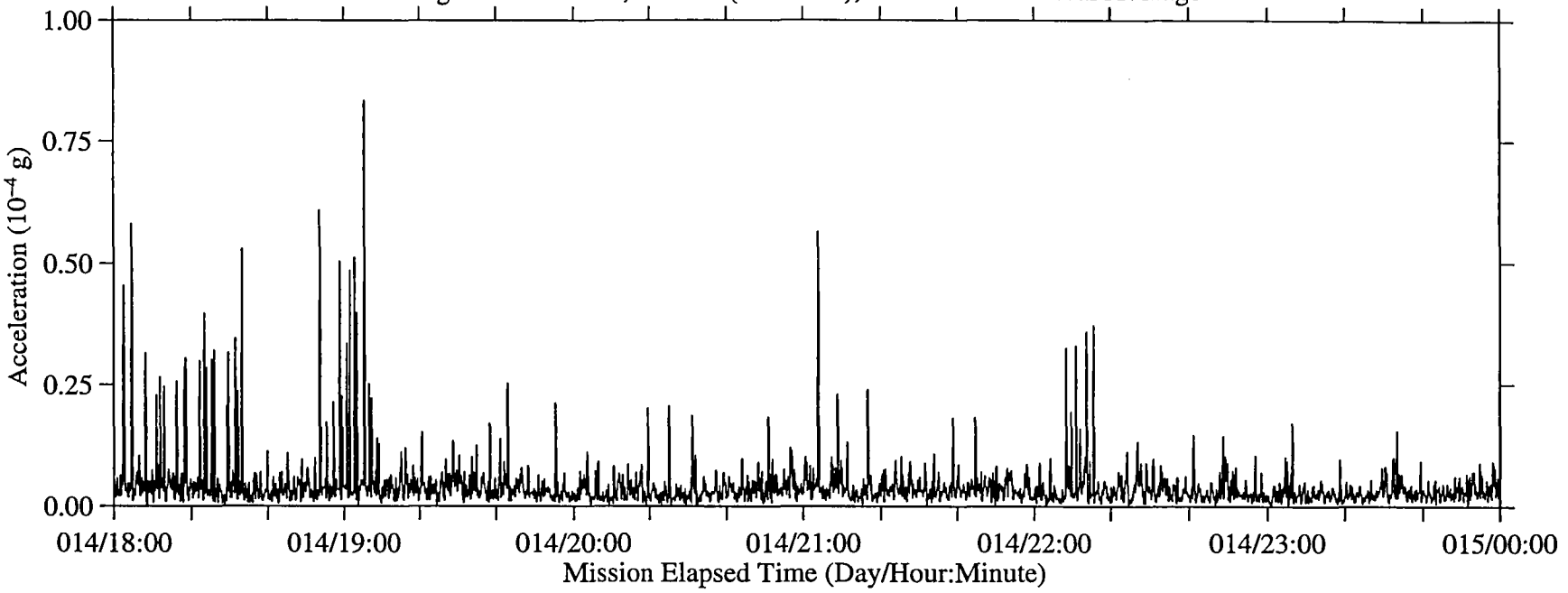

Figure 117b: LMS, Head C (fc=25 Hz), Ten Second Interval RMS

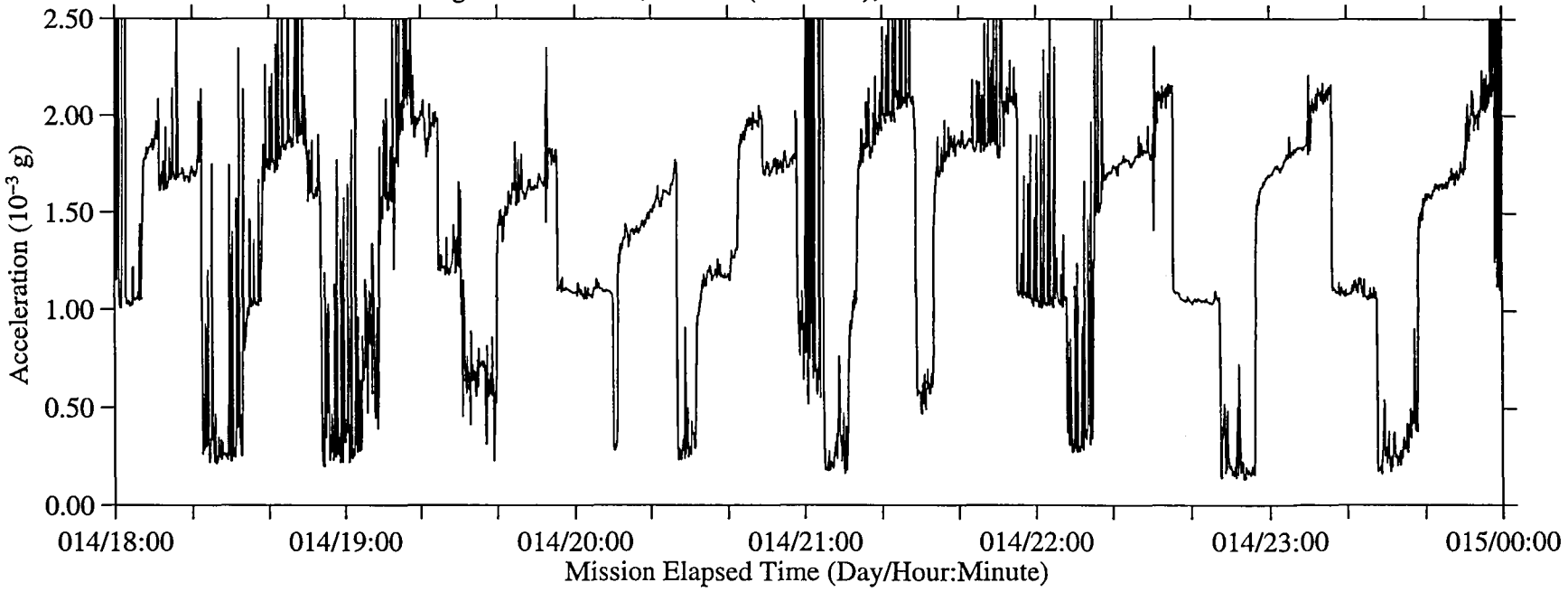

Figure 118: LMS, Head C (fc=25 Hz)

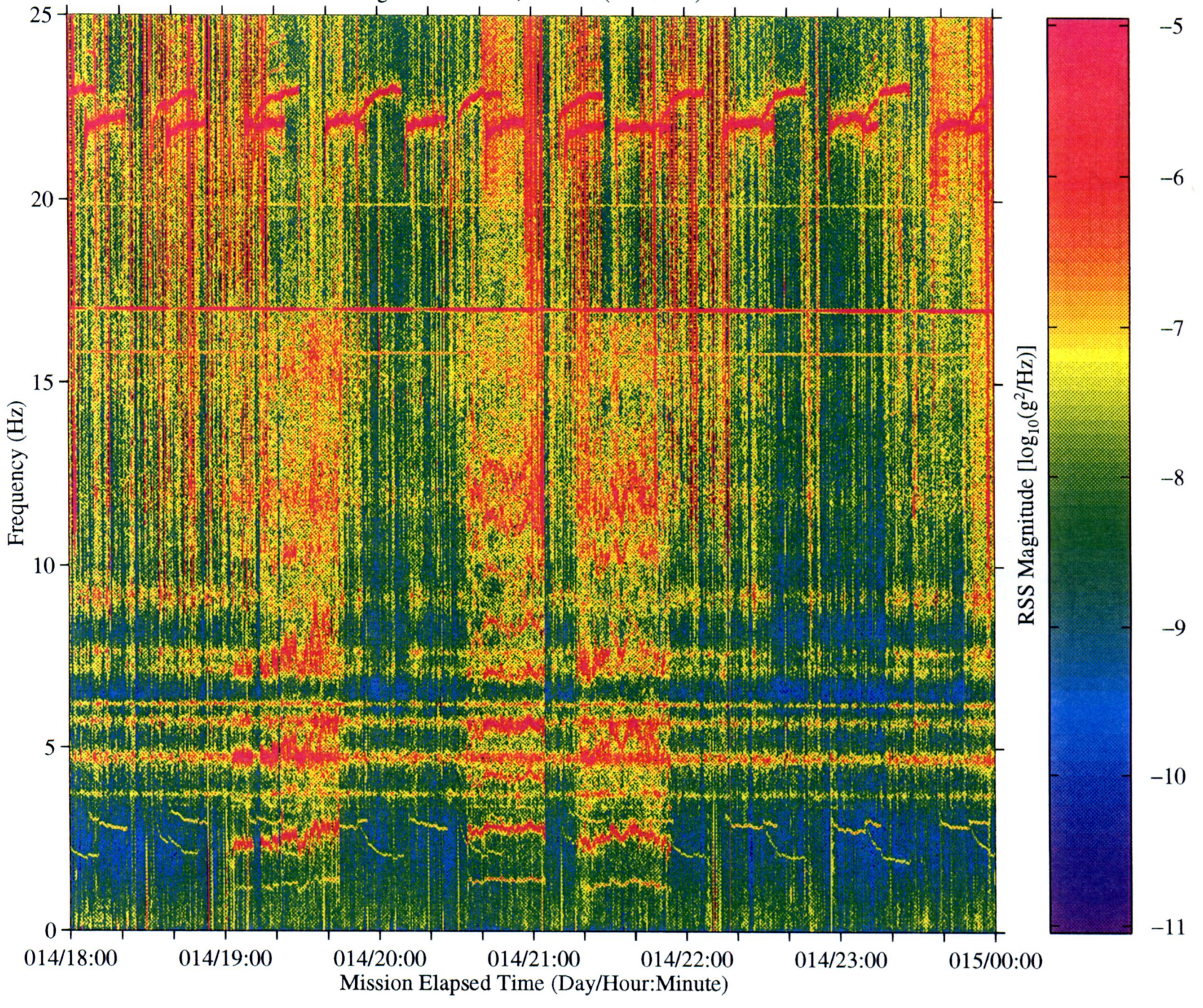

Figure 119a: LMS, Head C (fc=25 Hz), Ten Second Interval Average

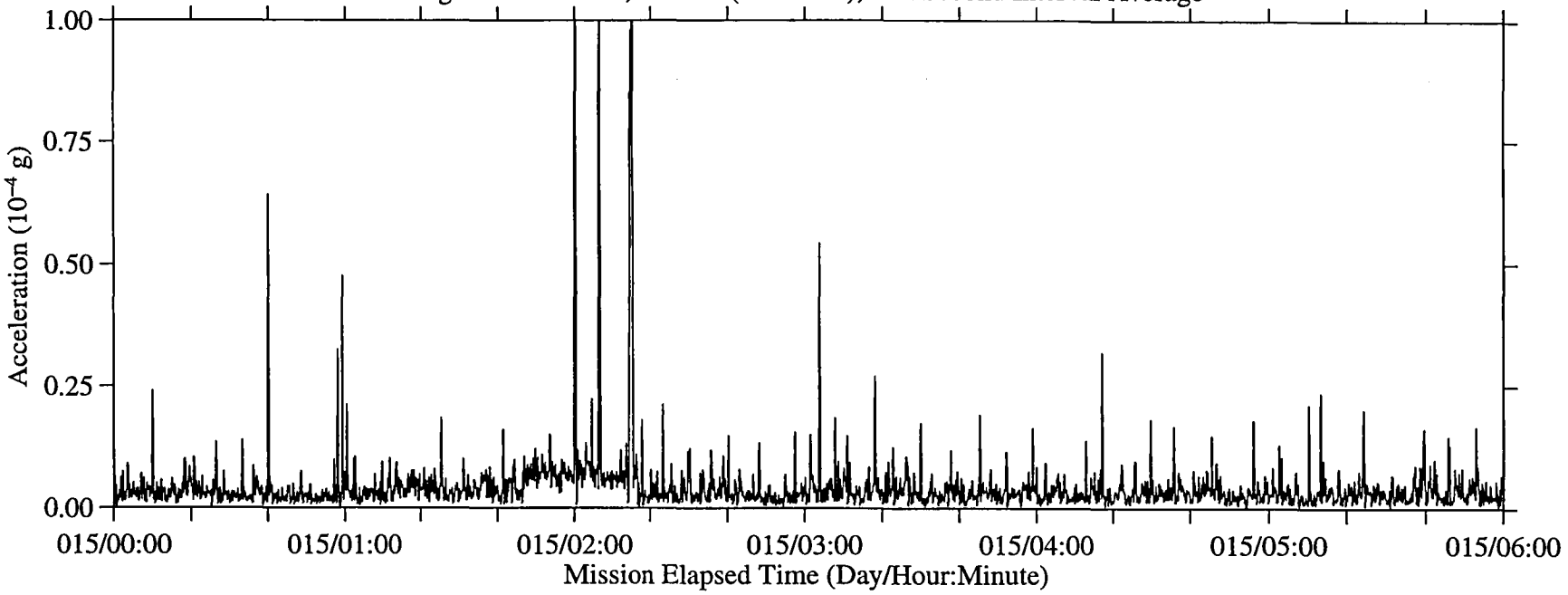

Figure 119b: LMS, Head C (fc=25 Hz), Ten Second Interval RMS

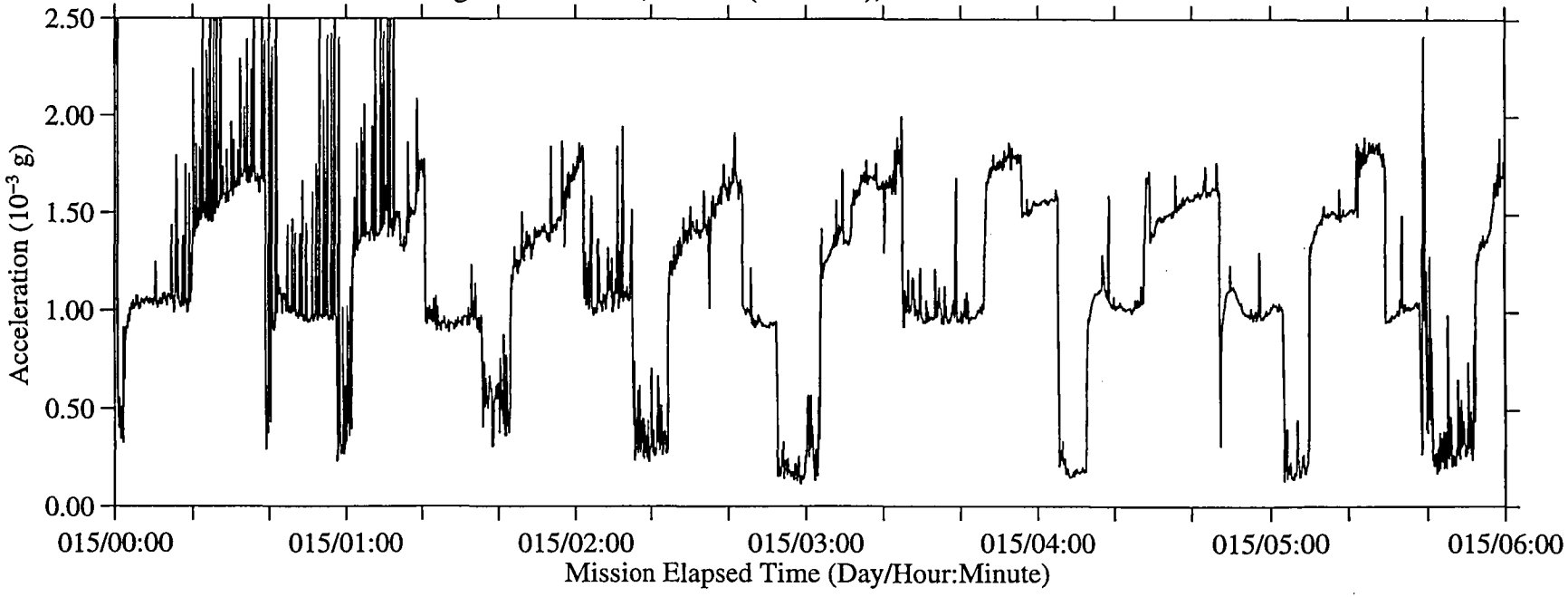

Figure 120: LMS, Head C (fc=25 Hz)

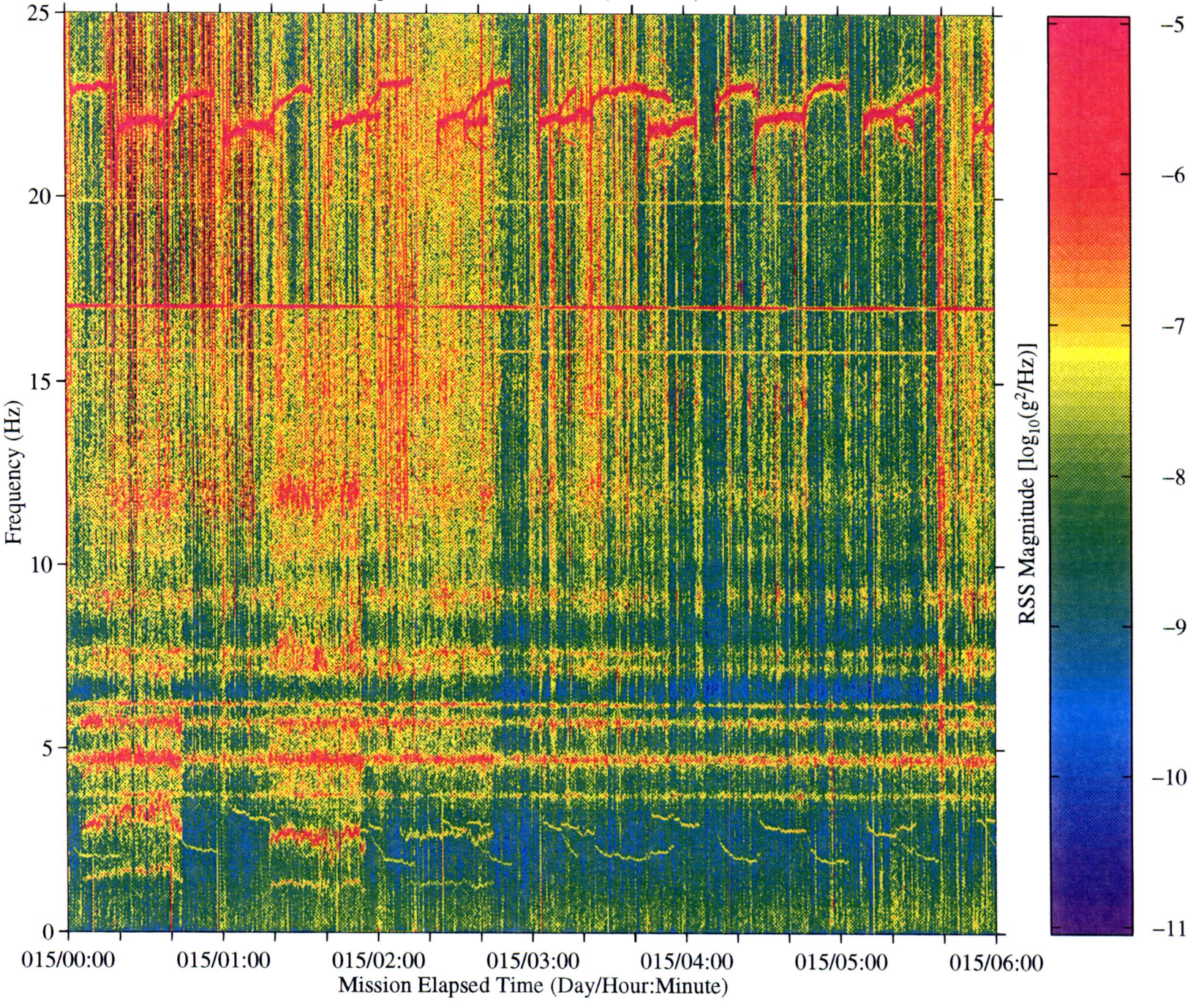

Figure 121a: LMS, Head C (fc=25 Hz), Ten Second Interval Average

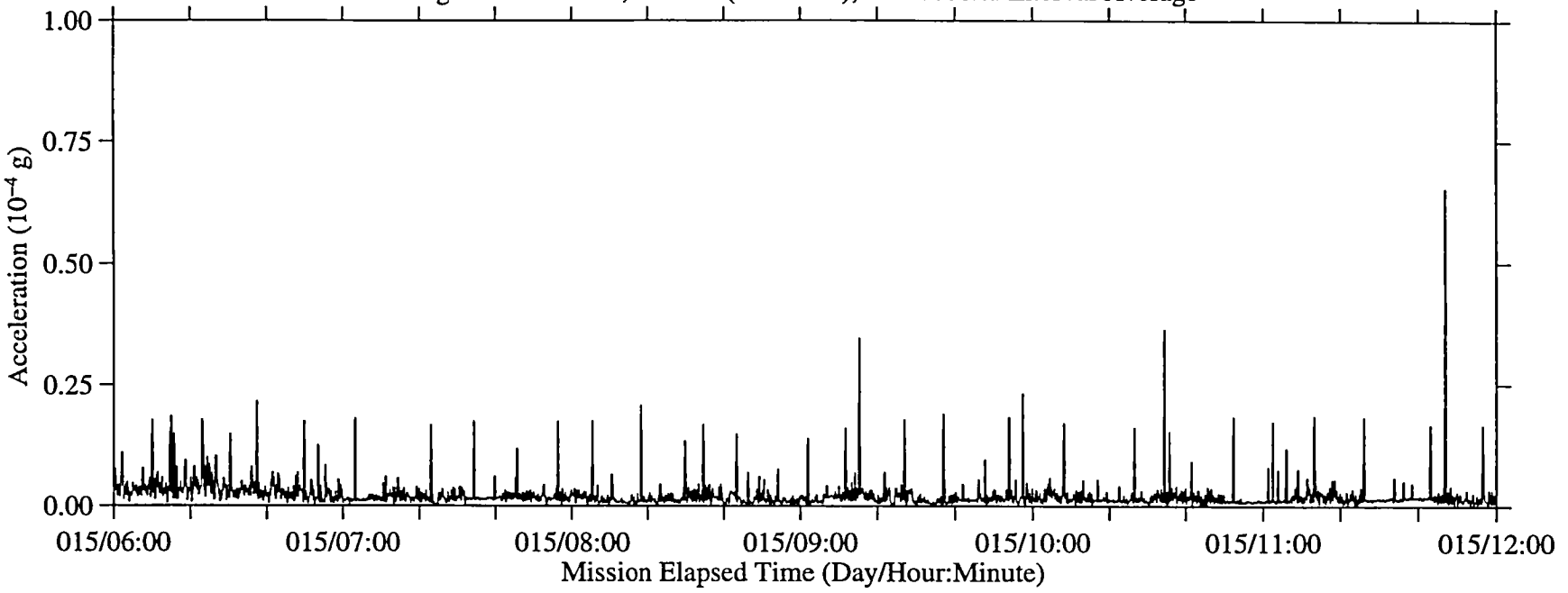

Figure 121b: LMS, Head C (fc=25 Hz), Ten Second Interval RMS

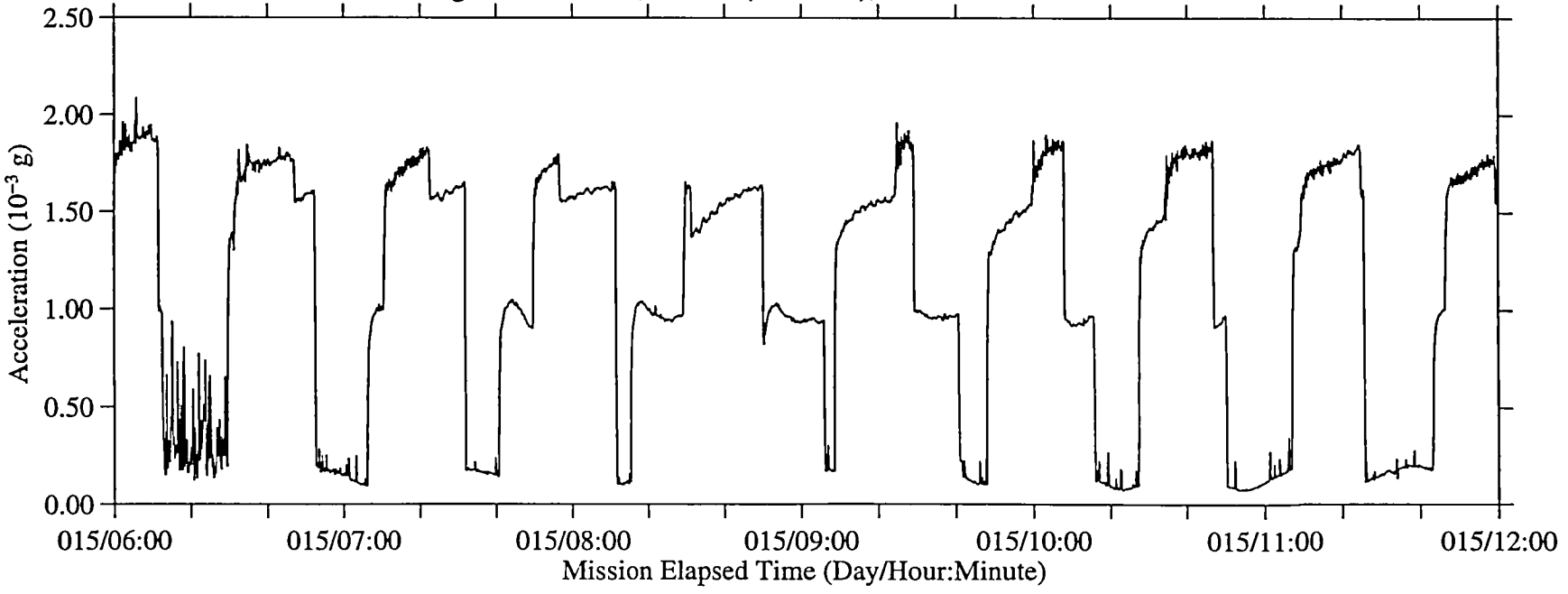

Figure 122: LMS, Head C (fc=25 Hz)

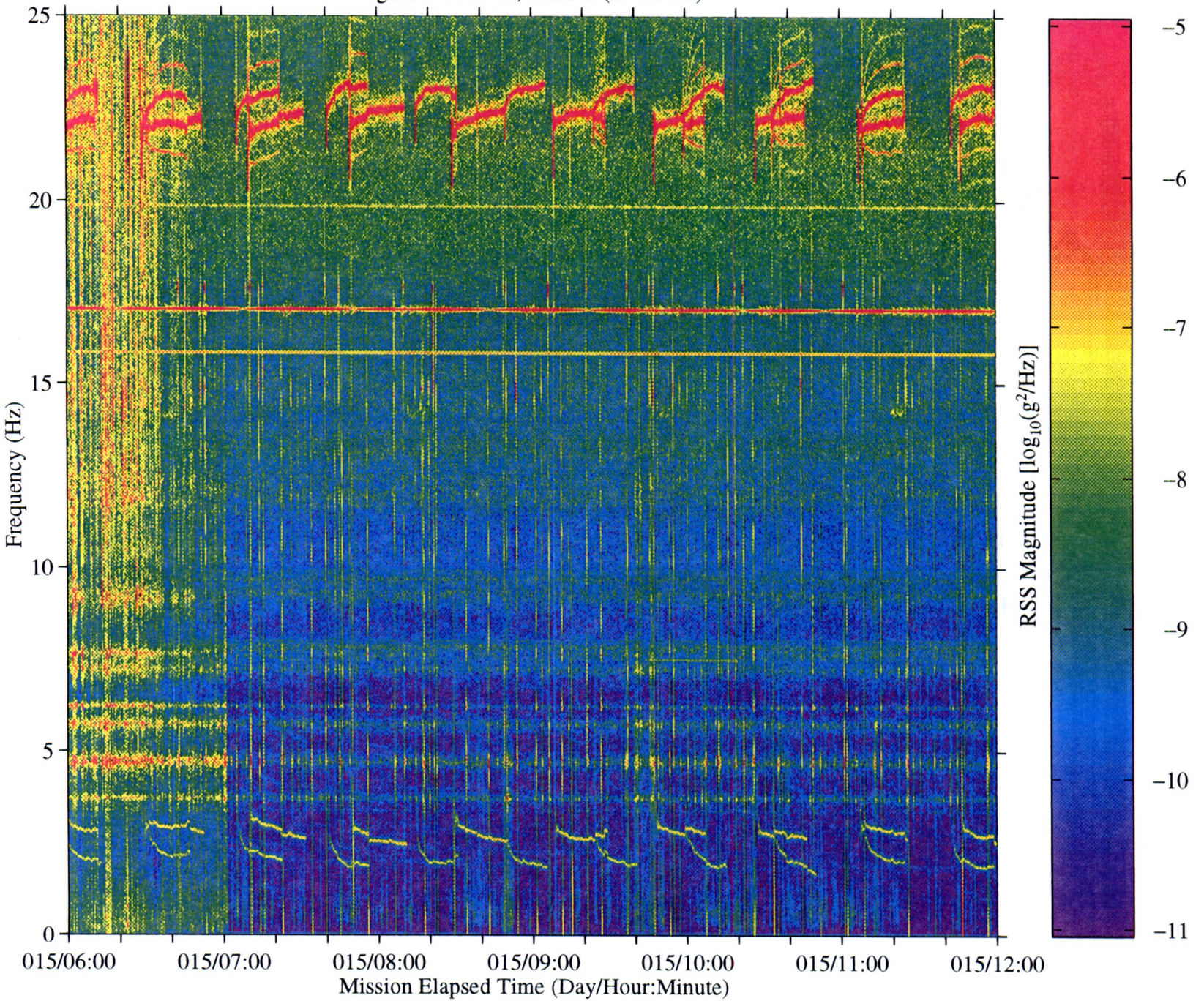

Figure 123a: LMS, Head C (fc=25 Hz), Ten Second Interval Average

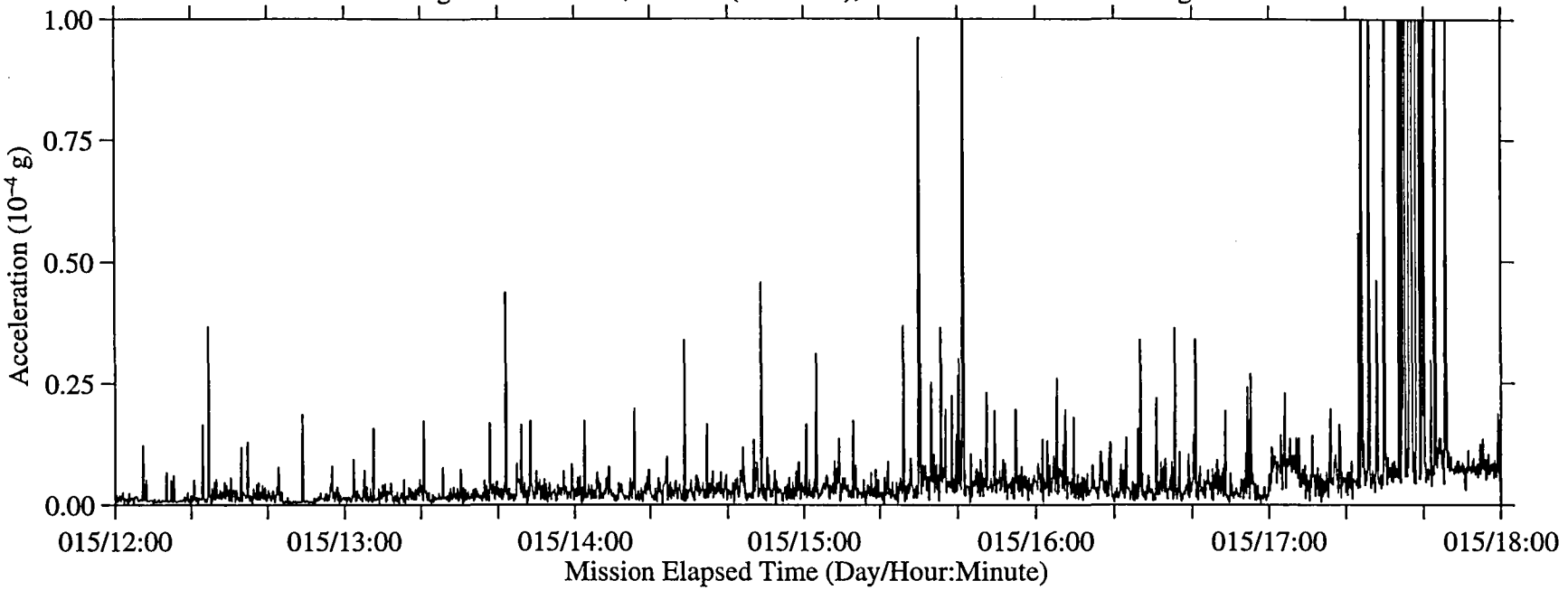

Figure 123b: LMS, Head C (fc=25 Hz), Ten Second Interval RMS

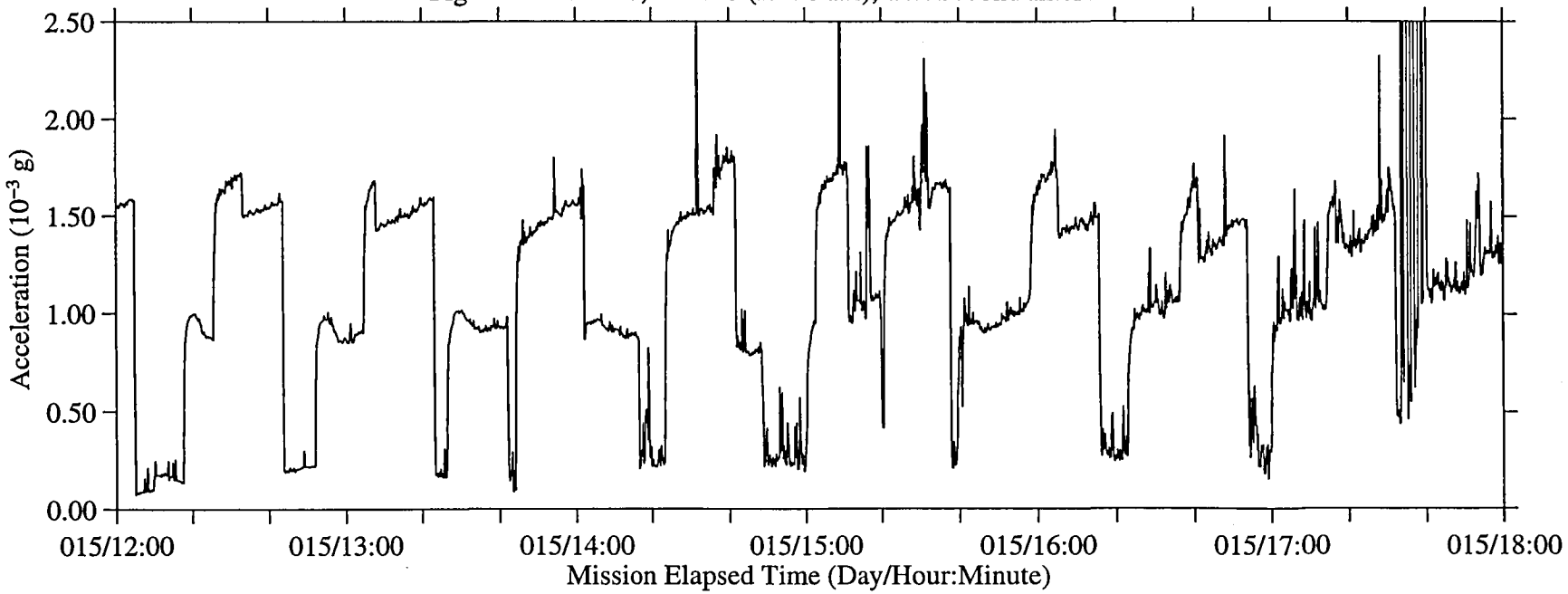

Figure 124: LMS, Head C (fc=25 Hz)

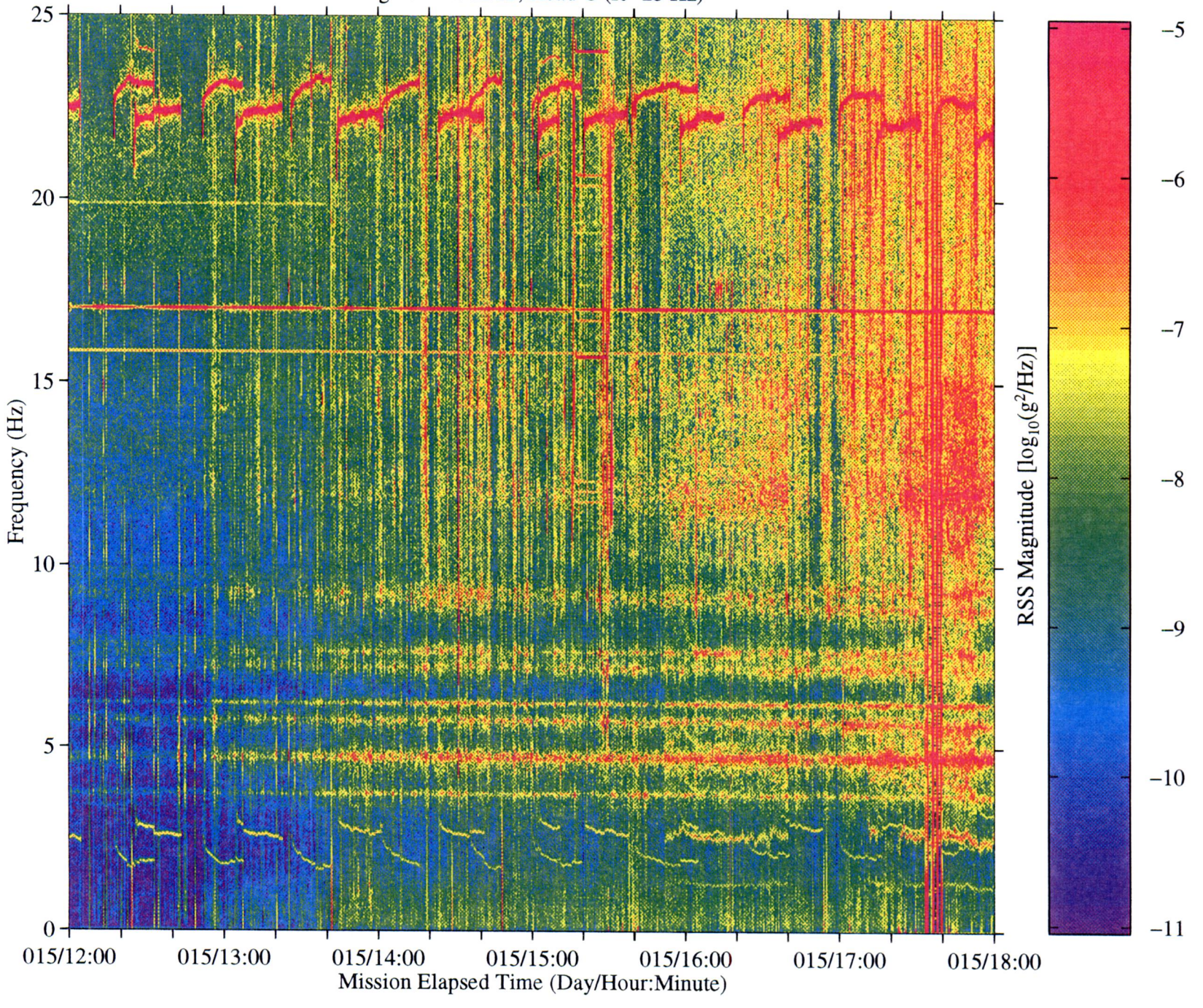

Figure 125a: LMS, Head C (fc=25 Hz), Ten Second Interval Average

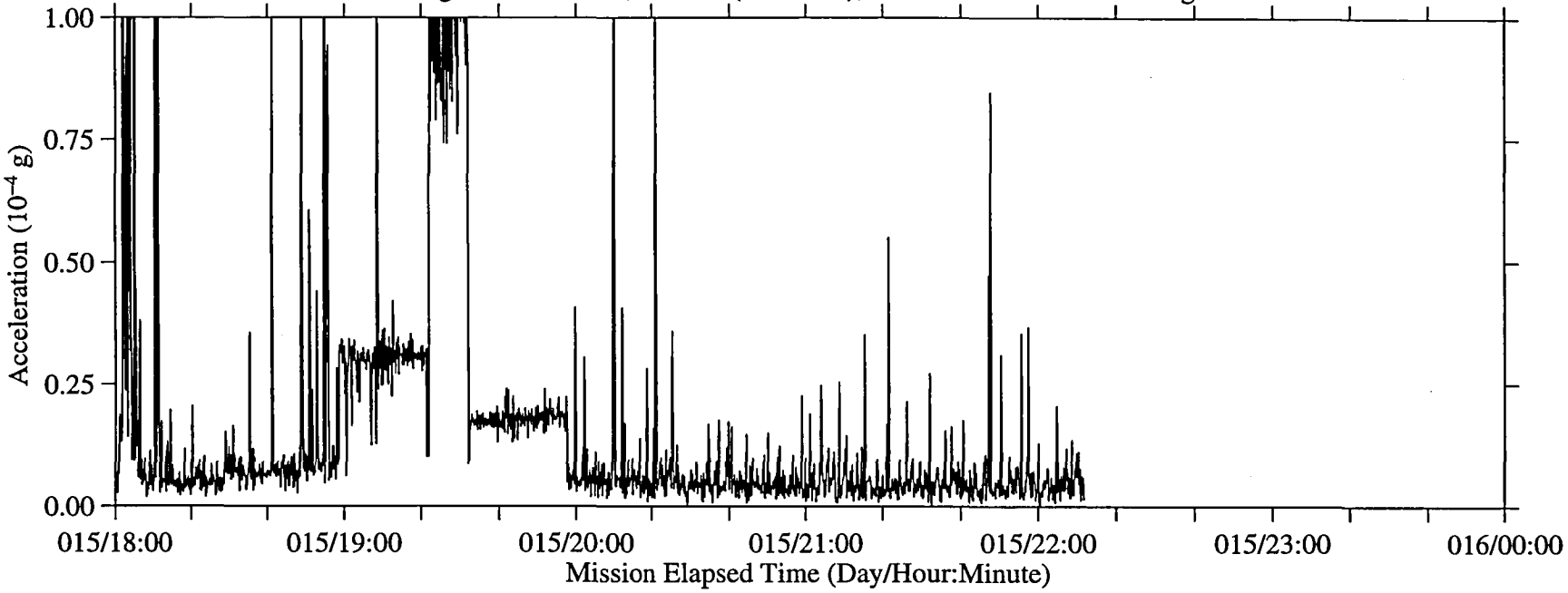

Figure 125b: LMS, Head C (fc=25 Hz), Ten Second Interval RMS

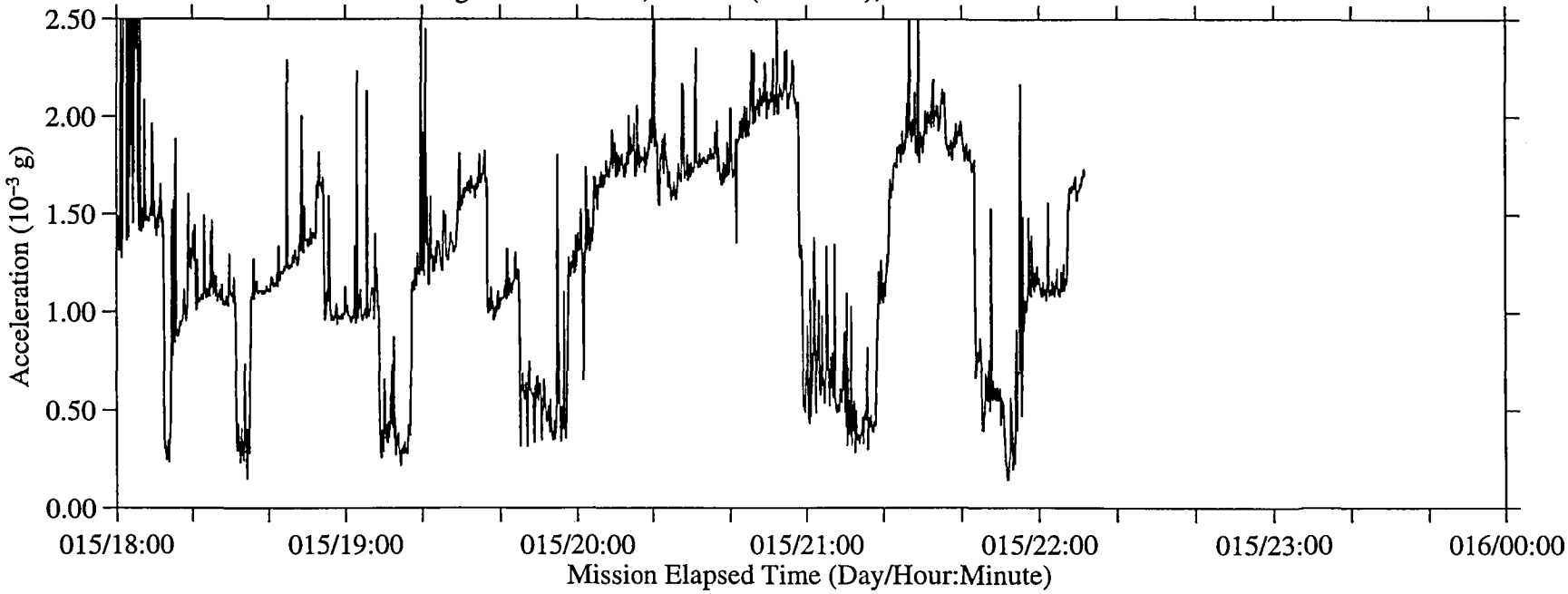

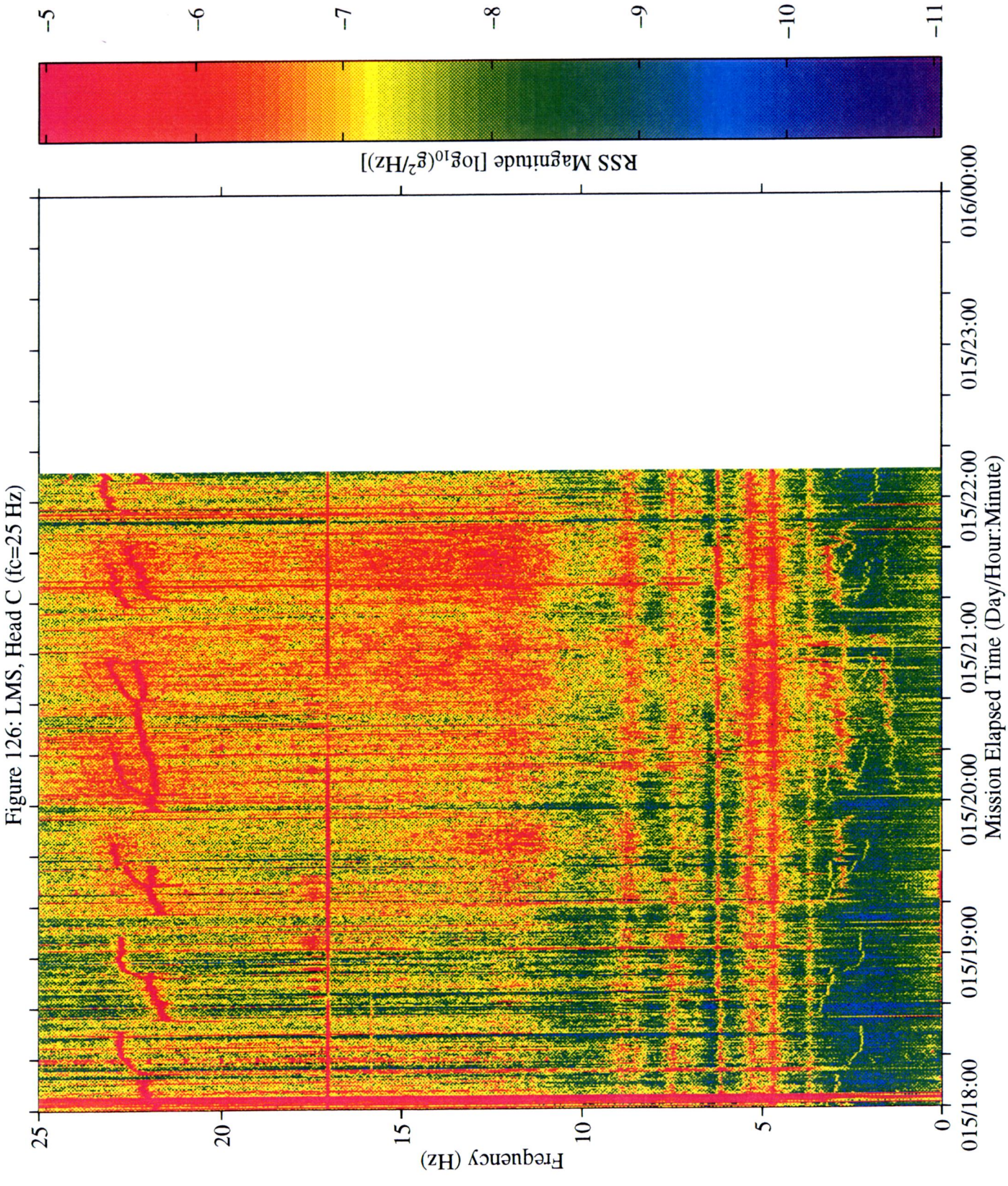

Figure 126: LMS, Head C (fc=25 Hz)

Appendix C User Comment Sheet

We would like you to give us some feedback so that we may improve the Mission Summary Reports. Please answer the following questions and give us your comments.

1. Do the Mission Summary Reports fulfill your requirements for acceleration and mission information?
_____Yes _____No If not why not?

Comments:

_____

_____

2. Is there additional information which you feel should be included in the Mission Summary Reports?
_____Yes _____No If so what is it?

Comments:

_____

_____

3. Is there information in these reports which you feel is not necessary or useful?

_____Yes _____No If so, what is it?

Comments:

_____

_____

4. Do you have internet access via: (____)ftp (____)WWW (____)gopher (____)other? Have you already accessed SAMS data or information electronically?

_____Yes _____No

Comments:

_____

_____

Completed by: Name:_____ Telephone_____

Address:_____ Facsimile_____

_____ E-mail addr_____

Return this sheet to:
Duc Truong
NASA Lewis Research Center
21000 Brookpark Road MS 500-216
Cleveland, OH 44135

or
FAX to PIMS Project: 216-433-8660
e-mail to: pims@lerc.nasa.gov.

REPORT DOCUMENTATION PAGE

Form Approved
OMB No. 0704-0188

1. AGENCY USE ONLY (*Leave blank*)	2. REPORT DATE	3. REPORT TYPE AND DATES COVERED
	January 1997	Technical Memorandum

4. TITLE AND SUBTITLE

Summary Report of Mission Acceleration Measurements for STS–78
Launched June 20, 1996

5. FUNDING NUMBERS

WU–963–60–0D

6. AUTHOR(S)

Roshanak Hakimzadeh, Kenneth Hrovat, Kevin M. McPherson,
Milton E. Moskowitz, and Melissa J.B. Rogers

7. PERFORMING ORGANIZATION NAME(S) AND ADDRESS(ES)

National Aeronautics and Space Administration
Lewis Research Center
Cleveland, Ohio 44135–3191

8. PERFORMING ORGANIZATION REPORT NUMBER

E–10608

9. SPONSORING/MONITORING AGENCY NAME(S) AND ADDRESS(ES)

National Aeronautics and Space Administration
Washington, DC 20546–0001

10. SPONSORING/MONITORING AGENCY REPORT NUMBER

NASA TM–107401

11. SUPPLEMENTARY NOTES

Roshanak Hakimzadeh and Kevin M. McPherson, NASA Lewis Research Center; Kenneth Hrovat, Milton E. Moskowitz, and Melissa J.B. Rogers, Tal-Cut Company, 24831 Lorain Road, Suite 203, North Olmsted, Ohio 44070. Responsible person, Roshanak Hakimzadeh, organization code 6727, (216) 433–8738.

12a. DISTRIBUTION/AVAILABILITY STATEMENT

Unclassified - Unlimited
Subject Categories 20, 35, and 18

This publication is available from the NASA Center for AeroSpace Information, (301) 621–0390.

12b. DISTRIBUTION CODE

13. ABSTRACT (*Maximum 200 words*)

The microgravity environment of the Space Shuttle Columbia was measured during the STS–78 mission using accelerometers from three different instruments: the Orbital Acceleration Research Experiment, the Space Acceleration Measurement System and the Microgravity Measurement Assembly. The quasi-steady environment was also calculated in near real-time during the mission by the Microgravity Analysis Workstation. The Orbital Acceleration Research Experiment provided investigators with real-time quasi-steady acceleration measurements. The Space Acceleration Measurement System recorded higher frequency data on-board for post-mission analysis. The Microgravity Measurement Assembly provided investigators with real-time quasi-steady and higher frequency acceleration measurements. The Microgravity Analysis Workstation provided calculation of the quasi-steady environment. This calculation was presented to the science teams in real-time during the mission. The microgravity environment related to several different Orbiter, crew and experiment operations is presented and interpreted in this report. A radiator deploy, the Flight Control System checkout, and a vernier reaction control system reboost demonstration had minimal effects on the acceleration environment, with excitation of frequencies in the 0.01 to 10 Hz range. Flash Evaporator System venting had no noticeable effect on the environment while supply and waste water dumps caused excursions of 2×10^{-6} to 4×10^{-6} g in the Y_b and Z_b directions. Crew sleep and ergometer exercise periods can be clearly seen in the acceleration data, as expected. Accelerations related to the two Life Science Laboratory Equipment Refrigerator/Freezers were apparent in the data as are accelerations caused by the Johnson Space Center Projects Centrifuge. As on previous microgravity missions, several signals are present in the acceleration data for which a source has not been identified. The causes of these accelerations are under investigation.

14. SUBJECT TERMS

Microgravity environment; SAMS; OARE; MMA; Acceleration measurements; STS–78; LMS; Life and microgravity space lab

15. NUMBER OF PAGES

193

16. PRICE CODE

A09

17. SECURITY CLASSIFICATION OF REPORT	18. SECURITY CLASSIFICATION OF THIS PAGE	19. SECURITY CLASSIFICATION OF ABSTRACT	20. LIMITATION OF ABSTRACT
Unclassified	Unclassified	Unclassified	

National Aeronautics and
Space Administration

Lewis Research Center
21000 Brookpark Rd.
Cleveland, OH 44135-3191